Development of lymphatic drug delivery platforms for the treatment of carcinomas
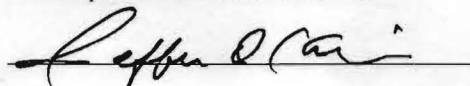
By

Shuang Cai

Submitted to the graduate degree program in Pharmaceutical Chemistry and the Graduate Faculty of the University of Kansas in partial fulfillment of the requirements for the degree of Doctor of Philosophy.
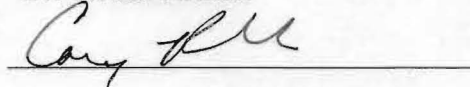
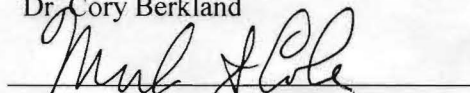Chairperson Dr. Laird Forrest

Dr. Jeff Krise

Dr. Teruna Siahaan

Dr. Cory Berkland

Dr. Mark Cohen

Date Defended: April 26, 2011

The Dissertation Committee for Shuang Cai

certifies that this is the approved version of the following dissertation:

Development of lymphatic drug delivery platforms for the treatment of carcinomas

Chairperson: Dr. Laird Forrest

Date approved: April 26, 2011

Abstract

Many cancers, such as breast cancer, lung cancer, and head and neck cancer, preferentially metastasize via the lymphatic system prior to their systemic invasion. Conventional chemotherapy has limited penetration into the lymphatics due to its anatomy, because drug molecules have to diffuse from the blood capillaries into the surrounding tissues and further enter the lymph vessels to reach the diseased lymph nodes. Therefore, chemotherapy can be of limited benefit in treating lymph node disease. In addition, due to the systemic administration and wide distribution, conventional intravenous chemotherapy causes a variety of organ toxicities, including but not limited to: renal toxicity, cardiotoxicity, and hepatic toxicity. This limits its use in the clinic, expecially for the elderly or late-stage patients who cannot tolerate systemic toxicities. Therefore, there is a critical need to develop of a localized drug delivery platform that confines the anti-cancer drugs to the site of the disease.

This dissertation focuses on the development of subcutaneously delivered drug platforms for the treatment of cancers that are known to be lymphatically metastatic. The goal is to improve the anti-cancer efficacy and reduce the non-specific organ toxicities of small molecule chemotherapeutic agents. To achieve this goal, three polymer-based anti-cancer conjugates: hyaluronan-cisplatin (HA-Pt), hyaluronan-doxorubicin (HA-DOX), and sugar star polymer-nitric oxide prodrug 1 (sugar-NO1), were synthesized, characterized, and evaluated in preclinical rodent models.

The route of drug administration along with the controlled release of the drug from the platforms, both play an important role in improving the biopharmaceutical properties of these conjugates. This is demonstrated by the extended systemic rentention, as well as the elevated local accumulation of the drug in the draining lymph nodes of the tumor, when compared to

standard intravenous chemotherapy. The HA-Pt and HA-DOX conjugates exhibited reduced renal toxicity and cardiotoxicity, respectively, relative to the conventional intravenous chemotherapy in rats. Because of the improved pharmarcokinetic and toxicological profiles of the polymer-drug conjugates, animals that were treated with the subcutaneous conjugates demonstrated enhanced inhibition of the tumor progression and increased survival rates. To understand the increased anti-cancer activity of the conjugates on a cellular level, the interaction and internalization of the nanocarriers into tumor cells was also investigated using a gold nanoparticle tagged HA-Pt conjugate and a fluorescently labeled HA-DOX conjugate.

In the clinic, cisplatin and doxorubicin are often administered in combination with other anti-tumor agents as a "chemo cocktail" to prevent chemoresistance. Additionally, nitric oxide has been shown to improve the cytotoxicity of cisplatin therapy via a synergistic effect. Therefore, the development of a nitric oxide prodrug cisplatin combinational therapy, with increased anti-proliferative activity against cancer cells, was investigated; and it is also presented in this disssertation and compared to cisplatin treatment alone.

In conclusion, this thesis work has led to the successful preclinical development of two localized drug delivery platforms and one promising candidate for the treatment of metastatic carcinomas. The motivation for drug delivery scientists to develop more efficacious and less toxic chemotherapies will be presented.

Dedicated to:

My parents, Guiling Wang and Wenyu Cai, and my husband, Xiaoning Li,

for

their constant love, support and encouragement.

Acknowledgements

First and foremost, I would like to express my gratitude and appreciation to my advisor, Dr. Laird Forrest, for his guidance, encouragement, and continuous support throughout my degree program and also with my professional development. I appreciate the numerous opportunities he provided me to explore new research ideas, to present my work at scientific conferences, to apply for fellowships and awards, and to gain internship experience. I am truly grateful for his inspiring mentorship and genuine friendship.

I would like to thank my committee members, Drs. Jeff Krise, Teruna Siahaan, Cory Berkland, and Mark Cohen for taking time out of their busy schedules to read my dissertation and for offering valuable suggestions.

Also, I give many thanks to all present and past Forrest lab members: Adel Alhowyan, Yomna Badawi, Taryn Bagby, Lei Cheung, Jason Christian, Dr. Hassam-Mustafa Diab, Dr. Shaofeng Duan, Dr. Padmaja Gunda, David Hart, Yepeng Luan, Sharadvi Thati, Dr. Yumei Xie, Qiuhong Yang, Ti Zhang, and Yunqi Zhao, as well as friends and staff members of the department. I am truly thankful for your friendship and assistance over the past four years.

Additionally, I would like to thank Drs. Valentino Stella, John Stobaugh, Russell Middaugh, Christian Schoneich, Jennifer Laurence, and Teresa DiColandrea for being such wonderful teachers.

Finally, thank you to my parents, Guiling Wang and Wenyu Cai, for always being there to help me, to guide me, and to laugh with me. Thank you to my husband, Xiaoning Li, for his endless support, patience, and love. I would not have been able to make it through my graduate career without you.

Table of Contents

Chapter 1

Introduction

1. Objectives

The overall purpose of this study was to develop localized intralymphatic chemotherapy methods using polymer-based nanocarriers for the treatment of metastatic cancers, such as breast cancer and head and neck cancer. This thesis work can be divided into four parts: 1) Development of nanoconjugates for the delivery of cisplatin and nitric oxide prodrugs to the head and neck lymphatics of rodents, and the evaluation of the *in vitro* efficacy of the nanoconjugates in head and neck squamous cell carcinoma (HNSCC) cell lines; 2) Development of nanoconjugates for doxorubicin delivery to the breast lymphatics of rodents and the evaluation of the *in vitro* efficacy of doxorubicin nanoconjugates in breast cancer cell lines; 3) Examination of the safety, long-term toxicity, and efficacy, of lymphatic nanoconjugate chemotherapy in rodents and compare these to intravenous delivery; and 4) Assessment of the internalization of the carrier and cisplatin/doxorubicin in cancer cells and murine tumors.

In this chapter, a series of clinical and investigational applications of localized chemotherapy will be presented, with the goal of emphasizing their improvements compared to the conventional intravenous chemotherapy. In the following chapters, the development, characterization, *in vitro* and *in vivo* evaluation, of three polymer-based chemotherapeutic conjugates will be described.

2. Localized chemotherapy

The most common types of cancer therapies include surgery, radiation, chemotherapy, and their combinations. In the past decades, new treatment regimens have been discovered and implemented in the clinic, to concurrently or successively complement the standard procedures

in cancer therapy, and provide patients with improved treatment outcomes and fewer side effects. Some of these clinical and investigational treatment methods include antiangiogenesis therapy [1-3], immunotherapy [4-6], gene therapy [7-9], bone marrow transplantation, and peripheral blood stem cell transplantation [10-12]. Due to the complex nature of the molecular targets of these newer therapies and the relatively short history since their clinical introduction, they are not as widely used as conventional chemotherapy.

Most cancer patients will receive some type of chemotherapy during their treatments in the form of adjuvant, neoadjuvant, or palliative therapy. Although the first line chemotherapies have provided lifesaving treatments for numerous cancer patients, their potential life-threatening side effects should not be overlooked. The most severe side effects of chemotherapy are mainly caused by the systemic toxicities of the anti-cancer drugs. Because the conventional chemotherapy is administered intravenously via a catheter, the cytotoxic drugs travel throughout the systemic circulation of the patient and accumulate in his or her healthy organs, such as the kidneys, heart, and liver, which eventually cause organ toxicities over time.

One of the issues with infusion chemotherapy is that the effective dose of conventional cytotoxic agents is often greater than or close to the maximum tolerable dose in the patient, depending on his or her disease stage and health condition. Therefore, to minimize the systemic exposure of the highly toxic chemotherapeutic agents, alternative locoregional drug delivery routes have been explored in both preclinical investigations and clinical trials. To date, several localized chemotherapies have been adapted into clinical practices, providing cancer patients with additional options of therapy with fewer side effects. In this section, six types of localized chemotherapy will be described, which include: isolated limb perfusion (ILP), heated intraperitoneal chemotherapy (HIPEC), intrapleural perfusion hyperthermo-chemotherapy

(IPPHC), isolated hepatic perfusion chemotherapy (IHP), transarterial chemoembolization (TACE), and lymphatic chemotherapy.

2.1 Isolated limb perfusion chemotherapy (ILP)

Isolated limb perfusion was initially introduced in the clinic in 1958 by the American surgeons, Creech and Krementz, as regional chemotherapy, using an extracorporeal circuit for the treatment of extremity melanoma [13]. Initially, the ILP procedure was performed at room temperature, but this procedure was later modified by Stehlin to be performed as a hyperthermic perfusion at 41-43 ˚C [14]. ILP works by temporarily isolating the arm or leg of the patient from the circulatory system using a tourniquet, and perfusing a highly concentrated anti-cancer agent, such as melphalan, for a short period of time. Typically several temperature probes are inserted into the subcutaneous tissue of the patient to monitor his/her body temperature. For example, ILP of the leg is performed by making a small incision close to the iliac vein of the patient; a catheter is then inserted into the iliac vein where the anti-cancer drug melphalan is perfused (Figure 1). Meanwhile another catheter is inserted into the draining artery, where the blood is collected and the melphalan solution is allowed to circulate for 1-2 hours. During the perfusion, a tourniquet is secured at the base of the leg, preventing the highly concentrated anti-cancer agent from entering the systemic circulation and reaching the healthy organs, such as the liver and kidneys. The ILP allows 10 to 20-fold higher regional drug concentrations to be administered compared to intravenous melphalan chemotherapy; therefore, it often leads to improved disease control, especially the malignancy is confined to the limbs.
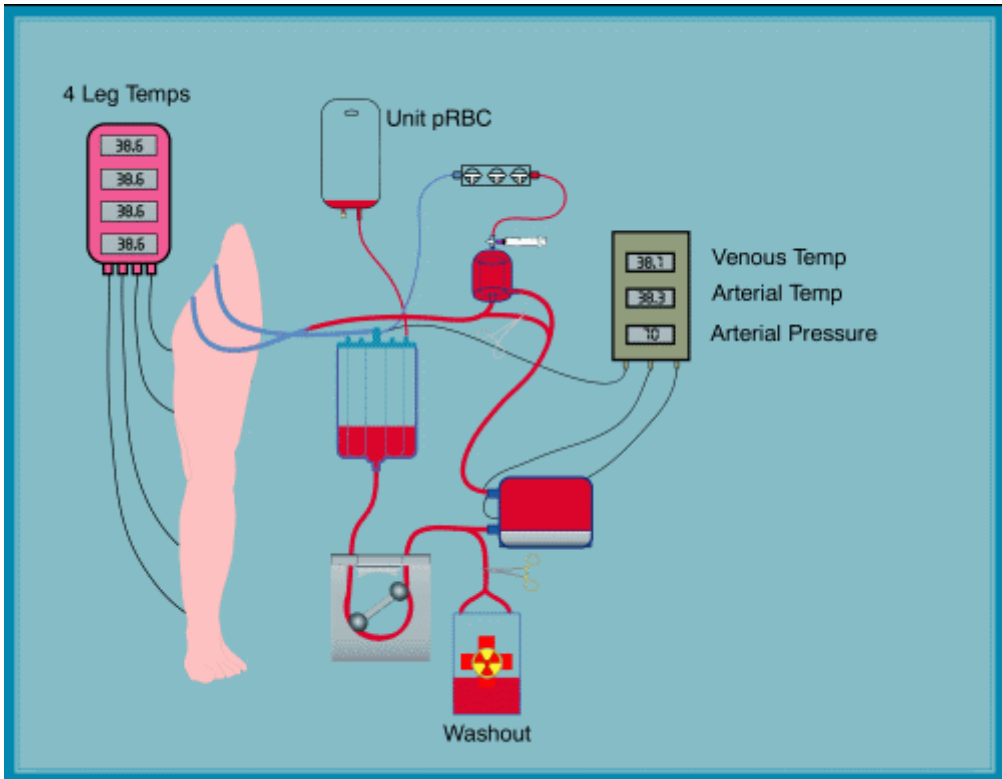
Figure 1. Schematic representation of isolated limb perfusion. Figure originally published on the internet. See reference [15].

Koops and Vaglini reported the impact of ILP in a multicenter randomized phase III clinical trial, as a preventive chemotherapy for melanoma patients who have a high risk of developing regional micrometastases [16]. A total of 832 patients were enrolled in the trial; 53% had a primary tumor with a thickness of 1.5-3 mm, and the remainder had a primary tumor thicker than 3 mm. The control group had 412 patients, who received a complete excision of the primary tumors without chemotherapy. The second group had a total of 420 patients, who were treated with hyperthermic ILP of melphalan after the initial resection. At the end of the follow-up period (median duration of 6.4 years), it was found that patients who received ILP exhibited reduced occurrence of in-transit metastases (control: 6.6% vs. ILP: 3.3%) and regional lymph node involvement (control: 16.7% vs. ILP: 1.6%). However, the rate of the occurrence of distant metastasis or overall survival was not statistically altered.

Melphalan was the first and most effective anti-cancer agent utilized in ILP. Due to the short half life ($t_{degradation}$=50 min) and the severe toxicity of melphalan in local limb tissues, there have been a number of clinical trials investigating alternative chemotherapeutic agents. One of the agents was cisplatin, which appeared to be effective for the treatment of melanoma in preclinical studies. Thompson and Gianoutsos conducted a cisplatin pilot trial in patients with recurrent melanoma [17]. Unfortunately, cisplatin ILP failed to demonstrate either disease inhibition or improved tissue toxicity, compared to melphalan therapy, in the majority of the patients. Another platinum-based cytotoxic agent, carboplatin, was also investigated in clinical trials. Even though partial response was observed in some patients, severe local toxicities such as motor-sensory neuropathy and oedema, were reported in all patients. The pharmacokinetic data demonstrated extremely high drug concentration in the regional skin; hence, further evaluation of

carboplatin-related treatment regimens was not warranted [18]. To date, melphalan remains to be the most successful anti-cancer drug for ILP in the treatment of localized melanomas.

Since melphalan became a commonly accepted treatment strategy, combination therapies using melphalan and other anti-cancer agents were extensively investigated in the 1990s, with the goal of further improving the rate of response and survival. Of these clinical investigations, the most successful regimen introduced tumor necrosis factor alpha (TNF-α) into the standard melphalan treatment. Eggermont and Lienard simultaneously reported the improved efficacy of melphalan and TNF-α combination chemotherapy in multicenter trials for the treatment of both melanoma and soft-tissue sarcoma [19-20]. To explore the underlying mechanism that leads to the synergistic effect between melphalan and TNF-α, a number of studies were conducted using animal xenograft models. Among the hypotheses of the synergism, de Wilt's explanation was widely accepted, in which he and his coworkers discovered that the addition of TNF-α resulted in a six-fold increase of melphalan tumor accumulation in a rat model. Hence, it was not surprising that the combination therapy increased the inhibition of tumor progression relative to melphalan treatment alone [21].

Strategies for localized chemotherapy, such as ILP, greatly reduce the systemic side effects of anti-cancer agents by confining the drug to the blood capillaries of the tumor-bearing limb. Systemic toxicities of melphalan ILP were only observed when systemic leakage had occurred due to the incomplete isolation of the perfused artery. A clinical study of 438 melphalan ILPs was conducted by Klaase et al. to determine the incidence of systemic leakage and the significant factors that caused the leakage [22]. Of all patients who received melphalan ILP, 12.6% exhibited systemic drug leakage ≥ 1% of the administered drug; additionally, 6.2% and 1.4% of the patients had 5% and 10% systemic drug leakage, respectively. Since > 90% of the

melphalan was confined to limb, the low amount of melphalan that leaked to the systemic circulation lead to relatively mild side-effect compare to systemic regimens, for example, transient bone marrow depression. The most significant factors associated with systemic leakage were determined to be the level of isolation, the diameter of the venous cannula, and the extent of the ligation of the perfused iliac vein.

The emergence of melphalan and TNF-α combination in ILP led to the clinical evaluation of the side effects caused by TNF-α systemic leakage. In a trial in the Netherlands, patients with recurrent melanoma received ILP of the combination of the two anti-cancer agents [23]. The pharmacokinetic data reported a 11.4 to 31.5-fold increase in the systemic TNF-α concentration in patients who had drug leakage compared to patients without systemic leakage. Even though the systemic concentration of TNF-α was greatly altered, only mild side effects manifested, including: fever, nausea, and grade I/II hepatotoxicity, which represented the common toxicities of ILP using melphalan alone. Their findings suggested that the combination of melphalan and TNF-α did not cause increased systemic toxicities relative to melphalan treatment alone; thus, the combination regimen was recommended for ILP procedures considering its improved efficacy.

Although ILP demonstrated improved efficacy and survival rate in patients with melanoma, it is still a complex and invasive procedure. To develop a simpler yet effective alternative, Thompson and coworkers at the Sydney Melanoma Unit introduced isolated limb infusion (ILI) technique to the clinic in the 1990s [24]. ILI is a low-flow ILP, in which catheters are percutaneously inserted into the axial artery and vein of the diseased limb. The solution of a cytotoxic agent, such as melphalan, is infused and circulated for 15 to 60 minutes. A tourniquet is applied at the base of the limb to prevent systemic drug leakage. Unlike ILP, surgery is no

longer necessary for this procedure; thus, the patient recovers quickly after the treatment. A number of clinical trials were conducted to evaluate the feasibility and efficacy of this newer procedure and compared it to ILP [24-27]. Lindner et al. reported a satisfactory response rate of 85% for patients with melanoma who were treated with ILI [28]. Of these patients, 41% had complete response and 44% had partial response. The response rate is comparable to the reported effectiveness of ILP. Another ILI trial conducted by Thompson et al. also demonstrated similar results, suggesting that ILI is a less invasive but equivalently effective alternative of ILP [24]. Fewer patients (32%) developed severe limb and systemic toxicities compared to the ones treated with ILP [29]. This is especially beneficial for elderly patients who cannot tolerate the surgery involved in ILP or its associated side effects. In conclusion, ILI appears to demonstrate similar effectiveness and a lower morbidity rate compared to ILP.

2.2 Heated intraperitoneal chemotherapy (HIPEC)

Intraperitoneal chemotherapy was developed by Sugarbaker et al. in the 1980s to treat peritoneal carcinomas, including gastric and colorectal cancers, as well as cancers that originated elsewhere in the body but have metastasized to the surface or interior of the peritoneal cavity. In HIPEC, a heated, high-dose of an anti-cancer drug is circulated for a short period of time through the peritoneal cavity (Figure 2). HIPEC is often used as an adjuvant therapy after complete resection of the primary malignancies, to eradicate the residue disease at the site of the tumor. A clinical trial of patients with gastrointestinal carcinoma reported the advantageous pharmacokinetics of HIPEC, in which the median area-under-the-curve ratios of i.p./i.v. were determined to be 117 and 22 for 5-FU and mitomycin C chemotherapy, respectively [30].
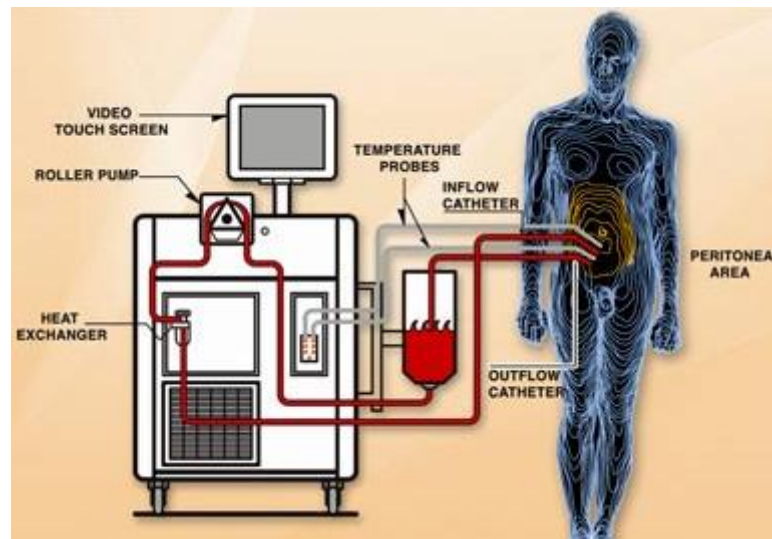
Figure 2. Schematic representation of heated intraperitoneal chemotherapy. Figure originally published on the internet. See reference [31].

To justify the addition of HIPEC to the standard procedures of peritoneal cancer therapy, clinical trials were conducted to compare the treatment outcome of surgery alone to the combination regiment of HIPEC and complete resection in patients with advanced gastric carcinomas. In a clinical trial in Japan, 141 patients with advanced gastric cancer along with invasion were registered, seventy-one were treated with HIPEC using 5-FU after the complete gastric resection, and the remainder received surgery alone [32]. The results revealed greatly reduced peritoneal recurrence rate over 7-year follow-up period (27% vs. 47%, p=0.0000847), and improved 2, 4, and 8-year survival rates in the HIPEC cohort.

Besides 5-FU and mitomycin C, other anti-cancer agents have been investigated for HIPEC. One of these investigational candidates for HIPEC is oxaliplatin, which is a platinum-based anti-cancer agent often used in the intravenous treatment of colorectal cancer. Elias et al. conducted a phase II study of oxaliplatin in patients with advanced colorectal cancer in France [33]. They reported a prolonged 3-year survival rate of 65%, and 68% of the living patients were free of peritoneal recurrence at the conclusion of the follow-up period (18.3 to 49.6 months).

Many late-stage cancer patients with unresectable tumors that cannot be effectively treated with available therapies receive palliative surgery preceding systemic chemotherapy to relieve disease-associated pain and improve their quality-of-life. Verwaal et al. conducted a randomized trial in the Netherlands to compare HIPEC of 5-FU-leucovorin in combination with aggressive cytoreduction surgery, with the standard treatment regimen of palliative surgery followed by systemic chemotherapy, in patients with peritoneal carcinomatosis from colorectal cancer [34]. Aggressive cytoreduction is the surgical removal of any detectable microscopic tumors or metastases, often by debriding of the intestine and other tissue surfaces within the

peritoneal cavity, after the complete excision of the primary tumor. Verwaal et al. reported a prolonged median survival period of 22.3 months for patients who received the experimental therapy with HIPEC, compared to 12.6 months for patients who received the standard treatment. Further, a significant improvement in survival was observed for patients with five or less metastatic lesions in the peritoneal cavity, relative to patients who had seven or more metastases at the time of the surgery.

Cytoreduction, also known as debulking, may reduce the rate of recurrence for some patient populations. It is not always recommended, because the aggressive resection may result in the removal of surrounding non-cancerous tissues, causing severe complications and increased mortality. A clinical trial, conducted by Jacquet et al., evaluated the post-treatment complications and the major risk factors of the HIPEC-cytoreduction combination procedure in patients with peritoneal carcinomatosis from adenocarcinoma of the colon or appendix [35]. The major complications included: anastomotic leaks, bowel perforations, bile leaks, and pancreatitis, which resulted in a 35% morbidity rate and 5% mortality rate. The complications were believed to be associated with the extent of the surgery, the length of the operation, and the temperature of the perfused chemotherapeutic agents [35-36]. To investigate the role of hyperthermia in localized chemotherapy, a trial was conducted in patients with colon cancer. The authors reported that both normothermic and hyperthermic intraperitoneal chemotherapies were clinically safe and feasible. Even though the patients who received the heated chemotherapy showed a higher incidence of anastomotic leakage, it was caused by the extensive resection of the colon, as opposed to the hyperthermic conditions of the perfusate [37].

2.3 Intrapleural perfusion hyperthermo-chemotherapy (IPPHC)

12

Since the clinical success of melphalan ILP was recognized, other localized treatment strategies have been investigated over the past decades. Intrapleural perfusion chemotherapy, a localized therapy for the treatment of pleural disseminated malignancies in the body cavity that surrounds the lungs, is one of these newer therapies developed in the 1990s. Pre-surgery, several temperature probes are inserted into the intercostal pleura to monitor the temperature of the pleural cavity (Figure 3). During the IPPHC procedure, the primary malignancy is first excised. Subsequently, an irrigation inlet catheter and a drainage outlet catheter are inserted into the pulmonary artery, and a highly concentrated anti-cancer drug, such as cisplatin, is perfused for one to two hours.

To determine the efficacy of IPPHC, a number of clinical trials were undertaken in patients with metastatic cancers that had spread to the pleura [38-41]. Matsuzaki et al. reported a trial conducted in Japan in which one cohort of patients received intrapleural perfusion of cisplatin after the removal of the malignancies, and the other cohort was treated with surgery alone [38]. The median survival of the experimental group was 2.3-fold longer than the standard surgery treated group (20 months vs. 6 months). Additionally, advantageous pharmacokinetic profiles were seen, demonstrated by the increased local concentration of cisplatin in the pleural cavity, along with minimal observed clinical complications. A similar clinical study was conducted a few years later by the same institution to compare the apoptotic status of the tumor tissue, pre- and post-IPPHC with cisplatin. An 8-fold increase in the number of the apoptotic cancer cells was detected immunochemically in the post-perfusion tissues compared to the untreated tumor tissues pre-treatment [39].
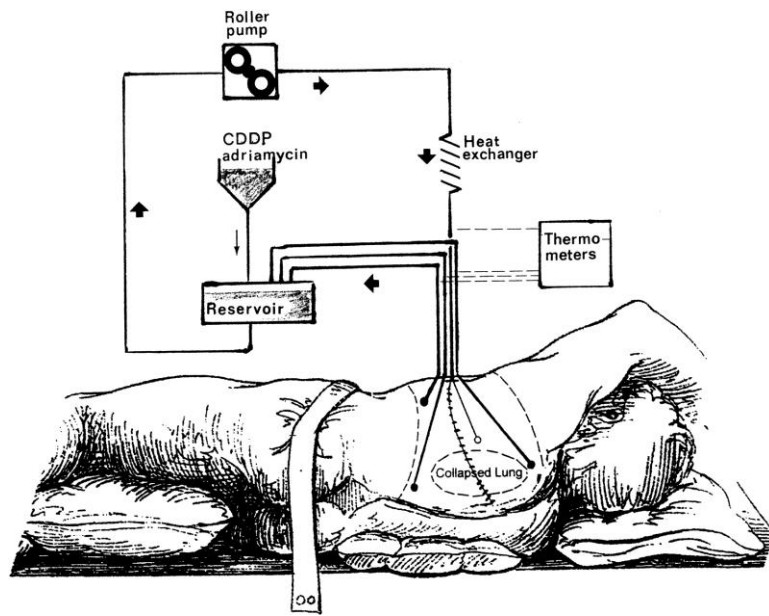
Figure 3. Schematic representation of intrapleural perfusion hyperthermo-chemotherapy. Reused with permission from [42].

Although intrapleural perfusion is often utilized as adjuvant chemotherapy after tumor excision, there is a possibility that a new modality consisting of presurgical IPPHC may provide better control of the tumor progression before the surgery is performed. Shigemura and coworkers evaluated this new modality in a 2003 pilot study for the treatment of lung cancer with carcinomatous pleuritis. A mean survival time of 19 months was reported for patients in the IPPHC and panpleuropneumonectomy combination arm [40]. No severe complications were observed in the study. Future trials with more patients and a longer follow-up time may be warranted to determine whether the new modality is superior to the previous regimen.

Cisplatin is the most commonly used anti-cancer agent for IPPHC, but mitomycin C is also a candidate for this procedure. To evaluate the effectiveness of IPPHC using cisplatin and mitomycin C combination treatment, a clinical trial was undertaken in patients with malignant pleural disease in France in 2003 [41]. The 1-year and 5-year survival rates of 74% and 27%, respectively, were reported, over a follow-up period of approximately 7.5 years. This combination regimen appeared to be especially effective for patients with T1 ("Tumor involves same side pleura of the chest wall, with or without focal involvement of the pleura on the outer side of lung.") or T2 ("Tumor involves same side pleura of the chest wall with at least one of the following features: confluent tumor on the outer surface of the lung, involvement of the muscles of the diaphragm, or involvement of the lung tissue deeper to the mesothum covering the lung.") mesothelioma [43], indicated by a median survival of 41.3 months. Therefore, patient staging and selection play a significant role in the design of a successful clinical trial for locoregional therapy.

2.4 Isolated hepatic perfusion chemotherapy (IHP)

Locoregional chemotherapy for the treatment of unresectable liver cancers was first developed by Ausman in 1961 as an isolated hepatic perfusion technique [44]; which isolates the hepatic blood flow from the systemic circulation and directs anti-cancer drugs through the hepatic artery and vein. Unresectable liver carcinoma and hepatic metastases disseminated from colorectal cancer and ocular melanoma are lethal diseases with a survival time of merely several months despite aggressive treatment. IHP offers the advantage of circulating a highly concentrated anti-cancer drug solution through the tumor-bearing liver. Because the maximum delivered dose is limited by the tolerance of only the liver, as opposed to the whole body, usually a much higher concentration of perfusate can be administered compared to intravenous chemotherapy. The most commonly used anti-cancer drugs for IHP consists of melphalan alone, melphalan TNF-α combination, or mitomycin C. At the beginning of an IHP procedure, a laparotomy is performed to locate the hepatic artery and vein for the insertion of the irrigation inlet catheter and the drainage outlet catheter. The gastroduodenal artery is cannulated for the insertion of the inlet catheter, and the retrohepatic inferior vena cava is dissected to position the outlet catheter. A perfusion circuit with a roller pump, a heat exchanger, and an oxygenator, is secured to perfuse the anti-cancer drug through the liver for an hour [45].

To examine the efficacy of this new procedure, Alexander et al. conducted a clinical trial of IHP using the melphalan and TNF-α combination in patients with unresectable primary or metastatic secondary liver cancers [46]. The patients received a one-hour hyperthermic perfusion of melphalan and TNF-α combination. Post treatment, 75% of the patients developed reversible hepatic toxicities. At the end of the follow-up period, 3% of the patients showed a complete response to the therapy, and 72% of the patients exhibited a partial response. The findings

suggested that the melphalan and TNF-α combination therapy might be an effective and safe treatment regimen for patients with unresectable liver cancers.

Whereas ILP requires only a small incision in the tumor-bearing limb, IHP for veinal and arterial access requires a laparotomy, thus it is a highly invasive and risky procedure in spite of the other advantages offered. To minimize the surgical invasion and reduce complication, the IHP technique was modified and adapted to a non-surgical procedure known as percutaneous hepatic perfusion (PHP). PHP is a non-invasive alternative to IHP, which delivers an anti-cancer drug to the liver at dramatically increased concentrations, with minimum systemic side effects. Because of the greatly reduced side effects and elimination of surgery, this procedure can be performed repeatedly four to six times within a month interval. During a PHP, an infusion catheter is inserted into the femoral artery through the skin and guided to the hepatic artery, and then a second catheter is inserted into the femoral artery on the other leg and guided to the inferior vena cava (Figure 4). After insertion, double balloons on the catheters are inflated to block the normal blood flow to complete the organ isolation. Subsequently, an anti-cancer drug is perfused through the liver for 30 minutes. At the end of the procedure, the two balloons are deflated and the catheters removed. To evaluate the feasibility and procedure-associated side effects of PHP, Ravikumar et al. carried out a pilot study in patients with advanced primary or metastatic liver cancers [47]. Patients were treated with percutaneous hepatic perfusion of either doxorubicin or 5-FU. In the dose escalation study, the dose-limiting toxicity was determined to be leucopenia in patients who received the highest dosage of doxorubicin or 5-FU. One of the benefits of PHP is that the procedure only requires an overnight hospital stay, and patients recovered quickly after the perfusion. A significant tumor response (> 95% reduction of tumor size) was observed in 9.5% of the patients. Because the size of the patient population was small
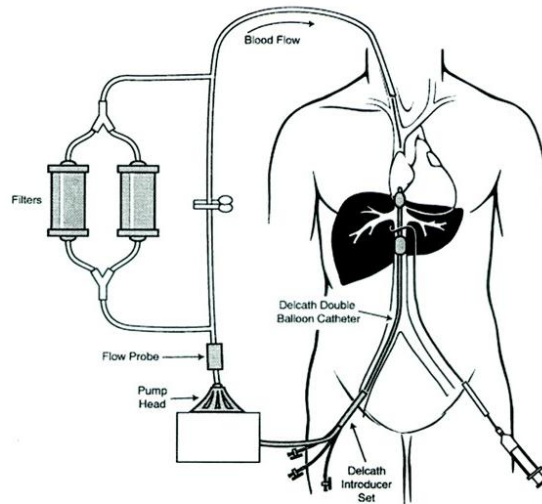
Figure 4. Schematic representation of percutaneous hepatic perfusion. Reused with permission from [48].

(23 patients), further randomized trials will have to be conducted to evaluate the efficacy and safety of PHO compared to IHP.

2.5 Transarterial chemoembolization (TACE)

TACE is a localized chemotherapy strategy used for the treatment of unresectable primary or metastatic liver carcinomas. It was developed by French surgeons Doyon and coworkers in 1974 [49]. Similar to PHP, TACE is another non-surgical approach to deliver anti-cancer agents to the liver via catheters that are inserted into the femoral veins. Unlike PHP, a TACE procedure does not require the double-balloon catheters. In a TACE procedure, drug-encapsulated degradable starch microspheres, liposomes, or other drug particle matrix are administered to the liver, to deliver the anti-cancer drug in a sustained release pattern (Figure 5). In the meanwhile, these particulates embolize the branches of the hepatic artery; thus, tumor deposits are deprived of nutrients and oxygen. Similar to the other locoregional therapies, TACE is confined to the tumor-bearing liver; hence, the systemic toxicities of the anti-cancer drug may be greatly reduced.

A nationwide clinical trial of TACE was undertaken in Japan to elucidate the impact of TACE on the survival of patients with unresectable hepatocellular carcinoma, which is the most common type of liver malignancy [50]. A total of 8510 patients were enrolled in the study, who received an emulsion of lipiodol, a contrast agent for *in vivo* imaging, and chemotherapeutic agents, such as cisplatin and doxorubicin, preceding the administration of gelatin sponge particles. Gelatin sponge particles were resorbable materials first introduced to the clinic in the mid 1960s in interventional radiology. The optimal size of gelatin sponge particle is believed to
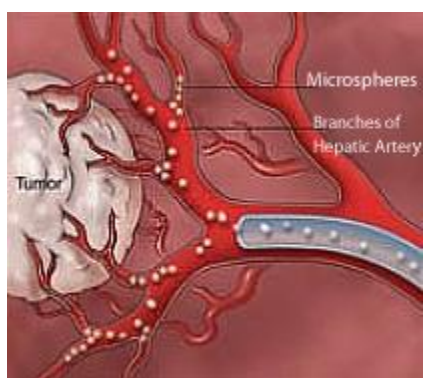
Figure 5. Drug releasing microspheres. Figure originally published on the internet. See reference [51].

be 500-1000 microns. After administration, they induce the formation of thrombus, causing occluding of the small end-arteries. In this trial, the median survival, 1-year, and 3-year survival rates were determined to be 34 months, 82%, and 47%, respectively. The mortality rate of treatment-related complications was determined to be 0.5%. Their results suggested that TACE may be a safe and feasible treatment modality, laying the foundation for further development to improve treatment effectiveness. However, the superiority of TACE over conventional intravenous chemotherapy remains controversial due to the mixed clinical results of its efficacy in treating liver cancers [52-54].

Although TACE is an independent procedure, it can be performed in combination with other procedures, such as a percutaneous ethanol injection (PEI), to improve the treatment efficacy and overall survival. Allgaier et al. conducted a trial of TACE and PEI combination therapy, and they compared it with TACE or PEI alone in patients with inoperable hepatocellular carcinoma [55]. The TACE and PEI combination cohort had a median survival of 25 months; whereas, TACE and PEI monotherapy cohorts had median survival times of 8 and 18 months, respectively. Although TACE-involved treatment modalities have shown some advantages over standard intravenous chemotherapy, the rate of procedure-related morbidity and mortality remain major issues. A clinical trial conducted by Poon et al. revealed overall treatment morbidities and mortalities of 23% and 4.3%, respectively, for patients with inoperable hepatocellular carcinoma [56]. The mortality rate was as high as 20% for patients with tumors greater than 10 cm at the time of the procedure or serum albumin concentrations lower than or equal to 35 g/L before the surgery. Therefore, careful evaluation of prognostic factors and patient selection are key factors in the design of successful TACE protocols.

In 2002, Camma et al. conducted a computerized meta-analysis of randomized controlled trials of TACE conducted between 1980 and 2000 for unresectable hepatocellular carcinomas, to evaluate whether the previously reported superiority of TACE is significant relative to other conservative modalities [57]. The survival data from the trials involving three intrahepatic procedures: TACE, TAC (transarterial chemotherapy), and TAE (transarterial embolization), were compared to the conventional intravenous chemotherapies. TAC and TAE are modified TACE procedures. In TAC chemotherapeutic agents are administered without embolizing particles, and in TAE particle-based artery-blocking embolizing materials are given without chemotherapeutic agents. The authors reported that TACE significantly prolonged the 2-year survival rate compared to standard intravenous chemotherapy for patients with unresectable hepatocellular carcinoma. However, TACE did not demonstrate significant benefits, in terms of efficacy, relative to TAE. Their findings were consistent with the controversial role of chemotherapeutic agents in TACE, considering the additional side effects that were caused by an anti-cancer drug. The data involved in the meta-analysis was generated from the trials of TACE using 5-FU as the anti-cancer drug. Further analysis using data from trials involving other chemotherapeutic agents may be informative in elucidating the impact of TACE over other therapy modalities.

2.6 Lymphatic chemotherapy

2.6.1 Overview of lymphatic drug delivery

The lymphatic system is a part of our immune system. The immune system is responsible for collecting and removing interstitial fluid from tissues; transporting fatty acids and vitamins to

the circulatory system; and carrying antigen-presenting cells to the lymph nodes via the lymph fluid, when an immune response is simulated by an invading microorganism. The lymphatic system is a unidirectional network that is comprised of lymph, lymph capillaries that carry the lymph, and connecting lymph nodes. The lymph fluid originates from the interstitial fluid, travels through the lymph vessels, and is filtered by the lymph nodes, before it ultimately returns to the circulatory system via the right or the left subclavian veins. Unlike the circulatory system, lymphatic system is unidirectional, and is regulated by a valve mechanism (Figure 6). The one-way valves are located in both afferent and efferent lymph vessels, and they move the lymph from one segment to another segment due to segmental contractions. Additionally, lymph flows slowly, because the lymphatic system lacks a "pump", such as the heart, to force the fluids to circulate. Similar to blood capillaries, lymph capillaries branch into every part of our body except for the brain; therefore, tumor cells may use the lymphatic system in their initial non-hematological spread.

When a primary tumor mass develops, it secretes lymphangiogenic cytokines that induce the formation of new lymph vessels [58]. The tumor cells invade the new lymph vessels and follow the lymph until entering the nearest draining lymph node, the sentinel lymph node, via the subcapsular sinus. The sentinel lymph node can trap the cancer cells, but if it does not successfully destroy the cancer cells, it may become the site of a secondary tumor and pass the tumor cells to the next draining lymph node. Ultimately, tumor cells may travel to the circulatory system and deposit in healthy organs resulting in the formation of distant metastases (Figure 7) [59]. Because lymphatic system plays a critical role in cancer metastasis, it has been recognized as a target for localized approaches to treat cancers that spread via the lymphatics, such as breast cancer, lung cancer, ovarian cancer, and head and neck cancer.
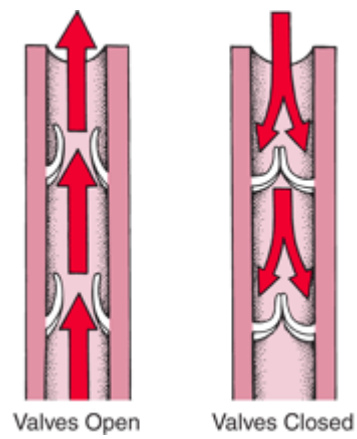
Figure 6. Open and closed valves. Figure originally published on the internet. See reference [60].
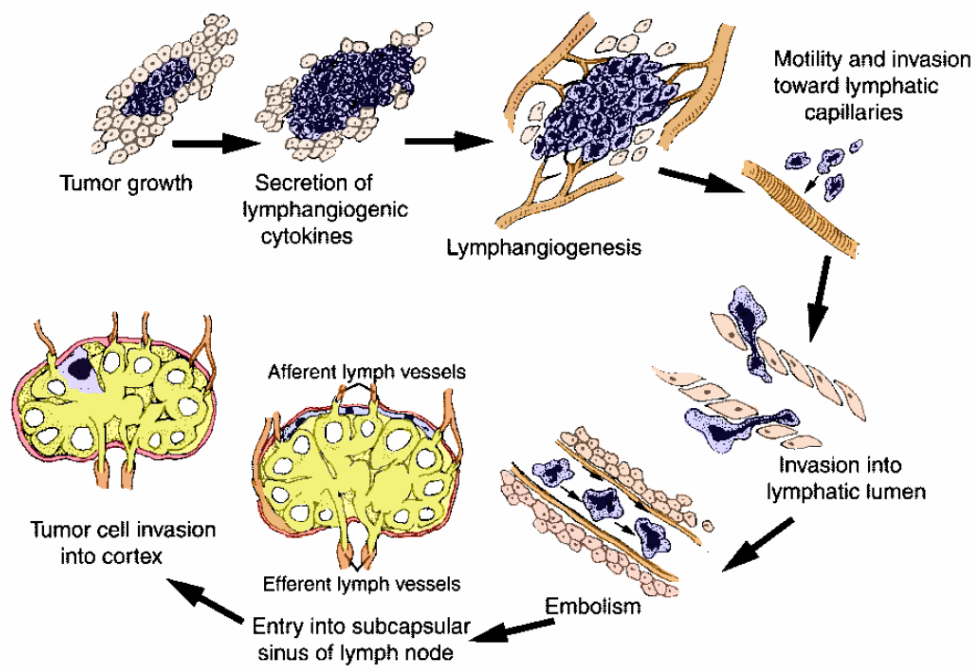
Figure 7. Cancer spread from primary tumor to draining lymph nodes. Figure originally published in [59]. Reused with permission.

The subcutaneous tissues contain a rich supply of lymph vessels, so they have become the most widely route used for delivering lymphatic-targeted chemotherapeutic agents in preclinical trials. The fate of subcutaneously injected materials depends on a variety of factors, including the size, charge, and immunogenicity. The optimal size range for lymphatic drainage is believed to be 10 to 100 nm. Molecules smaller than 10 nm mainly enter the systemic circulation through blood capillaries via diffusion; whereas, molecules larger than 100 nm have substantial local retention at the injection site. Therefore, molecules of 10 to 100 nm may be good candidates for subcutaneous injections for lymphatic drug delivery. Further, neutral or anionic materials were shown to demonstrate better lymphatic uptake compared to cationic materials [61]. This is likely due to the enhanced macrophage uptake and the subsequent lymphatic drainage of the neutrally or negatively charged particles. The interior wall of the lymphatic lumen bears negative charges; thus, the charge repulsion between the wall of the lymph vessel and the surface of the subcutaneously injected materials causes them to move faster towards the draining lymph nodes. Because most of the first-line cytotoxic drugs are small molecules, carriers that can deliver small-molecule drug cargo to target the lymphatics are of great interest to drug delivery scientists. The candidates in this category include a variety of biodegradable polymers [62-64], liposomes [65-67], micelles [68-69], and nanoparticles [61, 70] (reviewed in section 2.6.2 "Lymphatic drug delivery using engineered liposomes and solid lipid nanoparticles"). Anionic particles move faster in the interstitium because the internal wall of lymphatic lumen is slightly negatively charged. Charge repulsion makes it move faster. Charge may trigger macrophage uptake and drainage

Subcutaneous administration of these drug-loaded nanoformulations usually leads to enhanced accumulation and retention of the drug in the draining lymph nodes, in preclinical

animal models. These conjugates also take advantage of their controlled drug release properties to alter the pharmacokinetics of the anti-cancer drugs, by reducing the peak plasma concentration, as well as prolonging the systemic retention. The modified pharmacokinetics may further translate into an improved safety profile, by reducing the C_{max}-associated systemic side effects of the drug. In addition, a number of xenograft models suggest that subcutaneously injected carrier-based drug conjugates resulted in better treatment efficacy and survival compared to the conventional intravenous chemotherapy.

To demonstrate the previous statements in detail, the development, characterization and evaluation of such polymer-based drug conjugates will be presented in chapters two through five of this dissertation.

2.6.2 Lymphatic drug delivery and imaging using engineered liposomes

A wide spectrum of cancers, including breast, lung, and head and neck squamous cell cancers, metastasize through lymphatics to enter systemic circulation and develop secondary tumors. The lymphatics and sentinel lymph node, the first tumor draining lymph node, play a significant role in early stage diagnostics and subsequent therapies. Lymphatic delivery of drug encapsulated liposomal formulations has been investigated extensively in the past decade. A liposome is a vesicle containing lipid bilayer, composed of unimers which usually have a hydrophilic head and a hydrophobic tail and oriented so that the hydrophobic headgroups are inside the bilayer. Hydrophilic, lipid-insoluble drugs, or DNA can be encapsulated in the aqueous core within the liposome to improve their stability or bioavailability, compared to the free drugs or DNA. Current research on the lymphatic retention and imaging of subcutaneously,

intestinally, and pulmonary administration of engineered liposomes is discussed in this section. The primary improvements over conventional therapy are summarized in Table 1.

Traditional liposomal formulations utilize the encapsulation of anti-cancer drugs into liposomes for intravenous infusion for the treatment of various types of cancers. Doxil, a pegylated liposomal doxorubicin chemotherapy formulation, is widely used as first-line therapy of AIDS-related Kaposi's sarcoma, breast cancer, ovarian cancer, and other solid tumors [71-75]. The primary advantages of systemic liposomal chemotherapy encompass reduced side effects compared to the standard therapy, and prevention of the anti-cancer drug from enzymatic digestion in the systemic circulation. Another characteristic of pegylated liposomes is that their size can be adjusted through the modification of the PEG chains or lipid bilayer core of the carrier, promoting its potential use as a drug delivery vehicle to the lymphatics after subcutaneous injection [76].

In 2007, Moghimi et al. proposed that subcutaneously injected pentameric IgM may facilitate the lymphatic drainage and enhance lymphatic retention of IgG1-PEG-liposome conjugates; presumably attributed to the binding between IgM and macrophage Fc receptors in the draining lymph node sinuses, promoting the effective trapping of the therapeutic peptide or protein bound immune-PEG-liposomes [77]. In their previous study, they reported that pegylated immune-liposomes had more rapid lymphatic drainage from the injection site to the surrounding lymphatics due to the hydrophilic nature of the PEG moieties [78]. In their later study, they proved that concomitant administration of monoclonal IgM against rat IgG1 adjacent to the injection site of IgG1-PEG-liposomes could further enhance the lymphatic retention of the liposomal conjugates. It may be ascribed to the formation of IgM antibody-mediated vesicular aggregates in the lymphatic vessels. Harrington et al. reported improved delivery of anticancer drugs to tumors using pegylated liposomes as vehicles for intratumoral and subcutaneous

Route of administration	Improvement over standard therapy	References
Subcutaneous	Enhanced lymphatic retention	[76-79]
Intestinal	Increased bioavailability and stability	[80-81]
Pulmonary	Improved lymphatic penetration	[82-83]

Table 1. Summary of primary improvements of engineered liposomes over conventional therapy in vivo.

injection [76]. The authors compared the pharmacokinetics and tissue distribution, of subcutaneously or intratumorally injected pegylated liposome-encapsulated ^{111}In-labeled diethylenetriaminepentaacetic acid (IDLPL) with the unencapsulated IDLPL. The encapsulated form increased the carrier residence time and concentration in the head and neck tumors and their nodal metastases (both inguinal and axillary lymph nodes) in a nude mouse xerograph model, yielding a 11.6-fold increase in the area-under-the-curve (AUC) (96 hours).

A major issue of conventional liposomal formulations is that liposomes are poorly retained in the draining lymph nodes following injection (<2% injected dose). In order to enhance the retention of liposomes to lymph nodes, Phillips et al. developed an avidin activated biotin-coated liposome, resulting in prolonged lymphatic retention and extended lymph node localization, in an experimental rabbit model [79]. Biotin-coated liposomes were injected subcutaneously into both hind feet of rabbits, followed by an adjacent subcutaneous injection of avidin, causing the formation of liposomal aggregates in the lymphatic vessels. Twenty-four hours post injection, the retention of the liposomes was increased by 7.1 and 6.7-fold in the popliteal nodes and iliac nodes, respectively.

Intravenous liposomal doxorubicin (i.e. Doxil) has substantially improved pharmacokinetics compared to doxorubicin via the intravenous route, including improved AUC and half life. Ling et al. compared subcutaneous administration of liposomal doxorubicin with the standard intravenous doxorubicin treatment in a rabbit breast cancer model [84]. Female New Zealand rabbits were inoculated with VX2 carcinomas and treated three times with 1-mg/kg (doxorubicin equivalent) of subcutaneous liposomal doxorubicin, intravenous adriamycin, or saline, once the axillary lymph nodes reached 5 mm in diameter. Two days after the completion of the treatment, the nodal volume was measured and compared between different treatment groups. Data revealed that the liposomal doxorubicin treatment and intravenous doxorubicin

decreased the nodal volume by 57% and 27%, respectively, and increased the number of apoptotic cells by 3.2- and 2.0-fold, respectively, compared to the saline control. The subcutaneous administration of doxorubicin demonstrated a more robust inhibitory effect in relative to systemic doxorubicin, with a p value equals to 0.002 between the two treatment groups. Site inflammation including allergy and skin ulceration was not observed, likely due to the low dose of the drug administered, as well as the relatively short treatment period. In summary, the liposomal doxorubicin treatment exhibited effective inhibition of tumor progression and induction of apoptosis of metastatic cells, which may be a promising method for the treatment of node-positive advanced breast cancer.

The lymphatic administration route can also improve access to the systemic space and improve plasma pharmacokinetics compared to intravenous formuations. Trubetskoy et al. showed that subcutaneously injected liposome-encapsulated drugs can be absorbed into systemic circulation in response to manual massage of the injection site [85]. A five minute manual massage could induce release of up to 40% of the subcutaneously injected 200-nm ^{111}In-angiotensin II incorporated PEG-liposomes (made with egg phosphatidyl choline). In addition, when compared to the unmodified liposomes, the PEG-shielded liposomes had increased blood localization due to the reduced uptake by the lymph node macrophages. During the observation period of 45 minutes, the blood concentrations of the radioisotope-labeled, and drug-incorporated PEGylated liposomes remained constant, whereas the concentration of the plain liposomes decreased shortly post massage. The authors also suggested that the drug release pattern and the pharmacokinetic profile of the formulation could be modulated though the modification of the liposomal surface structure.

Oral delivery of therapeutics is the most convenient and widely employed route of drug delivery. However, a number of drugs exhibit poor oral bioavailability due to the degradation of

the active drugs in the gastrointestinal tract. The pH of stomach fluid may go as low as 1.0 in the fasted state and increase to 3.0 to 4.0 in the fed state. The extremely acidic environment facilitates the degradation of orally administered drugs. In the 1970s, liposomal formulations were developed as oral drug delivery carriers, shielding the labile drugs from the acidic environment via reduced rate of degradation and increased extent of uptake. Orally administered drug-incorporated liposomes enter the systemic circulation via the portal vein and intestinal lymphatics. Drugs entering the portal vein pass through the liver and undergo first-pass metabolism. However, drugs entering the intestinal lymphatic through the intestinal lumen first migrate to the lymphatic vessels and draining lymph nodes before entering systemic circulation; therefore, avoiding the liver and first-pass metabolism. Lymphatic uptake of therapeutics via the intestinal route plays a role in the increased bioavailability of a number of drugs [86].

Intestinal absorbability and stability are the primary formulation concerns when delivering drug-encapsulated liposomal formulations orally. In the 1980s, Hashida et al. studied the *in vivo* absorption characteristics of liposome-encapsulated carboxyfluorescein as a model liposomal drug and compared the plasma and lymph concentration profiles of the released carboxyfluorescein to that of the free dye [80]. There were no statistically significant differences in both the plasma and lymph between the two formulations, suggesting drug-encapsulated liposomes exhibited poor absorption across the intestinal mucosa. However, co-administration of lipid-surfactant mixed micelles greatly enhanced the permeability of the drug-trapped liposomes. This inductive effect was likely due to the interaction between the lipid-surfactant micelle and the lipid bilayer of the intestinal cell membrane.

A number of hydrophilic drugs exert poor lymphatic transport due to their low intestinal bioavailability, limiting their use in the clinic. In 2006, Ling et al. evaluated a liposome system for oral delivery of a poorly bioavailable hydrophilic drug, cefotaxime, in a rat model by

comparing three forms of the drug: liposomal formulation, aqueous free drug, and a physical mixture of the drug and liposomes [86]. The data revealed that the liposomal formulation of the drug exhibited a 2.7-fold increase in its oral bioavailability compared to the aqueous dosage, and a 2.3-fold increase for the physical mixture. In addition, they also reported that the liposomal formulation lead to a significant enhancement of the lymphatic localization of the drug relative to the other two formulations. Therefore, liposome systems may be useful carriers for poorly bioavailable hydrophilic drugs, promoting their lymphatic transport in the intestinal lymph as well as their systemic bioavailability.

Oral delivery of DNA vaccination remains a challenge due to the unsatisfactory stability of DNA vaccines and the need to induce an immunological response after immunization. Perrie et al. reported a novel liposome-mediated DNA vaccination using a dehydration-rehydration method, encapsulating plasmid DNA encoded for an enhanced green fluorescent protein into the liposomes [81]. Stability studies in a simulated intestinal media suggested the dehydration-rehydration vesicles incorporating the DNA (DRV-DNA) had a greater intestinal stability compared to the small unilamellar vesicles (SUV-DNA). In addition, the DRV-DNA, when administered orally in a mouse model, invoked a greater and longer IgA response compared to the naked DNA, suggesting a prolonged DNA retention and improved DNA protection of the DRV-DNA formulation.

The respiratory system consists of an upper respiratory tract, including the nose, nasal cavity, and pharynx; and a lower respiratory tract, including the lungs and trachea. The lungs are rich in lymphatic vessels, and a series of lymph nodes encompassing the hilar, mediastinal, carinal, and aortic nodes. Therefore, the lymphatics and lymph nodes can be readily accessed by pulmonary delivered aerosolized formulations [87].

Chemotherapy delivered by the pulmonary route could concentrate anticancer drugs in the lungs and draining lymph, while avoiding significant issues associated with systemic chemotherapy including serious non-target toxicities, poor drug penetration into the lymphatic vessels and surrounding lymph nodes, and first pass clearance in the case of orals. Latimer et al. investigated the feasibility of delivering liposomal formulation of paclitaxel and a vitamin E analog (α-TEA) in an aerosol for treatment of murine mammary tumors and metastases [82]. The pulmonary delivery of sequential combination treatments significantly decreased the mammary tumor burden compared to controls as well as the individually administered liposomal drugs. In addition, the aerosolized combination regimen reduced the total number of cells staining positive for cell markers CD31 and Ki67, suggesting an improved inhibition of lymphatic and pulmonary metastases. In a similar study, Lawson et al. compared the anti-proliferative efficacy of a dilauroylphosphatidylcholine liposome delivered 9-nitro-camptothecin (9-NC), α-TEA, and a combination therapy of 9-NC and α-TEA in a metastatic murine mammary tumor model. Each individual treatment and the combination treatment was encapsulated in liposomes and delivered via an aerosol to treat lung and the surrounding lymph node metastases. The Ki-67 immunostaining results revealed that there were less proliferative cells present in the animals treated with the combination therapy compared to the animals treated with 9-NC alone. However, there were no statistically significant differences between the 9-NC + α-TEA group and α-TEA group alone. All three treatments (9-NC alone, α-TEA alone, and 9-NC + α-TEA) showed elevated number of apoptotic cells by TUNNEL assay, when compared to the empty liposome control group. In addition, the in vivo anti-cancer efficacy studies demonstrated the combination treatment greatly hindered the tumor progression compared to each treatment alone, leading to the prolonged survival rate. [88].

Another application of pulmonary delivered liposomal formulations is to visualize deep lung lymphatic drainage after incorporating radioactive markers such as ^{99m}Tc into liposomes. Botelho et al. administered an aerosolized formulation of nanoradioliposomes to wild boars, and successfully visualized their deep lymphatic lung network and surrounding lymph nodes (Figure 8) [83]. The technique provided new information into the complex structure of the lymphatic network, which was not available through the use of conventional CT. In addition, it has become a new and non-invasive molecular imaging technique for the diagnosis of early dissemination of lung cancers.

Twenty-one therapeutic monoclonal antibodies have been approved by the FDA for immunological and oncological targeting since 1994, most of which belong to the IgG1 family. Lymphatic delivery of liposomal antibody formulations offers advantages over other routes due to the enhanced cellular uptake of the antibodies and the prolonged localization of the liposomal conjugates, resulting in improved efficacy. In 2004, Cui et al. developed a mannan-coated liposome protamine-DNA (LPD) nanoparticle formulation based on their previous studies of LPD nanoparticles [89]. The *in vitro* uptake of the mannan-coated LPD by antigen-presenting cells, DC2.4, was evaluated and compared to non-coated LDP. The data revealed that the mannan coating significantly enhanced cellular uptake of the nanoparticles by targeting the antigen-presenting cells; therefore, it may be a potential carrier for the delivery of biopharmaceuticals. In a separate experiment, they investigated the *in vivo* immunity of mannan-coated LPD against HPV-positive TC-1 lung cancer in C57BL/6 mice, by incorporating the major histocompatibility complex class-I (MHC class-I) restricted peptide antigen from HPV 16 E7 protein. It was reported that both preventive and therapeutic efficacy of the LPD/E7 formulation was greatly enhanced due to the mannan coating.
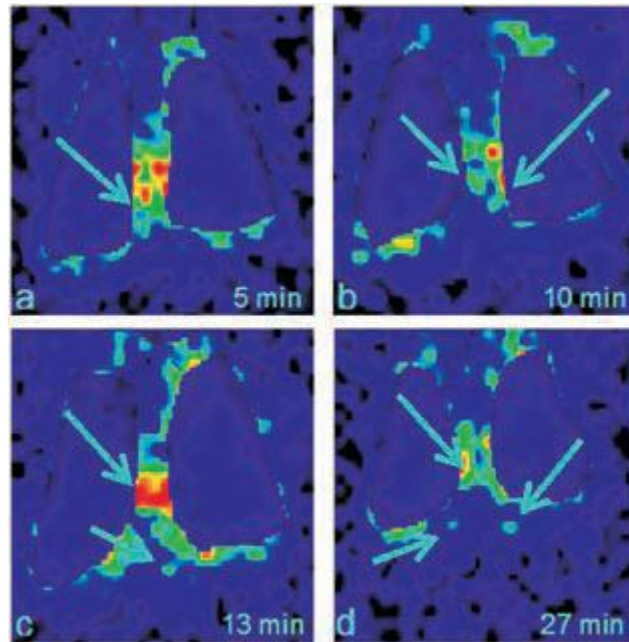
Figure 8. Thoracic images in posterior view obtained after ^{99}mTc-Liposome aerosol inhalation, in the pig nº 18. a) 5 min after the inhalation – visualization of hilar draining chains; b) 10 min after the inhalation – individualization of hilar draining chains; c) 13 min after the inhalation – transdiaphragmatic drainage; d) 30 min after the inhalation – initial visualization of the aortic chain ganglia.Figure originally published in [83]. Reused with permission.

HIV is life-threatening disease worldwide. Approximately forty-two million people live with HIV worldwide, half of which are in African countries. HIV infection in humans causes immune system failure, resulting in millions of deaths due to pathogen infections. Therefore, anti-HIV treatment regimens are in great need worldwide. Desormeaux et al. described a method for the synthesis of PEG stabilized immunoliposomes conjugated to anti-HLA-DR antibodies, that effectively delivered indinavir to the lymphoid tissues of female C3H mice for the treatment of HIV-1 [90]. The subcutaneous administration of anti-HLA-DR immunoliposomes demonstrated a 2.9-fold greater accumulation in the cervical lymph nodes of C3H mice compared to the standard liposome formulation. In addition, the PEG stabilized immunoliposomes delivered high concentration of indinavir to the lymphoid tissues for at least 15 days post-injection. A single subcutaneous dose (2 μmol lipids/g tissue) of the sterically stabilized immunoliposomes demonstrated a 0.9 to 1.9-fold greater AUC in the cervical, brachial, mesenteric, inguinal, and popliteal lymph nodes of C3H mice compared to the conventional immunoliposomal formulation. The encapsulation of anti-viral drugs into sterically stabilized immunoliposomes introduced a novel drug delivery approach for the treatment of life-threatening HIV-1 disease by greatly increasing the drug concentration in the diseased lymph nodes. In 2000, Bestman-Smith et al. optimized the anti-HIV liposomal formulations for accumulation in lymphoid organs by targeting the primary HLA-DR expressing cellular reservoirs of HIV-1. The liposomal formulations of interest were made from a combination of dipalmitoylphosphatidylcholine, dipalmitoylphosphatidylglycerol, distearoylphosphatidylethanol amine-N-[poly(ethyleneglycol)-2000], and dipalmitoylphosphatidylethanolamine-N-(4-(p-maleimidophenyl)butyryl). They compared four types of liposomal formulations, including: conventional liposomes, sterically stabilized liposomes, conventional immunoliposomes bearing anti-HLA-DR, and sterically stabilized immunoliposomes bearing anti-HLA-DR Fab' fragments

at the end termini of PEG chains [91]. Greater accumulation of liposomes were observed for the PEGylated immunoliposomes compared to the other three treatments in most of the evaluated lymph nodes and the spleen in female C3H mouse model; introducing a novel approach to concentrate drugs in HIV-1 reservoirs and improve their efficacy.

Another potential clinical application of liposomal formulations is cancer vaccination. Although cancer diagnostic and therapeutic technologies have been greatly improved in the past two decades, there is still a critical need for cancer prevention medications, such as effective and safe cancer vaccinations. In 2001, Mui et al. reported their study of a liposomal nanoparticle-encapsulated oligodeoxynucleotides (ODN)-cytosine-guanine (CpG) formulation (LN-ODN-CpG); which demonstrated enhanced stimulatory activity of LN-ODN-CpG against the immune response, by triggering the Toll-like receptor 9 in an ICR mouse model. The lipid particle carriers were synthesized using distearoylphosphatidylcholine /cholesterol/ dioleoyl-3-*N*, *N*-dimethylammoniumpropane/1-*O*-(2'-(ω-methoxypolyethyleneglycol)succinoyl-2-*N*-myristoyl sphingosine with a molar ratio of 20:45:25:10 [92]. In a following study from their group in 2007, they explored the feasibility of using subcutaneously injected LN-ODN-CpG formulation as a cancer vaccine adjuvant along with co-administration of tumor-associated antigens to induce antigen specific adaptive immune response in murine cancer models of thymoma and melanoma. They also compared the lymphatic uptake of fluorescently labeled free and liposome-encapsulated ODN-CpG conjugates. Post subcutaneous injection of either free ODN-CpG or LN-ODN-CpG (5 mg/kg on an ODN-CpG basis), mice were sacrificed and their draining lymph nodes were excised at pre-determined time intervals. The results revealed that the LN-ODN-CpG treatment demonstrated a two to nine-fold increase in lymph node uptake of the ODN-CpG compared to the free ODN-CpG, suggesting the possibility of using the liposomal nanoparticles as a cancer vaccination for lymphatically metastatic cancers [93].

A similar study was conducted by Kojima et al in 2008 using an ovalbumin (OVA) -encapsulated oligomannose-coated liposomal (OML) vaccination against OVA-expressing E.G7-OVA tumor in a C57BL/6 mouse model. All of the mice previously immunized with the OVA-OMLs developed effective anti-cancer immunity and completely rejected the tumor. In addition, a single subcutaneous injection of the OVA-OML treatment led to significantly reduced tumor progression in tumor-bearing mice [94].

There has been a series of clinical trials to evaluate the efficacy and safety of liposomal cancer vaccinations [95-96]. A phase IIB trial of the L-BLP25 liposome vaccine was conducted in patients with stage IIIB and IV non-small cell lung cancer. The L-BLP25 liposome vaccine is a liposome-based peptide vaccine derived from the mucin 1 antigen. In the trial, patients were randomly divided into two groups: the L-BLP25 group, in which patients were treated with weekly immunizations of the liposomal vaccine following a single intravenous dose of cyclophosphamide; or the control group, in which patients were treated with cyclophosphamide alone. Although the results demonstrated a 4.4-month increase in survival for the patients that were treated with the vaccination, the difference was not statistically significant [95]. Nevertheless, no vaccine-related toxicities were observed in the patients in the L-BLP25 treatment group.

Lymphatic system is a complex network, consisting of lymph vessels and lymph nodes, which are connected by the lymph vessels. Imaging of the lymphatics plays a role in disease discovery and diagnosis. In addition to the conventional computed tomography (CT) technique, newer tools such as scintigraphy and lymphography have also been widely utilized in the past two decades. Scintigraphy, a valuable tool to capture two-dimensional images of a body radiation source after intravenous injection of a readily cleared radioactive chemical into the patient, has been used extensively in the past decade for the development and evaluation of

gamma-emitting radionuclide labeled liposomal formulations. Pillips et al. reported a series of applications of scintigraphic imaging using technetium-99m (^{99m}Tc) labeled liposomes [97], including examination of bone fracture healing, detection of viral infection, and intraarticular and intralymphatic delivery of liposomal formulations. In addition, Phillips et al. also compared a series of ^{99m}Tc labeled liposomes, including: ^{99m}Tc sulfur colloid, filtered ^{99m}Tc sulfur colloid, filtered ^{99m}Tc sulfur colloid with reduced heating time, and ^{99m}Tc human serum albumin, in rabbits for optimal detection of the sentinel lymph nodes (Figure 9) [98]. Similar radioactive imaging techniques may be used for the evaluation and optimization of new radioactive liposomes for improved sentinel lymph node diagnostics.

Lymphoscintigraphy is a relatively new technology, which is only been widely used clinically since the 1990s. It is a type of nuclear medicine imaging, generating two-dimensional scintigrams of the lymphatic system including lymph nodes and vessels. A radioactive substance is administered as an intravenous injection, oral, or pulmonary dosage. The radioactive material is taken up by the draining lymph nodes after passing through lymph ducts; in the meantime, it generates gamma rays that can be detected by a gamma camera or positron emission tomography scanner. It is commonly used as a tool to identify sentinel lymph nodes [99] and diagnose disease conditions such as lymphoma [100] and lymphedema [101-102]. In 2002, Plut et al. developed a formulation kit by chemically combining a pyrogen-free low molecular weight isosulfan blue dye solution and ^{99m}Tc labeled liposomes, producing a radioactive blue liposomal formulation for pre-surgical injections clinically [103]. This formulation avoids the non-synchronized distribution and clearance kinetics of the small molecular weight dye and the radioactive liposomes when they are administered separately. In the clinic, patients usually receive an injection of a colored dye solution before operation, providing visualization of the lymphatic network, followed by another injection of a radioactive formulation. The radiotracer can be
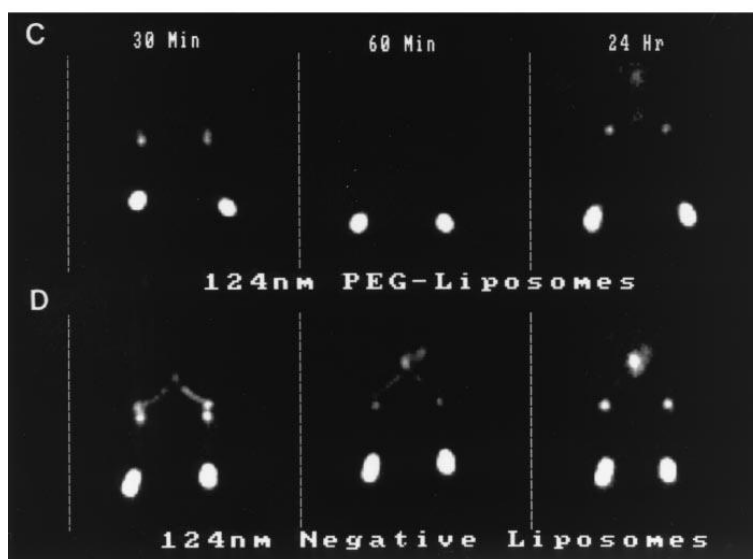
Figure 9. Gamma camera images of the lower portion of rabbits following subcutaneous injection (0.3 ml) of various [99mTc] liposomes in each hind foot at either 30 minutes, 60 minutes or 24 hours post injection. The images show the injection site in the hind feet, the popliteal node region and iliac node region. (C) 124 nm PEG-liposomes (both feet); (D) 124 nm Negative-liposomes (both feet). Figure originally published in reference [98]. Reused with permission.

detected using lymphoscintigraphy, leading to the identification of draining lymph nodes, including the sentinel lymph node. However, the two injections do not occur simultaneously, thus causing the differing distribution and clearance kinetics of the two substances. In order to overcome this issue and simplify the pre-surgical injection procedure, the kit was developed by combining the isosulfan blue dye with the ^{99m}Tc labeled liposomes.

Magnetic resonance imaging (MRI) could become another useful tool for imaging the lymphatic system. MRI has the potential to overcome the poor resolution of ^{99m}Tc, but lymphcentric contrast agents are required to provide clinically useful imaging of the lymphatic system. Fujimoto et al. developed gadolinium-diethylenetriamine pentaacetic acid (Gd-DTPA) labeled liposomes using long-circulating palmityl-D-glucuronide liposomes. After a subcutaneous injection of the liposomal formulation into the hind feet of rabbits, the popliteal lymph nodes as well as the deep retroperitoneal lymph node were detected. The enhanced lymphatic liposomal accumulation was likely due to the trapping of liposomes by the macrophages [104-106].

Rapid clearance post injection is the major drawback of liposomal formulations; therefore, a liposomal drug delivery system with prolonged retention is of high interest to physicians. Avidin/biotin-liposome systems overcome this limitation by forming avidin biotin-liposome aggregates after subsequent injections into the primary intraperitoneal of biotin coated liposomes followed by avidin [107-108]; thus, retaining the liposomes in the diseased tissues and the draining lymph nodes. Zavaleta et al. compared three avidin/biotin-liposome systems with different dosing sequences of avidin and biotin-liposomes in a rodent ovarian cancer xenograft model [107]. Lymphatic uptake of the liposomes was significantly enhanced in the rats treated with the subcutaneous injection of biotin-liposomes 2 hours post avidin injection. A similar study was conducted using a slightly modified avdin/^{99m}Tc-blue-biotin-liposome

system by Medina et al. to target the mediastinal node, and to determine the most effective injection site and tissue biodistribution of ^{99m}Tc-labeled liposomal formulations in rats [109]. The pharmacokinetics and movement pattern of the avdin/^{99m}Tc-blue-biotin-liposome formulation post intraperitoneal injected was evaluated using scintigraphic imaging. Their results suggested that lymph node targeting effect was independent of the cavity in which the formulation was inected, however, was closely related to the dosage administered.

2.6.3 Lymphatic drug delivery and imaging using solid lipid nanoparticles

Solid lipid nanoparticles (SLN) are a class of particulate drug carriers [110] made from lipids that remain in the solid state at room and body temperatures. Lipids utilized for SLN are typically physiological lipids, including: fatty acids, steroids, waxes, mono-, di-, or triglyceride mixtures. A wide variety of biocompatible surfactants are used to stabilize SLN; therefore, SLN have the advantage of physical stability with low toxicity. SLN are becoming increasingly used for the protection of labile drugs from degradation in the body and for controlled sustained release [111].

The application of SLN formulations for anticancer drug delivery has overcome many obstacles commonly seen in conventional cancer chemotherapy, such as limited specificity, high toxicity and tendency of drug resistance [112]. Various anticancer drugs, including: etoposide [113], methotrexate [114], and idarubicin [115] have been incorporated into SLN by different research groups and evaluated. Conventional administration routes (e.g. intravenous route) have shown relatively low tumor uptake [113], due to the hindrance of drug-loaded SLN to access the solid tumor [116], and reduced circulation time, due to the fast clearance by mononuclear phagocyte system, which in turn decrease the specific targeting effect. For this reason, various

alternative application routes, such as duodenal [115, 117-119], subcutaneous [113] and pulmonary [120] routes have been studied.

Drugs with poor oral bioavailability due to low solubility in GI tract or pre-systemic hepatic metabolism (first-pass effect) can be incorporated into SLN; allowing transported into systemic circulation via the intestinal lymphatics and bypassing first-pass metabolism, enhancing the drug bioavailability. A series of studies related to the absorption and distribution of SLN after duodenal administration has been carried out by Bargoni, Cavalli, and their colleagues [115, 117-119]. In one of the above studies [117], ^{131}I-17-iodoheptadecanoic acid labeled drug-free SLN were administered into the duodenal lumen of fed rats. Transmission electron microscopy and photon correlation spectroscopy analysis of the lymph and blood samples indicated that SLN were taken up and transported predominantly by the lymphatics rather than by systemic circulation, confirming the transmucosal transport of SLN. However, the author suggested that the significant difference in the SLN uptake between the lymphatic system and blood was probably the result of the totally blocked passage of the SLN from the lymph to the blood, because of the designed experimental conditions for sample collection and the physiologically impaired transportation and absorption of SLN caused by surgery-related paralysis of the intestine of the animals. A later comparison study [118] of the drug release, absorption, and distribution, of tobramycin-loaded SLN (tobra-SLN), prepared from stearic acid, phosphatidylcholine, and taurocholate, in the plasma and lymph after duodenal administration, revealed that the AUC for tobra-SLN was 24-fold higher than intravenous administration of the same SLN formulation and 120-fold higher than free tobramycin solution after intravenous injection. In addition, this study suggested the potential of SLN as sustained release system, as the half-life of tobramycin increased from 57 min (tobramycin solution) to 283 min (tobra-SLN

44

intravenously administered) to 1371 min (tobra-SLN duodenally administered). The enhancement of drug absorption and bioavailability for tobra-SLN after duodenal administration was ascribed mostly to the preferred transmucosal transport of tobramycin SLN to the lymph compared to the blood. In a similar study applying idarubicin loaded SLN (IDA-SLN) conducted by the same group, the enhancement in drug bioavailability was observed also when the IDA-SLN was administered through the duodenal route when compared to the intravenous route [115].

The influence of the subcutaneous route on the tumor uptake and biodistribution of drug-loaded SLN was evaluated by Reddy et al [113]. They prepared etoposide -loaded tripalmitin (ETPL) SLN radiolabeled with ^{99m}Tc, and the ETPL nanoparticles were administered subcutaneously, intraperitoneally, and intravenously, to mice bearing Dalton's lymphoma tumors. Gamma scintigraphy and the radioactivity measurements were used to determine biodistribution and tumor uptake of the ETPL SLN in the blood and organs. The data 24 hours after subcutaneous administration indicated that the ETPL SLN exhibited a noticeably higher degree of tumor uptake (8 and 59 fold higher than that of the intraperitoneal and intravenous routes, respectively) and reduced build-up in RES organs (i.e. liver, lung and spleen) compared to the other two routes. The tumor concentration of the ETPL SLN one hour after subcutaneous injection was 23.3% of that at 24 hours post injection, showing a lower extent of initial uptake compared to intraperitoneal and intravenous routes, whose initial uptake ratios were 29.7% and 48.1%, respectively. The gradual increase in tumor uptake of the drug from the subcutaneous injection site after the low initial uptake indicated that the drug-loaded SLN could be used for sustained drug release therapy. Therefore, a proximal subcutaneous injection could be proposed as the optimal route for lymphatic chemotherapy over intraperitoneal and intravenous routes.

Small cell lung cancer represents about 15% of all lung cancer cases, and it can spread through the lymphatic system, with intrathoracic lymph node metastasis to about 70% of the limited stage patients and to nearly 80% of the extensive stage patients [121]. In the case of the other more common type of lung cancer- non small cell lung cancer, greater than 80% of stage IV patients showing extensive metastasis to the lymphatics [122]. Since lymphatic drainage takes great part in alveolar clearance of foreign materials with submicron size, targeted delivery of anticancer drug to the lymphatic from the pulmonary route could be developed.

Videira et al. [120] evaluated the bio-distribution of inhaled ^{99m}Tc-HMPAO-radiolabelled SLN (rl-SLN) with an average size of 200 nm, and compared the results with the distribution of the free tracer (^{99m}Tc-HMPAO) administered via the same route. The gamma scintigraphic images showed significant accumulation of the rl-SLN in the lungs followed by a high distribution rate into lymphatic tissues and inguinal lymph nodes, through alveolar clearance, which indicated that the rl-SLN were mainly cleared from lungs via the lymphatics. However, in the case of the free tracer, it was quickly cleared from lungs by the systemic circulation. In addition, about 24% of the ^{99m}Tc-HMPAO activities still remained in the lungs four hours after administration of the rt-SLN, demonstrating a significant degree of retention of the intact SLN. This is consistent with the proposed sustained release effect of SLN by Müller et al. [110]; who proposed that during the production of SLN, drug molecules were dispersed into the solid lipid matrix. Due to the reduced mobility of the drug moiety in the lipid crystal lattice, prolonged drug release from SLN can be achieved.

Although the uptake of SLN into the lymphatic system and the distribution within the lymphatics varies with the different administration routes, they are largely determined by the physicochemical characteristics of the SLN [123-124], including: particle size, surface charge,

and hydrophobicity of the particles. When the SLN are injected subcutaneously, the particle size becomes the major determinant of lymphatic uptake from interstitial fluid [123, 125]. Due to the structure of interstitium, with narrow aqueous channels of about 100 nm in diameter, SLN need to be sized between 10 to 100 nm to easily travel through these channels into lymph from the injection site. In comparison, particles larger than 100 nm will be retained at the injection site, and those smaller than 10 nm tend to undergo re-absorption back into the blood capillaries. Support for this size dependency on the lymphatic uptake of colloids was observed in a lymphatic uptake and distribution study by Oussoren et al [125] using liposomes. In addition to the proper particle size, negative surface charge and hydrophobicity of the SLN have been shown to facilitate the lymphatic drainage from the injection site and localization in the lymph nodes [123].

Solid lipid nanoparticles are complicated colloidal particle systems; the physicochemical characteristics of SLN are impacted by the components and the composition, along with the intermolecular interactions between the drug loaded and SLN components. In a study of methotrexate (MTX) SLN formulation for oral lymphatic delivery, Paliwal et al. [114] assessed the influence of the lipid on the characteristics of the SLN. The SLN were prepared using four different lipids (stearic acid, monostearin, tristearin and Compritol 888 ATO) by the solvent diffusion method; particle size, zeta potential, shape, drug entrapment efficiency, in vitro release profile, and pharmacokinetics characteristics, of the four MTX SLNs were compared. The MTX SLN prepared from Compritol 888 ATO, a highly lipophilic atomized mixture of mono-, di-, tri-behenates of glycerol, generated the smallest, most uniform SLN with the highest entrapment efficiency. The Compritol 888 ATO based SLN (MTX-CA) yielded a 10% higher MTX loading; the longer chain length of glyceryl behenate in the Compritol 888 ATO could enhance the

intermolecular entrapment of the MTX by interchain intercalation. In addition, the crystal lattice of SLN prepared from Compritol 888 is less perfect in comparison with those made from relatively pure lipids, thus leaving more space for the drug to be loaded. The bioavailability and intestinal lymphatic uptake of MTX SLNs were evaluated after intraduodenal administration to albino rats. While all four of the MTX formulations exhibited a significant increase in the AUC and lymphatic drug concentration compared to the free drug solution, with MTX-CA having the highest bioavailability and lymphatic absorption. The author ascribed these results to the MTX-CA having the smallest size and the solubilization characteristics of the mono-glyceryl behenate in Compritol 888 ATO. Therefore, the Compritol 888 ATO SLN formulation was proposed to be the preferred carrier for oral lymphatic delivery.   However, it is noteworthy that the Compritol 888 ATO formulation showed a relatively low negative value for the zeta potential (-12mV). A similar finding was observed in the study of ^{99m}Tc-radiolabelled SLN [120] using the same lipid. Low zeta potential is an indicator of reduced storage stability, due to the possible conversion of the SLN dispersion into a viscous gel; this transformation could be related to a change in the lipid crystals [111]. However, this phenomenon could be hindered by addition of the proper surfactant and optimizing the lipid concentration.

The emulsifier composition and concentration influence the partitioning of the drug between the oil and aqueous phases during the SLN formation, which has direct effects on the SLN quality. For this reason Sanjula et al. [126] compared the physiochemical characteristics, in vitro release, and in vivo absorption, of Carvedilol-loaded SLN with varied ratios of poloxamer 188, a water soluble nonionic emulsifier. They demonstrated that a high concentration of poloxamer 188 resulted in reduced drug entrapment efficiency and aggregation of the SLN, which in turn decreased the amount of drug that could be released from the SLN, thus lowering

the bioavailability. This observation was consistent with a study by the Paliwal et al., who used soya lecithin as an emulsifier in Methotrexate SLN [114]. In the latter study, as the amount of soya lecithin increased from 1.0% to 1.5%, the drug entrapment efficiency and the percentage release of drug decreased. A possible explanation is that when the concentration of the emulsifier is above a certain value at which it can sufficiently cover the lipid core, the SLN dispersion is stabilized; above this value, the extra surfactant tends to form micelles that entrap the hydrophobic drug within their cores. Therefore, the portion of drug that partitioned into the lipid matrix decreased, resulting in the reduced entrapment efficiency of the SLN formulation. Further, the increased size and aggregation, introduced by the additional surfactant, reduced the hydrophobicity of the SLN, thus decreasing the lymphatic uptake [123-124].

Adjusting the amount of drug loaded in the SLN can change the physicochemical characteristics of SLN, including: particle size, total particle number, and surface area in SLN dispersion. These variations could impact the in vitro release behavior and in vivo pharmacokinetic parameters. In a comparative study [119] using three tobramycin loaded SLN formulations with different percentages of drug (1.25%, 2.50% and 5.00%), Cavalli et al. found that after duodenal administration, the lower the percentage of tobramycin loaded into the SLN, the slower the drug was released, the higher the bioavailability, and the longer residence time. The SLN with 1.25% drug loading yielded the smallest particle sizes (less than 100 nm); hence, this SLN dispersion had the largest total number of particles in the given volume of SLN dispersion. These factors contributed to the prolonged drug circulation. Tobramycin-SLN has been reported to be successfully transported by the transmucosal pathway to lymphatic system after duodenal administration [117]. In this study, analysis of the lymph and lymph nodes showed that the tobramycin concentration was significantly higher in lymph nodes than in lymph

after duodenal administration; indicating that the drug retention in the lymph nodes was followed by slow drug release to the lymphatic system.

Lymphatic chemotherapy holds great promise as an alternate therapy for patients with metastatic cancers. Despite the advances in cancer prevention and treatment in the past decades, recurrence still often occurs after treatment is completed, due to the inability to eradicate disease residing in the deep tissues and distant lymph nodes or dose-limiting toxicity of existing protocols that prevent patients from receiving full recommended regimens. Lymphatic therapy using drug-encapsulated liposomes and solid lipid nanoparticles emerges as a new technology to provide better penetration into the lymphatics where residual disease exists. It can be used in the clinic either as a neoadjuvant to achieve early disease control, or be administered post primary treatment to serve as a cleanup therapy to eradicate micro-metastases and nano-metastases, preventing cancer recurrence. In addition, solid lipid nanoparticle formulations provide a number of advantages for delivery of poorly water-soluble, unstable, and cytotoxic drugs, to the lymphatic system. By optimizing the preparation procedure and choosing the proper administration route, significant enhancements in bioavailability and lymphatic uptake can be achieved.

3. Overview of thesis

In section 2 of this introduction, the therapeutic improvements of localized chemotherapies have been discussed and compared to the conventional systemic chemotherapy, laying the foundation of the following chapters. The hypothesis of this thesis work is that locoregional lymphatic delivery of small-molecule chemotherapeutic agents will increase drug

concentrations in the tumors and lymph nodes, reducing the progression rate of distant metastases, and the overall drug-induced toxicity, compared to the standard intravenous therapy. The hypothesis will be evaluated against two types of cancers using two model drug delivery platforms in chapters two through five. In the section, the contents of each chapter are described.

3.1 Intralymphatic delivery of hyaluronic acid-cisplatin conjugates for the treatment of breast cancer and head and neck cancer

Chapter two describes the synthesis and characterization of a hyaluronic acid-cisplatin conjugate for the subcutaneous delivery of cisplatin to the rodent lymphatics. The *in vitro* drug release kinetics, anti-proliferative activity, pharmacokinetics, and safety of the conjugate, are presented. In addition, murine xenograft models of Part A) breast cancer, and Part B) head and neck cancer are described for the evaluation of the anti-cancer efficacy of the hyaluronic acid-cisplatin conjugate.

3.2 Intralymphatic delivery of hyaluronic acid-doxorubicin conjugates for the treatment of breast cancer

Chapter three provides information on the development and evaluation of a hyaluronic acid-doxorubicin conjugate for the localized, controlled delivery of doxorubicin to the breast lymphatics. The stability, toxicity, pharmacokinetics, and in vivo anti-cancer efficacy, of the conjugate are also discussed.

3.3 Combination chemotherapy

Chapter four discusses the development and *in vitro* optimization of combination chemotherapy using cisplatin and nitric oxide releasing prodrugs. To determine the optimal dosage and dosing schedule of the combinational treatment, a series of cell-based assays were performed in head and neck cancer and breast cancer cell lines. The mechanism that leads to the enhanced cytotoxicity of the combination regimens is presented.

3.4 Internalization of nanocarriers into tumor cells

Built upon the previous three chapters, chapter five focuses on the investigation of how carrier-based chemotherapies internalize into tumor cells. The synthesis of a gold tagged hyaluronic acid-cisplatin conjugate and a near-IR dye labeled hyaluronic acid-doxorubicin conjugate, are described. In addition, this chapter discusses findings regarding the internalization and cellular distribution of the carriers using transmission electron microscopy and fluorescence microscopy techniques.

4. References

[1] P. Wheatley-Price, F.A. Shepherd, Targeting angiogenesis in the treatment of lung cancer, J Thorac Oncol, 3 (2008) 1173-1184.

[2] V. Martin, D. Liu, C. Gomez-Manzano, Encountering and advancing through antiangiogenesis therapy for gliomas, Curr Pharm Des, 15 (2009) 353-364.

[3] A. Grothey, E. Galanis, Targeting angiogenesis: progress with anti-VEGF treatment with large molecules, Nat Rev Clin Oncol, 6 (2009) 507-518.

[4] L. Vidal, A. Gafter-Gvili, O. Shpilberg, Immunotherapy for patients with follicular lymphoma: the contribution of systematic reviews, Acta Haematol, 125 (2011) 23-31.

[5] J.L. Brun, V. Dalstein, J. Leveque, P. Mathevet, P. Raulic, J.J. Baldauf, S. Scholl, B. Huynh, S. Douvier, D. Riethmuller, C. Clavel, P. Birembaut, V. Calenda, M. Baudin, J.P. Bory, Regression of high-grade cervical intraepithelial neoplasia with TG4001 targeted immunotherapy, Am J Obstet Gynecol, 204 (2011) 169 e161-168.

[6] H. Song, G. Sgouros, Radioimmunotherapy of solid tumors: searching for the right target., Curr Drug Deliv., 8 (2011) 26-44.

[7] X.Y. Bak, H.L. Dang, J. Yang, K. Ye, E.X. Lee, S.K. Lim, S. Wang, Human Embryonic Stem Cell-derived Mesenchymal Stem Cells as Cellular Delivery Vehicles for Prodrug Gene Therapy of Glioblastoma., Hum Gene Ther, Epub ahead of print (2011).

[8] A. Kitamura, K. Matsushita, Y. Takiguchi, H. Shimada, Y. Tada, M. Yamanaka, K. Hiroshima, M. Tagawa, T. Tomonaga, H. Matsubara, M. Inoue, M. Hasegawa, Y. Sato, D. Levens, K. Tatsumi, F. Nomura, Synergistic effect of non-transmissible Sendai virus vector encoding the c-myc suppressor FUSE-binding protein-interacting repressor plus cisplatin in treatment of malignant pleural mesothelioma., Cancer Sci., Epub ahead of print (2011).

[9] R.M. Eager, J. Nemunaitis, Clinical development directions in oncolytic viral therapy., Cancer Gene Ther., Epub ahead of print (2011).

[10] I.F. Khouri, R. Bassett, N. Poindexter, S. O'Brien, C.E. Bueso-Ramos, Y. Hsu, A. Ferrajoli, M.J. Keating, R. Champlin, M. Fernandez-Vina, Nonmyeloablative allogeneic stem cell transplantation in relapsed/refractory chronic lymphocytic leukemia: Long-Term Follow-Up, Prognostic Factors, and Effect of Human Leukocyte Histocompatibility Antigen Subtype on Outcome., Cancer, Epub ahead of print (2011).

[11] J.S. Bubalo, G. Cherala, J.S. McCune, M.Y. Munar, S. Tse, R. Maziarz, Aprepitant Pharmacokinetics and Assessing the Impact of Aprepitant on Cyclophosphamide Metabolism in Cancer Patients Undergoing Hematopoietic Stem Cell Transplantation., J Clin Pharmacol, Epub ahead of print (2011).

[12] E. Goussetis, P. Constantoulakis, V. Kitra, I. Peristeri, M. Mastrominas, M. Baka, M. Papadimitropoulos, C. Karamolegos, A. Paisiou, H. Vasilatou-Kosmidis, S. Graphakos, Successful bone marrow transplantation in a pediatric patient with chronic myeloid leukemia from a HLA-identical sibling selected by preimplantation HLA testing., Pediatr Blood Cancer, Epub ahead of print (2011).

[13] O.J. Creech, E.T. Krementz, R.F. Ryan, J.N. Winblad, Chemotherapy of cancer: regional perfusion utilizing an extracorporeal circuit., Ann Surg, 148 (1958) 616-632.

[14] J.S.J. Stehlin, Hyperthermic perfusion with chemotherapy for cancers of the extremities., Surg Gynecol Obstet, 129 (1969) 305-308.

[15] http://web.mac.com/djf3/davidfary/Isolated_Limb_Perfusion.html.

[16] H.S. Koops, M. Vaglini, S. Suciu, B.B. Kroon, J.F. Thompson, J. Gohl, A.M. Eggermont, F. Di Filippo, E.T. Krementz, D. Ruiter, F.J. Lejeune, Prophylactic isolated limb perfusion for localized, high-risk limb melanoma: results of a multicenter randomized phase III trial. European Organization for Research and Treatment of Cancer Malignant Melanoma Cooperative Group Protocol 18832, the World Health Organization Melanoma Program Trial 15, and the North American Perfusion Group Southwest Oncology Group-8593, J Clin Oncol, 16 (1998) 2906-2912.

[17] J.F. Thompson, M.P. Gianoutsos, Isolated limb perfusion for melanoma: effectiveness and toxicity of cisplatin compared with that of melphalan and other drugs., World J Surg, 16 (1992) 227-233.

[18] D. Daryanani, E.G. de Vries, H.J. Guchelaar, T.W. van Weerden, H.J. Hoekstra, Hyperthermic isolated regional perfusion of the limb with carboplatin., Eur J Surg Oncol., 26 (2000) 792-797.

[19] A.M. Eggermont, A.N. van Geel, J.H. de Wilt, T.L. ten Hagen, The role of isolated limb perfusion for melanoma confined to the extremities, Surg Clin North Am, 83 (2003) 371-384, ix.

[20] D. Lienard, A.M. Eggermont, H.S. Koops, B. Kroon, G. Towse, S. Hiemstra, P. Schmitz, J. Clarke, G. Steinmann, F. Rosenkaimer, F.J. Lejeune, Isolated limb perfusion with tumour necrosis factor-alpha and melphalan with or without interferon-gamma for the treatment of in-transit melanoma metastases: a multicentre randomized phase II study, Melanoma Res, 9 (1999) 491-502.

[21] J.H. de Wilt, T.L. ten Hagen, G. de Boeck, S.T. van Tiel, E.A. de Bruijn, A.M. Eggermont, Tumour necrosis factor alpha increases melphalan concentration in tumour tissue after isolated limb perfusion., Br J Cancer, 82 (2000) 1000-1003.

[22] J.M. Klaase, B.B. Kroon, A.N. van Geel, A.M. Eggermont, H.R. Franklin, Systemic leakage during isolated limb perfusion for melanoma., br J Surg, 80 (1993) 1124-1126.

[23] B.C. Vrouenraets, B.B. Kroon, A.C. Ogilvie, A.N. van Geel, O.E. Nieweg, A.J. Swaak, A.M. Eggermont, Absence of severe systemic toxicity after leakage-controlled isolated limb perfusion with tumor necrosis factor-alpha and melphalan., Ann Surg Oncol, 6 (1999) 405-412.

[24] J.F. Thompson, P.C. Kam, R.C. Waugh, C.R. Harman, Isolated limb infusion with cytotoxic agents: a simple alternative to isolated limb perfusion., Semin Surg Oncol., 14 (1998) 238-247.

[25] P. Lindnér, A. Doubrovsky, P.C. Kam, J.F. Thompson, Prognostic factors after isolated limb infusion with cytotoxic agents for melanoma., Ann Surg Oncol., 9 (2002) 127-136.

[26] H.M. Kroon, M. Moncrieff, P.C. Kam, J.F. Thompson, Outcomes following isolated limb infusion for melanoma. A 14-year experience., Ann Surg Oncol., 15 (2008) 3003-3013.

[27] M.S. Brady, K. Brown, A. Patel, C. Fisher, W. Marx, A phase II trial of isolated limb infusion with melphalan and dactinomycin for regional melanoma and soft tissue sarcoma of the extremity., Ann Surg Oncol., 13 (2006) 1123-1129.

[28] P. Lindnér, A. Doubrovsky, P.C. Kam, J.F. Thompson, Prognostic factors after isolated limb infusion with cytotoxic agents for melanoma., Ann Surg Oncol, 9 (2002) 127-136.

[29] G.M. Beasley, R.P. Petersen, J. Yoo, N. McMahon, T. Aloia, W. Petros, G. Sanders, T.Y. Cheng, S.K. Pruitt, H. Seigler, D.S. Tyler, Isolated limb infusion for in-transit malignant melanoma of the extremity: a well-tolerated but less effective alternative to hyperthermic isolated limb perfusion., Ann Surg Oncol., 15 (2008) 2195-2205.

[30] P.H. Sugarbaker, T. Graves, E.A. DeBruijn, W.J. Cunliffe, R.E. Mullins, W.E. Hull, L. Oliff, P. Schlag, Early postoperative intraperitoneal chemotherapy as an adjuvant therapy to surgery for peritoneal carcinomatosis from gastrointestinal cancer: pharmacological studies., Cancer Res., 50 (1990) 5790-5794.

[31] http://healthinfoispower.wordpress.com/2008/06/16/encouraging-survival-data-associated-with-maximal-cytoreduction-and-hyperthermic-intraperitoneal-chemotherapy-using-pegylated-liposomal-doxorubicin/.

[32] S. Fujimoto, M. Takahashi, T. Mutou, K. Kobayashi, T. Toyosawa, Successful intraperitoneal hyperthermic chemoperfusion for the prevention of postoperative peritoneal recurrence in patients with advanced gastric carcinoma., Cancer, 85 (1999) 529-534.

[33] D. Elias, L. Sideris, M. Pocard, C. Edè, D. Ben Hassouna, M. Ducreux, V. Boige, J.F. Côté, P. Lasser, Efficacy of intraperitoneal chemohyperthermia with oxaliplatin in colorectal peritoneal carcinomatosis. Preliminary results in 24 patients., Ann Oncol, 15 (2004) 781-785.

[34] V.J. Verwaal, S. van Ruth, E. de Bree, G.W. van Sloothen, H. van Tinteren, H. Boot, F.A. Zoetmulder, Randomized trial of cytoreduction and hyperthermic intraperitoneal chemotherapy versus systemic chemotherapy and palliative surgery in patients with peritoneal carcinomatosis of colorectal cancer., J Clin Oncol, 21 (2003) 3737-3743.

[35] P. Jacquet, A.D. Stephens, A.M. Averbach, D. Chang, S.E. Ettinghausen, R.R. Dalton, M.A. Steves, P.H. Sugarbaker, Analysis of morbidity and mortality in 60 patients with peritoneal carcinomatosis treated by cytoreductive surgery and heated intraoperative intraperitoneal chemotherapy., Cancer, 77 (1996) 2622-2629.

[36] A.D. Stephens, R. Alderman, D. Chang, G.D. Edwards, J. Esquivel, G. Sebbag, M.A. Steves, P.H. Sugarbaker, Morbidity and mortality analysis of 200 treatments with cytoreductive surgery and hyperthermic intraoperative intraperitoneal chemotherapy using the coliseum technique., Ann Surg Oncol, 6 (1999) 790-796.

[37] A.M. Averbach, D. Chang, P. Koslowe, P.H. Sugarbaker, Anastomotic leak after double-stapled low colorectal resection., Dis Colon Rectum., 39 (1996) 780-787.

[38] Y. Matsuzaki, K. Shibata, M. Yoshioka, M. Inoue, R. Sekiya, T. Onitsuka, I. Iwamoto, Y. Koga, Intrapleural perfusion hyperthermo-chemotherapy for malignant pleural dissemination and effusion., Ann Thorac Surg, 59 (1995) 127-131.

[39] Y. Matsuzaki, M. Edagawa, T. Shimizu, M. Hara, M. Tomita, T. Ayabe, T. Onitsuka, Intrapleural hyperthermic perfusion with chemotherapy increases apoptosis in malignant pleuritis., Ann Thorac Surg, 78 (2004) 1769-1772.

[40] N. Shigemura, A. Akashi, M. Ohta, H. Matsuda, Combined surgery of intrapleural perfusion hyperthermic chemotherapy and panpleuropneumonectomy for lung cancer with advanced pleural spread: a pilot study., Interact Cardiovasc Thorac Surg, 2 (2003) 671-675.

[41] O. Monneuse, A.C. Beaujard, B. Guibert, F.N. Gilly, P. Mulsant, P.Y. Carry, M. Benoit, O. Glehen, Long-term results of intrathoracic chemohyperthermia (ITCH) for the treatment of pleural malignancies., Br J Cancer., 88 (2003) 1839-1843.

[42] E. de Bree, S. van Ruth, P. Baas, E.J. Rutgers, N. van Zandwijk, A.J. Witkamp, F.A. Zoetmulder, Cytoreductive surgery and intraoperative hyperthermic intrathoracic chemotherapy in patients with malignant pleural mesothelioma or pleural metastases of thymoma., Chest, 121 (2002) 480-487.

[43] http://medicineworld.org/cancer/mesothelioma/staging-of-pleural-mesothelioma.html.

[44] R.K. Ausman, Development of a technic for isolated perfusion of the liver., N Y State J Med, 61 (1961) 3993-3997.

[45] A. Grover, H.R.J. Alexander, The past decade of experience with isolated hepatic perfusion., Oncologist., 9 (2004) 653-664.

[46] H.R.J. Alexander, D.L. Bartlett, S.K. Libutti, D.L. Fraker, T. Moser, S.A. Rosenberg, Isolated hepatic perfusion with tumor necrosis factor and melphalan for unresectable cancers confined to the liver., J Clin Oncol., 16 (1998) 1479-1489.

[47] T.S. Ravikumar, G. Pizzorno, W. Bodden, J. Marsh, R. Strair, J. Pollack, R. Hendler, J. Hanna, E. D'Andrea, Percutaneous hepatic vein isolation and high-dose hepatic arterial infusion chemotherapy for unresectable liver tumors., J Clin Oncol., 12 (1994) 2723-2736.

[48] J.F. Pingpank, S.K. Libutti, R. Chang, B.J. Wood, Z. Neeman, A.W. Kam, W.D. Figg, S. Zhai, T. Beresneva, G.D. Seidel, H.R. Alexander, Phase I study of hepatic arterial melphalan infusion and hepatic venous hemofiltration using percutaneously placed catheters in patients with unresectable hepatic malignancies., J Clin Oncol., 23 (2005) 3465-3474.

[49] D. Doyon, A. Mouzon, A.M. Jourde, C. Regensberg, C. Frileux, Hepatic, arterial embolization in patients with malignant liver tumours (author's transl). Ann Radiol (Paris), 17 (1974) 593-603.

[50] K. Takayasu, S. Arii, I. Ikai, M. Omata, K. Okita, T. Ichida, Y. Matsuyama, Y. Nakanuma, M. Kojiro, M. Makuuchi, Y. Yamaoka, L.C.S.G.o. Japan., Prospective cohort study of transarterial chemoembolization for unresectable hepatocellular carcinoma in 8510 patients., Gastroenterology., 131 (2006) 461-469.

[51] TACE, http://www.cpmc.org/learning/documents/tace.html.

[52] R.S. Oliveri, J. Wetterslev, C. Gluud, Transarterial (chemo)embolisation for unresectable hepatocellular carcinoma., Cochrane Database Syst Rev, Epub ahead of print (2011).

[53] J.H. Zhong, L.Q. Li, Postoperative adjuvant transarterial chemoembolization for participants with hepatocellular carcinoma: A meta-analysis., Hepatol Res., 40 (2010) 943-953.

[54] E.G. Giannini, G. Bodini, M. Corbo, V. Savarino, D. Risso, M.A. Di Nolfo, P. Del Poggio, L. Benvegnù, F. Farinati, M. Zoli, F. Borzio, E. Caturelli, M. Chiaramonte, F. Trevisani,

I.L.C.I.L.C. GROUP., Impact of evidence-based medicine on the treatment of patients with unresectable hepatocellular carcinoma., Aliment Pharmacol Ther., 31 (2010) 493-501.

[55] H.P. Allgaier, P. Deibert, M. Olschewski, C. Spamer, U. Blum, W. Gerok, H.E. Blum, Survival benefit of patients with inoperable hepatocellular carcinoma treated by a combination of transarterial chemoembolization and percutaneous ethanol injection--a single-center analysis including 132 patients., Int J Cancer., 79 (1998) 601-605.

[56] R.T. Poon, H. Ngan, C.M. Lo, C.L. Liu, S.T. Fan, J. Wong, Transarterial chemoembolization for inoperable hepatocellular carcinoma and postresection intrahepatic recurrence., J Surg Oncol., 73 (2000) 109-114.

[57] C. Cammà, F. Schepis, A. Orlando, M. Albanese, L. Shahied, F. Trevisani, P. Andreone, A. Craxì, M. Cottone, Transarterial chemoembolization for unresectable hepatocellular carcinoma: meta-analysis of randomized controlled trials., Radiology., 224 (2002) 47-54.

[58] S.A. Stacker, M.G. Achen, L. Jussila, M.E. Baldwin, K. Alitalo, Lymphangiogenesis and cancer metastasis., Nat Rev Cancer., 2 (2002) 573-583.

[59] S.D. Nathanson, Insights into the mechanisms of lymph node metastasis, Cancer, 98 (2003) 413-423.

[60] valve, http://grovebiol.co.uk/humphys3transpt.aspx.

[61] D.A. Rao, M.L. Forrest, A.W. Alani, G.S. Kwon, J.R. Robinson, Biodegradable PLGA based nanoparticles for sustained regional lymphatic drug delivery., J Pharm Sci, 99 (2010) 2018-2031.

[62] J. Liu, D. Meisner, E. Kwong, X.Y. Wu, M.R. Johnston, Translymphatic chemotherapy by intrapleural placement of gelatin sponge containing biodegradable Paclitaxel colloids controls lymphatic metastasis in lung cancer., Cancer Res., 69 (2009) 1174-1181.

[63] S.D. Chipman, F.B. Oldham, G. Pezzoni, J.W. Singer, Biological and clinical characterization of paclitaxel poliglumex (PPX, CT-2103), a macromolecular polymer-drug conjugate., Int J Nanomedicine., 1 (2006) 375-383.

[64] S. Cai, Y. Xie, N.M. Davies, M.S. Cohen, M.L. Forrest, Carrier-based intralymphatic cisplatin chemotherapy for the treatment of metastatic squamous cell carcinoma of the head & neck, Therapeutic Delviery, 1 (2010) 237-245.

[65] L. Feng, L. Zhang, M. Liu, Z. Yan, C. Wang, B. Gu, Y. Liu, G. Wei, G. Zhong, W. Lu, Roles of dextrans on improving lymphatic drainage for liposomal drug delivery system., J Drug Target., 18 (2010) 168-178.

[66] K.A. Lawson, K. Anderson, R.M. Snyder, M. Simmons-Menchaca, J. Atkinson, L.Z. Sun, A. Bandyopadhyay, V. Knight, B.E. Gilbert, B.G. Sanders, K. Kline, Novel vitamin E analogue and 9-nitro-camptothecin administered as liposome aerosols decrease syngeneic mouse

mammary tumor burden and inhibit metastasis., Cancer Chemother Pharmacol., 54 (2004) 421-431.

[67] V.S. Trubetskoy, K.R. Whiteman, V.P. Torchilin, G.L. Wolf, Massage-induced release of subcutaneously injected liposome-encapsulated drugs to the blood., J Control Release, 50 (1998) 13-19.

[68] V.S. Trubetskoy, M.D. Frank-Kamenetsky, K.R. Whiteman, G.L. Wolf, V.P. Torchilin, Stable polymeric micelles: lymphangiographic contrast media for gamma scintigraphy and magnetic resonance imaging., Acad Radiol, 3 (1996) 232-238.

[69] H. Yoshikawa, Y. Satoh, N. Naruse, K. Takada, S. Muranishi, Comparison of disappearance from blood and lymphatic delivery of human fibroblast interferon in rat by different administration routes., J Pharmacobiodyn., 8 (1985) 206-210.

[70] G. Luo, X. Yu, C. Jin, F. Yang, D. Fu, J. Long, J. Xu, C. Zhan, W. Lu, LyP-1-conjugated nanoparticles for targeting drug delivery to lymphatic metastatic tumors., Int J Pharm, 385 (2010) 150-156.

[71] V. Frenkel, A. Etherington, M. Greene, J. Quijano, J. Xie, F. Hunter, S. Dromi, K.C. Li, Delivery of liposomal doxorubicin (Doxil) in a breast cancer tumor model: investigation of potential enhancement by pulsed-high intensity focused ultrasound exposure, Acad Radiol, 13 (2006) 469-479.

[72] M.E. O'Brien, N. Wigler, M. Inbar, R. Rosso, E. Grischke, A. Santoro, R. Catane, D.G. Kieback, P. Tomczak, S.P. Ackland, F. Orlandi, L. Mellars, L. Alland, C. Tendler, Reduced cardiotoxicity and comparable efficacy in a phase III trial of pegylated liposomal doxorubicin HCl (CAELYX/Doxil) versus conventional doxorubicin for first-line treatment of metastatic breast cancer, Ann. Oncol., 15 (2004) 440-449.

[73] T. Tejada-Berges, C.O. Granai, M. Gordinier, W. Gajewski, Caelyx/Doxil for the treatment of metastatic ovarian and breast cancer, Expert Rev Anticancer Ther, 2 (2002) 143-150.

[74] L.M. Prescott, Doxil offers hope to KS sufferers, J Int Assoc Physicians AIDS Care, 1 (1995) 43-44.

[75] A. Soundararajan, A. Bao, W.T. Phillips, R.r. Perez, B.A. Goins, [(186)Re]Liposomal doxorubicin (Doxil): in vitro stability, pharmacokinetics, imaging and biodistribution in a head and neck squamous cell carcinoma xenograft model, Nucl Med Biol, 36 (2009) 515-524.

[76] K.J. Harrington, G. Rowlinson-Busza, K.N. Syrigos, P.S. Uster, R.G. Vile, J.S. Stewart, Pegylated liposomes have potential as vehicles for intratumoral and subcutaneous drug delivery, Clin Cancer Res, 6 (2000) 2528-2537.

[77] S.M. Moghimi, M. Moghimi, Enhanced lymph node retention of subcutaneously injected IgG1-PEG2000-liposomes through pentameric IgM antibody-mediated vesicular aggregation, Biochim Biophys Acta, 1778 (2008) 51-55.

[78] S.M. Moghimi, The effect of methoxy-PEG chain length and molecular architecture on lymph node targeting of immuno-PEG liposomes, Biomaterials, 27 (2006) 136-144.

[79] W.T. Phillips, R. Klipper, B. Goins, Novel method of greatly enhanced delivery of liposomes to lymph nodes, J Pharmacol Exp Ther, 295 (2000) 309-313.

[80] N. Hashida, M. Murakami, H. Yoshikawa, K. Takada, S. Muranishi, Intestinal absorption of carboxyfluorescein entrapped in liposomes in comparison with its administration with lipid-surfactant mixed micelles, J Pharmacobiodyn, 7 (1984) 195-203.

[81] Y. Perrie, M. Obrenovic, D. McCarthy, G. Gregoriadis, Liposome (Lipodine)-mediated DNA vaccination by the oral route, J Liposome Res, 12 (2002) 185-197.

[82] P. Latimer, M. Menchaca, R.M. Snyder, W. Yu, B.E. Gilbert, B.G. Sanders, K. Kline, Aerosol delivery of liposomal formulated paclitaxel and vitamin E analog reduces murine mammary tumor burden and metastases, Exp Biol Med (Maywood), 234 (2009) 1244-1252.

[83] M.F. Rabaca Roque Botelho, M.A. Tavares Marques, C.M. Freitas Gomes, A. Marques Ferreira da Silva, V.A. Andrade Figueiredo Bairos, M.A. de Matos Santos Rosa, A. Pena Abrunhosa, J.J. Pedroso de Lima, Nanoradioliposomes molecularly modulated to study the lung deep lymphatic drainage, Rev Port Pneumol, 15 (2009) 261-293.

[84] R. Ling, Y. Li, Q. Yao, T. Chen, D. Zhu, Y. Jun, J. Chen, Lymphatic chemotherapy induces apoptosis in lymph node metastases in a rabbit breast carcinoma model, J Drug Target, 13 (2005) 137-142.

[85] V.S. Trubetskoy, K.R. Whiteman, V.P. Torchilin, G.L. Wolf, Massage-induced release of subcutaneously injected liposome-encapsulated drugs to the blood, J Control Release, 50 (1998) 13-19.

[86] S.S. Ling, E. Magosso, N.A. Khan, K.H. Yuen, S.A. Barker, Enhanced oral bioavailability and intestinal lymphatic transport of a hydrophilic drug using liposomes, Drug Dev Ind Pharm, 32 (2006) 335.

[87] S.L. Kraft, D. Dailey, M. Kovach, K.L. Stasiak, J. Bennett, C.T. McFarland, D.N. McMurray, A.A. Izzo, I.M. Orme, R.J. Basaraba, Magnetic resonance imaging of pulmonary lesions in guinea pigs infected with Mycobacterium tuberculosis, Infect Immun, 72 (2004) 5963-5971.

[88] K.A. Lawson, K. Anderson, R.M. Snyder, M. Simmons-Menchaca, J. Atkinson, L.Z. Sun, A. Bandyopadhyay, V. Knight, B.E. Gilbert, B.G. Sanders, K. Kline, Novel vitamin E analogue and 9-nitro-camptothecin administered as liposome aerosols decrease syngeneic mouse mammary tumor burden and inhibit metastasis, Cancer Chemother Pharmacol, 54 (2004) 421-431.

[89] Z. Cui, S.J. Han, L. Huang, Coating of mannan on LPD particles containing HPV E7 peptide significantly enhances immunity against HPV-positive tumor, Pharm Res, 21 (2004) 1018-1025.

[90] A. Desormeaux, M.G. Bergeron, Lymphoid tissue targeting of anti-HIV drugs using liposomes, Methods Enzymol, 391 (2005) 330-351.

[91] J. Bestman-Smith, P. Gourde, A. Desormeaux, M.J. Tremblay, M.G. Bergeron, Sterically stabilized liposomes bearing anti-HLA-DR antibodies for targeting the primary cellular reservoirs of HIV-1, Biochim Biophys Acta, 1468 (2000) 161-174.

[92] B. Mui, S.G. Raney, S.C. Semple, M.J. Hope, Immune stimulation by a CpG-containing oligodeoxynucleotide is enhanced when encapsulated and delivered in lipid particles, J Pharmacol Exp Ther, 298 (2001) 1185-1192.

[93] S. de Jong, G. Chikh, L. Sekirov, S. Raney, S. Semple, S. Klimuk, N. Yuan, M. Hope, P. Cullis, Y. Tam, Encapsulation in liposomal nanoparticles enhances the immunostimulatory, adjuvant and anti-tumor activity of subcutaneously administered CpG ODN, Cancer Immunol Immunother, 56 (2007) 1251-1264.

[94] N. Kojima, L. Biao, T. Nakayama, M. Ishii, Y. Ikehara, K. Tsujimura, Oligomannose-coated liposomes as a therapeutic antigen-delivery and an adjuvant vehicle for induction of in vivo tumor immunity, J Control Release, 129 (2008) 26-32.

[95] C. Butts, N. Murray, A. Maksymiuk, G. Goss, E. Marshall, D. Soulières, Y. Cormier, P. Ellis, A. Price, R. Sawhney, M. Davis, J. Mansi, C. Smith, D. Vergidis, P. Ellis, M. MacNeil, M. Palmer, Randomized phase IIB trial of BLP25 liposome vaccine in stage IIIB and IV non-small-cell lung cancer, J Clin Oncol, 23 (2005) 6674-6681.

[96] J. Neidhart, K.O. Allen, D.L. Barlow, M. Carpenter, D. Shaw, P.L. Triozzi, R.M. Conry, Immunization of colorectal cancer patients with recombinant baculovirus-derived KSA (Ep-CAM) formulated with monophosphoryl lipid A in liposomal emulsion, with and without granulocyte-macrophage colony-stimulating factor, Vaccine, 22 (2004) 773-780.

[97] W.T. Phillips, B. Goins, Assessment of liposome delivery using scintigraphic imaging, J Liposome Res, 12 (2002) 71-80.

[98] W.T. Phillips, T. Andrews, H. Liu, R. Klipper, A.J. Landry, R. Blumhardt, B. Goins, Evaluation of [(99m)Tc] liposomes as lymphoscintigraphic agents: comparison with [(99m)Tc] sulfur colloid and [(99m)Tc] human serum albumin., Nucl Med Biol, 28 (2001) 435-444.

[99] S.P. Bagaria, M.B. Faries, D.L. Morton, Sentinel node biopsy in melanoma: technical considerations of the procedure as performed at the John Wayne Cancer Institute, J Surg Oncol, 101 (2010) 669-676.

[100] T. Yamamoto, M. Tamura, T. Hamauzu, A. Nakayama, K. Kawasugi, M. Kamakura, T. Kinoshita, Y. Kuyama, M. Yamanaka, L.M. Wang, M. Sanaka, S. Mineshita, Intestinal Behçet's disease associated with non-Hodgkin's lymphoma, J Gastroenterol, 32 (1997) 241-245.

[101] J.A. Luongo, L.R. Scalcione, D.S. Katz, E.Y. Yung, Progression of clinically stable lymphedema on lymphoscintigraphy, Clin Nucl Med, 34 (2009) 585-588.

[102] P. Bourgeois, J.L. Dargent, D. Larsimont, D. Munck, F. Sales, M. Boels, C. De Valck, Lymphoscintigraphy in angiomyomatous hamartomas and primary lower limb lymphedema, Clin Nucl Med, 34 (2009) 405-409.

[103] E.M. Plut, G.H. Hinkle, W. Guo, R.J. Lee, Kit formulation for the preparation of radioactive blue liposomes for sentinel node lymphoscintigraphy, J Pharm Sci, 91 (2002) 1717-1732.

[104] Y. Fujimoto, Y. Okuhata, S. Tyngi, Y. Namba, N. Oku, Magnetic resonance lymphography of profundus lymph nodes with liposomal gadolinium-diethylenetriamine pentaacetic acid, Biol Pharm Bull, 23 (2000) 97-100.

[105] B. Misselwitz, A. Sachse, Interstitial MR lymphography using Gd-carrying liposomes, Acta Radiol Suppl, 412 (1997) 51-55.

[106] V.S. Trubetskoy, J.A. Cannillo, A. Milshtein, G.L. Wolf, V.P. Torchilin, Controlled delivery of Gd-containing liposomes to lymph nodes: surface modification may enhance MRI contrast properties, Magn Reson Imaging, 13 (1995) 31-37.

[107] C.L. Zavaleta, W.T. Phillips, A. Soundararajan, B.A. Goins, Use of avidin/biotin-liposome system for enhanced peritoneal drug delivery in an ovarian cancer model, Int J Pharm, 337 (2007) 316-328.

[108] L.A. Medina, S.M. Calixto, R. Klipper, W.T. Phillips, B. Goins, Avidin/biotin-liposome system injected in the pleural space for drug delivery to mediastinal lymph nodes, Journal of Pharmaceutical Sciences, 93 (2004) 2595-2608.

[109] L.A. Medina, S.M. Calixto, R. Klipper, Y. Li, W.T. Phillips, B. Goins, Mediastinal node and diaphragmatic targeting after intracavitary injection of avidin/99mTc-blue-biotin-liposome system, J Pharm Sci, 95 (2006) 207-224.

[110] R.H. Müller, K. Mäder, S. Gohla, Solid lipid nanoparticles (SLN) for controlled drug delivery - a review of the state of the art, Eur J Pharm Biopharm, 50 (2000) 161-177.

[111] W. Mehnert, K. Mäder, Solid lipid nanoparticles: production, characterization and applications, Adv Drug Deliv Rev, 47 (2001) 165-196.

[112] H.L. Wong, R. Bendayan, A.M. Rauth, Y. Li, X.Y. Wu, Chemotherapy with anticancer drugs encapsulated in solid lipid nanoparticles, Adv Drug Deliv Rev, 59 (2007) 491-504.

[113] L. Harivardhan Reddy, R.K. Sharma, K. Chuttani, A.K. Mishra, R.S. Murthy, Influence of administration route on tumor uptake and biodistribution of etoposide loaded solid lipid nanoparticles in Dalton's lymphoma tumor bearing mice, J Control Release, 105 (2005) 185-198.

[114] R. Paliwal, S. Rai, B. Vaidya, K. Khatri, A.K. Goyal, N. Mishra, A. Mehta, S.P. Vyas, Effect of lipid core material on characteristics of solid lipid nanoparticles designed for oral lymphatic delivery, Nanomedicine, 5 (2009) 184-191.

[115] G.P. Zara, A. Bargoni, R. Cavalli, A. Fundarò, D. Vighetto, M.R. Gasco, Pharmacokinetics and tissue distribution of idarubicin-loaded solid lipid nanoparticles after duodenal administration to rats, J Pharm Sci, 91 (2002) 1324-1333.

[116] R.K. Jain, Barriers to drug delivery in solid tumors, Sci Am, 271 (1994) 58-65.

[117] A. Bargoni, R. Cavalli, O. Caputo, A. Fundarò, M.R. Gasco, G.P. Zara, Solid lipid nanoparticles in lymph and plasma after duodenal administration to rats, Pharm Res, 15 (1998) 745-750.

[118] R. Cavalli, G.P. Zara, O. Caputo, A. Bargoni, A. Fundarò, G. M.R., Transmucosal transport of tobramycin incorporated in SLN after duodenal administration to rats. Part I--a pharmacokinetic study., Pharmacol Res, 42 (2000) 541-545.

[119] R. Cavalli, A. Bargoni, V. Podio, E. Muntoni, G.P. Zara, M.R. Gasco, Duodenal administration of solid lipid nanoparticles loaded with different percentages of tobramycin, J Pharm Sci, 92 (2003) 1085-1094.

[120] M.A. Videira, M.F. Botelho, A.C. Santos, L.F. Gouveia, J.J. de Lima, A.J. Almeida, Lymphatic uptake of pulmonary delivered radiolabelled solid lipid nanoparticles, J Drug Target, 10 (2002) 607-613.

[121] J.A. Elliott, K. Osterlind, F.R. Hirsch, H.H. Hansen, Metastatic patterns in small-cell lung cancer: correlation of autopsy findings with clinical parameters in 537 patients, J Clin Oncol, 5 (1987) 246-254.

[122] L.E. Stenbygaard, J.B. Sørensen, H. Larsen, P. Dombernowsky, Metastatic pattern in non-resectable non-small cell lung cancer, Acta Oncol, 38 (1999) 993-998.

[123] A.E. Hawley, S.S. Davis, L. Illum, Targeting of colloids to lymph nodes: influence of lymphatic physiology and colloidal characteristics Adv Drug Deliver Rev, 17 (1995) 129-148.

[124] W.N. Charman, V.J. Stella, Lymphatic Transport of Drugs, CRC Press, 1992.

[125] C. Oussoren, J. Zuidema, D.J. Crommelin, G. Storm, Lymphatic uptake and biodistribution of liposomes after subcutaneous injection.: II. Influence of liposomal size, lipid composition and lipid dose, Biochim Biophys Acta, 1328 (1997) 261-272.

[126] B. Sanjula, F.M. Shah, A. Javed, A. Alka, Effect of poloxamer 188 on lymphatic uptake of carvedilol-loaded solid lipid nanoparticles for bioavailability enhancement, J Drug Target, 17 (2009) 249-256.

Chapter 2

Intralymphatic Delivery of Hyaluronic Acid-Cisplatin Conjugates

for the Treatment of Breast Cancer and Head and Neck Cancer

1. Introduction

Since the FDA's approval of cisplatin in 1977 for the treatment of metastatic ovarian cancer [1], cisplatin (*cis*-diamminedichloroplatinum or CDDP) has emerged as the principal chemotherapeutic agent for many solid tumors, despite newer platinum drugs with fewer side-effects. CDDP has a high initial response rate in many cancers including head and neck squamous sarcomas, lymphomas, small cell and non-small cell lung, testicular, ovarian, gastric, esophagus, and pancreatic cancers [2]. Although not clinically employed as a single agent, CDDP is highly active in combination chemotherapeutic regimens for breast cancer [3], but the significant dose-limiting toxicity of CDDP has hampered its use in many patients.

Nephrotoxicity is the most dangerous and insidious of CDDP's side-effects, exhibited by renal tubular inflammation and necrosis, as CDDP is filtered by the kidneys [4]. After intravenous administration, CDDP tightly binds to plasma proteins and becomes highly concentrated in the plasma compared to other organs [5]. CDDP efficacy is well-correlated with the area-under-the-curve (AUC), but not with the maximum plasma concentration (C_{max}) [6]; however, toxicity is increased by high peak drug concentrations, as seen immediately after bolus injection or during short i.v. infusions, further increasing the risk of nephrotoxicity [2]. Fractional or metronomic dosing schedules that divide the same total dose of CDDP over several, e.g. daily, smaller injections, have been shown to significantly reduce nephrotoxicity and ototoxicity [6-7] due to lower peak plasma concentrations. However, metronomic dosing requires a more frequent dosing schedule, longer in-hospital stays, and increased care costs thereby limiting its use.

Locally advanced breast cancer in women remains a challenge for treatment, with current multimodality therapy resulting in moderate toxicity both locoregionally and systemically. Locoregional relapse of breast cancer can occur in up to 13% of patients, and a complete axillary lymphadenectomy can reduce this risk to less than 2% but carries its own surgical risks and morbidity including numbness in the upper medial arm, axilla and chest wall; increased incidence of skin and wound infections; and painful lymphedema in up to 30% to 50% of patients [8-9]. Cytotoxic chemotherapies also have poor penetration to the locoregional lymphatics in the breast because of separation of the lymphatics from the systemic vasculature as well as lymphatic mono-directional flow [10]. Platinum-based chemotherapy is the most commonly used chemotherapeutic in the United States but carries its own morbidity including dose-limiting nephrotoxicity and neurotoxicity. CDDP is not commonly used as a single-agent treatment for breast cancer although it is a part of several combination regimens, but CDDP may have a place in patient populations that have failed to respond to anthracyclines and taxanes. Triple-negative breast cancers are commonly resistant to standard regimens, but there is increasing evidence that these patients may have increased platinum sensitivity [11]. Recent studies report that BRCA1 breast cancers are highly sensitive to platinum regimens because of the role BRCA1 plays in DNA double-strand repair [12-13]. Herein, we sought to investigate the feasibility of developing a lymphatic drug delivery system to maximize the efficacy and long-term survival rate of cisplatin-based chemotherapy in treating locally advanced breast cancer and to reduce its dosing frequency and the associated patient hospital-stay. The development and *in vivo* evaluation of this cisplatin-based locoregional chemotherapy will be discussed in Part A of this chapter.

Cisplatin is commonly used as the first-line chemotherapy for head and neck squamous cell carcinoma (HNSCC). HNSCC is the sixth most common cancer worldwide, encompassing epithelial carcinomas and squamous cell carcinomas, which are characterized by their pathological characteristics [14]. Cancer in the head and neck region can arise from soft tissues, bones, and a variety of glands in the upper aerodigestive tracts, including: the oral cavity, oropharynx, hypopharynx, larynx, nasopharynx, paranasal sinuses and salivary glands [15]. Approximately 60,000 Americans are diagnosed with head and neck cancer each year. It has been noted that according to the statistics, that the largest group is head and neck squamous cell carcinoma, where malignancies originate in the most superficial layer of the tissues or organs in the head and neck region. Early stage (Stage I and II) localized HNSCC has good disease prognosis and local tumor control, yielding a stable survival rate of approximately 81% in the past decade. In contrast, patients with regional or metastatic disease have a poor survival rate, as low as 52% and 26%, respectively, which has improved only slightly in the past twenty years [14]. Late stage (Stage III or IV) patients are usually diagnosed with the involvement of multiple lymph nodes or distant metastasis. In most cases, the patients have to undergo neck dissection to examine the area of tumor lymphatic drainage and excise the diseased cervical lymph nodes in the lymphatic basin, preventing further disease recurrence.

Historically, patients with unresectable HNSCC have been treated with radiation therapy. Unfortunately, the five-year survival was unsatisfactory and disease recurrence usually occurred within two years after the radiation therapy. For HNSCC patients, there was an imperative need for a more effective, and less invasive regimen after ablation of the primary tumor. Therefore, concurrent chemoradiotherapy has been readily accepted as a neoadjuvant, as well as an adjuvant therapy for better local and regional control of the disease. Platinum-based chemotherapy

administered concomitant with radiation therapy has now become the first-line therapeutic strategy in the clinic due to the radiosensitizing properties and cytotoxic efficacy of cisplatin [16]. Several Phase III clinical trials in locally advanced HNSCC exhibited promising results of a three-drug chemotherapy regimen with cisplatin, taxane, and 5-fluorouracil, with improved overall survival, particularly for patients with unresectable tumors [17]. However, some clinical trials with cisplatin and 5-fluorouracil combinational adjuvant chemotherapy followed by radiotherapy, showed only minimal improvements in the disease-free survival and locoregional control, in comparison with patients who received radiation therapy alone [16]. In addition, most chemotherapeutics, including cisplatin, have poor penetration to the lymphatic basin due to its anatomy and mono-directional flow, limiting their efficacy in treating late stage patients. Hence, we sought to develop a lymphatic carrier-based platinum chemotherapy for the treatment of locally advanced head and neck squamous cell cancer. The development and *in vivo* evaluation of hyaluronan-cisplatin conjugates will be presented in Part B of this chapter.

2. Synthesis and characterization of hyaluronan-cisplatin (HA-Pt) conjugates

Cisplatin (CDDP) was conjugated to hyaluronan (HA, 35,000 Da) with and without the addition of silver nitrate (26 mg) as an activating agent. Typically, HA (100 mg) and CDDP (45 mg) were dissolved in H_2O (20 mL) and stirred in the dark for three days under argon at ambient temperature (ca. 25 ℃). The reaction mixture was filtered (0.2-μm nylon membrane) and dialyzed against ddH_2O (10,000 MWCO; Pierce, Rockford, IL) for 48 h at 4 ℃ protected from light. Following dialysis, the crude product was concentrated and stored at 4 ℃.

The degree of CDDP substitution was determined by atomic absorption spectroscopy (AAS) (Varian SpectrAA GTA-110 with graphite furnace). The furnace program was as follows: ramp 25 to 80 °C, hold 2 s, ramp to 120 °C, hold 10 s, ramp to 1000 °C, hold 5 s, ramp to 2700 °C, hold 2 s, cool to 25 °C over 20 s. The graphite partition tube was cleaned every 100 samples by baking at 2800 °C for 7 s. Argon was used as the injection and carrier gas.

Cisplatin was highly conjugated to HA, with typical conjugations of 0.25 w/w cisplatin/complex using a starting ratio of 0.5 w/w cisplatin/HA. Up to 0.75 w/w cisplatin/complex was attempted with decreasing efficiency (Table 1). The conjugation efficiency remained the same both in the presence or absence of the activating agent, silver nitrate. The AAS produced a linear concentration curve from 10 to 450 ng/mL (R^2=0.9998), with a limit of detection of 5 ng/mL and a limit of quantification of 10 ng/mL (5% standard deviation).

3. *In vitro* release

The *in vitro* release rate of the active hydrated form of the cisplatin (*cis*-$[Pt(NH_3)_2(H_2O)_2]^+$) from the HA-Pt conjugate was determined in both water and phosphate buffered saline (PBS, pH 7.4, 140 mM NaCl) solution. HA-Pt was added to a 10,000 MWCO dialysis bag (Pierce, Rockford, IL) and placed in a water or PBS bath and stirred at 37 ˚C. The bath volume (3 L) was replaced every 4 h to maintain sink conditions. Samples were taken from the dialysis bag at predetermined time points, and the remaining Pt concentration was determined by AAS.

The release rate of cisplatin from complexes was determined in both phosphate buffered saline and water. The Cl⁻ in saline was expected to more rapidly displace cisplatin, increasing the

Cisplatin added w/w cisplatin/HA	Conjugated w/w cisplatin/HA	Conjugation Efficiency, %
0.03	0.022	73 %
0.08	0.040	50 %
0.15	0.086	57 %
0.20	0.119	60 %
0.30	0.149	50 %
0.40	0.210	53 %
0.50	0.254	51 %
0.60	0.263	44 %
0.70	0.241	34 %

Table 1. Conjugation efficiency of cisplatin to HA. Efficiency calculated as (cisplatin added/cisplatin incorporated) $\times$ 100%.

release rate. The release of drug showed pseudo first order release kinetics with a release half-life of 42 h in water and 10 h in physiological saline (Figure 1).

4. Cytotoxicity

The metastatic human breast cancer cell line MDA-MB-468LN (isolated from patient's lymph nodes), was maintained in modified Eagle's medium alpha (MEMα) supplemented with 10% fetal bovine serum, 1% L-glutamine, and 0.4 mg/mL G418 (geneticin). The lymphatically metastatic head and neck cancer cell line MDA1986, was maintained in Dulbecco's modified Eagle's medium (DMEM) supplemented with 10% fetal bovine serum and 1% L-glutamine. Additional cell lines included MDA-MB-231, MCF-7 and JMAR, which were maintained in DMEM with 10% fetal bovine serum and 1% L-glutamine. Preceding proliferation studies, cells were trypsinized and seeded into 96-well plates (5,000 cells/well). After 24 h, CDDP, HA-Pt, or HA was added (n=12; 6 or 7 concentrations), and 72 h post-addition, resazurin blue in 10 μl of phosphate-buffered saline was added to each well (final concentration of 5 μM). After 4 h, well fluorescence was measured (λ_{ex} 560 nm, λ_{em} 590 nm) using a spectroflurometer (SpectraMax Gemini; Molecular Devices, Sunnyvale, CA). IC_{50} was determined as the midpoint between untreated (positive) and cell-free (negative) controls for each plate.

HA-Pt conjugates had similar anti-proliferative activity to free cisplatin in cell culture. Toxicity was evaluated in the human breast cancer cell lines MDA-MB-468LN, MDA-MB-231 and MCF-7 and human head and neck cancer cell line MDA-1986 (Table 2). Two types of HA-Pt conjugates were evaluated, including HA-Pt formulation with sliver and silver-free HA-Pt
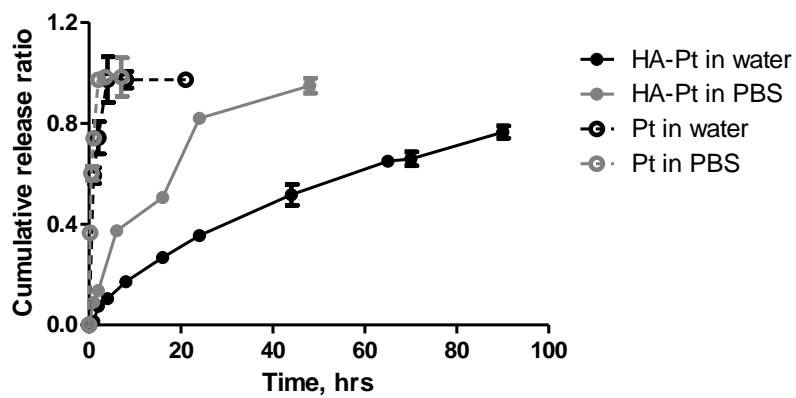
Figure 1. *In vitro* drug release in water and physiological PBS at 37 °C.

Treatment/IC$_{50}$	MDA-MB-468LN	MDA-MB-231	MCF-7	MDA-1986	JMAR
HA	> 10 mg/mL	> 10 mg/mL	> 10 mg/mL	> 10 mg/mL	Not tested
CDDP	5 µg/mL	6 µg/mL	6 µg/mL	2 µg/mL	2 µg/mL
HA-Pt (Ag free)	10 µg/mL	10 µg/mL	11 µg/mL	2 µg/mL	2 µg/mL
HA-Pt (w/ Ag)	9 µg/mL	4 µg/mL	6 µg/mL	Not tested	Not tested

Table 2. IC50 values of HA-Pt and CDDP in various human cancer cell lines.

conjugates. In all cell lines, there was no significant difference in toxicity between HA-Pt and cisplatin. Carrier HA had no toxicity to human cells over the concentration range examined (up to 10 mg/mL).

5. Pharmacokinetics and tissue distribution

Sprague-Dawley rats (female, 200-250 g) were cannulated in the left jugular vein under isoflurane anesthesia and were allowed to recover overnight. Animals were then administered i.v. CDDP, i.v. HA-Pt, s.c. HA-Pt, or s.c. CDDP (1.0 or 3.3 mg/kg equivalent cisplatin; n=5 for each group) under isoflurane anesthesia. Subcutaneous injections were given in the uppermost right mammary fat pad of the animal. Whole blood was withdrawn (200 µl) from the cannula at 0, 5, 30 min, 1, 2, 4, 6, 12, 24, 48 and 96 h, after dosing and was placed into 2-ml centrifuge tubes pretreated with heparin. The cannula was washed before and after withdrawal with saline and then heparin locked. The whole blood was centrifuged at $17,000 \times$ g for 5 mins, and the plasma was frozen at -80 ℃ until analysis.

In the tissue distribution studies, age and weight matched animals were administered the drugs and euthanized at the previously stated time-points. The right ipsilateral axilla nodes (treated side) (Figure 2), left contralateral axilla nodes (control side), and major organs (liver, kidneys, heart, spleen, lungs, brain, muscle, and bladder) were excised; washed with 0.9% saline; and stored at -80 ℃ until analysis. Typically, a 50 mg tissue sample was digested using 1.5 ml of 6.7% nitric acid for 2 hours at 80 ℃. After digestion, samples were homogenized (Tissue Tearor; BioSpec Products Inc., Bartlesville, OK) and centrifuged. The supernatant and plasma samples
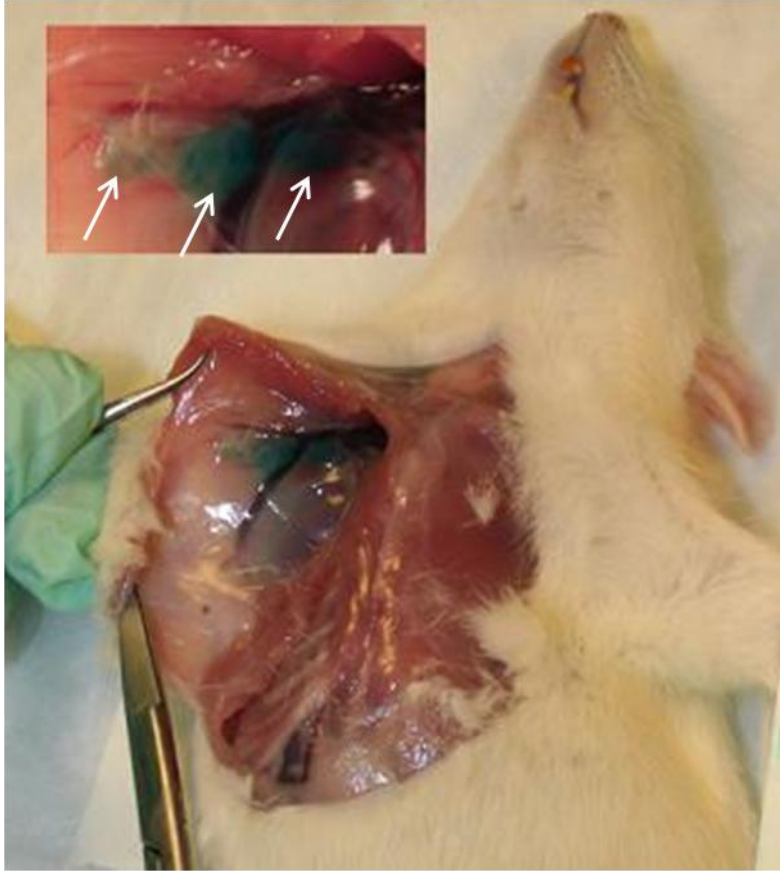
Figure 2. The axial lymph node package was excised after euthanizing animals (white arrows). In order to identify draining lymph nodes, 100 uL of patent blue was injected subcutaneously into the fatpad and the animal euthanized after 5 min (patent blue was not used in distribution studies).

were analyzed by AAS as described in the Synthesis section.

The pharmacokinetics parameters of HA-Pt and CDDP were determined by fitting individual animals' data to a two-compartment model with SAAM II (version 1.2, University of Washington) (Table 3). The area under the curve (AUC) of s.c. HA-Pt was 660% greater than i.v. CDDP. The plasma half life (t½) of s.c. HA-Pt was 200% greater than i.v. CDDP and 490% greater than i.v. HA-Pt. Clearance rates (Cl) of s.c. HA-Pt and i.v. HA-Pt were not significantly different, but the total body clearance (Cl) of i.v. CDDP was 590% greater than s.c. HA-Pt. The steady-state volume of distribution (Vss) of platinum was greater for the i.v. CDDP than s.c. or i.v. HA-Pt.

The s.c. HA-Pt preferentially accumulated in the draining ipsilateral axillary lymph nodes as compared to the i.v. CDDP control (Figure 3); preferential accumulation was still evident at 48 h post-injection despite an *in vitro* disassociation half-life of Pt from HA of 10 h. The ipsilateral axillary node AUC of HA-Pt when injected locally was 279% greater than i.v. CDDP node levels (p<0.001), and the peak node concentration (C_{max}) of HA-Pt was 520% greater than i.v. CDDP. The relative organ AUCs for i.v. CDDP were kidneys > axilla nodes > spleen > liver > bladder > brain > muscle > lungs > heart; for s.c. HA-Pt, ipsilateral axilla nodes > kidneys > liver > heart > contralateral axilla nodes > spleen > lungs > brain > muscle > bladder (Table 4). CDDP was injected s.c. as a comparision to the nanocarrier HA-Pt. There was no apparent increase in concentration in the draining lymph nodes, but the muscle tissue near the injection site had the highest platinum concentrate relative to the other tissues.

The pharmacokinetics of s.c. HA-Pt was greatly altered compared to the same carrier administered i.v. or the standard i.v. CDDP formulation. The greatly increased AUC of HA-Pt

Parameters	Unit	CDDP i.v.	HA-Pt i.v.	HA-Pt s.c.	CDDP s.c.
V_{ss}	l/kg	8.310±3.508	0.154±0.038	3.628±0.760	3.585±2.420
AUC_{0-inf}	(µg·h)/ml	14.104±4.570	141.176±38.878	107.122±59.062	56.707±27.102
Cl	l/(kg·h)	0.257±0.097	0.030±0.007	0.037±0.028	21.790±13.749
C_{max}	µg/ml	4.025±0.265	59.864±5.504	1.035±0.688	2.713±0.381
MRT	h	5.148±2.510	2.640±1.153	15.497±4.943	15.263±7.554
$t_{1/2}$ (β)	h	3.568±1.740	1.830±0.800	10.742±3.426	10.580±5.236

Table 3. Pharmacokinetics of formulations. Data were modeled using a two-compartment model for individual animals and then averaged for each group (n = 5, average ± STD).
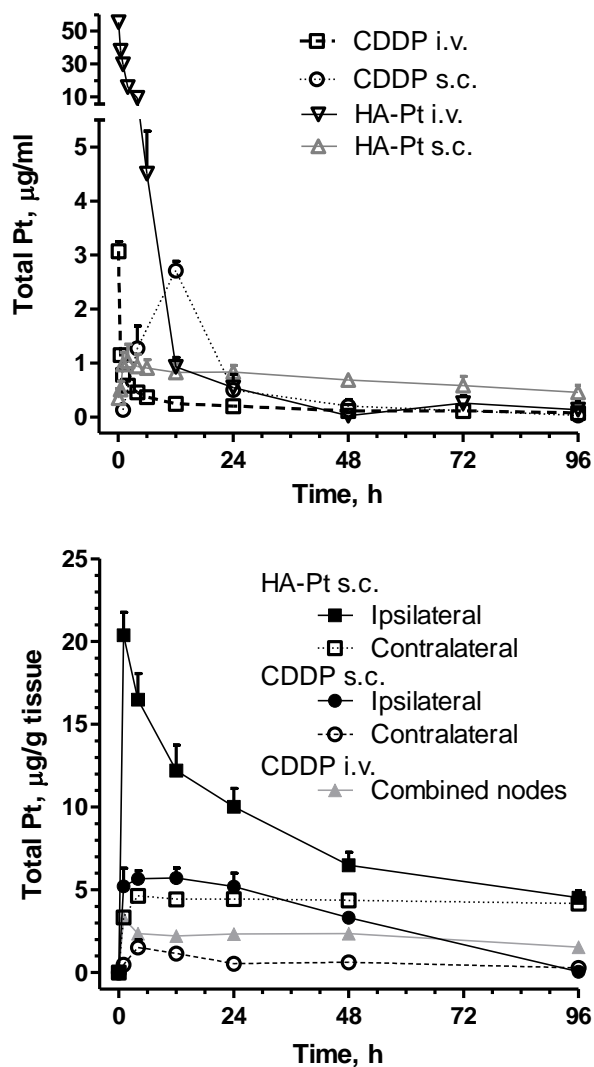
Figure 3. Plasma concentration of Pt after i.v. or s.c. injection of CDDP or HA-Pt (3.3 mg/kg Pt-basis) (Top panel). Concentration of Pt in ipsilateral (right) axillary nodes and contralateral (left) axillary nodes after i.v. or s.c. injection of CDDP or s.c. HA-Pt nanoconjugates (3.3 mg/kg Pt-basis) into the right mammary fatpad (Bottom panel).

Tissue	AUC$_{0-96 h}$, µg/g·h			C$_{max}$, µg/g (T$_{max}$)		
	CDDP i.v.	HA-Pt s.c.	CDDP s.c.	CDDP i.v.*	HA-Pt s.c.	CDDP s.c.
Heart	128 ±8	465 ±23	422±120	1.7±0.1 (1 h)	14.7±1.1 (1 h)	13.6±8.5 (4 h)
Lungs	139 ±7	347 ±13	170±92	2.2±0.1 (1 h)	7.5±0.7 (1 h)	9.0±6.7 (4 h)
Kidneys	291±8	669±28	517±76	4.6±0.4 (1 h)	12.3±2.5 (4 h)	10.5±3.1 (4 h)
Brain	152±11	344±22	341±57	2.3±0.1 (1 h)	7.5±2.0 (4 h)	9.4±4.2 (4 h)
Liver	178±5	495±20	359±33	2.9±0.2 (4 h)	10.6±2.2 (4 h)	10.8±2.5 (12 h)
Spleen	201±7	384±15	299±34	3.0±0.4 (1 h)	6.6±0.6 (4 h)	8.9±1.6 (4 h)
Muscle	151±9	262±15	367±27	2.2±0.2 (1 h)	8.5±2.1 (4 h)	11.9±5.9 (4 h)
Bladder	162±10	194±6	50±38	3.1±0.4 (1 h)	2.9±0.4 (4 h)	2.0±1.1 (1 h)
Ipsilateral axilla nodes	205±12 **	776±9	312±19	3.3±0.3 (1 h)	20.4±1.4 (1 h)	1.7±1.0 (4 h)
Contralateral axilla nodes	205±12 **	413±17	60±41	3.3±0.3 (1 h)	4.6±0.3 (4 h)	5.7±1.3 (12 h)

Table 4. Tissue AUC (average ± STD) and C_{max} (average ± STD) of 3.3 mg/kg i.v. CDDP and s.c. HA-Pt study groups. Two-way ANOVA analysis revealed study groups (CDDP and HA-Pt) differed significantly for all tissues, $p<0.001$ (n=5). * The first tissue sampling was at 1 hr so a C_{max} prior to this would not be detected. The first plasma sampling was at 5 mins. ** For i.v. CDDP, the bilateral axilla nodes were assayed together.

s.c. is consistent with sustained release of platinum by the nanocarrier. This effect may be due both to the delayed diffusion of platinum from the s.c. injection site and the slow release of conjugated platinum from the carrier as i.v. administration of HA-Pt also resulted in relatively large AUC. In a previous study, it was determined that CDDP administered s.c. gives rise to a comparable AUC (15), although this known vesicant can be highly inflammatory to tissues, which may alter the diffusion rate. The relatively small Vss and Cl and large AUC of i.v. HA-Pt indicates platinum release from the carrier may be slow. CDDP is readily eliminated renally but the highly molecular weight of HA-Pt precludes rapid renal clearance. Pharmacokinetic modeling suggests the nanocarrier also slowed the rate constant of distribution transfer of platinum from the plasma compartment to the tissues, which was approximately 10-fold slower for i.v. HA-Pt compared to i.v. CDDP. This was possible due to the ionization state and high molecular weight of hyaluronan, which is naturally cleared from the body by lymphatic transport into the systemic circulation followed by enzymatic degradation in the liver. CDDP administered s.c. did not significantly improve node concentrations, giving slightly lower exposure than i.v. CDDP. Indeed, the majority of CDDP administered s.c. was retained in the surrounding muscle tissue. Since CDDP is a known vesicant, subcutaneous administration is not a safe and feasible option in the absence of a drug carrier such as the hyaluronan nanoconjugate.

Clinical studies have indicated that CDDP's severe dose-limiting side-effects are likely due to the high peak plasma levels (C_{max}) experienced immediately after i.v. administration. Recent applications of metronomic dosing regimens have been shown to decrease toxicity although they are clinically cumbersome and inconvenient and resulted in increased costs to patients [6-7]. Based on our preliminary experience with this delivery system, locally administered nanocarrier chemotherapeutics may avoid high peak concentrations due to slow

release of platinum from the carrier, with a half-life in saline of around 11 h compared to 4 h for the standard CDDP formulation [18], and also as a result of slow platinum diffusion from the tissues or lymph into the systemic circulation after release from the carrier.

The increased tissue concentrations of platinum achieved with s.c. HA-Pt compared to i.v. CDDP carries two potential advantages: (1) This could result in a lower dose of platinum being required to achieve the same tissue effect such that the HA-Pt dose may be reduced by several fold and still maintain equivalent tissue levels; and (2) maintaining therapeutic systemic concentrations of drug is important for utilizing this drug as an adjuvant therapy since it is well known that most patients with cancers which have metastasized to the locoregional lymph nodes likely have micro in addition to systemic macrometastases. Therefore, this treatment if extendable to the clinical situation could potentially replace daily systemic intravenous therapy utilizing a less invasive and less-frequent dosing schedule, e.g. weekly subcutaneous dosing as compared to current therapy which is daily intravenous infusion, while simultaneously providing augmented local drug delivery and exposure over time to the locoregional tumor basin and lymphatics. The larger tissue AUC of s.c. HA-Pt may also increase rates of tumor apoptosis since a recent study found that a prolonged subtoxic level of CDDP can substantial improve tumor cell apoptosis compared to a single high dose [19]. Overall, assuming linear pharmacokinetics, the total platinum dose for local HA-Pt therapy could be reduced by 75% while maintaining the same systemic and node concentrations of platinum as i.v. CDDP, possibly with lower concentrations in the other tissues with the exception of the heart.

6. **Toxicology analysis: renal toxicity and ototoxicity**

Sprague-Dawley rats (35 females) were randomly divided into study groups of 5 animals each and dosed: 1.0 mg/kg s.c. HA-Pt (with and without silver; platinum equivalent to 1.0 mg/kg CDDP), 3.3 mg/kg s.c. HA-Pt (with and without silver), i.v. CDDP at 1.0 and 3.3 mg/kg, and s.c. HA (control; HA equivalent to 3.3 mg/kg HA-Pt). Each animal was administered a single bolus dose at the beginning of the 30-day study period. Urine samples were collected every day during the first two weeks of the study and every four days during third and fourth week of the studies except for the 3.3 mg/kg HA-Pt with silver group, which will be discussed later. In order to reduce the morbidity to animals, subjects were housed in metabolic cages for 12 h to collect approximately 5 ml of urine and then returned to cages with bedding until the next collection period. Urine samples were centrifuged at 17,000 x g for 5 mins and stored in -80 ℃ freezer until creatinine analysis.

Urine creatinine was analyzed using the QuantiChrom™ Creatinine Assay Kit according to the manufacturer's instructions (BioAssay Systems, Hayward, CA). The values of the optical density were measured using a UV plate reader. Creatinine concentration of the sample was calculated as $(OD_{SAMPLE\ 5} - OD_{SAMPLE\ 1}) / (OD_{STD\ 5} - OD_{STD\ 1})$ x [STD] (mg/dL). $OD_{SAMPLE5}$, $OD_{SAMPLE1}$, OD_{STD5}, and OD_{STD1} are OD_{510nm} values of sample and standard at 5 min and 1 min, respectively. [STD] is 50 mg/dl for the urine assay.

Urine creatinine levels are an indirect indicator of glomerular filtration rate, which can indicate changes in renal function and renal toxicity. A decrease in creatinine excretion corresponds to decreased renal function and possible renal toxicity or damage. Significant renal toxicity was observed in animals that received silver activated HA-Pt nanoconjugate (3.3 mg/kg), with a 30% decrease in creatinine excretion apparent at 3 days and a 70% decrease at 4 days

(Figure 4). All animals in this group died within one week of treatment due to drug-related cachexia. In contrast, the silver-free HA-Pt did not demonstrate significant toxicity, and creatinine levels remained near pre-dosing levels throughout the study's duration. Toxicity as measured by creatinine excretion was compared to the previous silver formulation, which had not been previously assessed. The silver-free formulations reported here demonstrate significantly less renal toxicity.

It was expected that lymphatic delivery of platinum would reduce systemic tissue exposure compared to i.v. CDDP, but s.c. HA-Pt had a much greater AUC than i.v. CDDP in most tissues including the kidneys (Table 4). The Vd is affected by the partition coefficient along with the tissue and plasma protein binding, which may be different between the parent CDDP and the nanoconjugate HA-Pt. However, the urine creatinine studies did not indicate an increase in toxicity. The reduction in toxicity could be due to protection of tissues by the nanocarrier; hyaluronan is frequently used in the clinic as a rescue therapy after accidental venipuncture by intravenous lines. The predominant chemical form of platinum in the kidneys may differ significantly between the two formulations as AAS measures only total elemental platinum, so it is unknown if the platinum from HA-Pt was detoxified before renal uptake. This could provide an explanation as to why the higher accumulated AUC seen in the kidney with HA-Pt was not as destructive as i.v. CDDP. CDDP ($Pt[(NH_3)_2Cl_2]$) is believed to become nephrotoxic after the displacement of a single chloride ion, which leads to the conjugation of a positively charged aqua ligand and glutathione, followed by a series of metabolic reactions ultimately leading to cysteine-conjugates that can produce highly reactive thiol species in the proximal tubule cells [20]. Since the mechanism of platinum release and metabolism from HA is still under investigation, it is unknown if platinum reaching the kidneys from HA-Pt complexes is significantly detoxified
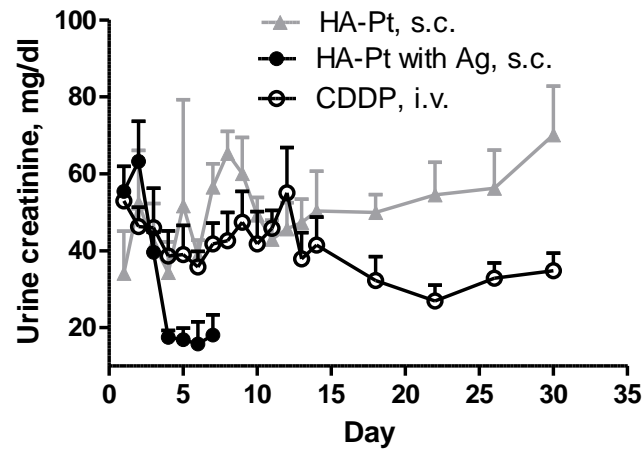
Figure 4. Urine creatinine concentration of animals that received 3.3 mg/kg HA-Pt with or without silver or i.v. CDDP (n=5, p<0.05).

unlike the free drug in the i.v. CDDP treatment. Future work is to examine the distribution of nanocarrier-bound and free platinum at the cellular level in the tissues and tumors of xenografts by transmission electron microscopy.

Cisplatin is known to induce dose-dependent ototoxicity, leading to mostly irreversible auditory impairment, primarily in the high frequencies, in both human and experimental animals [21-22]. Cisplatin is highly plasma protein bound after intravenous administration. Approximately 96% of the drug becomes biologically inactive after it binds to the plasma protein, principally serum albumin; whereas the monohydrated fraction of the free drug causes ototoxicity and injures the cochlea [22-23]. Cisplatin ototoxicity was likely due to the generation and release of reactive oxygen species post exposure of the mechanosensory hair cells to the active form of the drug [24]. The use of protective antioxidants was demonstrated to attenuate the injuries to the hair cells caused by cisplatin chemotherapy due to a free radical scavenging effect [25-27].

In order to check for ototoxicity from the cisplatin tratments, mice were tested for hearing loss. The hearing loss was measured in nude mice after three weekly doses of CDDP i.v. or HA-Pt s.c. chemotherapy. Saline was injected via tail vein into a group of control animals. At the fourth week, a probe was placed inside the external auditory canal of anesthetized mice and an acoustic stimulus was delivered using Smart OAE (Intelligent Hearing Systems, Miami, FL). Distortion product otoacoustic emission (DPOAEs) was recorded and graphed. Frequencies tested range from 3,000 to 32,000 Hz. The amplitude was recorded in dB SPL (decibel sound pressure level).

In this study, mice in both the control and treated groups (saline i.v., CDDP i.v. and HA-Pt s.c.) exhibited otoacoustic emission, which indicated that the cisplatin-targeted mechanosensory hair cells in the inner ear region remained functional. However, no statistically significant differences were observed between groups, which is likely due to the relatively low doses of cisplatin (3.5 mg/kg × 3 wks) that were administered. Zuur et al. reported that low-dose intravenous cisplatin chemotherapy caused less acute hearing loss, compared to high-dose therapy in a study of 60 patients [28]. Studies at a higher dose or more frequent dosing schedule may better reveal the influence of dosing to the degree of ototoxicity.

7. Pathology

Healthy Sprague-Dawley rats (250–300 g, Charles River) were randomly divided into 2 groups and administered CDDP intravenously via the tail vein or HA-Pt subcutaneously into the mammary fat pad (1.0 mg/kg or 3.3 mg/kg platinum basis, n = 5/group). The animals were euthanized after 4 weeks, and the liver, bilateral kidneys, spleen, lungs, heart, right (ipsilateral) and left (contralateral) axillary nodes, and brain were excised intact and stored in 80% alcoholic formalin solution overnight for fixation before slide mounting. Mounting using hematoxylin and eosin (H&E) staining were conducted by Veterinary Laboratory Resources (Kansas City, KS). The pathological examination was performed by a blinded board-certified veterinarian pathologist (University of Kansas Medical Center, Kansas City, KS).

At the conclusion of the 30-day toxicity study, animals were euthanized, and a full pathological examination was performed. Brain tissue and underlying tissue of the injection site were noted to be normal in appearance with no microscopic changes for all study groups. Very

mild changes in lymph nodes were detected for high-dose intravenous CDDP (3.3 mg/kg) and subcutaneous HA-Pt. Very mild morphological changes were observed in the livers for animals receiving both low-dose CDDP intravenously (1.0mg/kg) and low-dose HA-Pt subcutaneously as indicated by the presence of mild inflammation in the sinusoids (Figure 5). Mild degeneration with some sinusoidal necroses was observed for animals receiving high-dose intravenous CDDP and high-dose subcutaneous HA-Pt treatment. Necroses, however, were more severe in the intravenous CDDP group. In addition, 60% of animals receiving low-dose intravenous CDDP were observed to develop mild renal necrosis including hemorrhage into the renal tubules along with tubular edema. In contrast, none of the animals receiving low-dose subcutaneous HA-Pt had renal tubular necrosis. Similarly, 4 of 5 (80%) animals receiving high-dose intravenous CDDP compared with 1 of 5 (20%) animals receiving high-dose subcutaneous HA-Pt were diagnosed with mild renal tubular necrosis. Overall, the pathology studies showed that the HA-Pt conjugates had a lower incidence of both renal and hepatic toxicity compared with the conventional i.v. CDDP treatment at all dose ranges. Additionally, no neurotoxicity (in the brain tissue) or inflammation of injection site (in the underlying muscle tissue) was observed in the treated animals. A representative picture regarding the histological status of kidneys, liver, lymph nodes, brain and muscle tissue from each treatment group was collected, and diagnosed and classified into three categories (Grade 0, Grade 1 and Grade 2 with elevating severity of toxicity (Figure 6-10, Table 5).

8. Development of mouse xenograft models for *in vivo* imaging and efficacy evaluation

8.1 Part A: development of a breast cancer model for *in vivo* imaging
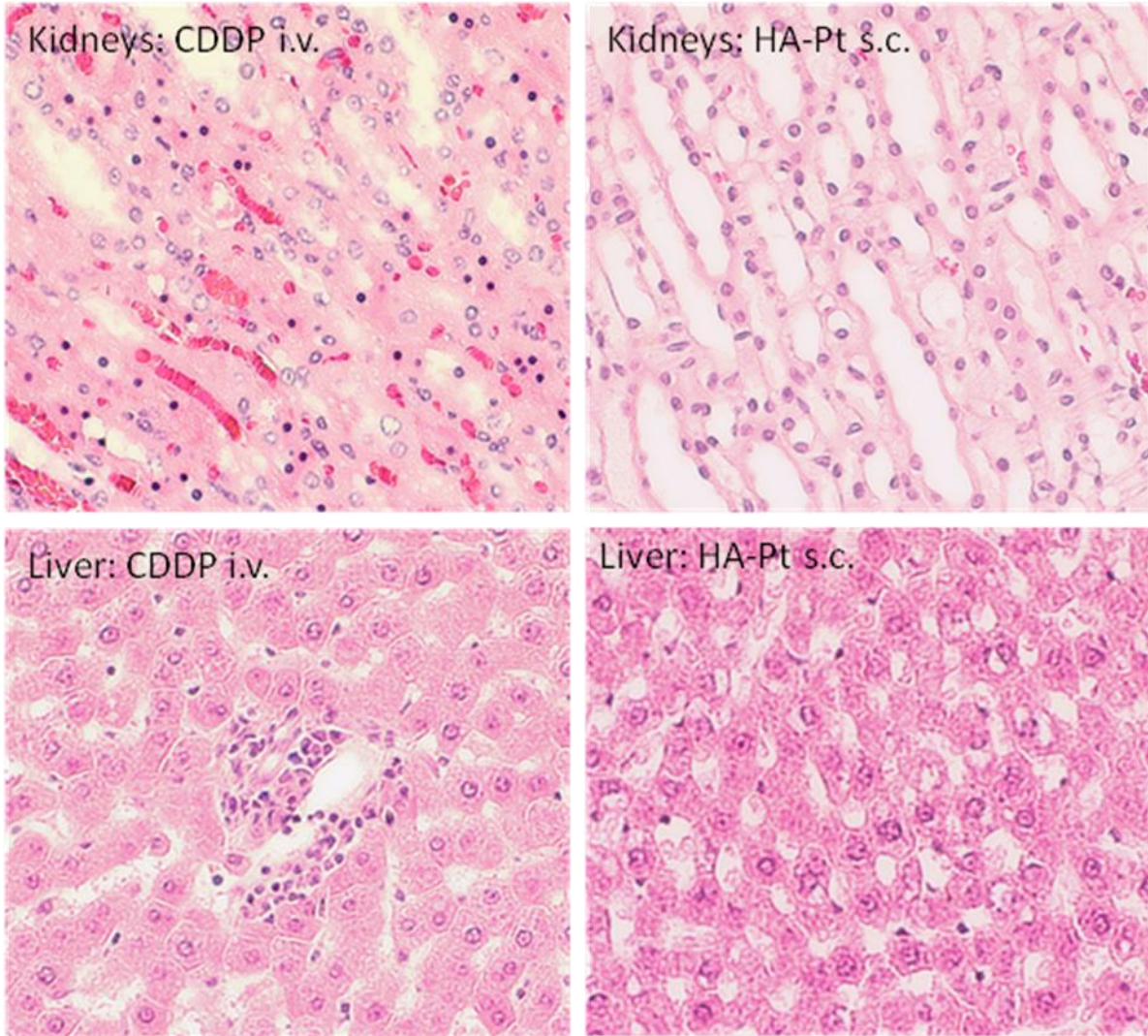
Figure 5. Kidneys of the subcutaneous HA-Pt group exhibited a normal appearance except for sparse minimal tubular cell necrosis, whereas the intravenous CDDP treatment group had pyknotic nuclei and apoptosis in the medullary tubular epithelia cells. Livers of the subcutaneous HA-Pt group showed very minor hepatitis, but otherwise appeared normal; whereas the intravenous CDDP treatment group had necrotizing lesions and hepatitis. Sprague-Dawley rats were injected subcutaneously into the mammary fat pad with HA-Pt or intravenously with CDDP (3.3mg/kg). Slides are typical of animals in each study group (n = 5).
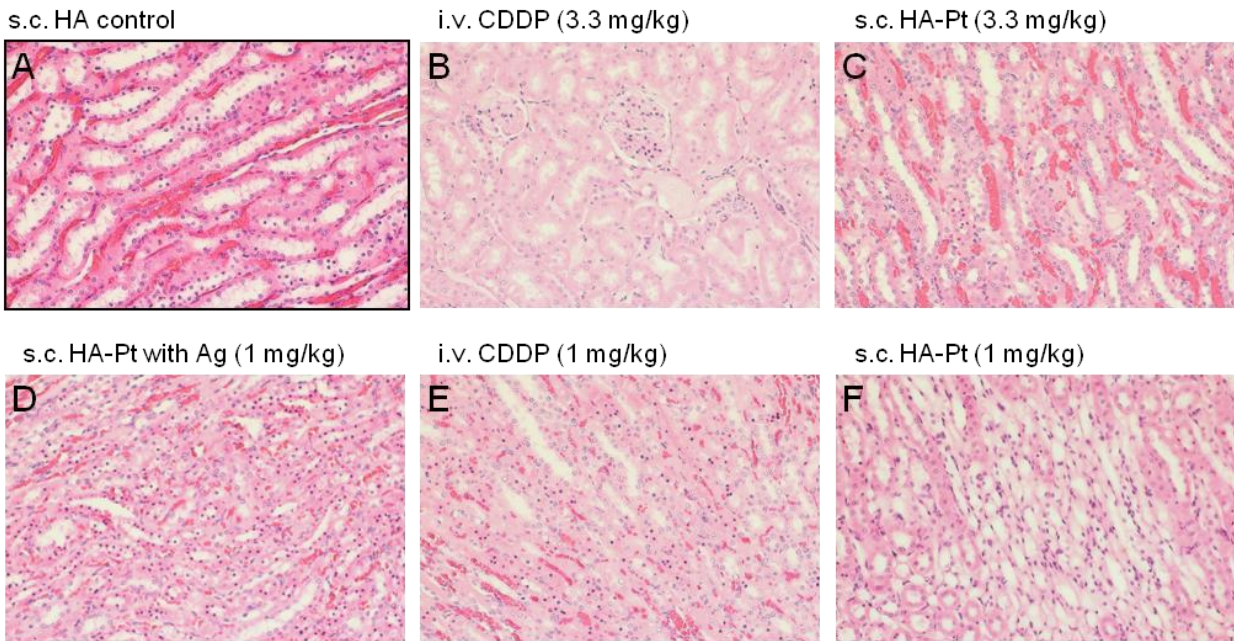
Figure 6. Kidney tissue analysis 30 days post injection. Tissues were stained with H&E. (A) Animals receiving s.c. injection of HA had normal findings; (B) animals receiving high dose i.v. CDDP had degenerative changes, such as pyknotic nuclei in corticomedullary tubular cells; (C) animals receiving SC high dose HA-Pt without silver had fairly a normal appearance, except for minor foci of the tubular cell necrosis at the corticomedullary junction; (D) animals receiving low dose s.c. HA-Pt with silver had widely spread pyknotic nuclei in medullary tubular epithelial cells; (E) animals receiving low dose i.v. CDDP had pyknotic nuclei in medullary tubular epithelial cells, an increase in dark purple staining suggesting nuclear staining and widespread apoptosis; (F) animals receiving low dose s.c. HA-Pt without silver had normal appearance, except for minimal renal tubular cell swelling and degeneration.
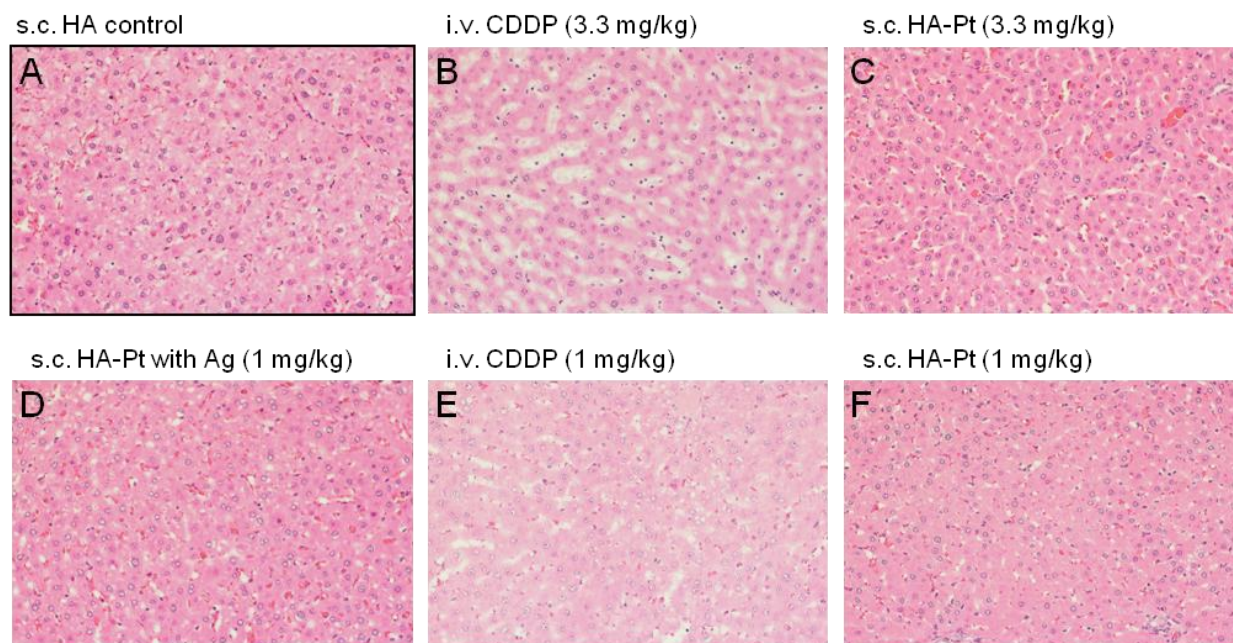
Figure 7. Liver tissue analysis 30 days post injection. Tissues were stained with H&E. (A) Animals receiving s.c. injection of HA had normal findings; (B) animals receiving high dose i.v. CDDP had moderate necrosis; (C) animals receiving high dose s.c. HA-Pt without silver had fairly normal appearance except for very mild degeneration; (D) animals receiving low dose s.c. HA-Pt with silver had fairly normal appearance except for very mild degeneration; (E) animals receiving low dose i.v. CDDP had fairly normal appearance except for very mild degeneration; (F) animals receiving low dose s.c. HA-Pt without silver had normal appearance.
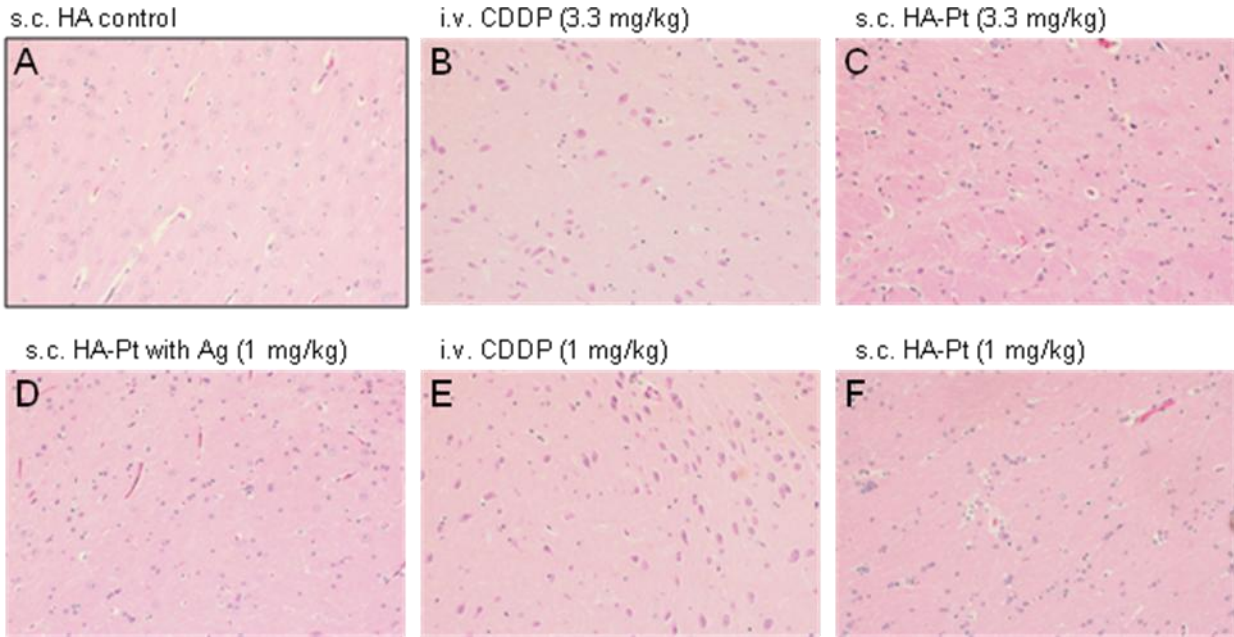
Figure 8. Brain tissue analysis 30 days post injection. Tissues were stained with H&E. (A) Animals receiving s.c. injection of HA had normal findings; (B) animals receiving high dose i.v. CDDP had normal appearance; (C) animals receiving high dose s.c. HA-Pt without silver had normal appearance; (D) animals receiving low dose s.c. HA-Pt with silver had fairly normal appearance; (E) animals receiving low dose i.v. CDDP had normal appearance; (F) animals receiving low dose s.c. HA-Pt without silver had normal appearance.
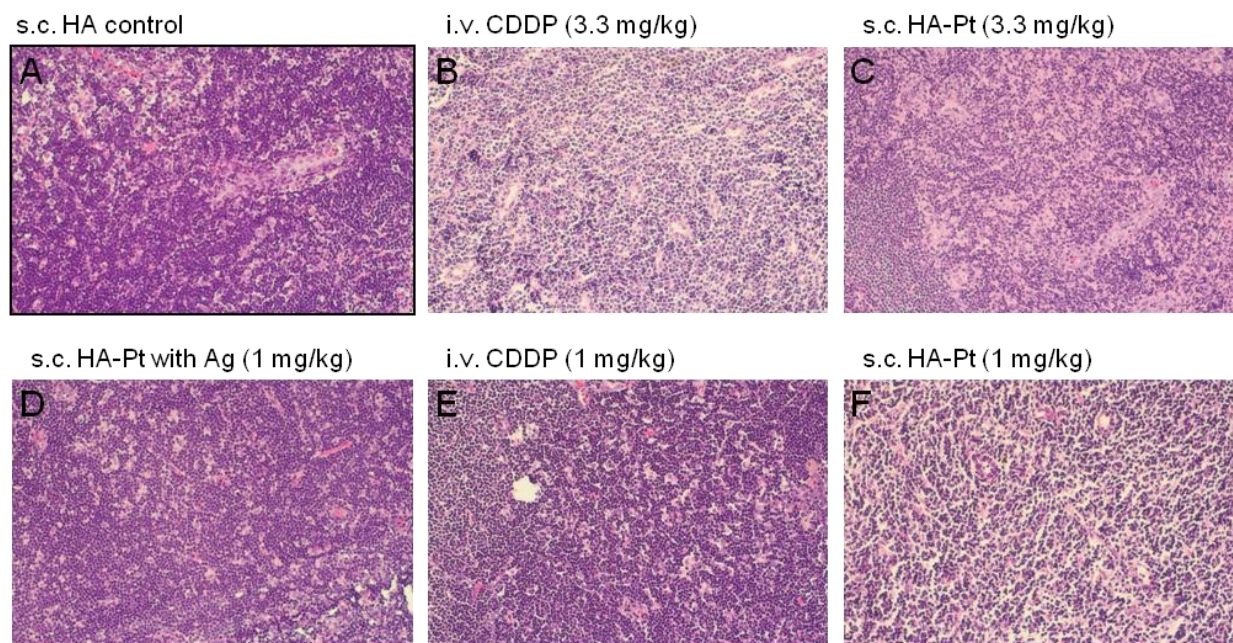
Figure 9. Lymphoid tissue analysis 30 days post injection. Tissues were stained with H&E. Animals receiving (A) s.c. injection of HA; (B) high dose i.v. CDDP; (C) high dose s.c. HA-Pt without silver; (D) low dose s.c. HA-Pt with silver; (E) low dose i.v. CDDP; and (F) low dose s.c. HA-Pt without silver all had normal lymph node appearance.
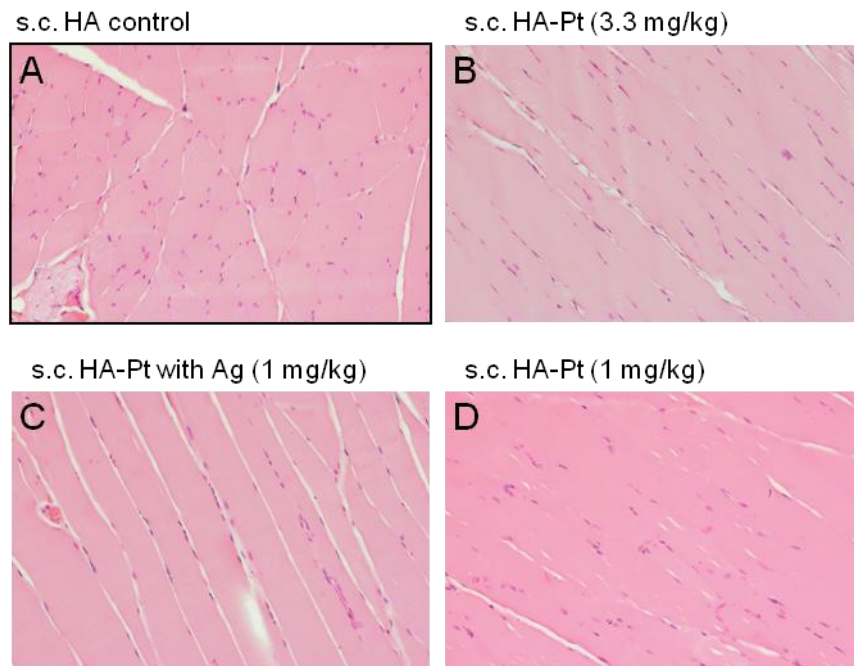
Figure 10. Analysis of underlying tissue at the injection site 30 days post injection. Tissues were stained with H&E. Animals receiving (A) s.c. injection of HA; (B) high dose s.c. HA-Pt without silver; (C) low dose s.c HA-Pt with silver; (D) low dose s.c HA-Pt without silver all had normal appearance.

Treatment	Liver	Kidney	Lymph nodes
Low Pt	40% Grade 0, 40% Grade 1, 20% Grade 2	20% Grade 0, 20% Grade 1, 60% Grade 2	100% Grade 0
Low HA-Pt	20% Grade 0, 60% Grade 1, 20% Grade 2	20% Grade 0, 80% Grade 1	60% Grade 0, 40% Grade 1
High Pt	60% Grade 1, 40% Grade 2	20% Grade 1, 80% Grade 2	80% Grade 0, 20% Grade 1,
High HA-Pt	20% Grade 0, 60% Grade 1, 20% Grade 2	20% Grade 0, 60% Grade 1, 20% Grade 2	60% Grade 0, 40% Grade 1,

Table 5. Diagnostic grading of the severity of organ toxicities.

For *Kidneys:*

Grade 0: Normal (no symptoms)

Grade 1: Minimal necrosis

Grade 2: Mild necrosis (includes degeneration and nuclear pyknosis)

For *Livers:*

Grade 0: Normal (no symptoms)

Grade 1: Inflammation (includes granulomas, microranulomas and hepatitis) or inclusions

  -Hepatitis: inflammation of the liver caused by a virus or a toxin

  -Granulomas: a tumor composed of granulation tissue resulting from injury or inflammation
  or infection.

  -Inclusions: any small intracellular body found within another (characteristic of certain
  diseases)

Grade 2: Degeneration or necrosis

For *Lymph nodes:*

Grade 0: Normal (no symptoms)

Grade 1: Mild lymphoid hyperplasia or depletion

The MDA-MB-468LN breast cancer cells were trypsinized (0.25% w/v trypsin) and prepared in 1X phosphate buffered saline solution at 3 different cell concentrations (10^5 cells/mL, 10^6 cells/mL, and 10^7 cells/mL). Cells (100 µL) were injected under pentobarbital sedation into the mammary fat pad of female nu/nu mice using a 27-G needle through a 5-mm incision (20–25 g, Charles River). The incision was closed with sterilized wound clips and was removed one week later, when the incision had healed.

Animals developed mammary tumors starting from the third week (Figure 11). The tumor size was measured twice a week with a digital caliper. Tumor volume was then calculated according to the following equation: tumor volume (mm^3) = 0.52 × (width)^2 × length (Figure 12). Animals were euthanized before the end of the study, when their tumor size reached 2,000 mm^3 or the body score index fell below 2.

The MDA-MB-468LN cell line was transformed with a green fluorescent protein to allow for tumor growth monitoring by whole-body fluorescent imaging, using a CSI Maestro imaging system (Version 2.4, Woburn, MA) with a 445- to 490-nm filtered halogen excitation light and a 515-nm longpass emission filter. The fluorescence was measured in 10-nm bandpass segments from 520 to 720 nm, using a cooled CCD camera using autoexposure. Images were then spectrally unmixed using the automatic deconvolution tools to limit skin and intestine autofluorescence resulting from the chlorophyll in the food (Figure 13). In addition, lymphatic metastases were observed after spectrum unmixing in the draining axillary lymph node package (Figure 14).

The drainage and localization of the lymphatic carrier was verified using a HA-Texas Red dye conjugate. Before imaging, mice were anesthesized, under isoflurane, and HA-Texas Red (10 mg/mL in saline, 20 µL) was injected subcutaneously near the left mammary fatpad of
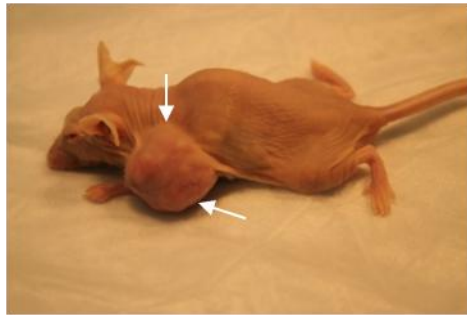
Figure 11. A nude mouse with a mammary tumor (white arrows).
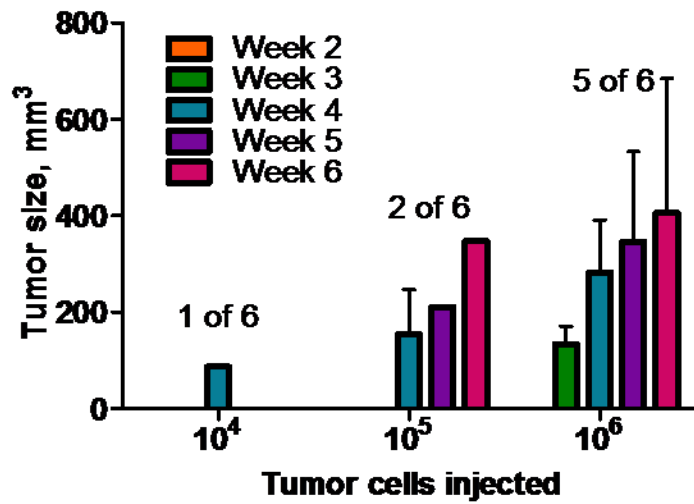
Figure 12. Measurement of tumor size from week 2 to 6. Nude mice were injected with 10^4, 10^5 or 10^6 cells/mouse (N=5).
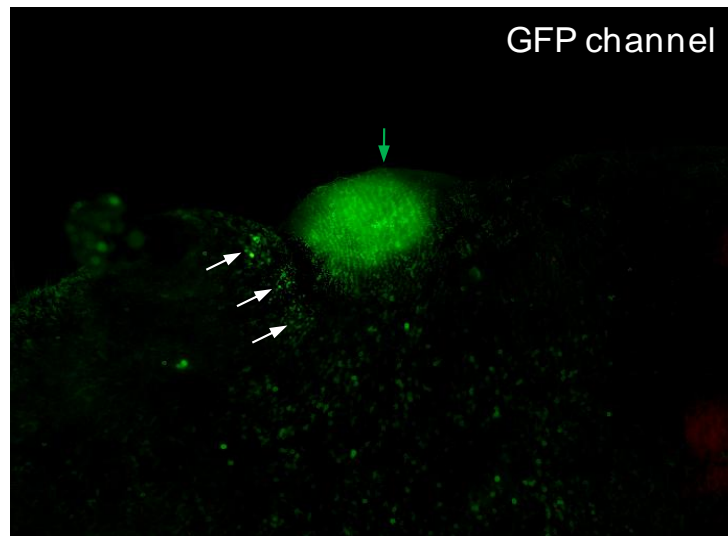
Figure 13. Images of lymphatically metastatic breast cancer xenograft before (top panel) and after (bottom panel) spectrum deconvolution. Tumor develops 3-5 wks after mammary fatpad injection; a primary tumor formed in the draining sentinel node (green arrow) with early metastases invading adjacent axillary nodes (white arrows indicating tumor cell clusters in axilla region).
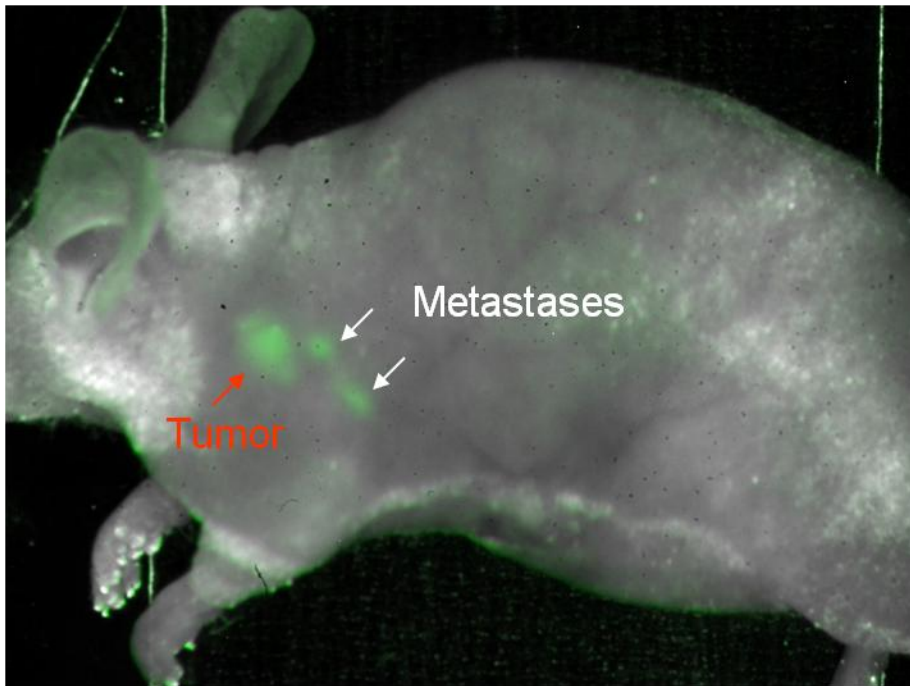
Figure 14. A nude mouse with a primary tumor (red arrow) and multiple metastases (white arrows) in the draining axillary lymph node package.

tumor bearing mice (before injection, Figure 15A). The injection area was massaged gently for 5 min and fluorescently imaged after 5 and 18 hrs (Figure 15B and 15C). Fluorescent conjugates of HA (1 dye/23 HA molecules) drained into the left lymphatic basins after a subcutaneous injection into the left mammary fatpad, with no observed bilateral drainage into the right basin. After 5 hrs, localization of HA in the nodes surrounding the tumor can be clearly observed (Figure 15B). Most of the carrier has localized in the basin of the tumor at 18 hrs with a lesser amount remaining the adjacent axillary node basins (Figure 15C).

8.2 Part A: evaluation of anticancer efficacy in breast cancer bearing mice

Three weeks after cancer cell injection, tumors of 50 mm^3 to 100 mm^3 were observed, and animals were randomly divided into 4 different treatment groups. Treatments including saline i.v., HA s.c., CDDP i.v. (3.3 mg/kg), and HA-Pt s.c. (3.3 mg/kg) were administered in the third and fourth weeks after tumor cells implantation. The tumor size was measured weekly and animal health was closely monitored.

Control animals showed a standard tumor growth curve at 10^6 cells/injection with tumor volumes exceeding 1,000 mm^3 at 6 weeks post-inoculation (Figure 16). Animals dosed with the HA carrier-only showed no difference from the saline control, confirming the *in vitro* data that HA has no direct anticancer activity. The i.v. CDDP-treated animals showed a tumor growth delay of about 3 weeks compared with the controls ($P < 0.05$) with a median survival of 12 weeks (compared with 7 weeks in the controls $P < 0.01$, Figure 16). HA-Pt treated animals had an initial delay in tumor growth of 5 weeks ($P < 0.01$ compared with controls), but this was not significant compared with intravenous CDDP; both curves intersected at the 11th week

113
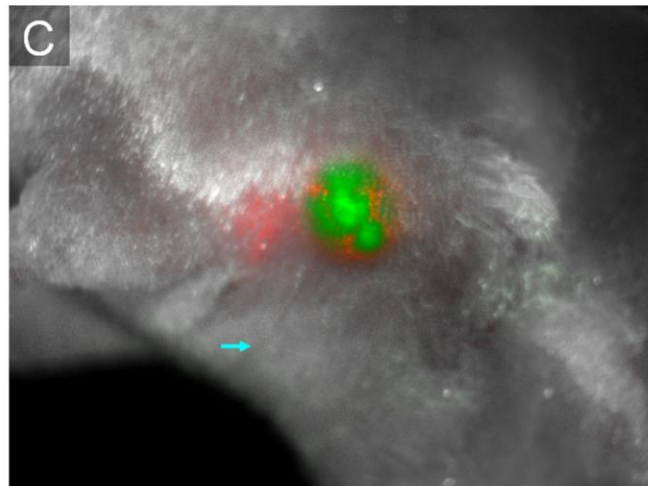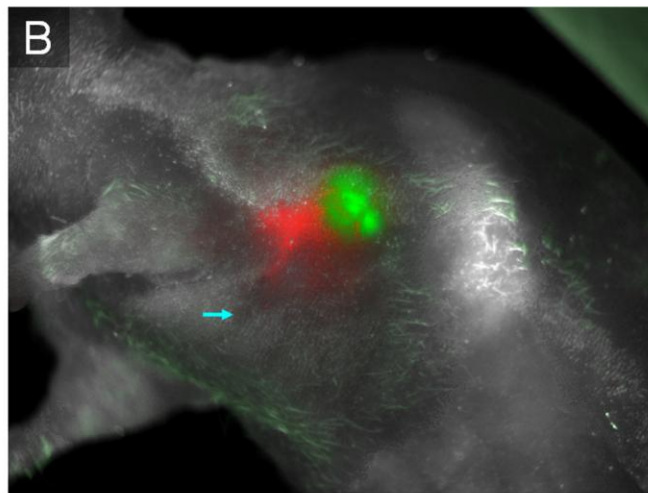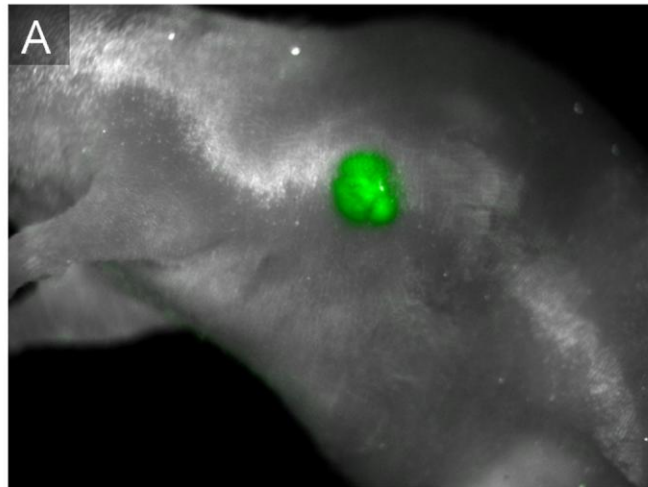
Figure 15. Nude mice bearing MDA-MB-468 breast lymphatic tumors (expressing green fluorescent protein [GFP], panel A) were subcutaneously injected with HA-Texas Red in the left mammary fat pad. After 5 hrs and 18 hrs (B and C, respectively), significant HA localization in the draining nodes, and it was co-localized with the tumor (GFP-channel in green, Texas Red channel in red, blue arrow denotes the injection site).
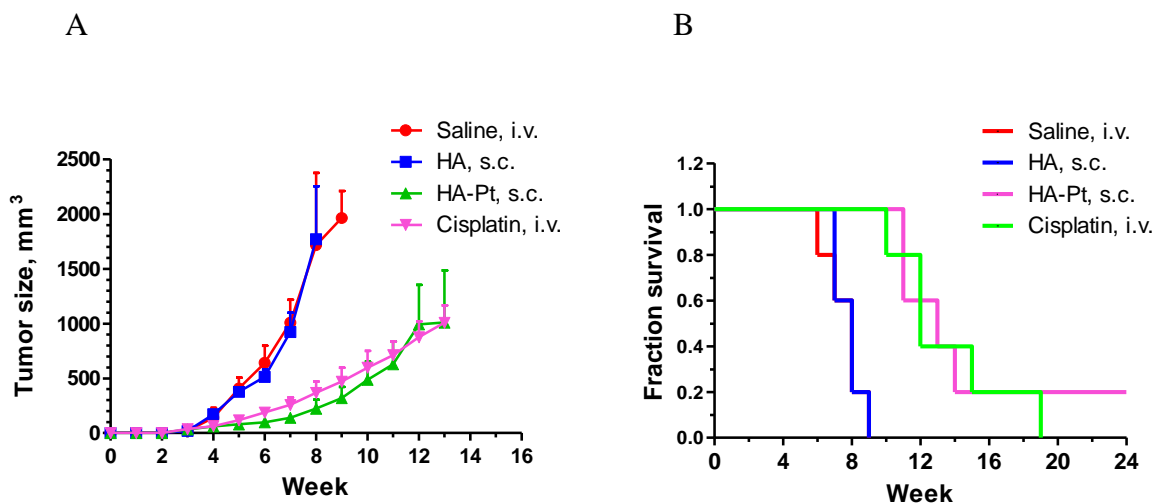
Figure 16. (A) Tumor volume and (B) survival rate. Treatments including saline i.v., HA s.c., CDDP i.v. (3.3 mg/kg), and HA-Pt s.c. (3.3 mg/kg) were administered in the third and fourth weeks after tumor cells implantation.

postinoculation, with a median survival of 12 weeks as well. However, there was one animal in the HA-Pt group who exhibited a complete response to treatment with no measurable tumor and survival well exceeding 24 weeks (upper limit of study). There were no complete responders in the intravenous CDDP group.

Lymphatically delivered chemotherapy through a subcutaneous injection is a novel approach to drug delivery that has only recently been shown by Dr. Forrest's group to be feasible with CDDP. Nanoconjugation of CDDP to hyaluronic acid not only allows for improved locoregional delivery of the drug to the site of greatest tumor burden in the breast and axillary tissues, but also decreases the level of renal toxicity associated with this drug. The toxicity data show that there is no significant injection site toxicity on pathological analysis, indicating that when bound to the carrier, CDDP does not lead to necrosis of the surrounding tissue. It is only after the carrier is cleaved from the conjugate by either hyaluronidase or receptor-mediated endocytosis (hyaluronan is a ligand for CD44, a receptor that is overexpressed on lymph nodes and many cancers including breast cancers and melanoma) that the drug becomes functionally active. In the tissue toxicology analysis, both renal and hepatic toxicity was significantly reduced in the HA-Pt–treated animals compared with the standard CDDP-treated group.

The other benefit noted in the HA-Pt nanoconjugate group involved efficacy in tumor growth inhibition and response *in vivo* in breast cancer xenograft. The HA-Pt versus CDDP tumor growth curves in Figure 16 showed that both drugs effectively delayed the tumor growth in an orthotopic, lymph node metastatic model of breast cancer. The HA-Pt group had an improved although not statistically significant arrest in tumor growth (about 2–3 weeks of additional delay compared with CDDP and a 5- to 6-week delay compared with controls). What was significant was a complete response was seen in 20% of the HA-Pt–treated group and in 0%

of the CDDP-treated group (Figure 16). These data support that HA-Pt injected subcutaneously in the breast has mildly improved efficacy over standard CDDP injected intravenously.

With improved efficacy and reduced toxicity with the nanoconjugate formulation in a metastatic breast cancer model *in vivo*, these data provide solid support for completing further preclinical proof of concept studies to advance this formulation into clinical applications. The benefits of a locally injectable chemotherapeutic over an intravenous infusion include potentially lower cost, because the patient does not have to be physically attached to an infusion pump with nurse or physician supervision, as well as the ability to deliver CDDP weekly with the sustained release properties of the nanoconjugate as opposed to daily administration, used most current intravenous protocols. The sustained-release properties of this nanoconjugate provide an excellent boost to locoregional tumor tissues, while maintaining therapeutic systemic levels and providing promise for potential future use in locally advanced breast cancer, in both the neoadjuvant and adjuvant setting. In addition, localized therapy may be an effective addition to systemic therapy in patients with metastatic disease; localized therapy can provide a higher dose of chemotherapeutic to the most vulnerable tissues than what is possible with systemic therapy alone.

Other published and ongoing studies have shown that HA-Pt given locoregionally provides adequate systemic levels of CDDP, including serum area under the curve levels greater than intravenous CDDP, but without the high (toxic) peak serum concentrations of intravenous therapy. As a result, it was hypothesize that these nanoconjugates would have a useful role in the treatment of locally advanced breast cancer in the neoadjuvant setting, providing enhanced locoregional drug efficacy while maintaining or even enhancing systemic therapy to distant

disease. Further studies will be necessary to evaluate long-term efficacy and toxicity in animal models as well as the role of this nanoconjugate in combination chemotherapy regimens.

8.3 Part B: development of a head and neck cancer model for *in vivo* imaging

The pCLNRX-turbo635 plasmid was constructed by inserting a 715-bp AfeI/HindIII fragment of the pTurboFP635C (Evrogen Inc, Moscow, Russia) into a 7675-bp AleI/HindIII fragment of the pCLNRX retrovirus expression vector (Imgenex, San Diego, CA). The incorporation of the insert was verified by sequencing. Packaging 293-GPG cells were used to generate retroviruses using $CaCl_2$ precipitation method; followed by infecting MDA-1986 human head and neck squamous cell cancer cells, and selection with 0.8 mg/mL G418 for two weeks. Stable protein production and the resulting strong, near-infared cell fluorescence was verified by fluorescence microscopy with a Texas Red filter on an upright microscope.

Stable MDA-1986/Turbo635 cells were prepared in 1×PBS solution at a cell concentration of 10^7 cells/mL. One hundred microliters of the cell solution was injected under pentobarbital sedation into the oral mucosa layer of nude mice using 27-ga needles. The tumor size was measured twice a week using digital calipers on mice anesthetized with 1.5-2 % isoflurane in 50% oxygen-50% ambient air mixture. Tumor volume was calculated using the equation: Tumor volume $(mm^3) = 0.52 \times (width)^2 \times length$.

Before imaging, mice were anesthetized, and Texas Red-HA (10 mg/mL in saline, 100 µL) was injected subcutaneously near the neck of the animal. The injection area was massaged gently for 5 min and fluorescently imaged over 24 hours (CRI Maestro Flex, CRI Inc., Woburn,

MA) using a 445- to 490-nm filtered halogen excitation light and a 515-nm longpass emission filter. Fluorescence was measured in 10-nm bandpass segments from 520 to 720 nm, using a cooled CCD camera using autoexposure. Images were spectrally unmixed using the automatic deconvolution tools (Maestro ver. 2.10) to limit skin and intestine autofluorescence resulting from the chlorophyll in the food.

In this study, an orthotopic murine tumor model of HNSCC was established by injecting human head and neck squamous cell cancer cells, MDA-1986, into the buccal mucosa of nude mice. The model exhibited rapid and sustained tumor growth, with average survival up to 12 weeks after tumor cell implantation. The primary tumor proceeded similar to highly aggressive human HNSCC, invading the mandible and metastasizing to the cervical nodes. To validate the tumor model and verify the incidence of distant metastasis, the intact primary tumor and the draining lymph nodes were removed from the animal and stored in formalin solution overnight for fixation, before the tissues were biopsied. H&E staining tests were conducted, and the histology slides showed muscular (middle panel) and glandular (right panel) invasion of the cancer cells into the lymphatics (Figure 17).

In order for the nanocarriers to deliver anticancer drugs to metastases in the head and neck locoregional lymphatics, the carriers should drain from the tumor area to the diseased lymph nodes. To verify the drainage into the diseased cervical lymph nodes, a HA-Texas Red conjugate was injected peritumorally, and the mouse was imaged 24 hours post injection (Figure 18). The nanoconjugates slowly diffused from the injection site to the primary tumor and peripheral locoregional lymphatics, which harbored the metastases. The targeted drainage of the HA conjugates toward the neoplastic tissue takes advantages of lymphangiogenesis, leading to
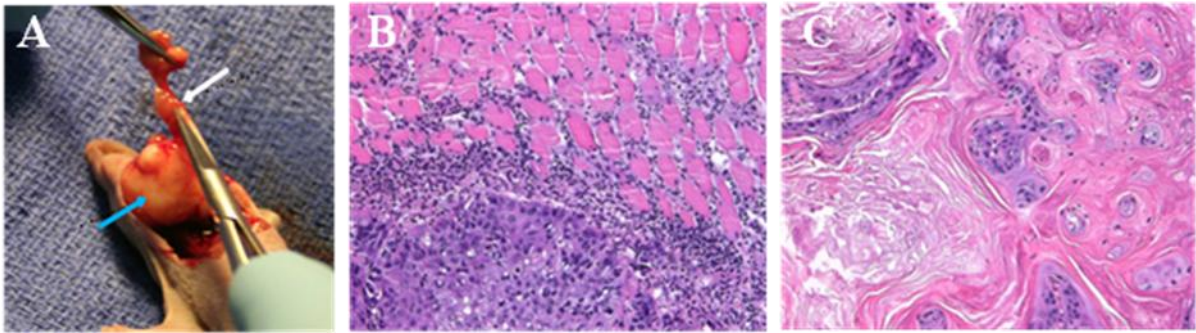
Figure 17. (A) Orthotopic mouse model of HNSCC showing the primary tumor (blue arrow) and the lymphatic metastases (white arrow). Histology slides show (B) muscular and (C) glandular invasion.
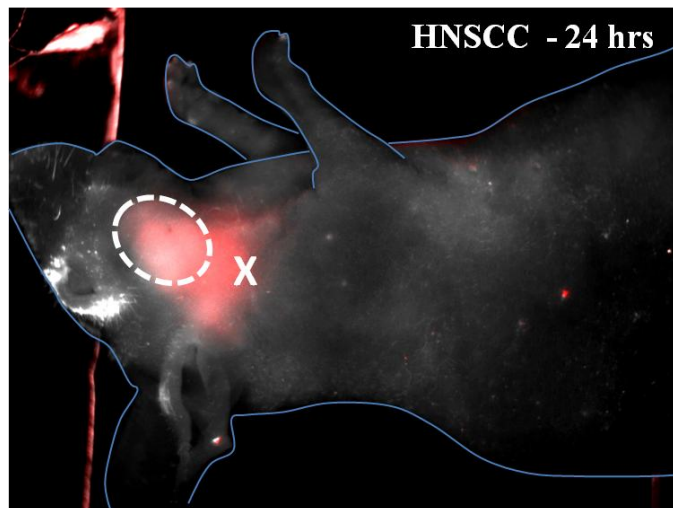
Figure 18. HA-Texas Red to the surrounding lymphatics (24 hours post injection). Dashed circle and × indicated the location of the primary tumor and the nearby injection site, respectively. [*]HNSCC: head and neck squamous cell cancer

the increased accumulation of the nanoconjugates adjacent to the tumor and the cervical lymph nodes. Other polymeric carriers, such as optically labeled dendrimers [29] or dextran [30-31] have also been used to enable visualization of the lymphatic drainage.

In order to visualize tumor progression in the early stages, the MDA1986 cell line was developed to express a red fluorescent protein. Initially, Turbo635 was inserted into the pLNCX2 vector (Clontech) under control of the CMV immediate promoter with a neomycin insert and the transfected cells were selected with G418. Although the resulting cells had strong fluorescence *in vitro*, the tumor implants resulted in no fluorescence; leading to the interpretation that the promoter was "shut off" in this cell line after implantation. Replacement of pLNCX2 with the Hsp70 promoter resulted in expression of the strong fluorescent reporter gene *in vitro* and *in vivo*.

8.4 Part B: evaluation of anticancer efficacy in head and neck cancer bearing mice

Female nude mice were injected with MDA-1986 cells and randomly divided into five groups including saline i.v. group (N = 5), HA s.c. group (N = 6), CDDP i.v. group (N = 5), HA-Pt s.c. group (N = 7), and HA-Pt i.v. group (N=6). Animals in each group were euthanized once their tumor size reached 1000 mm^3 or 12 weeks after tumor cells were implanted. In addition, animals were euthanized during the study if tumors became ulcerated or infections unrelated to tumor growth occurred. Facial tumors were observed two weeks after tumor cells were implanted. All treatments were administered on weeks 3, 4, and 5, after the tumor cell implantation. Three doses of 3.5 mg/kg CDDP, 3.5 mg/kg HA-Pt (on Pt basis), or physiological saline were administered intravenously via tail veins; or three doses of 3.5 mg/kg of HA-Pt (on Pt basis) or

HA were administered subcutaneously near the tumors. The size of the primary tumor was measured weekly. A similar study was conducted using male nude mice, which were treated with either CDDP i.v. (N = 4, 3.5 mg/kg × 3 wks) or HA-Pt s.c. (N = 4, equivalent dose on a platinum basis).

In this anticancer efficacy study, two groups of female nude mice treated with saline i.v. or HA s.c. developed tumors of approximately 1000 mm^3 on average after five weeks, which indicated that HA does not alter the natural progression of HNSCC. On the other hand, the female animals that were treated with three doses of either i.v. cisplatin or i.v. HA-Pt developed tumors of approximately 1000 mm^3 eight weeks post tumor cell implantation. In contrast, 57% of the female animals bearing HNSCC xenografts in the HA-Pt s.c. treated group (three equivalent doses of HA-Pt) were cured within six weeks, with no disease recurrence by the end of the study (Figure 19). In addition, the survival rate was greatly improved for the animals treated with HA-Pt s.c., when compared to either of the control groups (p<0.05 for both saline i.v. and HA s.c. groups) or CDDP i.v. (p<0.05) and HA-Pt i.v. (p<0.05) groups (Figure 19). No statistically significant differences were observed for intravenously treated CDDP and HA-Pt groups. Overall, the results of the tumor model suggests that HA-Pt conjugates achieved a higher anti-cancer efficacy relative to the conventional CDDP i.v. therapy, due to the route of drug administration, as well as the intrinsic properties of hyaluronan as a carrier for lymphatic drug delivery (Figure 19). HA-Pt slowly released the active form of the drug, which subsequently drained to the adjacent cervical lymph nodes and the surrounding lymphatic regions. The gradual release of CDDP did not cause any skin or tissue reaction at the injection site, even though CDDP is a well known vesicant. This is likely due to the protective effect of HA, which has been used as a rescue medication to alleviate local toxicity effects of chemotherapeutics.

A

B

C

D
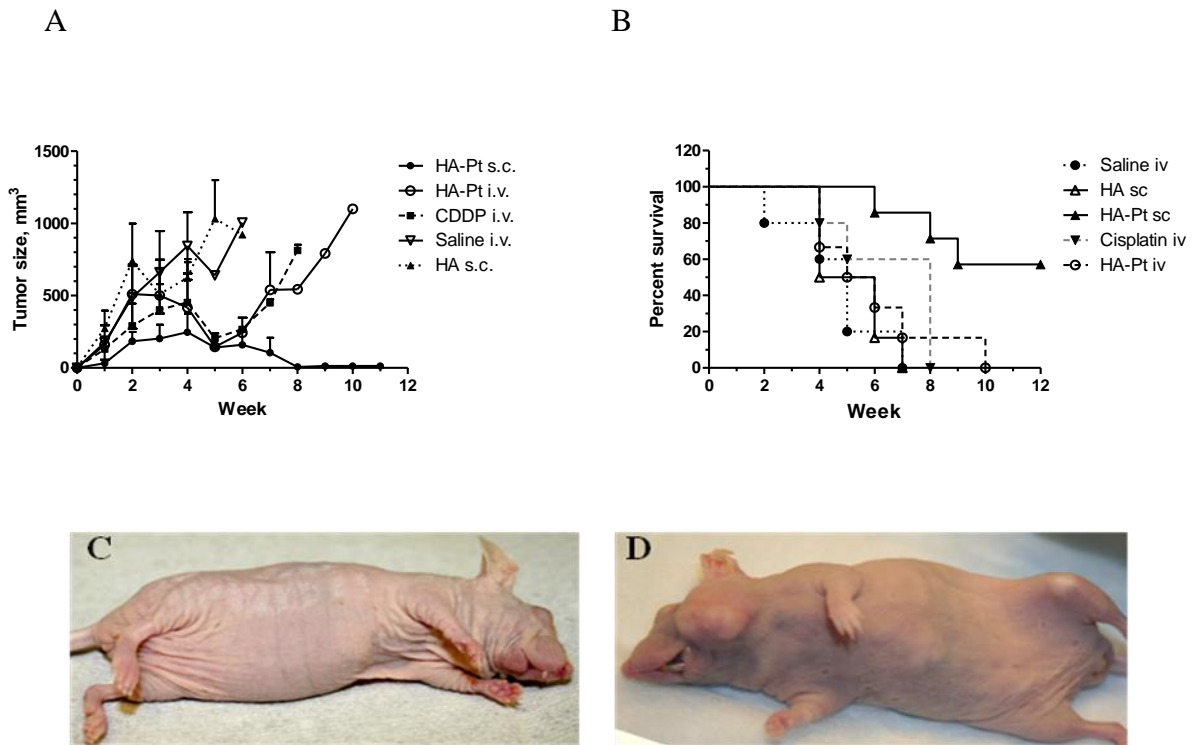
Figure 19. (A) Measurement of tumor sizes. Female animals were administered saline i.v., HA s.c., equivalent doses of CDDP i.v., HA-Pt s.c. and HA-Pt i.v. (3.5 mg/kg on Pt basis, $5 \leq N \leq 7$). (B) Survival curves of female animals treated by saline, HA, CDDP or HA-Pt ($5 \leq N \leq 7$) (Top Right Panel). (C) Lymphatic HA-Pt chemotherapy at 12 weeks. (D) Intravenous CDDP chemotherapy at 8 weeks. [*]HA-Pt: hyaluronan-cisplatin; CDDP: cisplatin; HA: hyaluronan; i.v.: intravenous; s.c.: subcutaneous.

Administration of anti-cancer drugs via polymeric delivery vehicles is a promising method for local delivery of concentrated chemotherapeutics, effectively treating lymphatically metastatic cancers. A study by Dunne et al. revealed that CDDP bound poly(ethylene oxide)-b-poly(lysine) block copolymers greatly hindered the tumor progression in a squamous cell cancer model of the upper aerodigestive tract in animals [32]. Another study done by Xie et al. reported an enhanced efficacy against laryngeal squamous cell carcinoma in rodents using paclitaxel-loaded poly(lactic-co-glycolic acid) microspheres compared with conventional paclitaxel therapy [33].

Another interesting observation was that the tumor progression of HNSCC exhibited a more aggressive pattern in male nude mice compared to female nude mice. All the male animals in the CDDP i.v. group reached an average tumor size of approximately 1000 mm^3 in two weeks (Figure 20) as opposed to eight weeks as seen in the previous female animals studies (Figure 19). On the other hand, 80% of the male animals in the HA-Pt s.c. group developed tumors of approximately 1000 mm^3 in three weeks and 20% of the animals were able to live through the end of the fourth week (Figure 20). Therefore, gender differences, as well as weight loss and stress may be contributing factors that are responsible for the differentiated carcinoma progression. In human studies, tobacco and alcohol consumption was believed to be the major, but not only, factors inducing the occurrence and recurrence of HNSCC. Other factors, such as age, weight loss, nutritional status, and complications, may also play a role in the survival of patients [34]. Dahlstrom et al. conducted a demographic study, of 172 patients that never smoked and never drank, that described the age and sex distribution of HNSCC patients, and identified the specific types of the most commonly diagnosed HNSCCs [35]. A similar study was also performed by Onyango et al, showing an overall male preponderance in the occurrence of
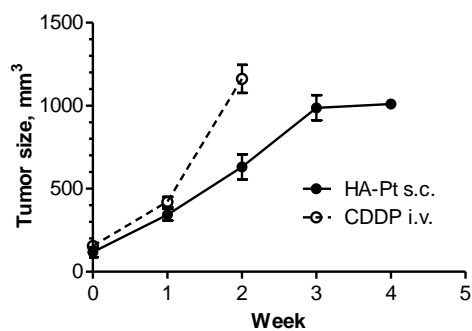
A
B
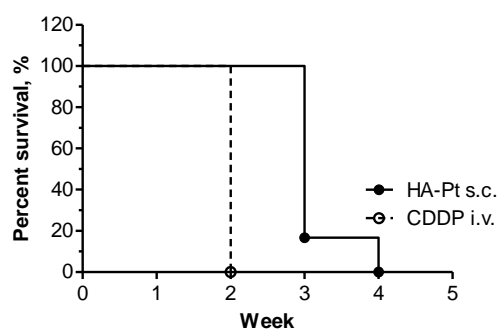
Figure 20. (A) Measurement of tumor sizes. Male animals were administered equivalent doses of CDDP i.v. and HA-Pt s.c. (3.5 mg/kg on Pt basis, N = 4 for CDDP i.v., N = 6 for HA-Pt s.c.). (B) Survival curves of male animals treated by CDDP or HA-Pt (N = 4 for CDDP i.v., N = 6 for HA-Pt s.c.).

HNSCC among 793 patience [36]. Additional factors affecting the disease progression and metastasis are still under investigation.

This study demonstrates that intralymphatic delivery of cisplatin may be a promising treatment regimen to deliver chemotherapeutics to the primary malignancy, locoregional lymphatics, and metastases, with greatly improved *in vivo* efficacy and survival compared with conventional cisplatin chemotherapy. Successful completion of this study may provide a platform for the development of other polymeric drug delivery models for the treatment of a wide spectrum of lymphatically metastic cancers. The platinum-based hyaluronan conjugates can either be administered as a neoadjuvant therapy prior to surgery to reduce tumor size and control cancer progression, or be given as an adjuvant therapy post surgery to reduce the risk of recurrence and eradicate cancer residuals, such as micrometastases. In addition, due to the sustained release characteristics of the conjugate, weekly or biweekly HA-Pt injections could replace the conventional daily infusion, leading to improved patient compliance and reduced healthcare costs.

Despite major strides in cancer prevention and treatment during the past decades, there has been only a modest improvement on the overall survival. Over half of HNSCC patients will face recurrence at some point, and these cancers recur because current imaging tools fail to detect occult disease or therapies fail to completely eradicate resistant disease. More frequent and intense radioimaging, or stronger regimens of chemotherapy and radiation, would be detrimental in the long run to patients' health, so new approaches are needed.

Localized therapies stand a stronger chance of eradicating residual disease, since higher doses of chemotherapy can be administered without dose-limiting toxicity to the heart, kidneys,

and liver. Localized chemotherapy is already used to great success in the treatment of peritoneal disease in colon cancer using heated intraperitoneal chemotherapy, limb melanomas with heated isolated limb perfusions, and liver cancer using isolated hyperthermic liver perfusion. However, there is no way to isolate most organs and tissues for concentrated chemotherapy, such as the breasts, the neck, and the lungs. For most tissues, the lymphatics are an ideal pathway for local therapy due to their importance in early cancer metastasis. Localized chemotherapy may become an important component in the treatment of early stage cancers that are still confined to the primary tumor and local lymphatics; yet, to date, there are no tools in the clinic to localize chemotherapy to the lymphatic system.

Localized delivery systems, such as the one described here can effectively treat these early stage diseases, and we believe that they will represent a new treatment option in the next 5 to 10 years. Next generation systems will incorporate both imaging and diagnostic capabilities in the drug or drug carriers, so that the staging (or restaging) of the disease can be followed immediately by treatment: to reduce treatment costs; limit the need for invasive surgeries and intravenous treatments; and increase the likelihood that all disease can be eliminated in the early, more controllable stages.

9. References

[1] FDA oncology tools approval summary for cisplatin for metastatic ovarian tumors, in, 2008.

[2] V. Launay-Vacher, J.B. Rey, C. Isnard-Bagnis, G. Deray, M. Daouphars, E.S.o.C.P.S.I.G.o.C. Care, Prevention of cisplatin nephrotoxicity: state of the art and recommendations from the European Society of Clinical Pharmacy Special Interest Group on Cancer Care, Cancer Chemother. Pharmacol., 61 (2008) 903-909.

[3] H.J. Stemmler, S. Kahlert, O. Brudler, M. Beha, S. Muller, B. Stauch, V. Heinemann, High efficacy of gemcitabine and cisplatin plus trastuzumab in patients with HER2-overexpressing metastatic breast cancer: a phase II study, Clin Oncol (R Coll Radiol), 17 (2005) 630-635.

[4] N. Pabla, Z. Dong, Cisplatin nephrotoxicity: mechanisms and renoprotective strategies, Kidney Int, 73 (2008) 994-1007.

[5] R. Safirstein, P. Miller, J.B. Guttenplan, Uptake and metabolism of cisplatin by rat kidney, Kidney Int, 25 (1984) 753-758.

[6] Y. Shimizu, K. Hasumi, Chemotherapy with consecutive low-dose CDDP combined with 5-FU for gynecologic malignancies, Gan To Kagaku Ryoho, 26 (1999) 1564-1574.

[7] C.L. Zuur, Y.J. Simis, R.S. Verkaik, J.H. Schornagel, A.J. Balm, W.A. Dreschler, C.R. Rasch, Hearing loss due to concurrent daily low-dose cisplatin chemoradiation for locally advanced head and neck cancer, Radiother. Oncol., 89 (2008) 38-43.

[8] J.M. Armer, The problem of post-breast cancer lymphedema: impact and measurement issues, Cancer Invest, 23 (2005) 76-83.

[9] A.J. Cochran, R. A.A., T. Saida, The place of lymphatic mapping and sentinel node biopsy in oncology., Int J Clin Oncol, 8 (2003) 139-150.

[10] Chen JH, Ling R, Yao Q, Li Y, Chen T, Wang Z, L. KZ, Effect of small-sized liposomal Adriamycin administered by various routes on a metastatic breast cancer model., Endocr Relat Cancer, 12 (2005) 93-100.

[11] Sirohi B, Arnedos M, Popat S, Ashley S, Nerurkar A, Walsh G, Johnston S, S. IE., Platinum-based chemotherapy in triple-negative breast cancer., Ann Oncol, 19 (2008) 1847-1852.

[12] Rhiem K, Wappenschmidt B, Bosse K, Köppler H, Tutt AN, S. RK., Platinum sensitivity in a BRCA1 mutation carrier with advanced breast cancer., Clin Oncol (R Coll Radiol), 21 (2009) 448-450.

[13] Byrski T, Huzarski T, Dent R, Gronwald J, Zuziak D, Cybulski C, Kladny J, Gorski B, Lubinski J, N. SA., Response to neoadjuvant therapy with cisplatin in BRCA1-positive breast cancer patients., Breast Cancer Res Treat, 115 (2009) 359-363.

[14] S.E. Kurtin, Systemic therapies for squamous cell carcinoma of the head and neck, Semin Oncol Nurs, 25 (2009) 183-192.

[15] Z. Gil, D.M. Fliss, Contemporary management of head and neck cancers, Isr Med Assoc J, 11 (2009) 296-300.

[16] A.A. Forastiere, Chemotherapy in the treatment of locally advanced head and neck cancer, J Surg Oncol, 97 (2008) 701-707.

[17] S.R. Chandana, B.A. Conley, Neoadjuvant chemotherapy for locally advanced squamous cancers of the head and neck: current status and future prospects, Curr Opin Oncol, 21 (2009) 218-223.

[18] S. Cai, Y. Xie, T. Bagby, M.S. Cohen, M.L. Forrest, Intralymphatic chemotherapy using a hyaluronan-cisplatin conjugate, J. Surg. Res., 147 (2008) 247-252.

[19] S. Kishimoto, Y. Kawazoe, M. Ikeno, S. Fukushima, Y. Takeuchi, Continuous exposure to low-dose cisplatin and apoptosis, Biol. Pharm. Bull., 28 (2005) 1954-1957.

[20] D.M. Townsend, M. Deng, L. Zhang, M.G. Lapus, M.H. Hanigan, Metabolism of Cisplatin to a nephrotoxin in proximal tubule cells, I. Am. Soc. Nephrol., 14 (2003) 1-10.

[21] C.L. Zuur, Y.J. Simis, R.S. Verkaik, J.H. Schornagel, A.J. Balm, W.A. Dreschler, C.R. Rasch, Hearing loss due to concurrent daily low-dose cisplatin chemoradiation for locally advanced head and neck cancer, Radiother Oncol, 89 (2008) 38-43.

[22] A. Ekborn, A. Lindberg, G. Laurell, I. Wallin, S. Eksborg, H. Ehrsson, Ototoxicity, nephrotoxicity and pharmacokinetics of cisplatin and its monohydrated complex in the guinea pig, Cancer Chemother Pharmacol, 51 (2003) 36-42.

[23] G.C. Vreeburg, P.M. Stell, J.D. Holding, W.E. Lindup, Cisplatin-albumin complex for treatment of cancer of the head and neck, J Laryngol Otol, 106 (1992) 832-833.

[24] W.J. Clerici, K. Hensley, D.L. DiMartino, D.A. Butterfield, Direct detection of ototoxicant-induced reactive oxygen species generation in cochlear explants, Hear Res, 98 (1996) 116-124.

[25] X. Huang, C.A. Whitworth, L.P. Rybak, Ginkgo biloba extract (EGb 761) protects against cisplatin-induced ototoxicity in rats, Otol Neurotol, 28 (2007) 828-833.

[26] K.C. Campbell, R.P. Meech, J.J. Klemens, M.T. Gerberi, S.S. Dyrstad, D.L. Larsen, D.L. Mitchell, M. El-Azizi, S.J. Verhulst, L.F. Hughes, Prevention of noise- and drug-induced hearing loss with D-methionine, Hear Res, 226 (2007) 92-103.

[27] M.T. Kalcioglu, A. Kizilay, M. Gulec, E. Karatas, M. Iraz, O. Akyol, M. Egri, O. Ozturan, The protective effect of erdosteine against ototoxicity induced by cisplatin in rats, Eur Arch Otorhinolaryngol, 262 (2005) 856-863.

[28] Y. Kamei, T. Kanno, M. Abe, Ossifying fibroma in the sylvian fissure: case report, Neurosurgery, 29 (1991) 120-123.

[29] H. Kobayashi, M. Ogawa, N. Kosaka, P.L. Choyke, Y. Urano, Multicolor imaging of lymphatic function with two nanomaterials: quantum dot-labeled cancer cells and dendrimer-based optical agents, Nanomed, 4 (2009) 411-419.

[30] S.C. Vieira, R.B. Sousa, M.B. Tavares, J.B. Silva, B.A. Abreu, L.G. Santos, B.B. da Silva, L.C. Zeferino, Preoperative pelvic lymphoscintigraphy is of limited usefulness for sentinel lymph node detection in cervical cancer, Eur J Obstet Gynecol Reprod Biol, 145 (2009) 96-99.

[31] M. McElroy, M. Bouvet, R.M. Hoffman, Chapter 2. Color-coded fluorescent mouse models of cancer cell interactions with blood vessels and lymphatics, Methods Enzymol, 445 (2008) 27-52.

[32] A.A. Dunne, H.G. Boerner, H. Kukula, H. Schlaad, S. Wiegand, J.A. Werner, M. Antonietti, Block copolymer carrier systems for translymphatic chemotherapy of lymph node metastases, Anticancer Res, 27 (2007) 3935-3940.

[33] M. Xie, L. Zhou, T. Hu, M. Yao, Intratumoral delivery of paclitaxel-loaded poly(lactic-co-glycolic acid) microspheres for Hep-2 laryngeal squamous cell carcinoma xenografts, Anticancer Drugs, 18 (2007) 459-466.

[34] S. van Bokhorst-de van der, P.A. van Leeuwen, D.J. Kuik, W.M. Klop, H.P. Sauerwein, G.B. Snow, J.J. Quak, The impact of nutritional status on the prognoses of patients with advanced head and neck cancer, Cancer, 86 (1999) 519-527.

[35] K.R. Dahlstrom, J.A. Little, M.E. Zafereo, M. Lung, Q. Wei, E.M. Sturgis, Squamous cell carcinoma of the head and neck in never smoker-never drinkers: a descriptive epidemiologic study, Head Neck, 30 (2008) 75-84.

[36] J.F. Onyango, D.O. Awange, A. Njiru, I.M. Macharia, Pattern of occurrence of head and neck cancer presenting at Kenyatta National Hospital, Nairobi, East Afr Med J, 83 (2006) 288-291.

Chapter 3

Intralymphatic Delivery of Hyaluronic Acid-Doxorubicin Conjugates

for the Treatment of Breast Cancer

1. Introduction

Doxorubicin (DOX) is among the most effective chemotherapeutics used for the treatment of cancers including breast, ovarian, sarcomas, pediatric solid tumors, Hodgkin's disease, multiple myeloma, and non-Hodgkin's lymphomas. Despite the success of DOX against many cancers, its use can be severely limited by its cardiac toxicity including development of a cardiomyopathy, often refractory to common medications, which can progress to biventricular failure and even death (reviewed in [1]). This damage is caused by the generation of reactive oxidative species, such as superoxide and hydrogen peroxide, upon the reduction of doxorubicin to form an election deficient semiquinone. In addition, doxorubicin is an iron chelator, chelating Fe(III) and perturbing the transportation of iron into cells. It causes iron-deficient cell death of myocytes [2]. Technologies such as polymeric micelles [3], synthetic polymer conjugates [4], and antibody targeted carriers [5], have demonstrated reduced or altered toxicity in Phase I trials, yet the therapeutic efficacy of these formulations has yet to be demonstrated. In the absence of safer, efficacious systemic formulations, localized delivery of DOX may improve tolerability and improve efficacy, especially in the treatment of early breast cancer.

Early breast cancers typically spread, initially from the primary tumor site to the regional lymph nodes in the axilla prior to systemic dissemination. Surgery and radiation therapy can be effective, but result in significant side effects including painful lymphedema [6]. There is debate over the risks verses the benefits of aggressive therapy for patients with isolated tumor cells or nanometastases in the axillary lymph nodes; however, recent studies support that there is a strong risk factor for metastatic relapse in patients with nodal nano-metastases, with occult lymph node disease accounting for up to 50% of metastatic recurrences [7] and a hazard ratio of 1.5 for patients with isolated cancer cells who do not receive adjuvant systemic chemotherapy [8]. We

therefore sought to develop a formulation of DOX that could be given locally and concentrated in the draining lymphatic basin of the breast, where early metastases are more prevalent, while sparing normal tissues from many of the organ toxicities associated with systemic chemotherapy. DOX is a potent vesicant, so direct s.c. injection (leading to lymphatic drainage) is not viable; however, conjugates of DOX and a lymphatically targeted carrier may avoid severe tissue toxicity through improved localization to the lymphatic basin. For this purpose, hyaluronan may be an ideal carrier.

Hyaluronan (HA) is a polysaccharide, of alternating D-glucuronic acid and *N*-acetyl D-glucosamine, found in the connective tissues of the body, and it is cleared primarily by the lymphatic system (12 to 72 hrs turnover half-life [9]). After entering the lymphatic vessels, HA is transported to the nodes, where it is catabolized by receptor-mediated endocytosis and lysosomal degradation. Several studies have correlated an increase in HA synthesis and uptake with cancer progression and metastatic potential [10-11]. Breast cancer cells are known to have greater uptake of HA than normal tissues [12], requiring HA for high P-glycoprotein expression, the primary contributor to DOX resistance [13]. The knockout of HA receptors has been reported to prevent migration of cancers that initially spread intralymphatically [14]. Furthermore, invasive breast cancer cells overexpress CD44, the primary receptor for HA [15], and are dependent on high concentrations of CD44-internalized HA for proliferation (reviewed in [12]). Doxorubicin conjugated to HA may represent a natural lymphatic and breast-cancer-targeted delivery platform to improve efficacy against lymphatic metastases.

Several HA-DOX conjugates have been reported which used irreversible or peptide linkers, which had considerable loss in anticancer activity [16-18]. We report herein a new pH-sensitive, reversible hydrazone linked HA-DOX conjugate with potent anticancer activity against

137

breast cancer cells *in vitro* demonstrating excellent cellular uptake and retention. Furthermore, HA is shown to drain to the axilla basin of rats after s.c. injection into the mammary fatpad, laying the foundation for future studies of pharmacokinetics, and anti-tumor activity in rodent models.

2. Synthesis and characterization of hyaluronan-doxorubicin (HA-DOX) conjugates

Direct conjugation of drugs to HA is inefficient due to the steric hindrance of the polysaccharide backbone and low reactivity of the carboxylate group. HA was derivatized with adipic acid dihydrazide (ADH), according to the procedure of Luo et al. [19]. Briefly, HA (200 mg, 35 kDa) was dissolved in 40 mL ddH$_2$O with ADH (436 mg) and 1-ethyl-3-[3-(dimethylamino)-propyl]carbodiimide (EDCI, 48 mg). The solution pH was adjusted to 4.75 with 1 N HCl, and checked again after 10 min. The reaction was quenched by addition of 0.1 N NaOH to pH 7.0. The reaction scheme is shown in Figure 1. The resulting solution was dialyzed against ddH$_2$O for two days with bath changes every 12 hrs. After dialysis, the product was filtered (0.2 μm polystyrene membrane, Millipore), and lyophilized. The degree of substitution was determined to be 33 % by ^{1}H NMR in D$_2$O using the ratio of ADH methylene protons to HA acetyl methyl protons.

Conjugation of DOX to HA was accomplished by formation of a hydrazone bond between the ketone of DOX and the hydrazide side chain of HA-ADH [20]. HA-ADH (110 mg) was dissolved in 30 mL of 2 mM sodium phosphate buffer (pH 6.5). DOX·HCl (2 mL, 2 mg/mL) was added dropwise in the HA-ADH solution. The solution was adjusted to pH 6.5 with 0.1 N NaOH and after 12 hrs, it was dialyzed against 2 mM sodium phosphate buffer (pH 7.8), with
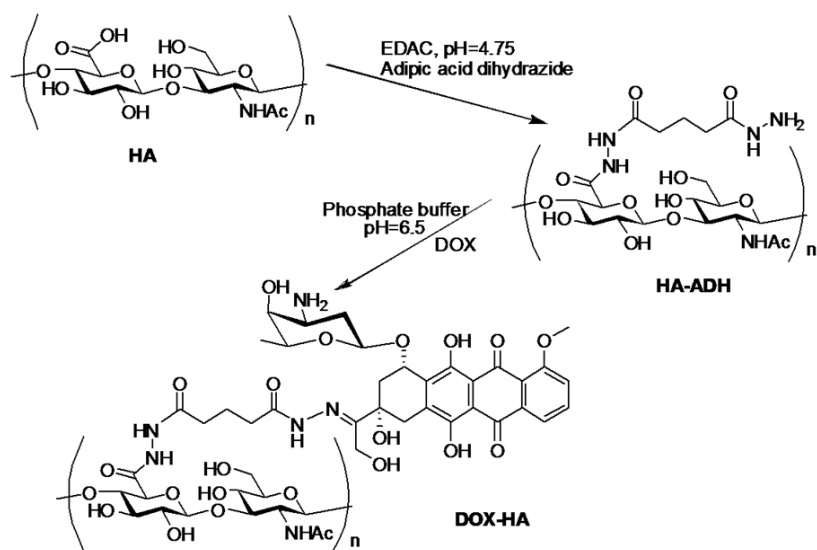
Figure 1. Synthesis of hyaluronan-doxorubicin (HA-DOX) conjugate.

139

twice daily changes until no further color change was observed (2 days). Solutions were protected from light at all times.

Gel permeation chromatography (GPC; Shodex HQ-806M column, 0.8 mL/min, 20 mM HEPES, pH 7.2) with refractive index and fluorescent detection (ex/em 480/590 nm) was utilized to verify drug conjugation by equivalent elution times. The HA (green) and bound DOX (blue) both eluted at approximately 11 minutes (Figure 2). The degree of conjugation was determined by UV/Vis spectrophotometry at 480 nm using a standard calibration curve (1-100 µg/mL). A series of concentrations of DOX standard solution was prepared to generate a calibration curve. The concentrations of the standard solution were 1, 2, 5, 10, 25, 50 and 100 µg/mL (R^2=0.99). Absorbance at 480 nm was measured and it was due to the UV absorbance of DOX; HA does not exhibit UV absorbance (data not shown). Specifically, the loading degree was calculated to be 5.2 % (wt/wt). In general, the optimal loading degree of DOX was maintained to be in a range of 5-15 % (wt/wt) to obtain the maximum solubility and the least volume of solution administered in the animal studies.

Nanocarrier strategies for the delivery of drugs have been investigated extensively in the past decade. Among candidates of potential nanocarriers, hyaluronan represents a very promising substrate by being both a biocompatible and nonimmunogenic molecule. It has been used as a carrier for the delivery of a variety of chemotherapeutic agents, for instance, cisplatin [21], paclitaxel [22] and mitomycin C [23]. Strategies with different choices of spacers for the delivery of doxorubicin have been explored for optimal entrapment efficiency [24], specific tumor targeting [25] and higher cellular uptake [26]. A liposome-encapsulated formulation of doxorubicin (Doxil[TM]) is currently available in human chemotherapy and produces major benefits, including reduced acute cardiotoxicity compared to i.v. DOX·HCl and improved
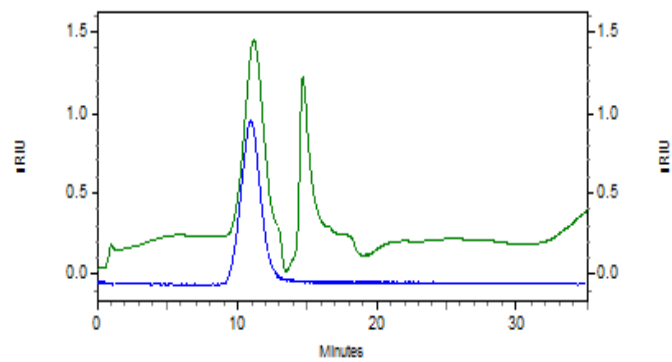
Figure 2. Chromatogram of HA-DOX (GPC). The HA (green) and bound DOX (blue) were both eluted at approximately 11 minutes.

biodistribution [27]. However, liposomal DOX can cause palmar plantar erythrodysesthesia, a dermatologic toxic reaction associated with the leakage of a small amount of the drug from the long-circulating liposomes into the cutaneous tissues of the palms and the soles of the feet [28]. A trial of DOX and liposomal DOX in 509 patients with metastatic breast cancer demonstrated reduced toxicity of liposomal DOX, but no increase in survival [29]. In this chapter, the development of a controlled-release HA-DOX conjugate will be described. The HA-DOX conjugate demonstrated improved efficacy in locally advanced disease and reduced side effects compared to conventional DOX and liposomal DOX treatments.

3. *In vitro* release

In order to determine the release profile of DOX from HA-DOX, the release was studied at three different pHs mimicking the pHs of normal cells and cancer cells. HA-DOX (20 mg) was dissolved in PBS (10 mL) adjusted to pH 5.0, 6.0 or 7.4 and sealed in dialysis tubing (10,000 MWCO, Pierce, Rockford, IL). The dialysis tubings were placed in a PBS bath at pH 5.0, 6.0 or 7.4; 100 µL aliquots were taken from the bags as predetermined time points, and were analyzed by GPC coupled with refractive index and fluorescence (ex/em 480/590) detectors. The PBS solution was changed 5 times daily, and the ratio of the peak areas of HA to DOX was calculated for up to 500 hrs.

HA-DOX conjugates were synthesized using a pH sensitive linker, resulting in adipic dihydrazide functionalized nanoconjugates. The conjugate releases doxorubicin in a pH dependent fashion via a Schiff base mechanism, yielding free DOX and the polymer. The release half life of DOX was determined to be 172 hrs at pH 7.4, 110 hrs at pH 6.0 and 45 hrs at pH 5.0

(Figure 3). The ratio of the release half lives of DOX from the polymer backbone at pH 5.0, 6.0 and 7.4, was determined to be approximately 1:2.4:3.8, clearly indicating the dependence of the hydrolysis of carbon-nitrogen double bond to pH changes. The extended half life at physiological pH was consistent with the sustained release characteristics of HA-DOX conjugates. Thus, the carrier releases the active form of the drug more rapidly *in vivo* in an acidic environment as in the hypoxic environment within solid tumor masses, which may preferentially concentrate drug near the primary tumor or distant metastases of breast cancer cells, compared to a relatively neutral environment that surrounds normal cells.

4. *In vitro* imaging and cytotoxicity

In order to confirm that the HA-DOX conjugate can enter cells, cancer cells were incubated with HA-DOX and imaged. Typically cell lines were seeded into 12-well plates (50,000 cells/well) containing a poly-L-lysine coated coverslip (Fisher Scientific). After 24 hrs, DOX, HA-DOX, or HA was applied, and after 6 hrs, the media was refreshed. After 12 hrs, cells were examined by fluorescent microscopy (ex/em 480/590). Images were adjusted for contrast and brightness with no further manipulation. Both free DOX and HA-DOX conjugate were taken up by MDA-MB-231 cells after 6 hours incubation (data not shown).

Cell growth inhibition was determined in 96-well plates (3,000 cells/well in 100 μL) (n=3, 12 wells/concentration). DOX or HA-DOX in PBS was applied after 24 hrs; 72 hrs post-addition, resazurin blue in 10 μL PBS was applied to each well (final 5 μM). After 4 hrs, well fluorescence was measured (ex/em 560/590) (SpectraMax Gemini, Molecular Devices), and the IC_{50} concentration determined as the midpoint between untreated (positive) and cell-free (negative) controls.
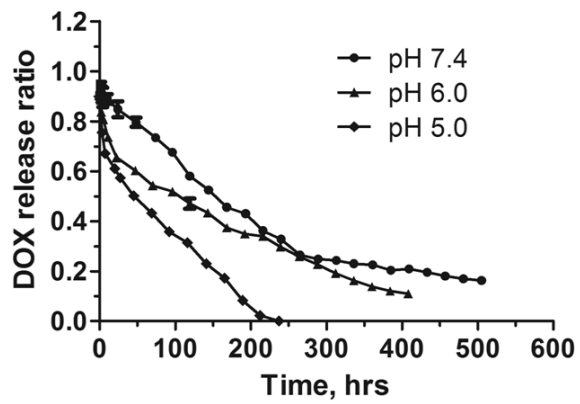
Figure 3. *In vitro* release of DOX from HA-DOX at pH 5.0, 6.0 and 7.4.

HA-DOX conjugates exhibit slightly lower toxicities than free doxorubicin in cell culture: MDA-MB-468LN, 221 and 515 nM (DOX and HA-DOX, respectively); MDA-MB-231, 147 and 588 nM; and MCF-7, 221 and 1287 nM. However, the conjugate remains potent for all the breast cancer cell lines tested with IC_{50} values in the nanomolar range. HA exhibits no toxicity to human cells over the concentration range examined (up to 10 mg/mL, data not shown).

5. Pharmacokinetics

Sprague-Dawley rats (200-300 g females, Charles Rivers) were placed under isoflurane anesthesia and cannulated at the jugular veins. Animals were allowed to recover with access to food and water overnight. Then they were injected s.c. (100 μL) into the left mammary fat pad with HA-DOX (4 mg/kg DOX·HCl equivalent, n=4), i.v. into the jugular vein with 2 mg/mL DOX·HCl in 0.9 % saline (4 mg/kg DOX·HCl equivalent, n=4), or s.c. (100 μL) into the left mammary fat pad with DOX·HCl (4 mg/kg DOX·HCl equivalent, n=4). Blood was sampled from the jugular vein (200-300 μL) at 0 min, 5 min, 30 min, 1h, 2h, 4h, 6h, 12h and 24 h. Plasma was separated by centrifugation from whole blood and stored at -80 ºC freezer until analysis. At 24 hours, the animals were euthanized by isoflurane overdose.

The pharmacokinetic parameters were determined using SAAM II Version 1.2 software. A two compartmental model was utilized for i.v. DOX, s.c. DOX, and s.c. HA-DOX data. Pharmacokinetic data were collected from 0 to 24 hours and were analyzed, resulting in a series of biexponential plasma level-time curves. Pharmacokinetic parameters such as volume of distribution, clearance, area under the curve, mean residence time and elimination half-time were determined as followed.

The pharmacokinetics of s.c. HA-DOX were compared to i.v. DOX and s.c. DOX in Sprague-Dawley rats. The peak plasma concentration of i.v. DOX was 18.8-fold greater than s.c. HA-DOX (Figure 4). The release of DOX from HA-DOX into the systemic circulation was slow, and the resulting plasma AUC of HA-DOX did not exhibit significant difference from i.v. therapy. The peak plasma concentration of s.c. DOX was 1.3 greater than s.c. HA-DOX and the AUC of s.c. DOX was slightly lower than s.c. HA-DOX. The serum DOX level measured in HA-DOX was associated with the free unbound drug instead of the sum of free drug and HA bound drug due to the difficulty cleaving DOX from the polymer backbone in serum samples. Thus, the actual total DOX level in the serum would be expected to be higher for s.c. HA-DOX, resulting in a greater AUC.

A two-compartment model was selected to describe the biexponential nature of the pharmacokinetics of HA-DOX and DOX. The predicted volume of distribution of i.v. DOX was determined to be approximately 3.4-fold greater than HA-DOX. In addition, both routes of drug administration (i.v. DOX and s.c. HA-DOX) resulted in similar values of Area-under-the-curve (AUC$_{0-24\ h}$), clearance and elimination half life. However, s.c. HA-DOX exhibited a 2.2-fold increase in systemic mean residence time, which is consistent with the sustained release nature of the polymer drug conjugate. Finally, the observed peak plasma concentration of i.v. DOX is shown to be 18.8-fold higher than that of the s.c. HA-DOX, which may cause potential tissue toxicity, such as cardiac toxicity (dose-limiting) and hepatoxicity (the liver is the major organ of DOX metabolism) (Table 1).

The previous study demonstrated that the intralymphatic delivery model using hyaluronan-cisplatin conjugate not only increases drug concentrations in loco-regional nodal tissues significantly compared to the standard cisplatin formulation, but it also exhibits sustained

146
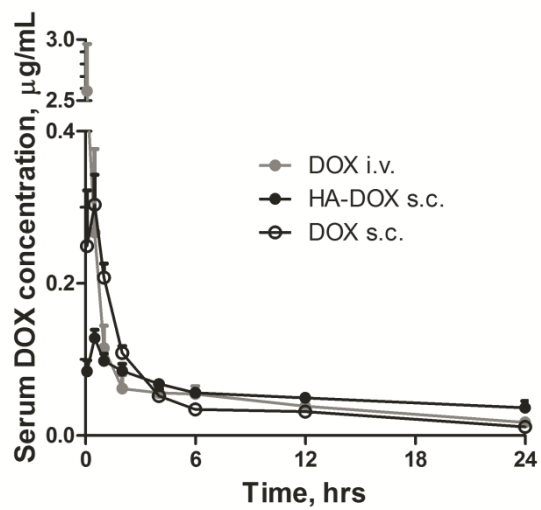
Figure 4. Serum concentration of doxorubicin. The animals were treated with i.v. DOX, s.c. HA-DOX and s.c. DOX.

Parameters	Unit	DOX (i.v.)	HA-DOX (s.c.)
V_d	L/kg	0.430 ± 0.272	0.096 ± 0.084
A	µg/mL	4.415 ± 1.515	30.974 ± 29.980
B	µg/mL	0.078 ± 0.013	0.086 ± 0.012
$AUC_{0-24\,h}$	(µg·h)/mL	2.061 ± 0.824	2.201 ± 0.905
Cl	L/(kg·h)	1.283 ± 0.404	1.261 ± 0.564
MRT (Syst)	h	$8.247 \pm 4.944^{*}$	$26.501 \pm 10.703^{*}$
$t_{1/2}\,(\beta)$	h	0.226 ± 0.072	0.199 ± 0.293
$C_{max}\,(t)$	µg/mL (min)	$2.580 \pm 0.670\,(5)^{*}$	$0.130 \pm 0.020\,(30)^{*}$

Table 1. The pharmacokinetic data were fitted using a two-compartmental model. Data are shown as means and standard deviation. *Study groups, i.v. DOX and s.c. HA-DOX, differed significantly for MRT(Syst) and $C_{max}(t)$. Significance defined as $p<0.05$ using student t-test (n=4).

release kinetics, allowing lower peak plasma concentration which could translate into lower organ toxicity over time [21]. In this study, the intralymphatic delivery strategy was successfully applied to the HA-DOX delivery system, reducing the C_{max} by approximately 19-fold without compromising the plasma drug AUC. In addition, only the free DOX released from HA, as opposed to the sum of free and bound drug, was detected and analyzed for the calculation of the total drug AUC in the plasma. The actual total DOX concentration in the plasma may be higher, allowing a greater AUC compared to the standard DOX treatment. This may result in a lower dose of doxorubicin being required to achieve the same plasma and tissue drug level. HA-DOX injections therefore, could be considered for weekly or even biweekly injections, with great potential to replace daily conventional intravenous doxorubicin chemotherapy both from a standpoint of improved toxicity profiles, but also in terms of improvements in compliance and completion of chemotherapeutic regimens.

In addition, the difference in the volume of distribution in the plasma compartment, V_d, between i.v. DOX group and s.c. HA-DOX group was possibly due to the easier access to the surrounding tissues for free doxorubicin molecules as opposed to polymer bound DOX conjugates. Doxorubicin with a log P value of 1.3, pKa of 8.4, and a molecular weight of 544 g/mol, rapidly crosses lipid membranes and binds to tissues, resulting in a larger V_d [30]. Finally, HA-DOX conjugates exhibited a 2.2-fold increase in systemic mean residence time relative to unbound i.v. DOX. The extended residence time of HA-DOX conjugates may decrease the frequency of doxorubicin chemotherapy and have potential to improve patient compliance and quality of life in a clinical setting. The sustained release drug-carrier model avoids peak and trough of plasma drug concentration in both drug distribution and elimination, leading to a well controlled drug level profile corresponding to its therapeutic index.

6. Toxicology

Renal toxicity is one of the side effects found with the administration of anthracycline antibiotics. The potential renal toxicity of DOX and HA-DOX was determined using lysosomal enzyme, β-N-Acetylglucosaminidase (NAG) (Sigma), which acts as an indicator of ongoing kidney damage. Two groups (n=3) of Sprague-Dawley rats were treated with 4 mg/kg of either i.v. DOX or s.c. HA-DOX. Animals were housed in metabolic cages and their urine was collected daily. The urine samples were centrifuged and stored at -80 ℃ freezer until analysis. The animals were euthanized after 8-10 days. The urine samples were analyzed for the concentration of NAG upon hydrolyzing the NAG substrate, 4-nitrophenyl.

NAG is a urinary enzyme that is sensitive to early renal tubular dysfunction. It is commonly and widely used as a biomarker for the early detection of renal tubular damage. NAG is expressed in normal kidney at a relatively constant level. However, elevated urinary NAG activity in chemotherapy treated animals may be associated with renal tubular dysfunction caused by the administered chemotherapeutic agent. The NAG activity in animals treated with s.c HA-DOX exhibited a relatively steady level during the study period of 9 days (Figure 5A). On the other hand, animals that were treated with i.v. DOX demonstrated a slight increase in NAG activity starting two days after drug administration (Figure 5B). A dose of 4 mg/kg DOX or HA-DOX may not be sufficient to induce significant renal tubular damage (Figure 5C).

Furthermore, cardiotoxicity is also a dose-limiting toxicity associated with doxorubicin therapy. The cardiac toxicity of DOX and HA-DOX was determined using a rat cardiac Troponin-I (cTnI) ELISA kit (Life Diagnostic). Sprague-Dawley rats were cannulated in the

A
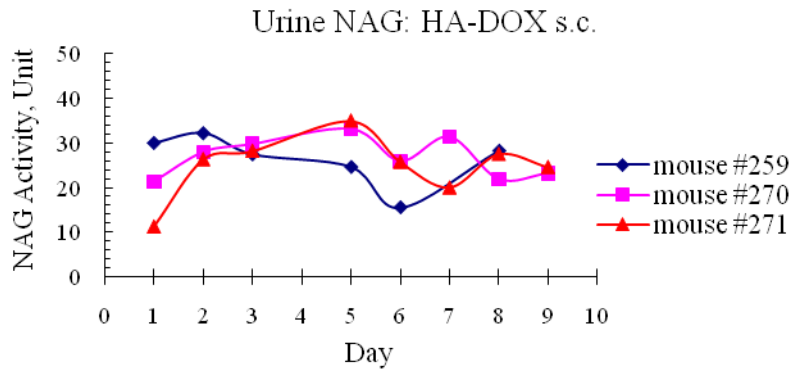
B
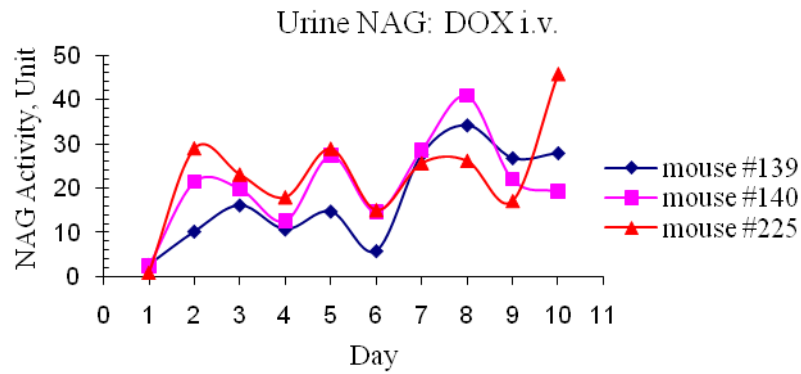
C
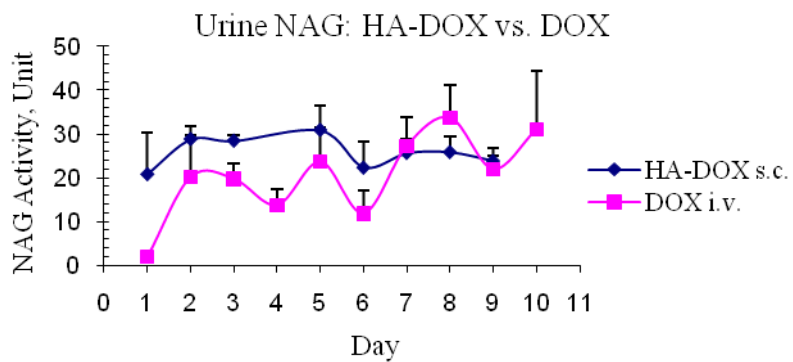
Figure 5. Urine NAG level of i.v. DOX or s.c. HA-DOX treated rats.

jugular vein and injected with 4 mg/kg DOX·HCl solution i.v. or HA-DOX s.c. into the mammary fat pad. Blood samples were collected at 0, 8, 16, 24 hrs and 2, 3, 4, 5 and 6 days from the jugular vein and centrifuged to obtain the plasma. Samples were stored at -80 ℃ freezer until analysis.

Doxorubicin-induced cardiomyopathy and congestive heart failure was believed to be dose-dependent. Troponin I is a cardio-specific protein that is released from injured myocytes. It is a highly sensitive and specific biomarker for cardiac damage. The cTnI levels, for i.v. DOX and s.c HA-DOX, were both below the detection limit of the commercial available cTnI assay kit (0.156 ng/mL); indicating that 4 mg/kg was a relatively low dose for an animal model of doxorubicin-induced cardiotoxicity.

7. Pathology

Sprague-Dawley rats were divided into two groups and treated with DOX s.c. or HA-DOX s.c. (n=6/group) at either 2 or 4 mg/kg. Three rats from each group were euthanized 6 hrs after drug administration and the other three were euthanized 24 hrs after drug administration. The liver, bilateral kidneys, spleen, lungs, heart, right (ipsilateral) and left (contralateral) axillary nodes, and brain, were excised intact and stored in 80 % alcoholic formalin solution overnight for fixation before slide mounting. The H&E staining were conducted by Veterinary Lab Resources (Kansas City, KS). The pathological examination was performed by a blinded board-certified veterinarian pathologist (University of Kansas Medical Center, Kansas City, KS). The heart, kidneys, liver, lymph nodes and underlying tissue of the injection site, were normal with no microscopic changes for all study groups.

In addition, the long term toxicity (8-10 days) of DOX and HA-DOX at 4 mg/kg was evaluated. The liver and lymph nodes were normal, with no microscopic changes for both study groups. The underlying tissue of the injection site was examined for the HA-DOX s.c. treated animals, and no microscopic changes were observed. Mild degeneration in the kidney was detected for both groups, indicated by sparse pyknotic nuclei and mild inflammation. In addition, 83% of animals (n=6) receiving 4 mg/kg i.v. DOX were observed to have myocyte degeneration, including myofiber necrosis and myocarditis. In contrast, none of the animals (n=5) receiving s.c. HA-DOX exhibited cardiac damage. Overall, the pathology studies demonstrated that the HA-DOX conjugates had a lower incidence of cardiac toxicity compared to the conventional intravenous DOX treatment (Figure 6).

In spite of the high efficacy of DOX chemotherapy, its clinical use is limited due to its dose-limiting cardiac toxicity, along with its renal toxicity and hepatoxicity. Tissue toxicities from doxorubicin are typically caused by the generation of oxygen species from the conversion of DOX to the semiquinone, yielding very reactive hydroxyl radicals. The free radicals may also cause damage to various membrane lipids and other cellular components [31]. Pathological examination 10 days following a single dose of doxorubicin revealed significant cardiac differences between the s.c. HA-DOX and i.v. DOX formulations. Of the animals that received i.v. DOX, 83% developed myocarditis and cardiac myocyte degeneration. Other significant lesions included thrombosis and muscle inflammation around the thrombus. In contrast, only 20 % of animals that received s.c. HA-DOX developed very subtle myocyte degeneration. No lesions or inflammation were observed for 80% of the animals in the s.c. HA-DOX group, which clearly demonstrates that the HA-DOX formulation greatly reduces the cardiac toxicity of doxorubicin in a rodent model. Furthermore, the pathology studies demonstrated that the skin
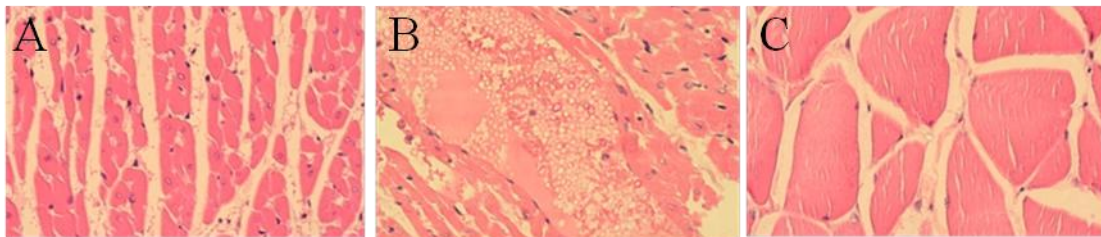
Figure 6. Heart tissues of (A) HA-DOX, (B) DOX and (C) underlying tissues of the HA-DOX injection site.

and cutaneous tissues at the injection site, were devoid of inflammation or necrosis at both 6 and 24 hours after HA-DOX injection. This finding may be corroborated clinically with the use of hyaluronan as a rescue medication, to alleviate the local toxicity effects of doxorubicin that has extravasated into the subcutaneous tissues following dislodgement of an i.v. catheter during intravenous administration. This effect was confirmed in tissue biopsies at the conclusion of the study (10 days post injection), which demonstrated no substantial damage to the underlying tissue at the injection site. Therefore, HA-DOX conjugates have the potential to reduce the incidence of local skin and soft tissue toxicity from doxorubicin chemotherapy, which would improve patient tolerance and compliance in clinical application.

Another strategy for reducing doxorubicin associated cardiac and liver toxicity is metronomic chemotherapy, which involves continuous administration of doxorubicin at regular short intervals, as opposed to bolus dosing with a higher concentration of the drug [32]. Metronomic dosing regimens decrease the non-specific toxicity of an anti-cancer drug in normal cells. In addition, in a study by Pastorino et al., a metronomic chemotherapy of a NGR peptide coupled liposomal doxorubicin formulation greatly hindered the progression of orthotopic neuroblastoma xenografts in immunodeficient mice [33]. This dosing regimen, however, has its own drawbacks clinically, in that more frequent intravenous doses are required, which adds to patient discomfort, time spent in infusions, and creates nursing as well as compliance issues.

8. **Tumor model and *in vivo* drug release**

MDA-MB-468LN human breast cancer cells (kind gift of Ann Chambers, London University) were implanted into the mammary fat pad of female nude mice from a small incision

using a 27-ga needle (100 µL, 10^6 cells) under pentobarbital sedation. The incision was closed using sterilized staples, which were removed when the incision healed. The MDA-MB-468LN human breast cancer cell line can be transfected with a GFP-neomycin expression vector and selected with G418, to express green fluorescent protein (GFP) so that metastasis can be monitored by whole animal fluorescent imaging. The tumor growth was monitored by fluorescent imaging using the CSI Maestro imaging system, and the tumor size was measured twice a week using digital calipers on mice anesthetized with 1.5-2 % isoflurane in 50 % oxygen-50 % ambient air mixture. The tumor volume was calculated using the equation: Tumor Volume (mm^3) = 0.52×(width)^2×length.

In order for the nanocarriers to deliver anticancer drugs to nano- and micrometastases in the breast locoregional lymphatics, carriers should drain from the injection site near the breast area to the diseased lymph nodes. The injected HA-DOX conjugates to verify drainage into the diseased lymph nodes, which were indicated by the dashed circle in the following figures. Nude mice with mammary tumors (approximately 500 mm^3) were injected peritumorally with a single dose of 3.5 mg/kg HA-DOX solution. The injection site and location of the primary tumor were also labeled on each figure. Drainage of HA-DOX to the locoregional lymphatics in the axilla, was characterized after a s.c. needle injection near a nodal breast tumor.

Mice were imaged, and the images of the primary tumor and lymphatic metastases were captured from day 1 to day 9 after drug administration. The distribution characteristics of HA-DOX were monitored, and percentage of DOX released calculated by spectrally unmixing of the tumor GFP, DOX, and skin autofluorescent signals, using the Maestro software. After one day, 10% of the initial HA-DOX drained to the tumor, and 66% drained to the tumor lymphatics and local tissues. After a week, 4% of original dose remained in the primary tumor, with 10% of the

156

initial dose in the surrounding area and adjacent lymph nodes. Clearance of drug from the tumor was 80% slower than from the surrounding tissues and lymphatics (Figure 7). Intravenous DOX could not be detected in the tumor or surrounding tissues by *in vivo* imaging at any time point (data not shown).

9. Anticancer efficacy in breast cancer bearing nude mice

Nude mice were injected with into the first mammary fat pad on the right side with 10^7 MDA-MB-468LN cells, and were randomly divided into four groups including: saline, HA, DOX, and HA-DOX (n=5/group). Animals of the saline and HA control groups were euthanized once their tumor size reached 2000 mm^3. Animals in the DOX or HA-DOX treatment groups were euthanized once their tumor reached 1000 mm^3 in size or 24 weeks after tumor cells were injected. In addition, animals were euthanized during the study if tumors ulcerated, or the animals acquired opportunistic infections. Mammary tumors were observed three weeks after tumor cells were implanted. All treatments were administered in the 3rd and 4th weeks after tumor cell implantation. Two doses of 3.5 mg/kg DOX or physiological saline were administered i.v. via the tail vein; whereas two doses of 3.5 mg/kg of HA-DOX (on DOX basis) or HA were administered s.c. 2-3 mm from the tumor margins. The size of the primary tumors was measured weekly.

Animals treated with saline or HA had an average tumor size of approximately 2000 mm^3 in nine weeks, which indicated that HA does not alter the natural progression of breast cancer. On the other hand, the animals that were treated with three weekly doses of i.v. DOX developed a tumor with an average size of 1000 mm^3 after approximately ten weeks. In contrast, animals in
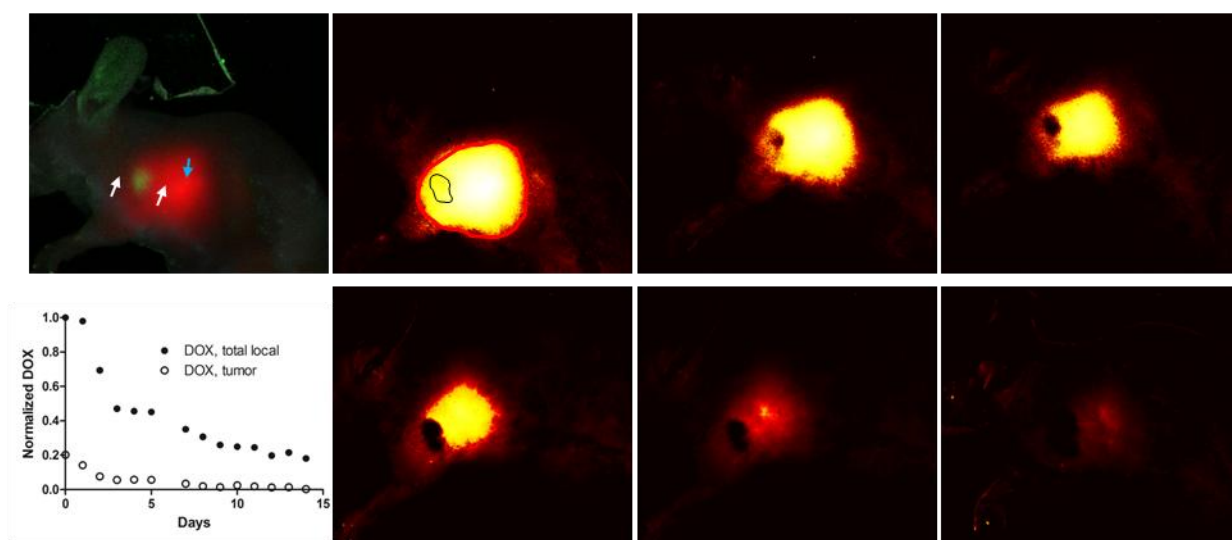
Figure 7. Imaging of HA-DOX in the primary tumor and the surrounding lymphatics (day 1-9). HA-DOX was injected peritumorally (white arrows) with most of the carrier draining to the adjacent nodes (blue arrow). After spectrum unmixing and false coloring, the total DOX (within the red circle) and tumoral DOX (within black circle) were integrated and normalized to day 0. Doxorubicin is falsely colored white-yellow-red with decreasing intensity.

the s.c. HA-DOX treated group (three weekly equivalent doses of HA-DOX) reached an average tumor size of around 300 mm^3 ten weeks after the tumor cell injection (Figure 8A). In addition, 100% animal death occurred 18 weeks after the tumor cell injection for DOX treated group (Figure 8B). In contrast, 50% of HA-DOX treated animals lived for the duration of the study (24 weeks) with an average tumor delay of 4 weeks. Overall, the result of the tumor model suggests that HA-DOX conjugates achieved a higher anti-cancer efficacy relative to the conventional i.v. DOX therapy. HA-DOX conjugates delayed the tumor progression by approximately 10 weeks and increased the survival of the animals relative to the i.v. DOX treatment (p<0.05). We believe the carrier slowly released the active form of the drug, which subsequently drained to the adjacent axilla lymph nodes and the surrounding lymphatic regions.

In conclusion, HA-DOX by weekly subcutaneous injections would have great benefits over standard or metronomic dosing regimens, both in terms of patient compliance and tolerance, but also with regard to potential improved toxicity and efficacy. Further translational efforts will focus on optimizing the dosing frequency and completing preclinical proof of concept.
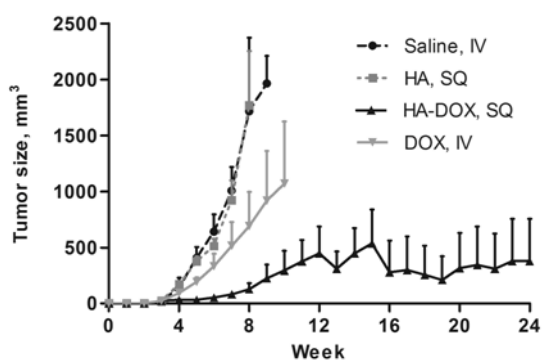
A.   B.
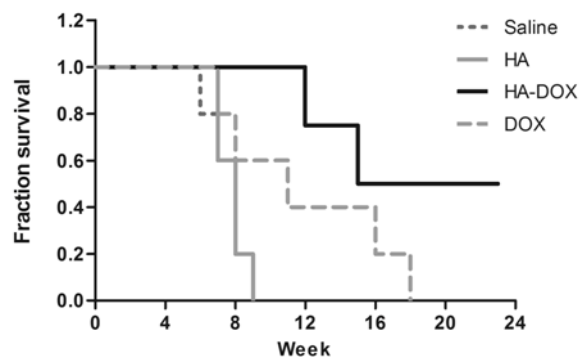
Figure 8. (A) Measurement of tumor volume and (B) survival curve of the tumor bearing animals.

10. References

[1] G. Takemura, H. Fujiwara, Doxorubicin-induced cardiomyopathy from the cardiotoxic mechanisms to management, Prog. Cardiovasc. Dis., 49 (2007) 330-352.

[2] X. Xu, R. Sutak, D.R. Richardson, Iron chelation by clinically relevant anthracyclines: alteration in expression of iron-regulated genes and atypical changes in intracellular iron distribution and trafficking, Mol. Pharmacol., 73 (2008) 833-844.

[3] Y. Matsumura, T. Hamaguchi, T. Ura, K. Muro, Y. Yamada, Y. Shimada, K. Shirao, T. Okusaka, H. Ueno, M. Ikeda, N. Watanabe, Phase I clinical trial and pharmacokinetic evaluation of NK911, a micelle-encapsulated doxorubicin, Br. J. Cancer, 91 (2004) 1775-1781.

[4] B. Rihova, J. Strohalm, J. Prausova, K. Kubackova, M. Jelinkova, L. Rozprimova, M. Sirova, D. Plocova, T. Etrych, V. Subr, T. Mrkvan, M. Kovar, K. Ulbrich, Cytostatic and immunomobilizing activities of polymer-bound drugs: experimental and first clinical data, J. Control. Release, 91 (2003) 1-16.

[5] A.W. Tolcher, S. Sugarman, K.A. Gelmon, R. Cohen, M. Saleh, C. Isaacs, L. Young, D. Healey, N. Onetto, W. Slichenmyer, Randomized phase II study of BR96-doxorubicin conjugate in patients with metastatic breast cancer, J. Clin. Oncol., 17 (1999) 478-484.

[6] National Cancer Institute: Breast cancer PDQ treatment, in, 2007.

[7] P. Querzoli, M. Pedriali, R. Rinaldi, A.R. Lombardi, E. Biganzoli, P. Boracchi, S. Ferretti, C. Frasson, C. Zanella, S. Ghisellini, F. Ambrogi, L. Antolini, M. Piantelli, S. Iacobelli, E. Marubini, S. Alberti, I. Nenci, Axillary lymph node nanometastases are prognostic factors for disease-free survival and metastatic relapse in breast cancer patients, Clin. Cancer Res., 12 (2006) 6696-6701.

[8] M.d. Boer, C.H.v. Deurzen, J.A.v. Dijck, G.F. Borm, P.J.v. Diest, E.M. Adang, J.W. Nortier, E.J. Rutgers, C. Seynaeve, M.B. Menke-Pluymers, P. Bult, V.C. Tjan-Heijnen, Micrometastases or isolated tumor cells and the outcome of breast cancer, N. Engl. J. Med., 361 (2009) 653-663.

[9] J.R. Fraser, T.C. Laurent, Turnover and metabolism of hyaluronan, Ciba. Found. Symp., 143 (1989) 41-53; discussion 53-49, 281-285.

[10] T. Ahrens, V. Assmann, C. Fieber, C. Termeer, P. Herrlich, M. Hofmann, J.C. Simon, CD44 is the principal mediator of hyaluronic-acid-induced melanoma cell proliferation, J. Invest. Dermatol., 116 (2001) 93-101.

[11] A. Dietrich, E. Tanczos, W. Vanscheidt, E. Schopf, J.C. Simon, High CD44 surface expression on primary tumours of malignant melanoma correlates with increased metastatic risk and reduced survival, Eur. J. Cancer, 33 (1997) 926-930.

[12] M. Gotte, G.W. Yip, Heparanase, hyaluronan, and CD44 in cancers: a breast carcinoma perspective, Cancer Res., 66 (2006) 10233-10237.

[13] S. Misra, S. Ghatak, B.P. Toole, Regulation of MDR1 expression and drug resistance by a positive feedback loop involving hyaluronan, phosphoinositide 3-kinase, and ErbB2, J. Biol. Chem., 280 (2005) 20310-20315.

[14] A. Bartolazzi, R. Peach, A. Aruffo, I. Stamenkovic, Interaction between CD44 and hyaluronate is directly implicated in the regulation of tumor development, J. Exp. Med., 180 (1994) 53-66.

[15] T. Asplund, P. Heldin, Hyaluronan receptors are expressed on human malignant mesothelioma cells but not on normal mesothelial cells, Cancer Res., 54 (1994) 4516-4523.

[16] S. Sugahara, S. Okuno, T. Yano, H. Hamana, K. Inoue, Characteristics of tissue distribution of various polysaccharides as drug carriers: influences of molecular weight and anionic charge on tumor targeting, Biol. Pharm. Bull., 24 (2001) 535-543.

[17] C. Cera, M. Palumbo, S. Stefanelli, M. Rassu, G. Palu, Water-soluble polysaccharide-anthracycline conjugates: biological activity, Anticancer Drug Des., 7 (1992) 143-151.

[18] K. Akima, H. Ito, Y. Iwata, K. Matsuo, N. Watari, M. Yanagi, H. Hagi, K. Oshima, A. Yagita, Y. Atomi, I. Tatekawa, Evaluation of antitumor activities of hyaluronate binding antitumor drugs: synthesis, characterization and antitumor activity, J. Drug Target., 4 (1996) 1-8.

[19] Y. Luo, G.D. Prestwich, Synthesis and selective cytotoxicity of a hyaluronic acid-antitumor bioconjugate, Bioconjugate chemistry, 10 (1999) 755-763.

[20] K.H. Bouhadir, E. Alsberg, D.J. Mooney, Hydrogels for combination delivery of antineoplastic agents, Biomaterials, 22 (2001) 2625-2633.

[21] S. Cai, Y. Xie, T. Bagby, M.S. Cohen, M.L. Forrest, Intralymphatic chemotherapy using a hyaluronan-cisplatin conjugate, J. Surg. Res., 147 (2008) 247-252.

[22] A.H.M. A.M. Al-Ghananeem, Y.M. Muammer, J.M. Balko, E.P. Black, W. Mourad, E. Romond, Intratumoral delivery of Paclitaxel in solid tumor from biodegradable hyaluronan nanoparticle formulations, AAPS PharmSciTech, 10 (2009) 410-417.

[23] R.M. D. Peer, Loading mitomycin C inside long circulating hyaluronan targeted nano-liposomes increases its antitumor activity in three mice tumor models, Int. J. Cancer, 108 (2004) 780-789.

[24] A.K. Yadav, P. Mishra, A.K. Mishra, S. Jain, G.P. Agrawal, Development and characterization of hyaluronic acid-anchored PLGA nanoparticulate carriers of doxorubicin, Nanomedicine, 3 (2007) 246-257.

[25] A.K. Yadav, P. Mishra, S. Jain, A.K. Mishra, G.P. Agrawal, Preparation and characterization of HA-PEG-PCL intelligent core-corona nanoparticles for delivery of doxorubicin, J. Drug Target., 16 (2008) 464-478.

[26] H. Lee, C.H. Ahn, T.G. Park, Poly[lactic-co-(glycolic acid)]-grafted hyaluronic acid copolymer micelle nanoparticles for target-specific delivery of doxorubicin, Macromol. Biosci. , 9 (2009) 336-342.

[27] R. Soloman, A.A. Gabizon, Clinical pharmacology of liposomal anthracyclines: focus on pegylated liposomal Doxorubicin, Clin. Lymphoma Myeloma, 8 (2008) 21-32.

[28] D. Lorusso, A.D. Stefano, V. Carone, A. Fagotti, S. Pisconti, G. Scambia, Pegylated liposomal doxorubicin-related palmar-plantar erythrodysesthesia ('hand-foot' syndrome), Ann. Oncol., 18 (2007) 1159-1164.

[29] M.E. O'Brien, N. Wigler, M. Inbar, R. Rosso, E. Grischke, A. Santoro, R. Catane, D.G. Kieback, P. Tomczak, S.P. Ackland, F. Orlandi, L. Mellars, L. Alland, C. Tendler, Reduced cardiotoxicity and comparable efficacy in a phase III trial of pegylated liposomal doxorubicin HCl (CAELYX/Doxil) versus conventional doxorubicin for first-line treatment of metastatic breast cancer, Ann. Oncol., 15 (2004) 440-449.

[30] P.E. Wallemacq, A. Capron, R. Vanbinst, E. Boeckmans, J. Gillard, B. Favier, Permeability of 13 different gloves to 13 cytotoxic agents under controlled dynamic conditions, Am. J. Health Syst. Pharm., 63 (2006) 547-556.

[31] R.D. Olson, P.S. Mushlin, Doxorubicin cardiotoxicity: analysis of prevailing hypotheses, FASEB J., 4 (1990) 3076-3086.

[32] A.J. Quesada, T. Nelius, R. Yap, T.A. Zaichuk, A. Alfranca, S. Filleur, O.V. Volpert, J.M. Redondo, In vivo upregulation of CD95 and CD95L causes synergistic inhibition of angiogenesis by TSP1 peptide and metronomic doxorubicin treatment, Cell Death Differ., 12 (2005) 649-658.

[33] F. Pastorino, C. Brignole, D. Marimpietri, M. Cilli, C. Gambini, D. Ribatti, R. Longhi, T.M. Allen, A. Corti, M. Ponzoni, Vascular damage and anti-angiogenic effects of tumor vessel-targeted liposomal chemotherapy, Cancer Res., 63 (2003) 7400-7409.

Chapter 4

Combination Chemotherapy

1. Introduction

Cancer cells undergo random and uncontrolable mutations, it is quite common for them to become resistant to a single type of chemotherapy. Usually the most successful cancer chemotherapy regimens involve the administration of multiple anti-cancer drugs simultaneously. Because different chemotherapies may have different mechanisms of action; it is difficult for cancer cells to become resistant to combination therapy. For instance, cisplatin crosslinks the DNA in cancer cells; doxorubicin inhibits protein biosynthesis in cancer cells; and taxane stabilizes microtubules, thus preventing cancer cells from entering mitosis.

Many cancer patients experience high initial cisplatin responsiveness during their treatment; however, the majority of the patients eventually develop cisplatin-resistant disease, either at the late stage of their cancer or when their cancer relapses. The mechanism of cisplatin resistance has been investigated extensively over the past decades. It is believed that cisplatin resistance is a complex process, in which many mechanisms are involved, such as: increased DNA repair of cancer cells [1], decreased intracellular drug accumulation [2], enhanced cisplatin efflux [3], and activated drug detoxification pathways [4].

To overcome chemoresistance, a number of combination therapy regimens have been investigated in clinical trials and preclinical studies. The first-line combination therapies for head and neck cancer include: combination of cisplatin, docetaxel and 5-FU, combination of cisplatin and cetuximab, and combination of 5-FU and carboplatin. Commonly used combination therapies for breast cancer include: combination of doxorubicin and cyclophosphamide, combination of cyclophosphamide, adriamycin and fluorouracil, and combination of carboplatin and paclitaxel.

Built upon the results of chapter 2, this chapter focuses on the development and evaluation of locoregional cisplatin-based combination chemotherapy for the treatment of breast cancer and head and neck cancer. As discussed in chapter 2, subcutaneous hyaluronan-cisplatin (HA-Pt) conjugates demonstrated a similar anti-cancer efficacy and survival rate as the conventional cisplatin therapy in a murine xenograft model of breast cancer. Based on a study conducted at Dr. Cohen's laboratory, when the HA-Pt conjugates were subcutaneously co-administered with the hyaluronan-doxorubicin (HA-DOX) conjugates, the anti-cancer effectiveness and survival rate were significantly improved compared to the intravenous combination therapy of doxorubicin and cisplatin. Efficacy results for breast tumor bearing mice treated with HA-conjugated doxorubicin/cisplatin (DOX/CDDP) at 50% MTD include: [complete responses (CR)=5, partial responses (PR)=2, and stable disease (SD)=1]. In comparison, mice given standard DOX/CDDP (50% MTD) demonstrated: [progressive disease (PD)=6, SD=1, and PR=1]. The results suggested that subcutaneous nanocarrier-delivery of doxorubicin and cisplatin significantly improved efficacy compared to standard agent combination therapy. Based on the success of this localized combination therapy, we sought to develop combination regimens of cisplatin and nitric oxide-producing prodrugs with the goal of improving the cytotoxicity and overcoming the chemoresistance of cisplatin therapy.

Recent investigations have discovered that nitric oxide (NO) may be involved in the reversal of cisplatin resistance in head and neck cancer [5], ovarian cancer [6-7] and lung cancer [8], via mechanisms of survivin modulation, depletion of cellular thiols, and inhibition of Bcl-2 ubiquitination, respectively. Similar re-sensitizing effects of nitric oxide were also reported in the reversal of doxorubicin chemo-resistance in human colon cancer [9]. Previously, a series of nitric oxide-producing prodrugs were synthesized in the Forrest laboratory. Herein, we sought to

169

develop combination chemotherapy regimens that utilize nitric oxide donors to regulate the cell sensitivity to cisplatin therapy in two cell culture models: head and neck squamous cell cancer cell line MDA-1986 and breast cancer cell line MDA-MB-468LN.

2. Synthesis of sugar star polymer-nitric oxide prodrug conjugates

A series of nitric oxide-releasing JS-K prodrug analogues (NO1 - NO4, Figure 1A) and a 4-arm sugar star polymer carrier [4-arm star poly-(1,2:3,4-*Di-O*-isopropylidene-6-*O*-methacryloyl-α-*D*-galactopyranose), Figure 1B] were previously synthesized in the Forrest laboratory. Subsequently, sugar star polymer-nitric oxide prodrug conjugates (Figure 1C and 1D) were developed by the formation of an ester bond between the nitric oxide-releasing prodrug and sugar star polymer, to deliver gaseous nitric oxide chemotherapy to cancer cells. The synthetic steps are presented in the Appendix.

3. *In vitro* release of nitric oxide

In order to better simulate *in vivo* drug release conditions, a series of *in vitro* nitric oxide release studies were carried out in cell culture media (DMEM with 10% bovine serum albumin and 1% L-glutamine) with human head and neck cancer cells, MDA-1986. The nitric oxide release kinetics were determined in 96-well plates with 3,000 cells per well. The concentration of nitrite, the breakdown product of gaseous nitric oxide, was measured using the Griess assay as an indirect measurement of the nitric oxide concentration in cell culture media. The assay is based on the reaction between sulfanilamide, N-1-napthyethylenediamine dihydrochloride and nitrite,

170

A.

NO1:

NO2:

JS-K (NO3):

NO4:
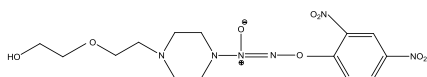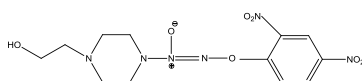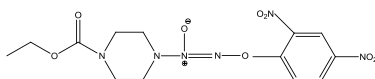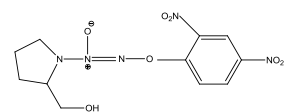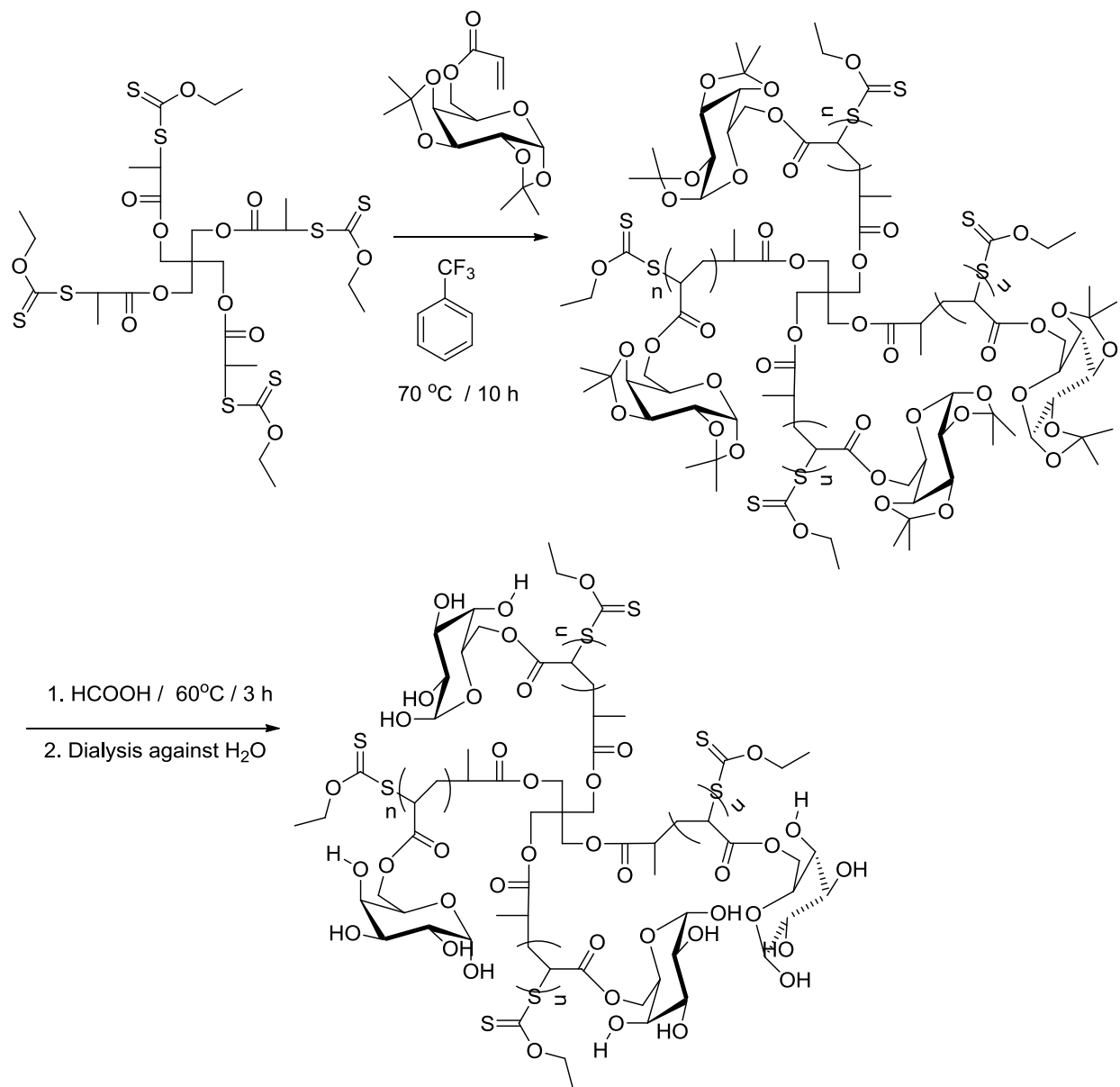
C.
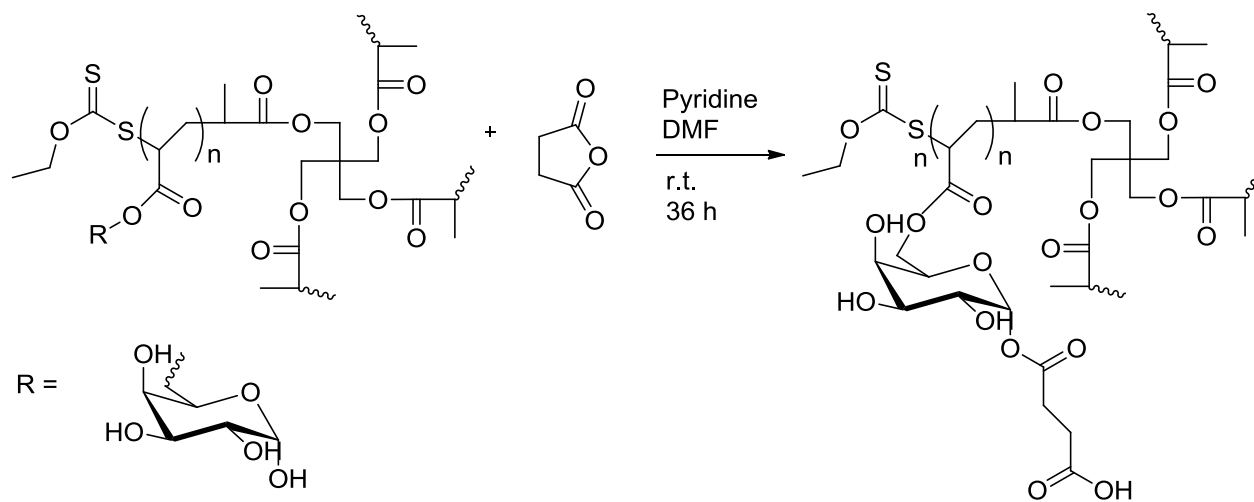
D.
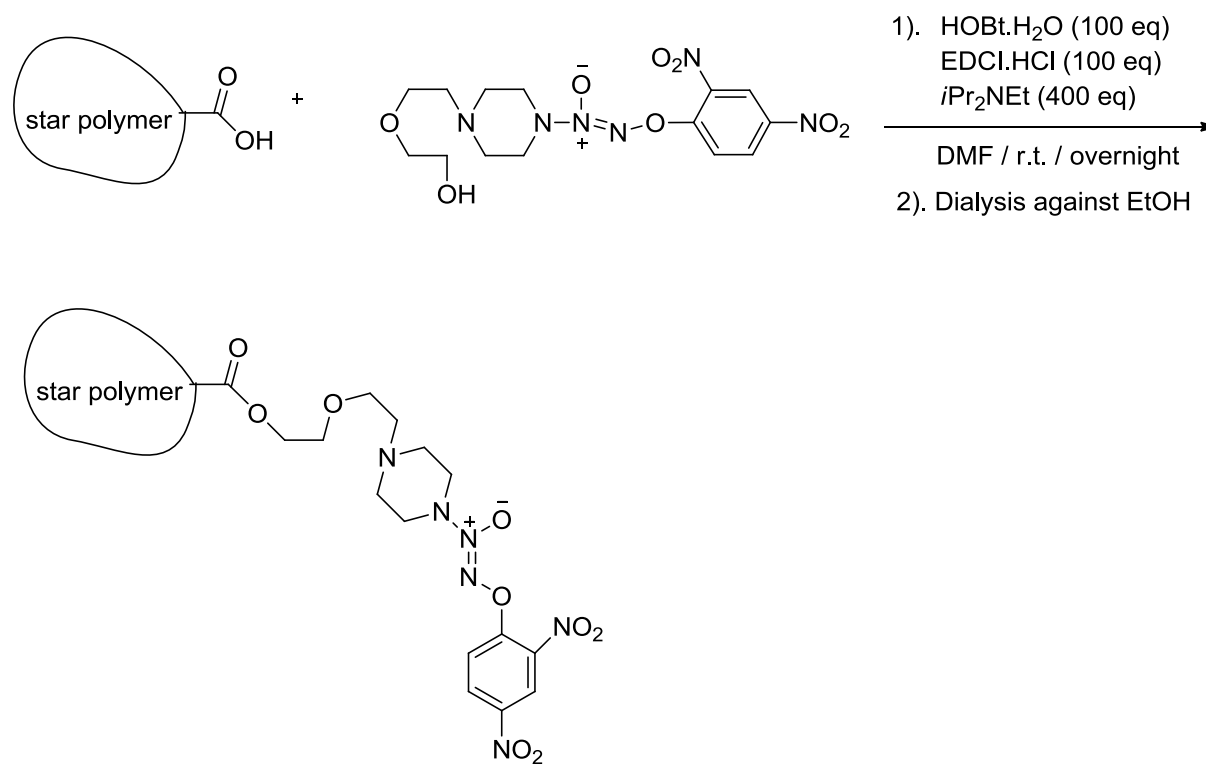
Figure 1. (A) Chemical structures of nitric oxide-releasing prodrugs 1-4 (NO1-NO4); (B) synthesis of the sugar star polymers; (C) synthesis of an acid derivative of the sugar star polymer; and (D) synthesis of sugar star polymer-nitric oxide prodrug 1 conjugate (sugar-NO1)

under acidic conditions to produce a fluorescent azo compound. A nitrite calibration curve was generated under the same condition using a series of nitrite solution (0, 1.56, 3.13, 6.25, 12.5, 25, 50, and 100 µM).

To determine the nitric oxide release from the prodrugs, MDA-1986 cells were seeded in six 96-well plates 24 hours prior to drug treatment (100 µL/well). On the following day, cells were treated with either one of the nitric oxide prodrugs (NO1, NO2 or JS-K) or the sugar polymer based nitric oxide prodrug conjugate number 1 (sugar-NO1) at three different concentrations (0.2, 0.1 and 0.05 mM). Fifty microliters of cell culture media were collected from each plate at 10 minutes, 2, 7, 22, 48 and 96 hours, post treatment to determine the nitrite content (N=5). The Griess reaction was performed according to the manufacturer's suggestions. The fluorescence intensity was measured between 520 nm and 550 nm using a fluorescence microplate reader. Thus, the nitrite concentration and the corresponding nitrite oxide levels were determined using the nitrite standard curve previously generated.

All three nitric oxide prodrugs, NO1, NO2 and JS-K, as well as the sugar-NO1 conjugate, released nitric oxide in a sustained, concentration-dependent pattern, generating half lives of 6, 7, 3, and 10 hours, respectively (Figure 2). The sugar-NO1 exhibited the longest release half-life, which was 2.3-fold longer than the standard NO-releasing drug, JS-K. Therefore, if the *in vitro* drug release kinetics correctly represent the *in vivo* conditions, the sugar-NO1 conjugate may be a promising candidate for the controlled release of nitric oxide in tumor-bearing animals.

4. Cytotoxicity of cisplatin-nitric oxide combination chemotherapy
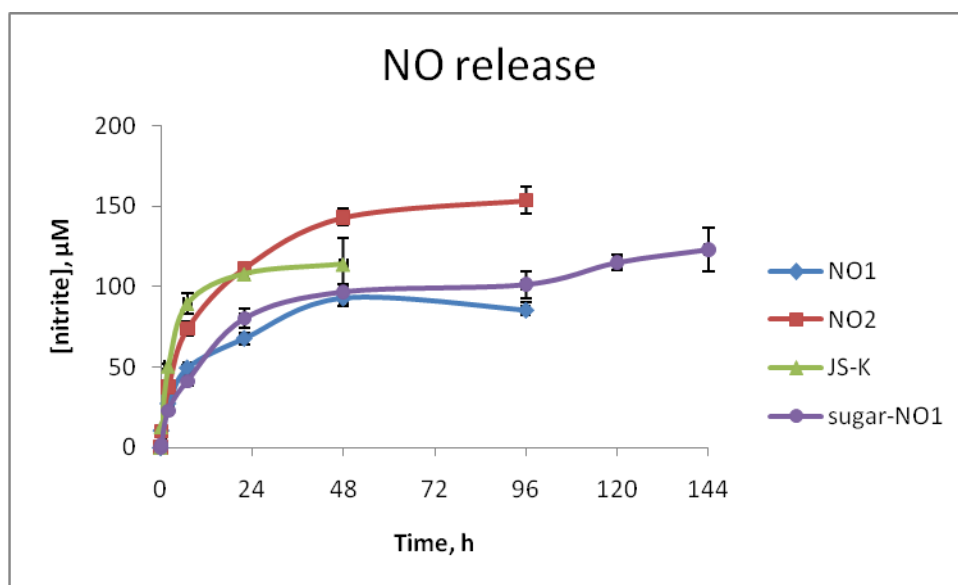
Figure 2. *In vitro* release of nitric oxide from NO1, NO2, JS-K, and sugar-NO1 (0.02 mM starting concentration on NO basis). Release studies were performed in DMEM with the presence of MDA-1986 cells. Release half lives were determined to be 6, 7, 3, and 10 hours, for NO1, NO2, JS-K, and sugar-NO1, respectively.

176

To select a model compound out of the four nitric oxide-releasing prodrugs synthesized for further investigation of CDDP/NO combination therapy, the cytotoxicity of these prodrugs was determined in the human head and neck cancer cell line MDA-1986 and human breast cancer cell line MDA-MB-468LN. Free NO1 and NO2 both had slightly lower *in vitro* toxicity when compared to JS-K in MDA-1986 cells; whereas, they both showed slightly higher *in vitro* toxicity in MDA-MB-468LN cells relative to JS-K (Table 1). In addition, the IC_{50} of the sugar star polymer-based conjugate was determined in the aforementioned cell lines. Even though the sugar-NO1 had higher IC_{50} values than JS-K and unbound NO1, the sustained nitric oxide-releasing platform may provide modified drug pharmacokinetics *in vivo*. NO4 had extremely high IC_{50} values; therefore, it was eliminated from the investigation in the remainder of the studies.

A cisplatin-NO combination therapy strategy was designed to further evaluate the *in vitro* toxicity of the chemotherapeutics against human head and neck cancer and breast cancer. Based on IC_{50} measurements, all the combination groups (CDDP + NO prodrug) revealed similar (NO1 and NO2) or lower (JS-K) toxicity compared to their nitric oxide prodrug counterparts. Interestingly, CDDP/NO1 combination ([NO1] = 5% IC_{50} of NO1) appeared to have an equivalent (MDA-1986) or improved (MDA-MB-468LN) efficacy compared to CDDP treatment alone. Therefore, we decided to select NO1 as our model nitric oxide-releasing compound to further evaluate the optimal dose, treatment schedule, and cytotoxicity of CDDP/NO1 combination therapy, in comparison to standard cisplatin treatment in a cell culture model.

5. **Determination of CDDP and NO1 concentrations for cell assays**

Treatment/Cell lines	IC_{50}: MDA-1986	IC_{50}: MDA-MB-468LN
CDDP	7.0 μM	17.0 μM
NO1	32.3 μM	23.6 μM
Sugar-NO1	86.0 μM	67.0 μM
NO1 + CDDP (25% × [IC_{50}])	39.8 μM	27.5 μM
CDDP + NO1 (5% × [IC_{50}])	7.0 μM	8.0 μM
NO2	56.6 μM	26.9 μM
NO2 + CDDP (25% × [IC_{50}])	41.7 μM	35.9 μM
NO3 (JS-K)	15.8 μM	42.1 μM
NO3 + CDDP (25% × [IC_{50}])	316.2 μM	203.7 μM
NO4	2.8 mM	4.4 mM
NO4 + CDDP (25% × [IC_{50}])	891 μM	631 μM

Table 1. IC_{50} values of CDDP, nitric oxide prodrugs (NO1-NO4), and combination treatments (NO1&CDDP and NO2&CDDP). Cell viability was determined in MDA-1986 and MDA-MB-468LN cell lines 72 hours post drug treatment (SD<15%).

Three concentrations of CDDP (0.01, 0.04 and 0.1 mM), three concentrations of NO1 (0.01, 0.03 and 0.1 mM), and two concentrations of sugar-NO1 (0.01 and 0.03 mM) were tested to determine the optimal dose ranges of each drug for cell viability assays. The highest concentrations of CDDP (0.1 mM) and NO1 (0.04 mM) both caused a large percentage (> 80%) of cell death, thus they were eliminated from the remainder of the experiments. The percentage of cell death was estimated by visual comparison of the surface area of the cell culture flask that was covered with the adherent cells between pre-treatment and post-treatment conditions. Three low concentrations of cisplatin, 0.01, 0.02 and 0.03 mM, which induced less than 20% cell death, were determined to be the working drug concentrations. Similarly, one relatively low concentration of NO1, 0.02 mM, which led to less than 10% death of MDA-1986 cells, was selected for further experiments.

6. Evaluation of CDDP/NO1 combination therapy in head and neck cancer cells

To compare the cytotoxicity of CDDP/NO1 combination therapy to cisplatin treatment alone, the post-treatment cell viability was assessed using resazurin assay. Resazurin is a non-fluorescent molecule that is converted to a highly fluorescent molecule, resorufin, once it is reduced in mitochondria, making it an indicator of the metabolic activity of cells (Figure 3). MDA-1986 cells were trypsinized and seeded into 96-well plates (10,000 cells/well) 24 hours before drug treatment. On day one, NO1 was added (0.02 mM), and on day two, CDDP was added (0.01, 0.02 and 0.03 mM). The dosing schedule was based on the study conducted by Fetz et al., which investigated the synergistic effect between nitric oxide-producing prodrugs and cisplatin [5]. On the third day, resazurin blue in 10 μL of phosphate-buffered saline was added to
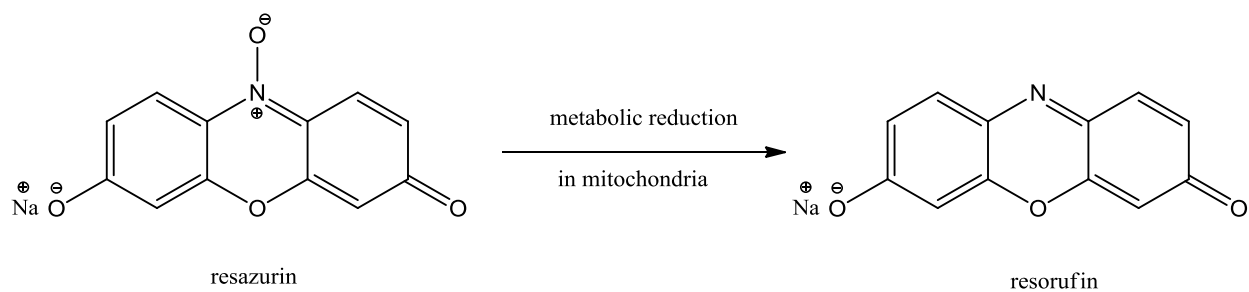
Figure 3. Conversion of resazurin to resorufin.

each well (final concentration of 5 µM). After 4 hours, the well fluorescence was measured (λ_{ex} 560 nm, λ_{em} 590 nm) using a fluorescent plate reader (SpectraMax Gemini; Molecular Devices, Sunnyvale, CA). The fluorescence intensity was then normalized against the untreated control.

The results of the resazurin assay indicate that all drug treatments caused reduced metabolic activity of the head and neck cancer cells compared to the untreated group (Figure 4). The CDDP/NO1 combination treatment resulted in a statistically significant reduction of cellular metabolic activity compared to cisplatin treatment alone ([CDDP]=0.02 and 0.03 mM, $p<0.05$). The improved effectiveness of the combination therapy over cisplatin treatment alone could be due to one of the two reasons: first, increased cell death; or second, improved suppression of cellular metabolic activity without causing cell death.

To determine the degree of cell death and understand the reduced metabolic activity generated by CDDP/NO1 combination therapy, trypan blue exclusion assay was conducted using an equivalent concentration of each drug and an identical dosing schedule as the previous resazurin assay (day 1: NO1 addition; day 2: CDDP addition; and day 3: assay). Trypan blue is a diazo dye that selectively stains dead cells by passing through the damaged or disrupted cellular membrane (Figure 5). Live cells have intact cellular membranes that are impermeable to trypan blue. Therefore, live and dead cells can be differentiated under a microscope. The trypan blue exclusion assay enables a direct evaluation of cell viability post drug treatment; whereas, the resazurin assay mainly measures the mitochondrial metabolic activity of cells. Reduced metabolic activity may not be directly correlated with cell death. The results of the trypan blue assay demonstrate that the CDDP/NO1 combination treatment caused significantly higher degree of cell death compared to cisplatin treatment alone at all concentrations ($p<0.05$), which is consistent with the results of the metabolic assay (Figure 6).
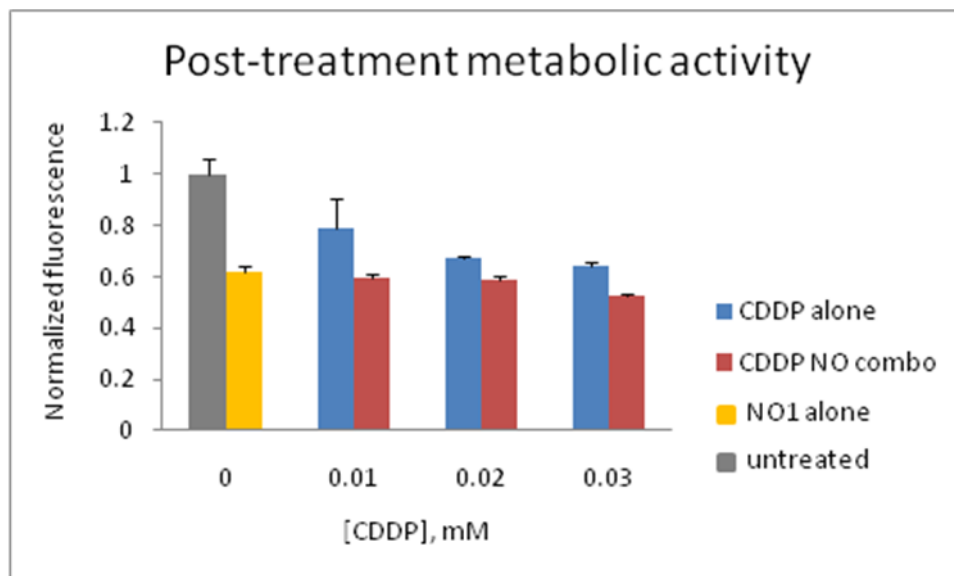
Figure 4. Measurement of metabolic activity in MDA-1986 cells using resazurin assay. Treatment groups included untreated control, NO1 alone (0.02 mM), CDDP alone (0.01, 0.02 and 0.03 mM), and CDDP/NO1 combination treatments ([NO1]=0.02 mM; [CDDP]=0.01, 0.02 or 0.03 mM). $p<0.05$ for [CDDP]=0.02 and 0.03 mM (N=4).
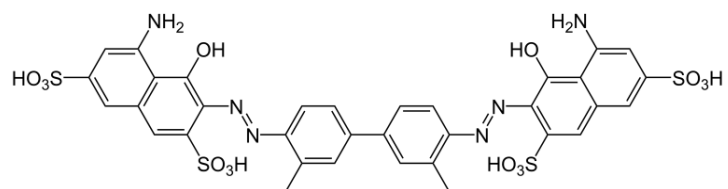
Figure 5. Chemical structure of trypan blue.
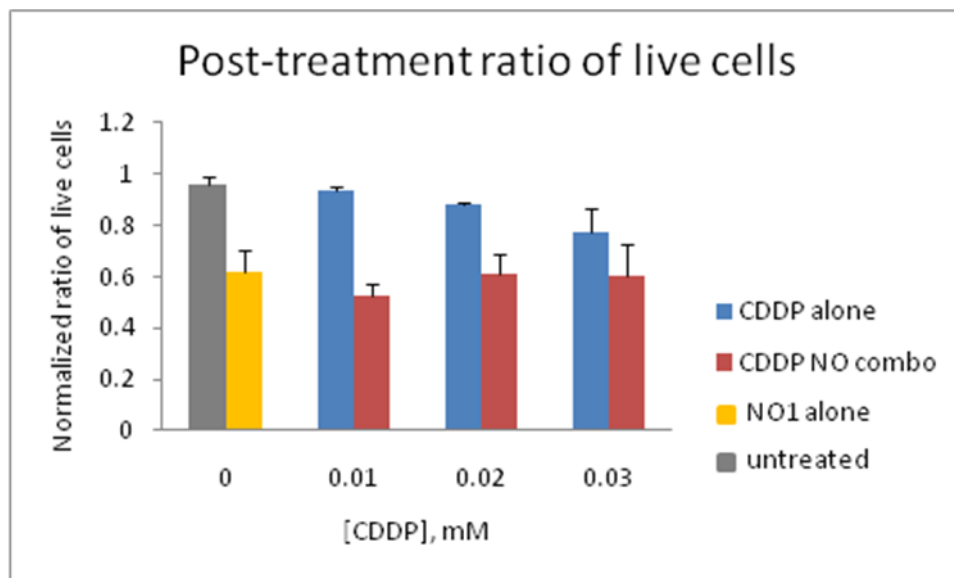
Figure 6. Determination of post-treatment cell counts using trypan blue exclusion assay. Treatment groups included untreated control, NO1 alone (0.02 mM), CDDP alone (0.01, 0.02 and 0.03 mM), and CDDP/NO1 combination treatments ([NO1]=0.02 mM; [CDDP]=0.01, 0.02 or 0.03 mM). $p<0.05$ for all CDDP concentrations (N=4).

The findings from the two assays (resazurin and trypan blue) led us to ask our next question: by which mechanism was the cell death caused in the combination therapy? Three of the known mechanisms of cell death include: apoptosis, necrosis and autophagy [10]. Apoptosis, also known as type I programmed cell death, is a process in which cells initiate intracellular suicide in response to stress, such as cytotoxic drug exposure. Apoptosis results in distinct morphological changes of cells including: cell membrane disruption, nuclear fragmentation and chromatin condensation. Unlike apoptotic suicide, necrosis is an "accident"-induced cell death pathway, which usually causes inflammatory response of the surrounding cells. The morphological changes involved in a necrotic pathway consist of the loss of plasma membrane integrity and leakage of cytoplasm [11]. Autophagy is another mechanism of programmed cell death (type II), which is characterized by the self-digestion of intracellular components via autolysosomal machinery. Autophagy can be induced by nutrient deprivation as well as insult by cytotoxic agents [12]. The underlying mechanisms of autophagy pathway are not yet clearly understood, but it is believed to be an alternative approach of cell death when apoptotic signaling fails. In a review article written by Edinger et al., a series of representative TEM images were provided to demonstrate the characteristic changes of cellular morphology during apoptosis-, necrosis-, or autophagy-mediated cell death (Figure 7) [10].

To decipher the specific mechanisms that contribute to the enhanced cytotoxicity of CDDP/NO1 combination therapy, apoptosis-mediated cell death mechanism was first investigated by the determination of caspase-3 activity of drug treated cells. Caspase-3 belongs to a family of cysteine-requiring aspartate proteases that mediate cell death in the process of apoptosis. *In vitro* caspase-3 activity can be determined using a fluorimetric assay that measures the fluorescent moiety 7-amido-4-methylcoumarin (AMC) that is released after the hydrolysis of
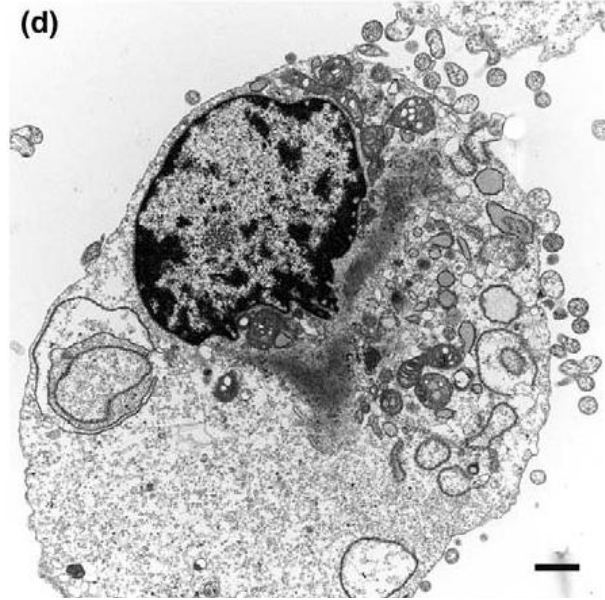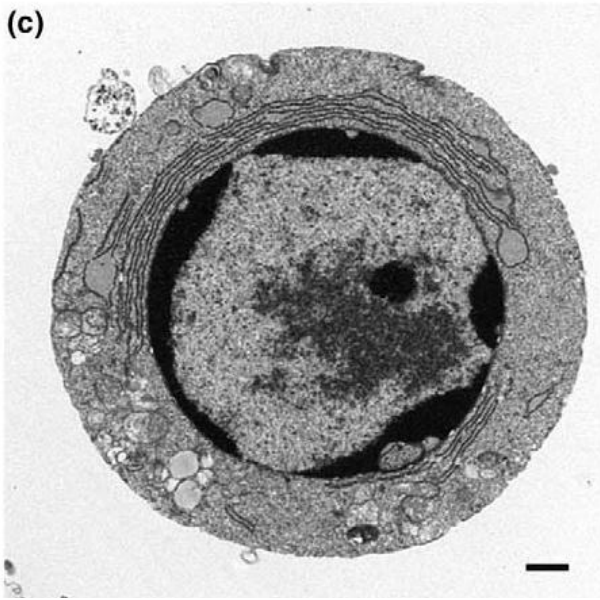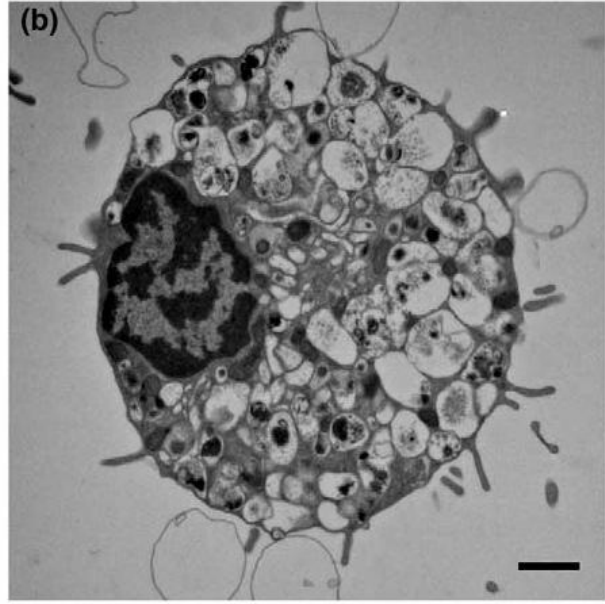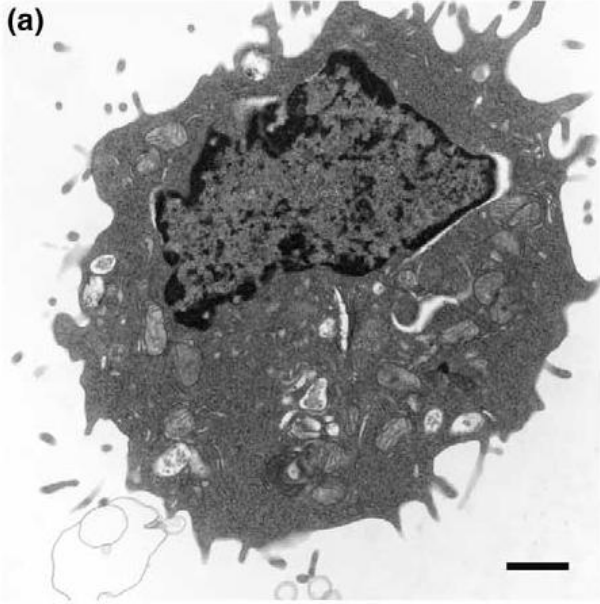
Figure 7. "Morphological features of autophagic, apoptotic and necrotic cells. (a) Normal, (b) autophagic, (c) apoptotic (d) and necrotic cells. Whereas the morphologic features of apoptosis are well defined, the distinction between necrotic and autophagic death is less clear. The bioenergetic catastrophe that culminates in cellular necrosis also stimulates autophagy as the cell tries to correct the decline in ATP levels by catabolizing its constituent molecules. Thus, vacuolation of the cytoplasm is observed in both autophagic cells (b) and in cells stimulated to undergo programmed necrosis (d). By contrast, ATP levels are maintained in normal (a) and apoptotic cells (c) consistent with the limited number of autophagic vacuoles in their cytoplasm. The scale bar represents 1 mm." Reviewed in [10].

a peptide substrate (Ac-DEVD-AMC) by caspase-3 (Figure 8). The excitation and emission wavelengths of AMC are 360 nm and 460 nm. To evaluate the combination therapy, first, a series of cisplatin and NO1 concentrations were tested in MDA-1986 cells to identify the optimal dosing windows for apoptosis induction for each drug. If the drug concentration is too high, it may kill the majority of the cells during incubation and before the caspase-3 activity can be measured. On the other hand, if the drug concentration is too low, the drug-induced production of caspase-3 may not be detectable using the commercially available apoptosis detection kit.

The apoptosis assay was conducted using an identical dosing schedule as the two previous assays (day 1: NO1 addition; day 2: CDDP addition; and day 3: assay). Measurements of caspase-3 activity in each treatment group were normalized against the untreated control. The results suggest that increasing the CDDP concentration produced elevated caspase-3 activity in MDA-1986 cells (Figure 9). In contrast, treatment with NO1 alone did not induce any statistically marked increase in caspase-3 activity. Since the NO1 concentrations employed were verified to cause cell death, this indicates that NO1 may trigger cell death through a mechanism other than apoptosis. In addition, all combination treatment groups demonstrated increased levels of caspase-3 activity with elevated CDDP concentrations. However, the degree of caspase-3 activity generated in cells that were treated with the CDDP/NO1 combination was similar or even lower than cisplatin treatment alone. In other words, the presence of nitric oxide did not seem to accelerate the apoptotic process of MDA-1986 cells in the timeframe of the experiment. If a comparison is made between cisplatin treatment alone (i.e. [CDDP]=0.03 mM) and cisplatin/NO1 combination treatment (i.e. [NO1]=0.02 mM; and [CDDP]=0.03 mM), a reduction of caspase-3 activity was observed for the combination group. It is likely that the combination therapy caused an increase in cell death; therefore, a lower number of apoptotic cells are present

$$\text{Ac-DEVD-AMC} \xrightarrow{\text{Caspase 3}} \text{Ac-DEVD} + \text{AMC}$$
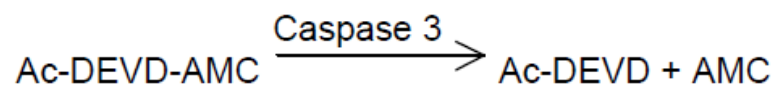
Figure 8. Hydrolysis reaction of the peptide substrate by caspase-3, producing a fluorescent molecule, AMC.
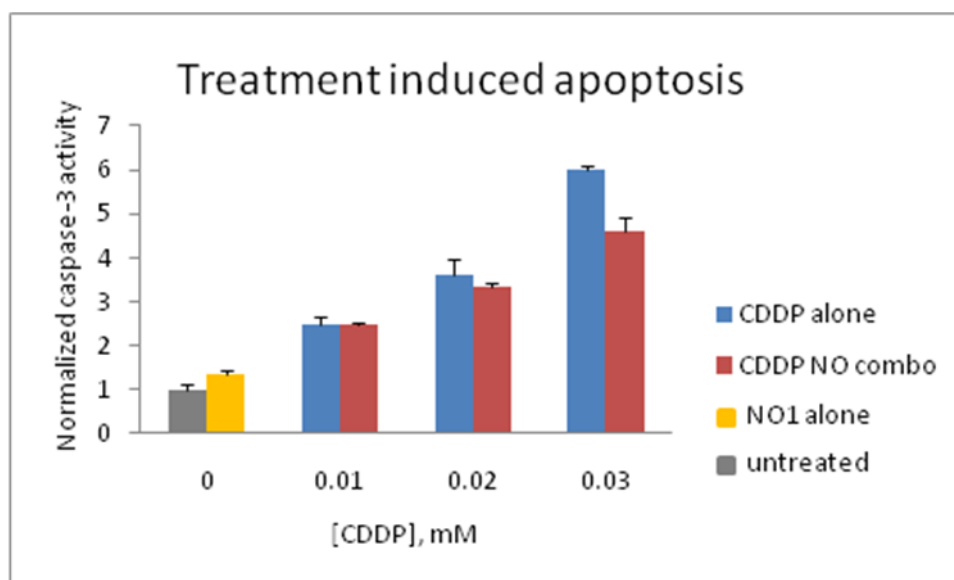
Figure 9. Measurement of caspase-3 activity in MDA-1986 cells. Treatment groups included untreated control, NO1 alone (0.02 mM), CDDP alone (0.01, 0.02 and 0.03 mM), and CDDP/NO1 combination treatments ([NO1]=0.02 mM; [CDDP]=0.01, 0.02 or 0.03 mM). $p<0.05$ for [CDDP]=0.03 mM (N=4).

that are able to produce caspase-3.

In conclusion, NO1, a new nitric oxide-producing prodrug, demonstrated similar anti-proliferative activity as the standard JS-K against HNSCC cells. The NO1/CDDP combination therapy exhibited enhanced cytotoxicity compared to cisplatin treatment alone *in vitro* ([NO1] =0.02 mM). The improved effectiveness of combination treatment was independent of cisplatin concentration; whereas, it was noted that the concentration of NO1 played a role in increasing the anti-cancer activity of the combination therapy. Namely, combination therapy with a high NO1 concentration (0.02 mM) resulted in enhanced cytotoxicity against HNSCC cell; in contrast, combination therapy with lower NO1 concentrations (0.002 and 0.005 mM) did not exert a toxic effect. This is consistent with the results from a study conducted by Fetz et al., in which the authors investigated CDDP/NO combination therapy using two nitric oxide-releasing prodrugs, SNAP and SNP [5]. They demonstrated the upregulation of survivin expression in HNSCC cells treated with a low concentration of the NO-donors. Because survivin expression is known to be associated with chemoresistance, this may provide an explanation to the lack of efficacy of the combination therapy. In addition, they reported forced overexpression of inducible NO synthase in HNSCC cells that were treated with a high concentration of the NO-donors, which triggered cell death and ultimately led to enhanced cytotoxicity of the combination therapy.

The effectiveness of CDDP/NO1 combination therapy may be further improved by incorporating the carrier-based sugar-NO1 conjugate in our future studies. Sugar-NO1 and NO1 demonstrated NO *in vitro* release half lives of 10 and 6 hours, respectively. According to a study conducted by Azizzadeh et al., NO-producing prodrugs with a longer release half life may be more potent inhibitors of DNA synthesis and mitotic activity in the S-phase compared to short-lived NO-prodrugs [13]. With carrier-based NO1 and cisplatin conjugates (sugar-NO1/HA-Pt),

we could achieve locoregional delivery of highly concentrated CDDP/NO combinational agents, further improving the efficacy of HA-Pt therapy in HNSCC xenograft model by incorporating the additional benefits of NO-prodrugs.

A number of studies reported that JS-K activated apoptotic signaling via a caspase-dependent pattern in cancer cells [14-15]. However, based on our preliminary studies, NO1 triggered cell death via a non-apoptotic pathway, because the caspase-3 activity of NO1-treated cells was shown to be similar to the untreated cells. Additionally, the caspase-3 activity after combination treatment even demonstrated a marked reduction relative to the cisplatin alone. In a recent study conducted by McMurtry et al., autophagic cell death was reported in breast cancer cells treated with JS-K [16]. The TEM images of JS-K treated cells revealed characteristic changes of cell morphology such as the formation of vesicle organelles suggesting the occurrence of autophagic cell death. To determine the mechanism of CDDP/NO-induced cell death, future studies will examine alternative mechanisms such as necrosis and autophagy.

7. References

[1] R. Rosell, R.V. Lord, M. Taron, N. Reguart, DNA repair and cisplatin resistance in non-small-cell lung cancer., Lung Cancer, 38 (2002) 217-227.

[2] S.Y. Loh, P. Mistry, L.R. Kelland, G. Abel, K.R. Harrap, Reduced drug accumulation as a major mechanism of acquired resistance to cisplatin in a human ovarian carcinoma cell line: circumvention studies using novel platinum (II) and (IV) ammine/amine complexes., Br J Cancer., 66 (1992) 1109-1115.

[3] Z.S. Chen, M. Mutoh, T. Sumizawa, T. Furukawa, M. Haraguchi, A. Tani, N. Saijo, T. Kondo, S. Akiyama, An active efflux system for heavy metals in cisplatin-resistant human KB carcinoma cells., Exp Cell Res, 240 (1998) 312-320.

[4] C. Peklak-Scott, P.K. Smitherman, A.J. Townsend, C.S. Morrow, Role of glutathione S-transferase P1-1 in the cellular detoxification of cisplatin., Mol Cancer Ther, 7 (2008) 3247-3255.

[5] V. Fetz, C. Bier, N. Habtemichael, R. Schuon, A. Schweitzer, M. Kunkel, K. Engels, A.F. Kovács, S. Schneider, W. Mann, R.H. Stauber, S.K. Knauer, Inducible NO synthase confers chemoresistance in head and neck cancer by modulating survivin., Int J Cancer, 124 (2009) 2033-2041.

[6] A. Bratasz, K. Selvendiran, T. Wasowicz, A. Bobko, V.V. Khramtsov, L.J. Ignarro, P. Kuppusamy, NCX-4040, a nitric oxide-releasing aspirin, sensitizes drug-resistant human ovarian xenograft tumors to cisplatin by depletion of cellular thiols., J Transl Med, 6 (2008) 9.

[7] A. Bratasz, N.M. Weir, N.L. Parinandi, J.L. Zweier, R. Sridhar, L.J. Ignarro, P. Kuppusamy, Reversal to cisplatin sensitivity in recurrent human ovarian cancer cells by NCX-4016, a nitro derivative of aspirin., Proc Natl Acad Sci U S A, 103 (2006) 3914-3919.

[8] P. Chanvorachote, U. Nimmannit, C. Stehlik, L. Wang, B.H. Jiang, B. Ongpipatanakul, Y. Rojanasakul, Nitric oxide regulates cell sensitivity to cisplatin-induced apoptosis through S-nitrosylation and inhibition of Bcl-2 ubiquitination., Cancer Res., 66 (2006) 6353-6360.

[9] C. Riganti, E. Miraglia, D. Viarisio, C. Costamagna, G. Pescarmona, D. Ghigo, A. Bosia, Nitric oxide reverts the resistance to doxorubicin in human colon cancer cells by inhibiting the drug efflux., Cancer Res., 65 (2005) 516-525.

[10] A.L. Edinger, C.B. Thompson, Death by design: apoptosis, necrosis and autophagy., Curr Opin Cell Biol., 16 (2004) 663-669.

[11] Z.F. Zakeri, H.S. Ahuja, Cell death/apoptosis: normal, chemically induced, and teratogenic effect., Mutat Res., 396 (1997) 149-161.

[12] S. Yousefi, H.U. Simon, Autophagy in cancer and chemotherapy., Results Probl Cell Differ. , 49 (2009) 183-190.

[13] B. Azizzadeh, H.T. Yip, K.E. Blackwell, S. Horvath, T.C. Calcaterra, G.M. Buga, L.J. Ignarro, M.B. Wang, Nitric oxide improves cisplatin cytotoxicity in head and neck squamous cell carcinoma., Laryngoscope., 111 (2001) 1896-1900.

[14] V. Udupi, M. Yu, S. Malaviya, J.E. Saavedra, P.J. Shami, JS-K, a nitric oxide prodrug, induces cytochrome c release and caspase activation in HL-60 myeloid leukemia cells., Leuk Res., 30 (2006) 1279-1283.

[15] P.J. Shami, J.E. Saavedra, L.Y. Wang, C.L. Bonifant, B.A. Diwan, S.V. Singh, Y. Gu, S.D. Fox, G.S. Buzard, M.L. Citro, D.J. Waterhouse, K.M. Davies, X. Ji, L.K. Keefer, JS-K, a glutathione/glutathione S-transferase-activated nitric oxide donor of the diazeniumdiolate class with potent antineoplastic activity., Mol Cancer Ther, 2 (2003) 409-417.

[16] V. McMurtry, J.E. Saavedra, R. Nieves-Alicea, A.M. Simeone, L.K. Keefer, A.M. Tari, JS-K, a nitric oxide-releasing prodrug, induces breast cancer cell death while sparing normal mammary epithelial cells., Int J Oncol., 38 (2011) 963-971.

Chapter 5

Internalization of Nanocarriers into Tumor Cells

1. Introduction

The mechanism of how cisplatin enters cancer cells is poorly defined. The two most common interpretations include passive diffusion [1-2] and carrier-mediated transport [3-5], both of which act via a transcellular route. The passive diffusion mechanism of cisplatin internalization is based on the evidence that the cellular accumulation of cisplatin is proportional to the drug concentration. It is driven by a concentration gradient, following Fick's Law. In addition, cellular accumulation of cisplatin was determined to be unsaturable, thus supporting the passive diffusion pathway. However, recent observations revealed that cisplatin may enter cells through an ion channel, supporting the carrier-mediated pathway. One of the possible transporters involved in cisplatin influx is believed to be the human copper transporter 1, which is the primary transporter responsible for the internalization of copper and silver [6]. Once cisplatin gains access into the cells, the intracellular disposition has not been fully described. Studies have shown that besides plasma membrane, cisplatin is present in the cytoplasm and nuclear matrices [2].

Our previous findings suggested that the hyaluronic acid-cisplatin (HA-Pt) conjugate had improved *in vivo* efficacy in head and neck cancer compared to the free cisplatin. In order to understand the enhanced anti-proliferative activity, herein we would like to examine the cellular localization and the mechanism of internalization of polymer-based cisplatin conjugates. By labeling HA with a very small gold nanoparticle, both the carrier and the drug may be detected using transmission electron microscopy, as both gold and platinum are electron-dense elements. In addition, a similar approach will be taken to evaluate the internalization and localization of hyaluronic acid-doxorubicin (HA-DOX) conjugates using a far-red dye tagged HA polymer.

2. Determination of hyaluronic acid-cisplatin cellular internalization using TEM

2.1 Sample preparation for TEM

A solution of cisplatin (CDDP) or hyaluronic acid-cisplatin (HA-Pt) conjugate was prepared prior to TEM viewing, with a concentration of approximately 1 mg/mL on a platinum basis. Ten microliters of the solution was coated onto the surface of a lacey carbon coated nickel TEM grid. Representative TEM images showed 5-nm cisplatin particles (Figure 1A), which were precipitated from 1 mg/mL cisplatin solution during drying, and 25-nm platinum-based HA-Pt conjugates (Figure 1B). Bound platinum on the side chains of HA formed hydrophobic regions during dehydration, leading to the formation of platinum clusters.

2.2 *In vitro* localization of cisplatin

MDA-1986 cells were seeded in 75 cm^2 cell culture flasks. Cisplatin treatment (0.1 mM) was added once the cells became adherent. Twenty-four or forty-eight hours post treatment, cells were harvested and fixed to make TEM cell pellets. Typically, cell culture fluid was removed from the flask and PBS was added and incubated for 3 minutes at room temperature. Once the PBS was removed, 2% gluteraldehyde in 0.1 M sodium cacodylate (pH 7.4) was added into the cell culture flask. After incubating the cells in the fixative for 15 minutes, the cells were scraped from the surface of the flask into a centrifuge tube. Subsequently, the cell suspension was centrifuged at 500 rpm for 5 minutes. The cell pellets were then rinsed in twice with 0.1 M sodium cacodylate buffer at pH 7.4 to remove the excess glutaraldehyde.
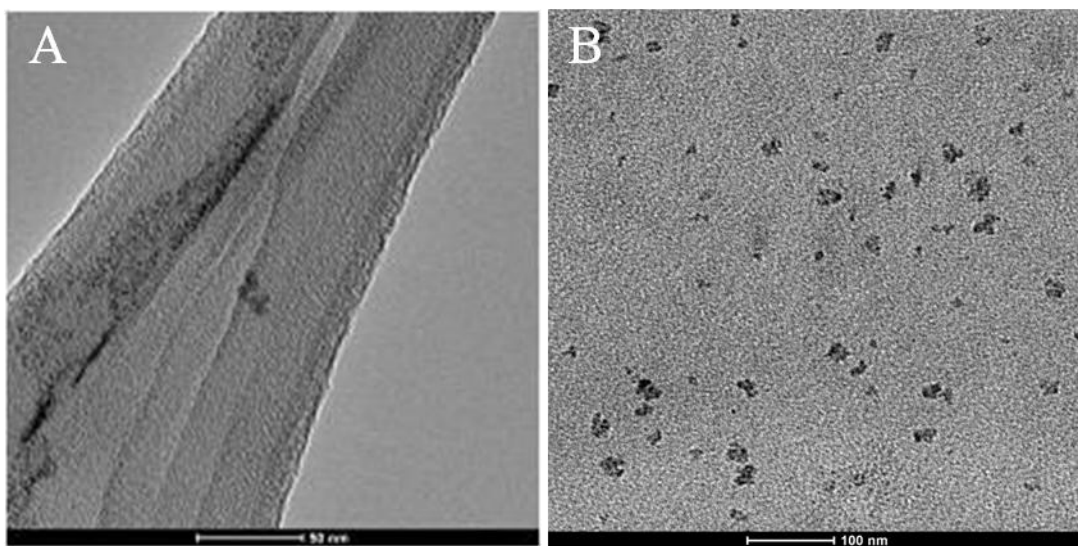
Figure 1. TEM images of (A) 5-nm cisplatin particles (precipitated during drying), and (B) 25-nm HA-Pt clusters.

Cells were post-fixed in 1% osmium tetroxide and 0.3% potassium ferricynide buffered in 0.1 M sodium cacodylate (pH 7.4) for one hour in a fume hood. Pellets were then rinsed three times with de-ionized distilled water. After rinsing, the pellets were dehydrated in a series of ethanol, as follows: 30%, 70%, 80%, 95%, 100% and 100%, for 10 minutes each step. Subsequently, pellets were placed in propylene oxide for 10 minutes in a fume hood and then were infiltrated overnight in a 50% propylene oxide and 50% Embed 812 resin medium mixture (5 mL of Embed 812, 4 mL of DDSA, 2 mL of NMA and 190 µL of DMP-30, purchased from Electron Microscopy Sciences, Hatfield, PA). The next day, cell pellets were placed into fresh 100% Embed 812 resin mixture for 30 minutes. The resin containing the cells was placed into tube with cells and placed into a 60 °C oven overnight to polymerize. The next day, the cell pellets were removed and oriented in a flat embedding mold, the mold was placed in a 60 °C oven overnight.

Samples were sectioned with a diamond knife (Leica Ultrtome) into 80-90 nm sections. The sections were then contrasted with 3% uranyl acetate for 15 minutes and rinsed, followed by Sato's modified lead citrate solution for 3 minutes. Finally, the sections were rinsed with water five times (one minute each time) and air dried for viewing by TEM.

Figure 2 is a representative TEM image of an untreated MDA-1986 cell. Cellular organelles were permanently fixed and darkly stained. The cell exhibited an intact cellular membrane, nucleus, mitochondria, vesicles, Golgi apparatus and endoplasmic reticulum (Figure 2). The dark wavy lines were caused by the wrinkling of the embedding material during drying. It was noted that the cellular compartments of untreated, healthy cells were evenly stained, thus, no enhanced contrast was observed.
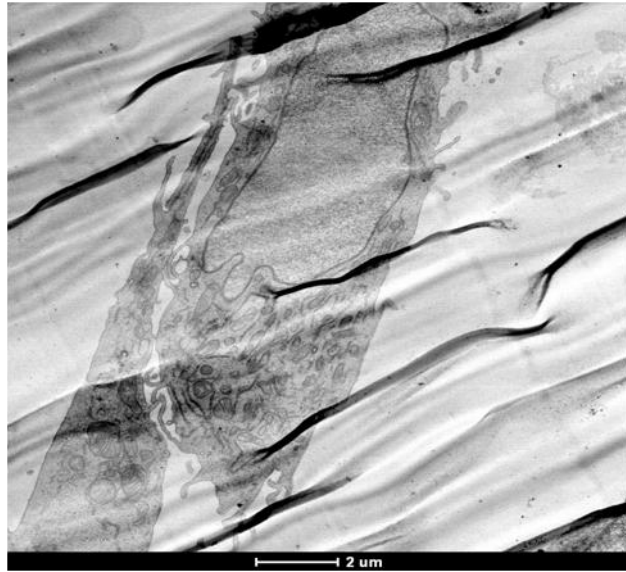
Figure 2. A representative TEM image of an untreated MDA-1986 cell.

Figure 3 shows a group of TEM images of cisplatin treated MDA-1986 cells. The cells were incubated in the presence of 1-µg/mL cisplatin for 48 hours before fixation. Cellular organelles such as mitochondria, Golgi apparatus, and vesicles, were clearly stained. Particulate-like enhancement was detected on the surface of the plasma membrane, in the cytoplasm, and surrounding vesicles [2], presumably because the electron-dense platinum was localized in these organelles. Interestingly, dark staining was also observed in the mitochondria, which is consistent with a number of recent discoveries of cisplatin mitochondria toxicity in head and neck cancer cells [7]. Future work will further explore the localization and mechanism of internalization of cisplatin and carrier-based cisplatin conjugates in cancer cells.

2.3 *In vivo* localization of HA-Pt conjugates

A mouse was inoculated with MDA-1986 cells to induce squamous cell carcinoma of the head and neck. HA-Pt was administered as a subcutaneous injection peritumorally with a dosage of 3.5 mg/kg. Twenty-four hours post dosing, the animal was euthanized by isoflurane overdose. The cervical lymph nodes draining the injection site were collected, fixed in formalin, and embedded in paraffin. Subsequently, the embedded lymph node tissues were sectioned into 4-µm sections using an ultratome and imaged with TEM. Platinum accumulation was detected in lymph node tissues, indicated by the red arrows highlighting the signal enhancement (Figure 4). Small particulates were in the size range of 100-200 nm; whereas, larger aggregates measured approximately 400-500 nm in size. The presence of platinum in HA-Pt treated tissue was verified by comparing it with tissue from an untreated animal using an energy dispersive x-ray detector (Figure 5). The results indicated that the conjugate drained and was retained in the surrounding
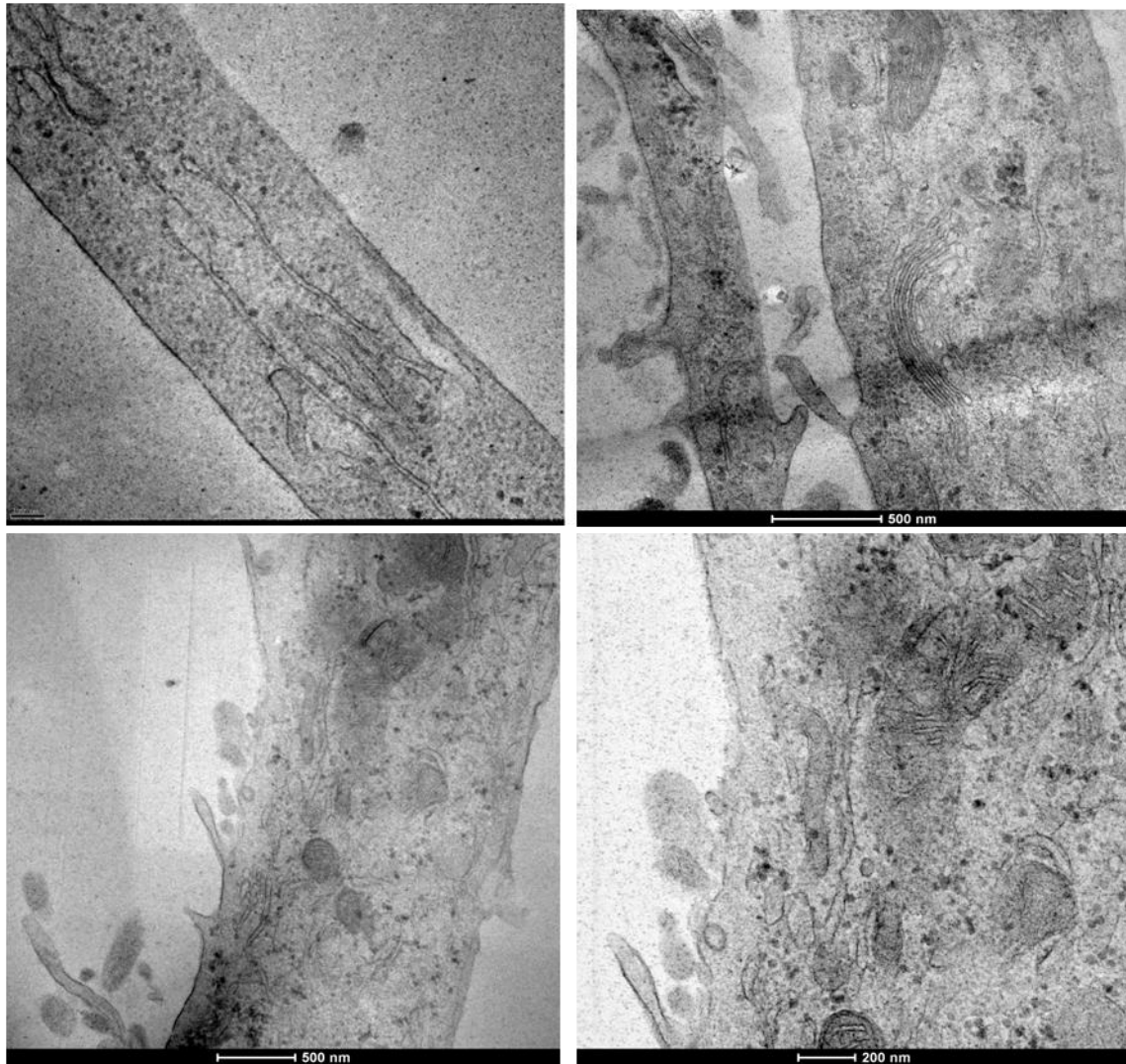
Figure 3. Representative TEM images of CDDP treated MDA-1986 cells.
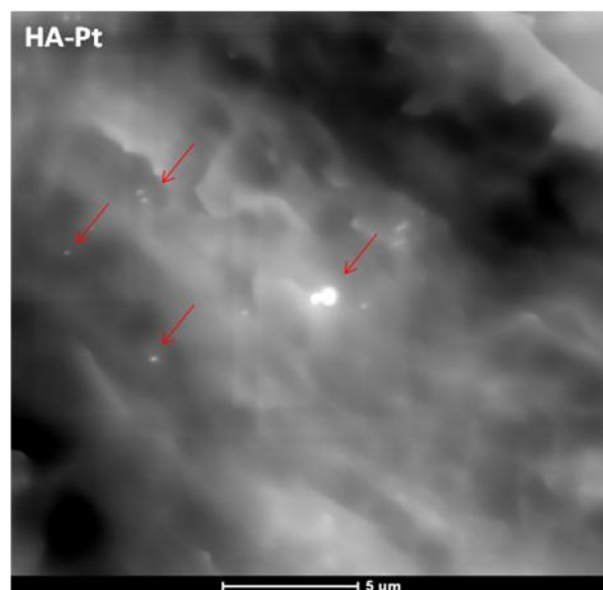
Figure 4. TEM image showing platinum accumulation in the cervical lymph node tissues of a HNSCC bearing mouse post s.c. injection of HA-Pt (3.5 mg/kg).
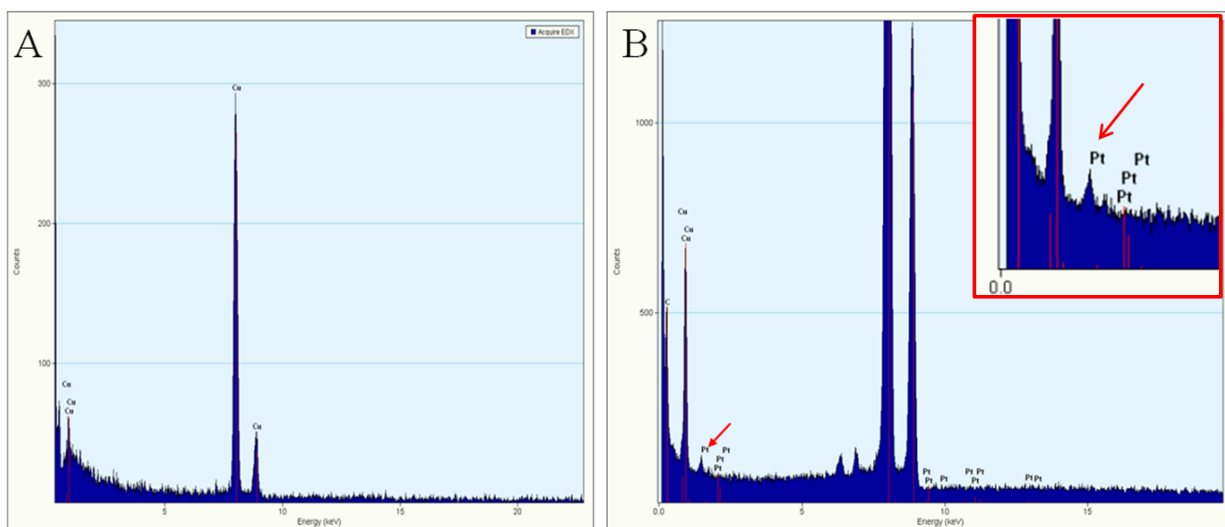
Figure 5. Elemental spectra of (A) untreated and (B) HA-Pt treated lymph node tissues of nude mice, generated by an energy dispersive x-ray detector.

lymphatics within 24 hours after subcutaneous injection. However, without organelle specific staining, the cellular localization of the conjugate remains unknown and is worth further investigation.

2.4 Synthesis of gold tagged HA-Pt conjugates

Colloidal gold nanoparticles were synthesized by quickly adding solution B (50-60 °C), which contained 4 mL of 1% w/v trisodium citrate·2H_2O, 5 mL of 1% w/w tannic acid, 5 mL of 25 mM K_2CO_3, and 6 mL of water, into solution A (60 °C), which contained 79 mL of water and 1 mL of 1% $HAuCl_4$, with continuous stirring. Addition must be rapid in order to form colloid nanoparticles with uniform size. The solution mixture was stirred rapidly, heated to a simmer, and then allowed to react until the color of the solution turned brown. Once the color change was complete, the solution was heated to a full boil and then allowed to cool to room temperature. Subsequently, a small amount of H_2O_2 was added into the colloidal gold solution to a final concentration of 0.1%. The solution was covered and stored at 4 °C until further use. Two representative TEM images of 3-nm gold colloidal nanoparticles are shown in Figure 6; the scale markers are 100 nm and 20 nm, respectively. An X-ray backscattering map was generated with an energy dispersive x-ray detector (Figure 7).

HA-ADH was synthesized as previously described (chapter 3.2). 2,5-dioxopyrrolidin-1-yl 5-(1,2-dithiolan-3-yl)pentanoate was then conjugated to HA-ADH in a H_2O/THF mixture (1:2) with 5% TEA (Figure 8). The reaction was allowed to proceed for 48 hours. The resulting HA-thioctic ester was purified via dialysis for 24 hours and lyophilized overnight. The next day equal
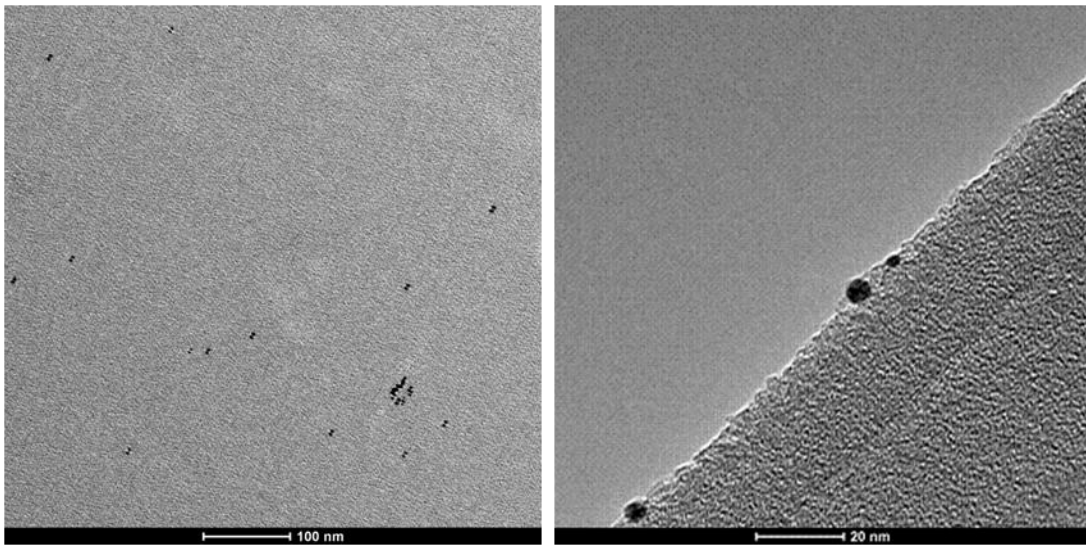
Figure 6. TEM images of 3-nm colloidal gold nanoparticles on a copper mesh TEM grid.
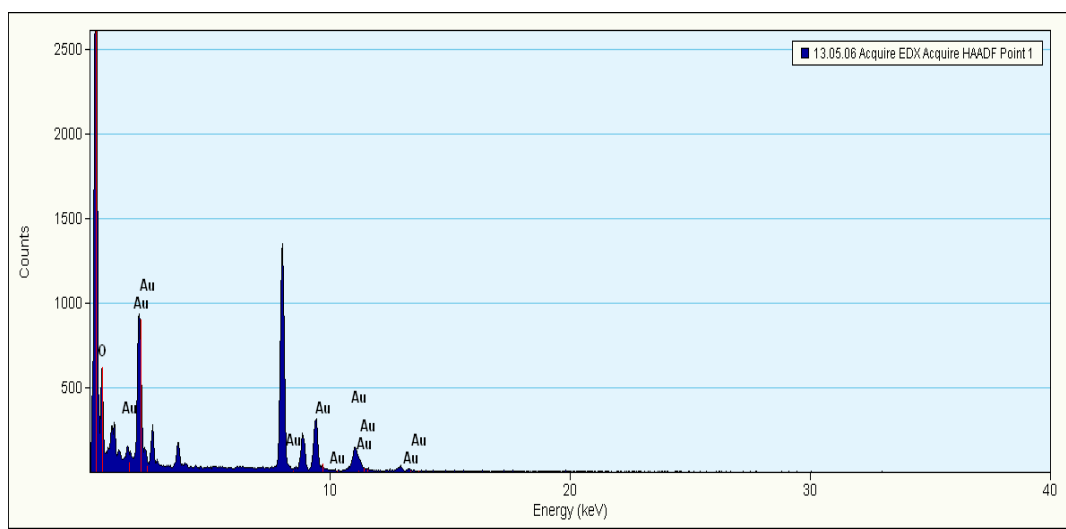
Figure 7. Elemental spectrum of 3-nm colloid gold nanoparticles.
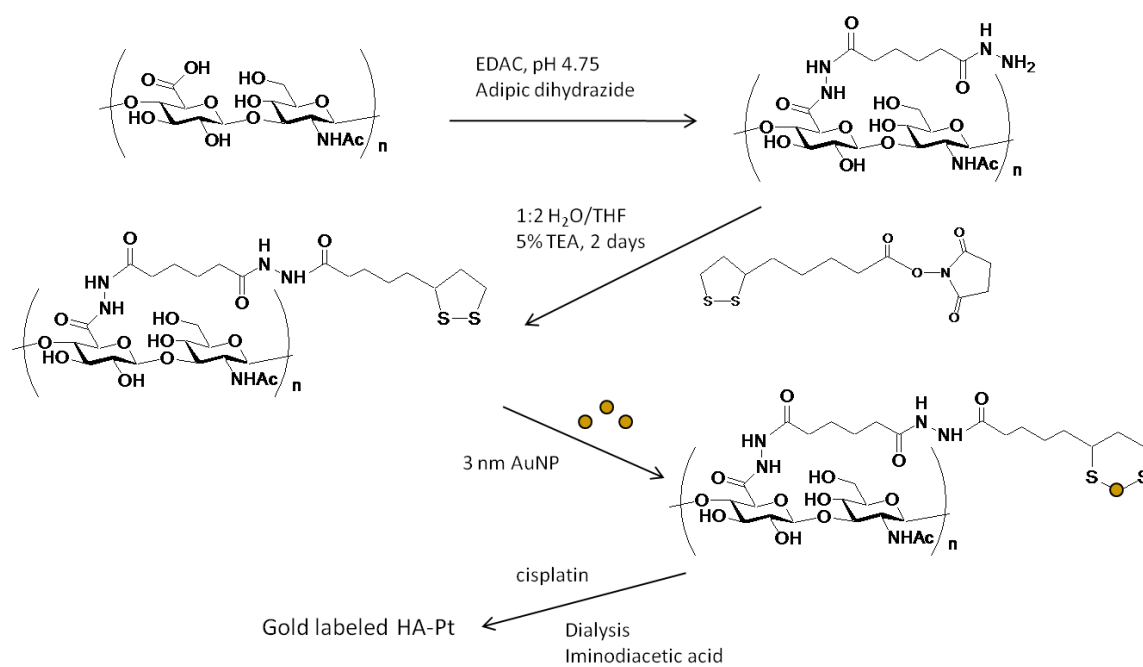
Figure 8. Synthetic scheme of gold tagged HA-Pt.

volumes of HA-thioctic ester solution in 20 mM HEPES at pH 7.4, and the colloidal gold solution were mixed, covered and stirred at room temperature for 24 hours. Finally, the resulting HA-Au conjugate was centrifuged to remove aggregates, dialyzed against water for 24 hours and lyophilized to obtain the gold tagged HA conjugate. Subsequently, cisplatin was attached to the carboxylic acid groups of HA, as described in chapter 2.2, leading to the formation of gold labeled HA-Pt.

The substitution degree of the cisplatin and gold was determined by atomic absorption spectroscopy and UV-Vis spectroscopy, respectively. No apparent peak shifts were observed on the UV spectrum of gold tagged HA compared to HA. This is likely due to the limited binding efficiency between the gold nanoparticles and the thiol moieties of the linker, leading to a very low conjugation degree. Thus the gold concentration could not be determined by UV-Vis spectroscopy. Future work will focus on the selection of gold binding linkers to produce stable gold tagged HA-Pt conjugates with an optimized loading degree of both the drug and the gold label. Further, the selection of heavy-metal staining and contrasting agents will be optimized. The metals used in this study include osmium, lead and uranium, all of which have similar electron densities as the targeted platinum and gold. They are very likely to cause signal overlapping under TEM, making identity assignment difficult. Hence, contrasting agents such as molybdenum derived materials will be investigated in future studies.

3. Determination of hyaluronic acid-doxorubicin cellular internalization using fluorescent microscopy

3.1 Synthesis of IR820 tagged hyaluronic acid-doxorubicin conjugates

Near-IR dye molecules, including IR820 (Figure 9A), have been used in our laboratory as a fluorescent tag of a variety of nanocarriers for *in vivo* whole body imaging as they produce minimum background fluorescence, facilitating spectra deconvolution in data analysis. Doxorubicin was conjugated to HA-IR820 (Figure 9B) via a dihydrazine linker. The synthesis was described in the "Synthesis and characterization of hyaluronan-doxorubicin (HA-DOX) conjugates" section in chapter 3. The resulting IR820 labeled HA-DOX conjugate (IR820-HA-DOX) had approximately 1% (wt/wt) of each of the two fluorophores (IR820, DOX). A minimum amount of DOX/IR820 substitution is desired because high degree of conjugation may yield more hydrophobic HA conjugates that could affect the cellular internalization of the drug as well as the carrier.

3.2 Cellular uptake of IR820 labeled hyaluronic acid-doxorubicin (IR820-HA-DOX)

A human head and neck squamous cell carcinoma cell line, MDA-1986, was employed to evaluate the internalization and cellular distribution of the drug bound vehicles (HA-DOX), by incorporating a fluorescent tag, IR820, to determine the cellular trafficking of the carrier as free HA cannot be detected by fluorescence microscopy. First, cells were treated with a series of concentrations of unbound doxorubicin (final concentration of 0.5, 1 and 5 µg/mL) and HA-IR820 (final concentration of 0.5, 1 and 1.7 µg/mL on IR820 basis) for 6 hours as control groups to determine the optimal working concentrations. Post treatment, cells were rinsed with PBS and imaged by fluorescence microscopy using the Texas red (DOX) and Cy5 (HA-IR820) filter sets.
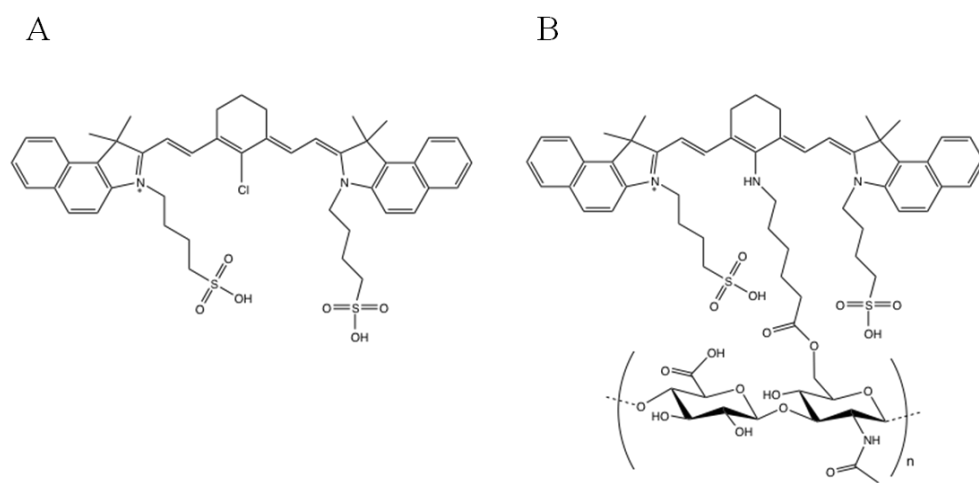
Figure 9. Chemical structures of (A) IR820 and (B) HA-IR820.

Doxorubicin has an excitation and an emission wavelength of 480 nm and 590 nm, respectively. IR820 is a laser dye, and HA-IR820 has an excitation and an emission wavelength of 675 nm and 730 nm, respectively. Thus, the fluorescent signals of doxorubicin and IR820 could be captured simultaneously using Texas red and Cy5 filter sets, respectively. In Figure 10, the cellular internalization of both doxorubicin (Images A, B and C) and HA-IR820 (Images D, E and F) are shown at three different concentrations. The intensity of the fluorescent signal was proportional to the concentration. Because the highest concentrations of doxorubicin (5 µg/mL) and IR820 (1.7 µg/mL) appeared to saturate the images, they were eliminated from further experiments. In addition, MDA-1986 cells are sensitive to doxorubicin treatment, thus prolonged exposure or elevated concentrations may lead to cell death, which is undesirable in this study. In order to minimize doxorubicin-induced cytotoxicity, which may alter the morphology of cells, MDA-1986 cells were only exposed to doxorubicin or IR820 labeled HA-DOX for one hour prior to imaging for the rest of the experiments.

In the non-overlaid fluorescent images, it was noticed that after entering the cell, doxorubicin was mainly localized in the nucleus with a smaller amount of drug remaining in the cytoplasm (Figure 11); whereas HA-IR820 had a greater cytoplasmic distribution compared to its nuclear accumulation (Figure 12). In addition, as a control, cells were treated with HA-DOX to demonstrate that HA-DOX can enter cells, before the experiments using IR820-HA-DOX were conducted (Figure 13). Similar to the free doxorubicin, cleaved doxorubicin (from the carriers) was mainly localized within the nucleus. Because large polymer conjugates, such as 35 kDa HA-DOX, may not be able to enter the nucleus, this suggests the cleaved doxorubicin was internalized into the nucleus. Therefore, it is possible that the conjugates release the free drug,
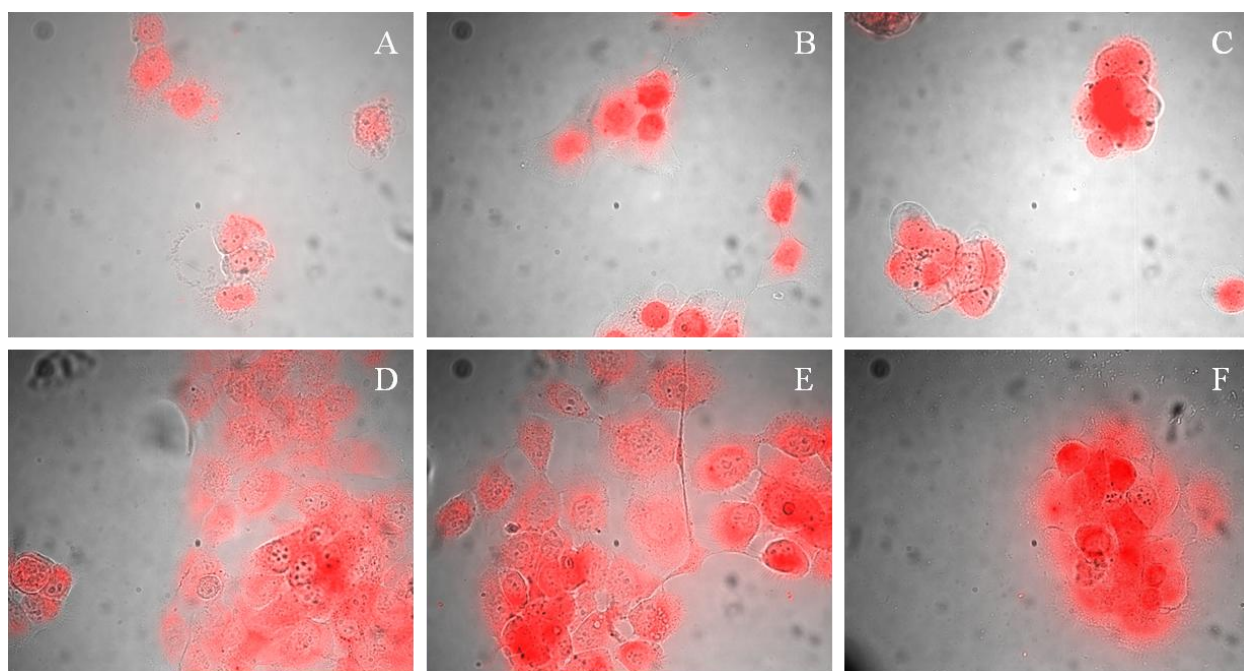
Figure 10. Uptake of doxorubicin (captured using a Texas red filter set; A: 0.5 µg/mL, B: 1 µg/mL, C: 5 µg/mL) and HA-IR820 (captured using a Cy5 filter set; D: 0.5 µg/mL, E: 1 µg/mL, F: 1.7 µg/mL) into MDA-1986 cells.
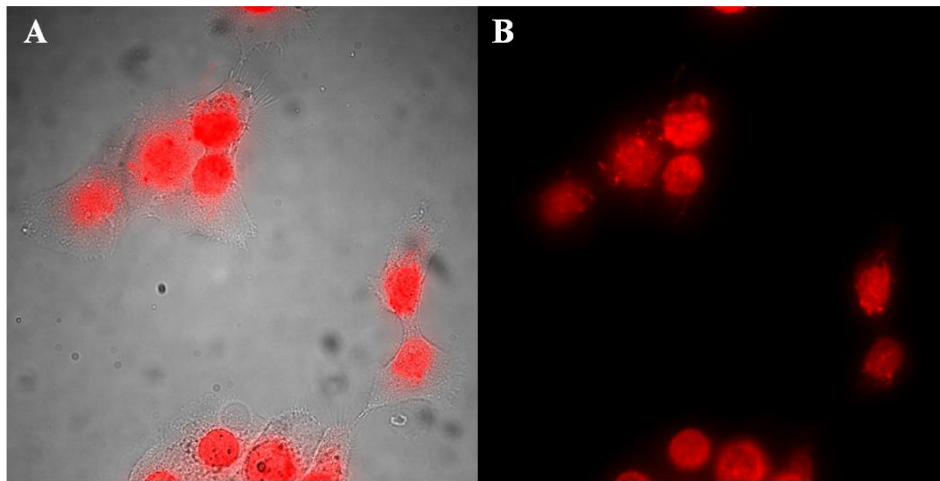
Figure 11. Cellular internalization of doxorubicin (A: overlaid cellular phase contrast/DOX fluorescent images, B: non-overlaid fluorescent DOX image). MDA-1986 cells were treated with a final concentration of 100 ng/mL doxorubicin for an hour prior to imaging. The representative images were taken using a Texas red filter set. The red color indicates the internalization of doxorubicin.
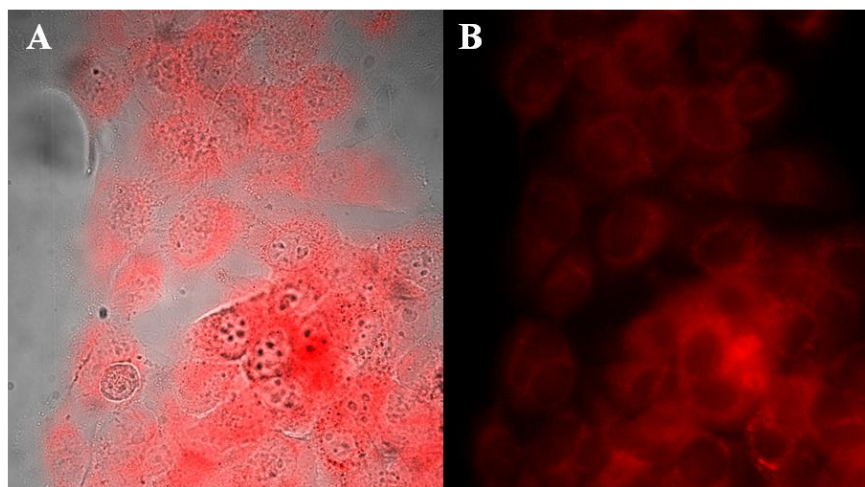
Figure 12. Cellular internalization of HA-IR820 (A: overlaid cellular phase contrast/HA-IR820 fluorescent images, B: non-overlaid HA-IR820 fluorescent image). MDA-1986 cells were treated with a final concentration of 100 ng/mL IR820 for an hour prior to imaging. The representative images were taken using a Cy5 filter set. The red color indicates the internalization of HA-IR820.
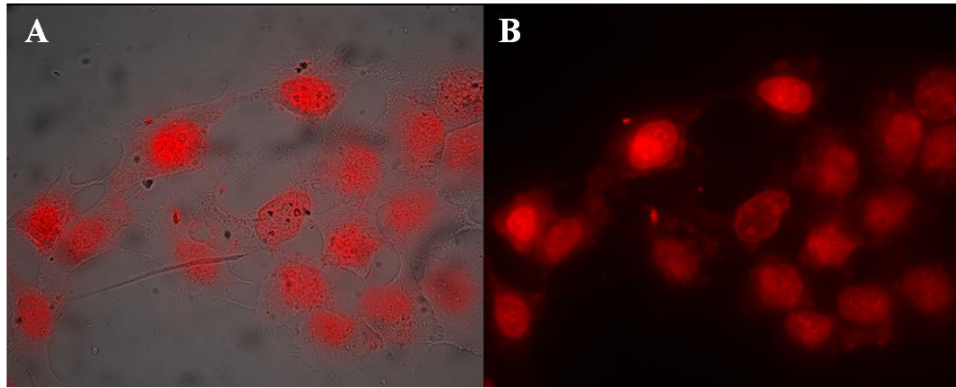
Figure 13. Cellular internalization of HA-DOX (A: overlaid cellular phase contract/HA-DOX fluorescent images, B: non-overlaid HA-DOX fluorescent image). MDA-1986 cells were treated with a final concentration of 100 ng/mL doxorubicin for an hour prior to imaging. The representative image was taken using a Texas red filter set. The red color indicates the internalization of HA-DOX.

and then the free drug enters the cells via mechanisms, such as, passive diffusion or active uptake. The other possibility is that the conjugates are internalized via receptor-mediated endocytosis (i.g. CD44, the primary receptor of HA), followed by the intracellular drug release, and the further nuclear uptake.

In order to simultaneously examine the cellular trafficking of the carrier and the drug, cells were treated with IR820 tagged HA-DOX prior to imaging. Unfortunately, due to the instability of the doubly labeled conjugate (IR820-HA-DOX), no fluorescent signal of IR820 was detected in cells, suggesting the degradation of the dye or the complex releases the dye from the carriers during the process of conjugating DOX onto HA-IR820 (Figure 14). This assumption led to the evaluation of the release kinetics of IR820 from HA. In order to determine its release half life, HA-IR820 solution was placed in dialysis tubing in a PBS bath at 37 °C. Aliquots of HA-IR820 solution were collected at 0, 1, 2, 4, 6, 24 and 30 hours, and the amount of IR820 was determined using a spectrophotometer. The release half-life was calculated to be approximately 18 hours (Figure 15). Because the time frame for conjugation of doxorubicin onto HA-IR820 and the subsequent dialysis lasted one to two days, it was not surprising that the majority of the dye may have been degraded or cleaved from the carriers, before the cell assay was conducted.

In future studies, three alternative approaches may be investigated. First, the order of the two conjugation reactions could be altered, which means a HA-DOX conjugate would be synthesized, followed by the conjugation of IR820. This approach may solve the previous issue because HA-DOX was determined to be more stable than HA-IR820 indicated by their release half lives (HA-IR820: $t_{1/2}$=18 hours, HA-DOX: $t_{1/2}$=172 hours). The second approach is to select a more stable dye with excitation and emission wavelengths differentiable from doxorubicin
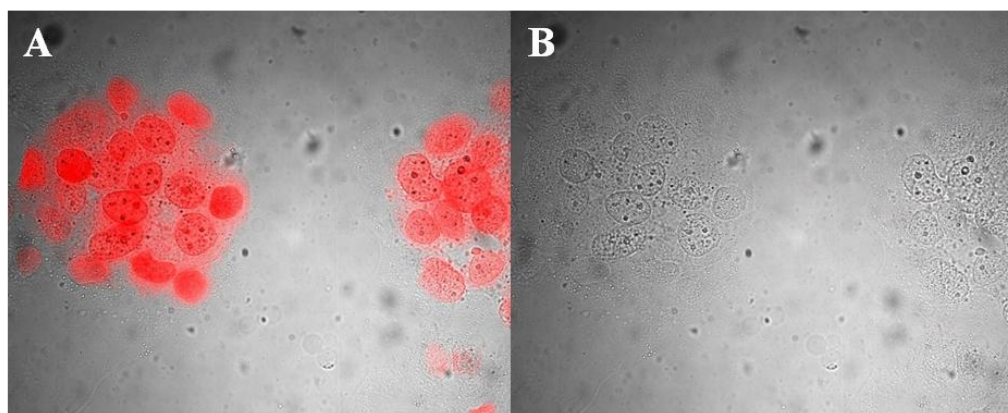
Figure 14. Cellular internalization of IR820 labeled HA-DOX conjugate (A: Texas red channel showing cellular internalization of doxorubicin, B: Cy5 channel showing cellular internalization of HA-IR820). MDA-1986 cells were treated with IR820 tagged HA-DOX for an hour prior to imaging. The red color in image A indicates the internalization of doxorubicin. No IR820 signal was detected in the Cy5 channel in image B, suggesting the degradation or release of the dye.
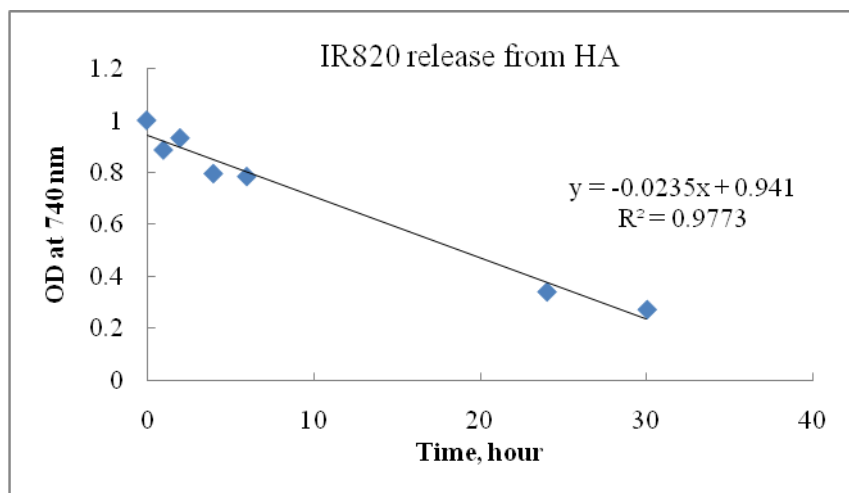
Figure 15. Release of IR820 from the carrier HA. The release study was conducted in PBS at 37 °C. The concentration of IR820 was determined using a spectrophotometer.

under a fluorescent microscope, preventing early degradation of the dye molecule. Another alternative method is to replace the current linker (Figure 16A) with a molecule that has two primary amines at both ends (Figure 16B), thus maximizing the release half life of the dye and improving the stability of the conjugates.

A

B
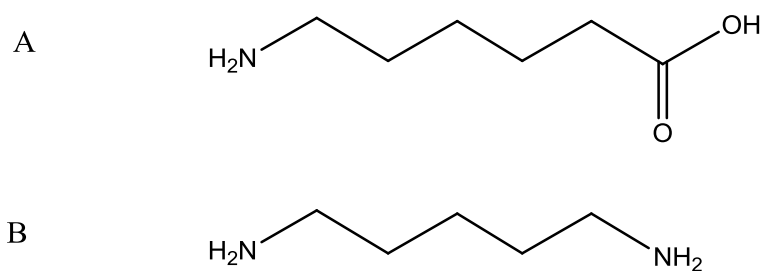
Figure 16. Chemical structures of A) the linker used in HA-IR820 conjugation reaction, B) modified linker for future study.

4. References

[1] A. Ghezzi, M. Aceto, C. Cassino, E. Gabano, D. Osella, Uptake of antitumor platinum(II)-complexes by cancer cells, assayed by inductively coupled plasma mass spectrometry (ICP-MS). J Inorg Biochem, 98 (2004) 73-78.

[2] G.L. Beretta, S.C. Righetti, L. Lombardi, F. Zunino, P. Perego, Electron microscopy analysis of early localization of cisplatin in ovarian carcinoma cells., Ultrastruct Pathol, 26 (2002) 331-334.

[3] M.D. Hall, M. Okabe, D.W. Shen, X.J. Liang, M.M. Gottesman, The role of cellular accumulation in determining sensitivity to platinum-based chemotherapy., Annu Rev Pharmacol Toxicol, 48 (2008) 495-535.

[4] J. Helleman, H. Burger, I.H. Hamelers, A.W. Boersma, A.I. de Kroon, G. Stoter, K. Nooter, Impaired cisplatin influx in an A2780 mutant cell line: evidence for a putative, cis-configuration-specific, platinum influx transporter., Cancer Biol Ther, 5 (2006) 943-949.

[5] D.P. Gately, S.B. Howell, Cellular accumulation of the anticancer agent cisplatin: a review., Br J Cancer, 67 (1993) 1171-1176.

[6] J. Lee, M.M. Peña, Y. Nose, D.J. Thiele, Biochemical characterization of the human copper transporter Ctr1, J Biol Chem, 277 (2002) 4380-4387.

[7] K.J. Cullen, Z. Yang, L. Schumaker, Z. Guo, Mitochondria as a critical target of the chemotheraputic agent cisplatin in head and neck cancer., J Bioenerg Biomembr, 39 (2007) 43-50.

Chapter 6

Future Work

1. Development of combination therapy

Our preliminary results of CDDP/NO1 combination chemotherapy demonstrated improved anti-proliferative activity against human head and neck cancer cells and human breast cancer cells. Therefore, further evaluation of a series of dose regimens will be conducted to identify the most efficacious drug combination and treatment schedule for each cancer cell line of interest. These cell lines include, but are not limited to the human head and neck squamous cell cancer cell line MDA-1986 (CDDP sensitive and CDDP resistant), human breast cancer cell lines MDA-MB-468LN, MDA-MB-231 and MCF-7, as well as human melanoma cell line A375.

To understand nitric oxide-induced mechanism of cell death, the apoptotic status of CDDP/NO1 treated cells were tested. The results suggest that the additive cytotoxicity of the combination treatment was not mediated via an apoptotic pathway. Therefore, future studies will investigate alternative cell death mechanisms such as necrosis and autophagy using lactate dehydrogenase release assay and Cyto-ID^{TM} autophagy detection kit, respectively; to determine the primary pathway of drug-induced cell death.

In addition, carrier-based nitric oxide prodrugs including sugar-NO1 will be tested in combination with cisplatin, to determine the efficacy of the controlled-release drug delivery platform *in vitro* and to determine the most responsive cancer type to this treatment. Subsequently, a corresponding xenograft model will be utilized to examine the *in vivo* toxicity and efficacy of the most promising combination regimen. If both equivalent or reduced toxicity and improved *in vivo* efficacy are observed post combination treatment, the concept will be adapted to other treatment regimens such as doxorubicin/NO-prodrugs.

2. *In vivo* evaluation of sugar star polymer-based NO prodrugs: pharmacokinetics, toxicity and anti-cancer efficacy

A series of star polymer-nitric oxide prodrug conjugates have been synthesized and characterized in our laboratory. In our preliminary studies, I have determined the *in vitro* release kinetics and toxicity of the formulations. In an on-going anti-cancer efficacy study, a sugar star polymer-NO1 conjugate was administered as a weekly subcutaneous injection in HNSCC bearing nude mice. The conjugate demonstrated 100% tumor inhibition effectivity, leading to a complete cure and prolonged survival of the animals (Figure 1). The next step of this study is to examine the pharmacokinetics, bio-distribution, and drug-induced toxicity, of the conjugates in Sprague-Dawley rats, and the anti-tumor activity and survival rate in tumor-bearing mice.

3. Determination of the cellular distribution of gold tagged HA-Pt and Cy7 tagged HA-DOX conjugates

In order to determine the tumor cell distribution of the carried-based chemotherapy, I synthesized a gold-tagged HA-CDDP conjugate via a disulfide bond between the 3-nm gold nanoparticle and the carrier HA. Transmission electron microscopy (TEM) will be used to determine the co-localization of the gold-tagged carrier as well as the platinum-based anticancer drug. In my initial studies, I characterized the conjugate using atomic absorption spectroscopy and UV-visible spectroscopy. Subsequently, the sample preparation procedures were optimized by examining a variety of drug concentrations, treatment durations, and staining/contrasting agents, in MDA-1986 cells. Finally, the TEM operation conditions were also optimized using TEM grids made of different materials, to minimize the background interference with the target
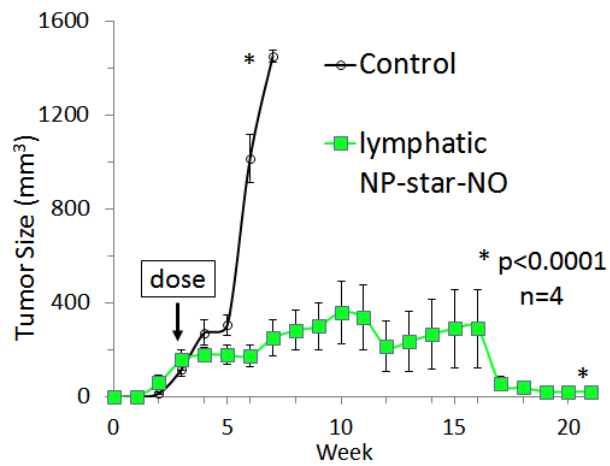
Figure 1. Locoregional chemotherapy with star polymer nanoparticles releasing NO (NP-star-NO) were highly efficacious, increasing mean survival by >10 weeks in xenografts of HNSCC. Dosing was 10 mg/kg NO-prodrug.

metals (Au and Pt). Future work will be conducted to determine the compartment-specific cellular localization and distribution of the polymer backbone and the cleaved active drug. Based on the information collected, we will be able to answer the questions: has the drug been released from the carrier before it enters the cell and are the carriers incorporated into the cell via endocytosis?

An alternative approach to investigate the cellular distribution of the carrier-based chemotherapy is to use fluorescently labeled HA-DOX. Because of the distinct fluorescence spectra of the Cy7 fluorophore and doxorubicin, the signals can be separated and analyzed using fluorescence microscopy. Further, Cy 7 is a more stable fluorescent dye than IR820 for the use in fluorescence microscopy. Therefore, the same goal may be accomplished and the questions of interest can be answered.

Appendix

1. Synthetic schemes of a sugar star polymer and nitric oxide prodrugs

1.1. Synthetic scheme of a sugar star polymer
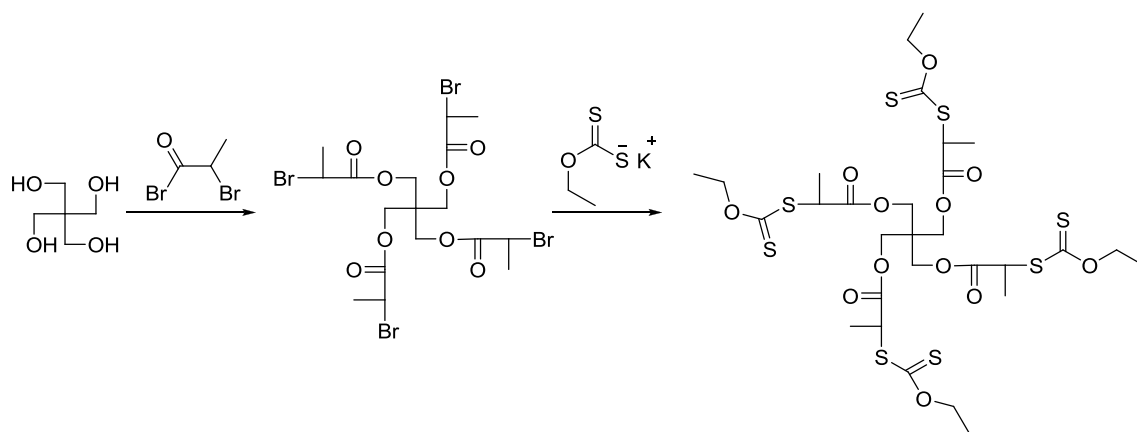
Scheme 1. Synthesis of MADIX/RAFT agents
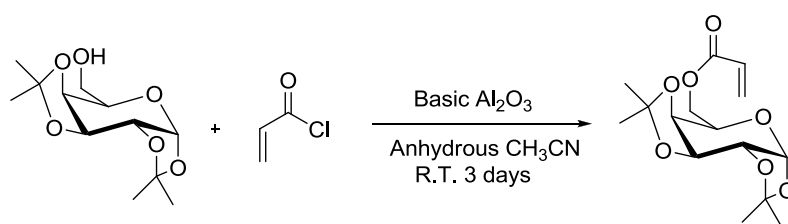
Scheme 2. Synthesis of *1,2;3,4-Di-O-isopropylidene-6-O-acryloyl-α-D-galactopyranose*
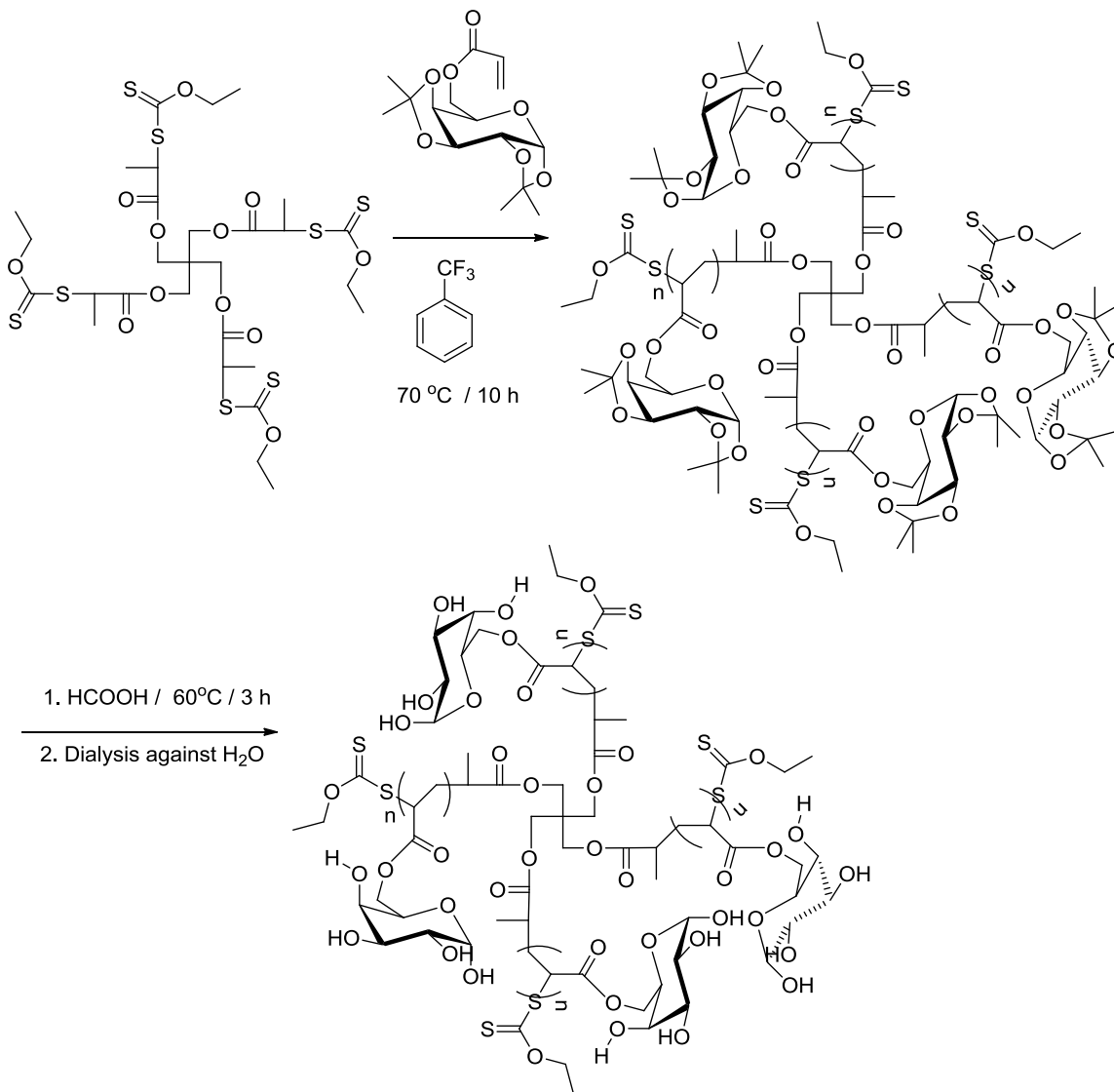
Scheme 3. Synthesis of a sugar star polymer

1.2. Synthetic scheme of nitric oxide prodrugs
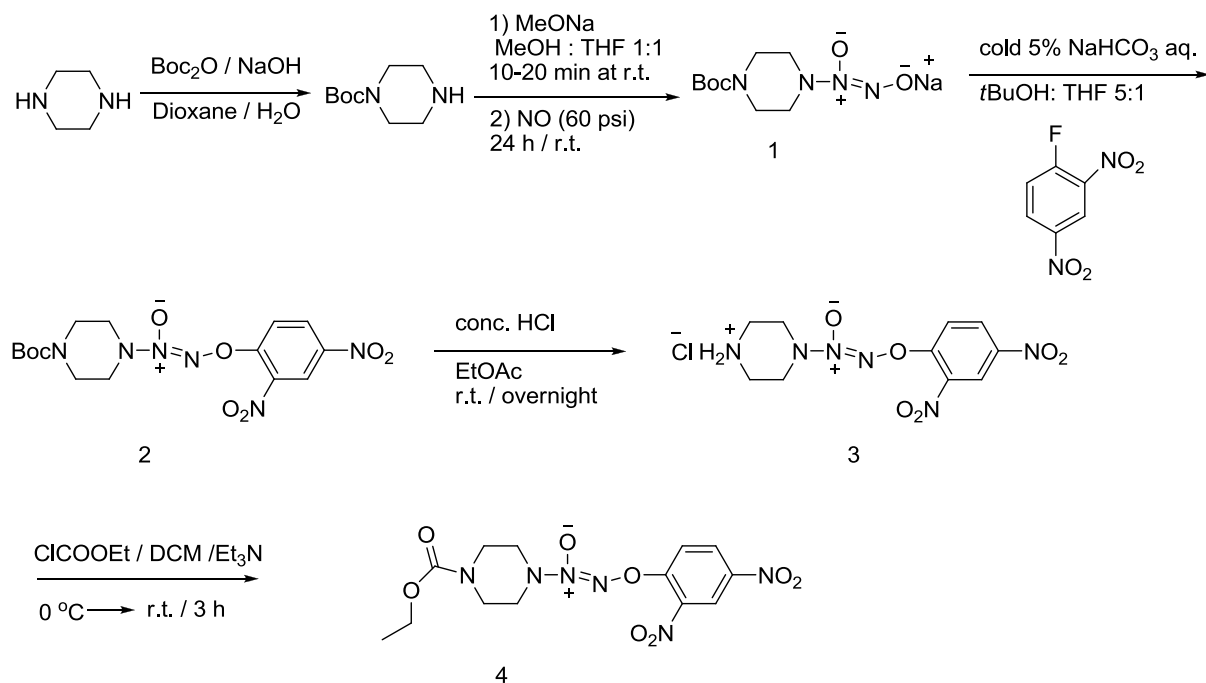
Scheme 4. Synthesis of JS-K
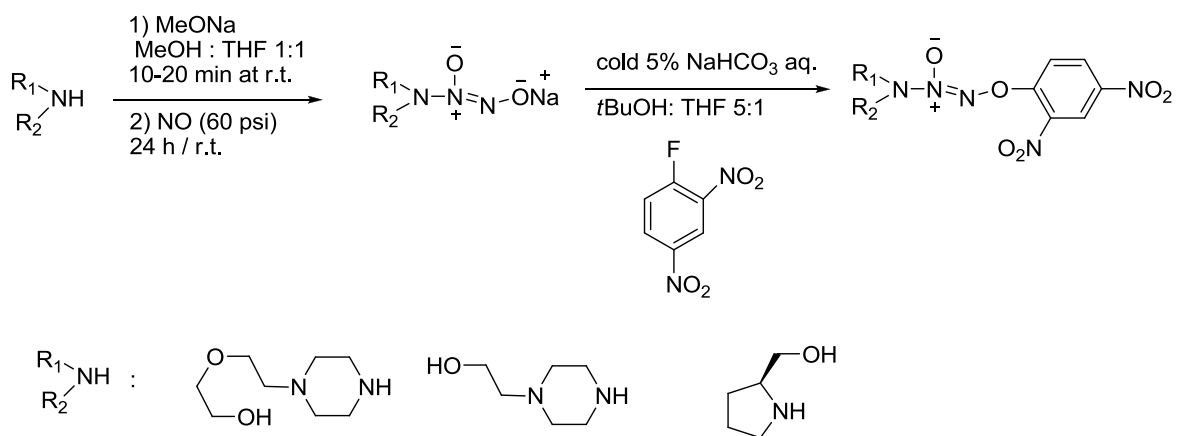
Scheme 5. Synthesis of JS-K analogues

2. Release of nitric oxide from JS-K, JS-K analogues and carrier-based prodrugs

A.
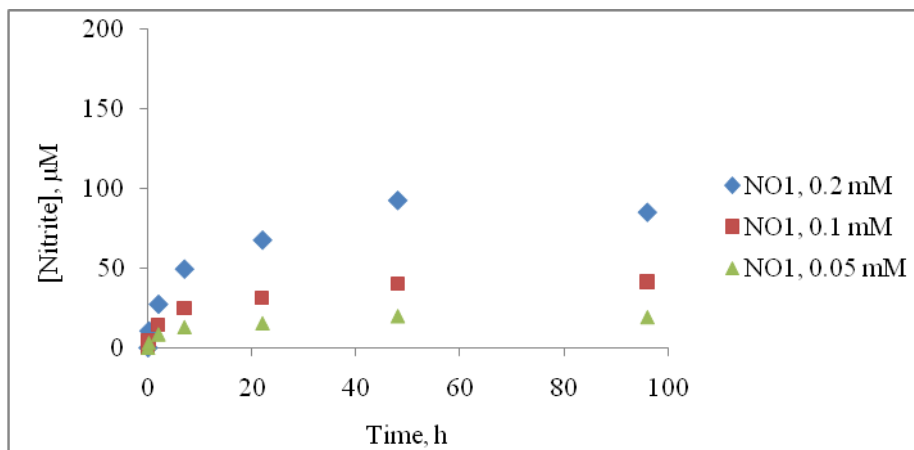
B.
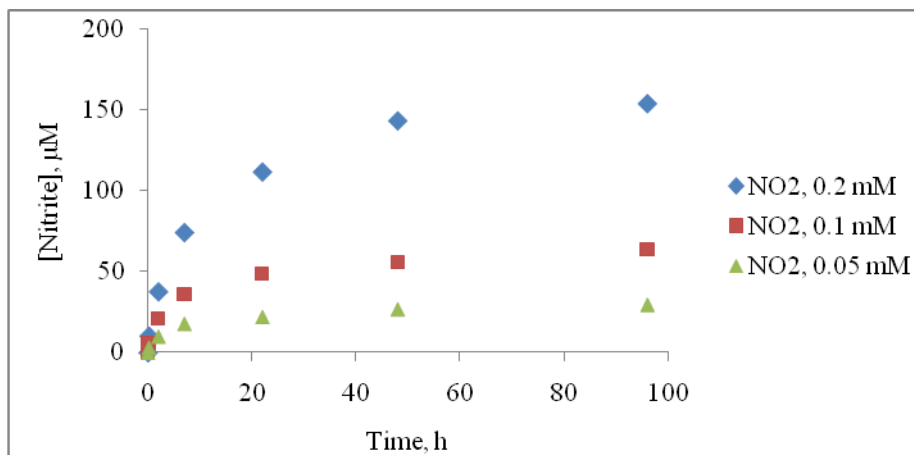
C.
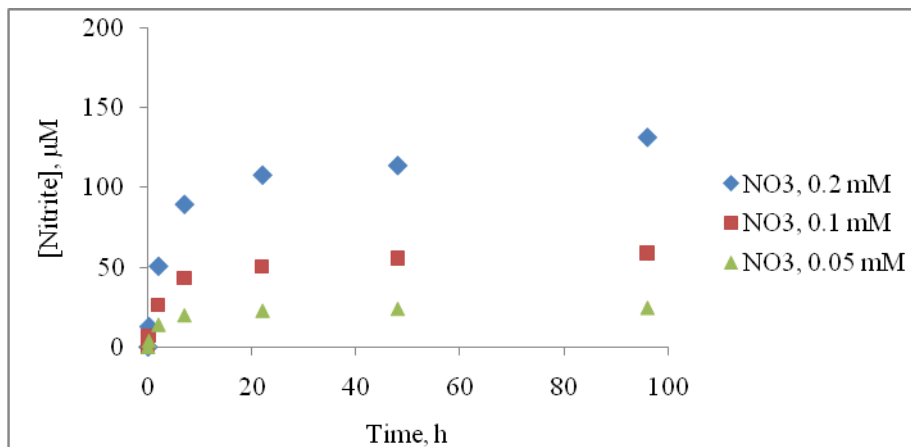
D.
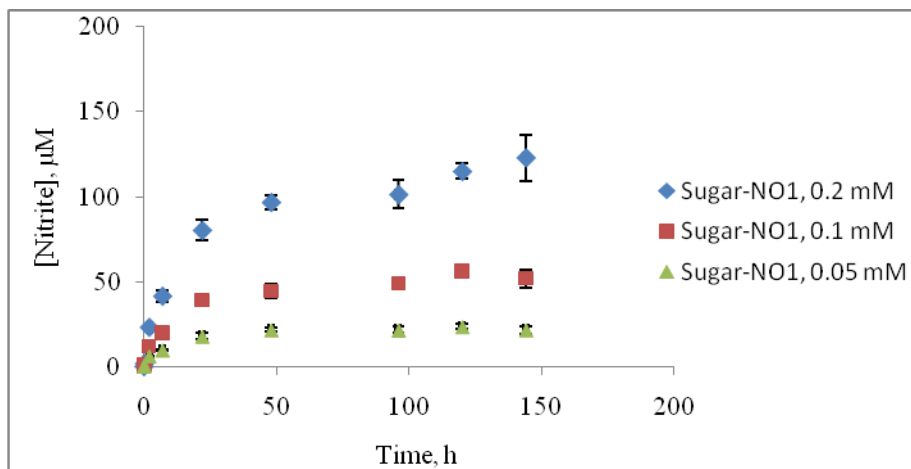
Figure 1. *In vitro* release of nitric oxide from (A) NO1, (B) NO2, (C) JS-K, and (D) sugar-NO1. Release studies were performed in DMEM with the presence of MDA-1986 cells. Release half lives were determined to be 6, 7, 3, and 10 hours, for NO1, NO2, JS-K and sugar-NO1, respectively.

3. Dosing schedule and results of caspase-3, resazurin and trypan blue assays in MDA-1986 cells

Experiment #	Cell line	Cells/well	Dose on day 1	Dose on day 2
1	MDA-1986	10,000	NO1	NO1+CDDP
2	MDA-1986	10,000	NO1	CDDP
3	MDA-1986	10,000	CDDP	NO1+CDDP
4	MDA-1986	10,000	CDDP	NO1
5	MDA-MB-468LN	5,000	NO1	NO1+CDDP
6	MDA-MB-468LN	5,000	NO1	CDDP
7	HUVEC	3,000	NO1	NO1+CDDP
8	HUVEC	3,000	NO1	CDDP

Table 1. Dose regimens of single drug treatment and combination therapy in three cell lines.
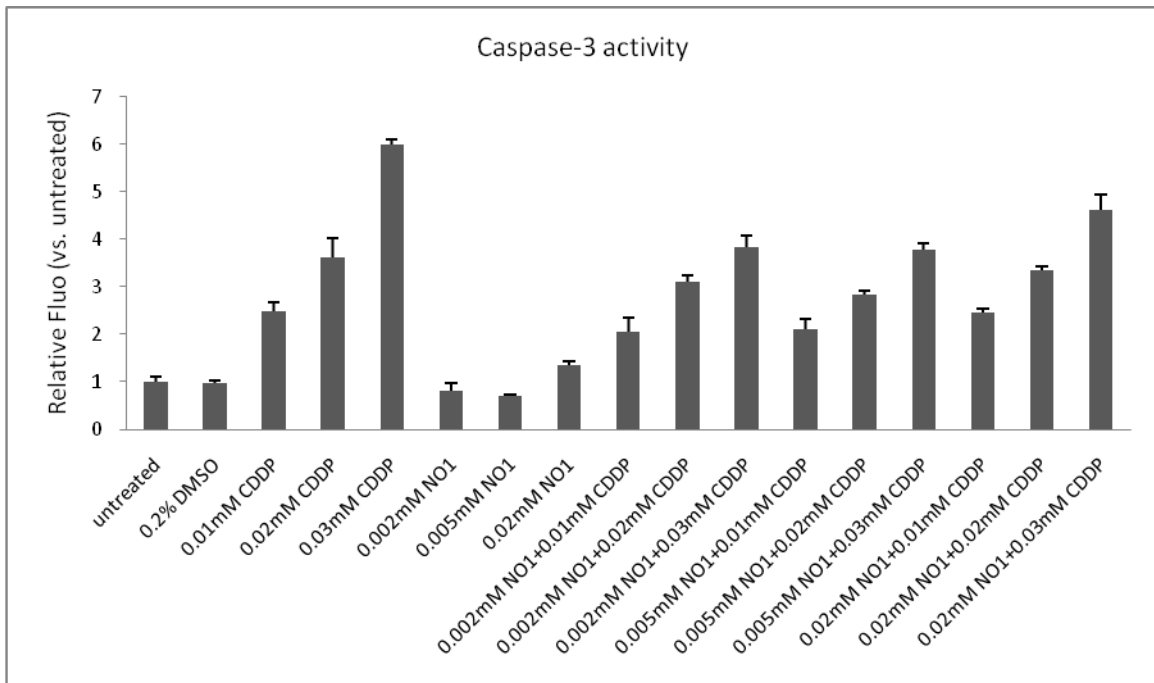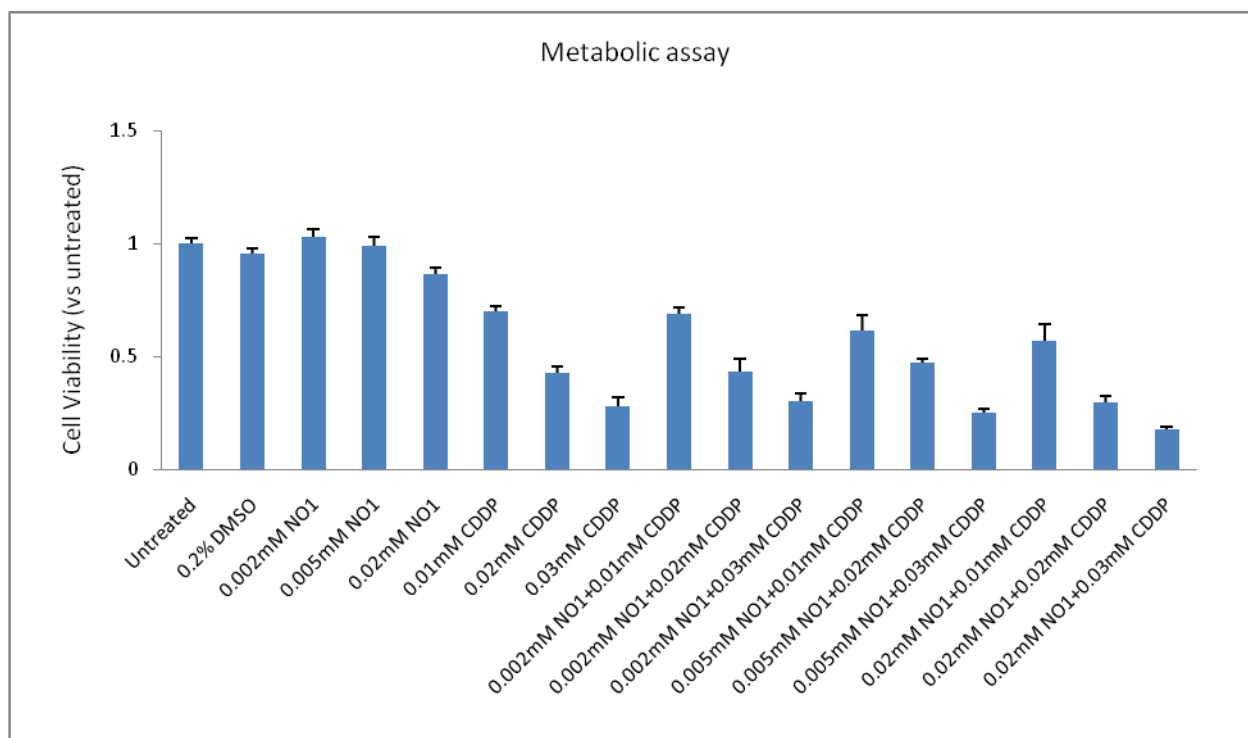
Figure 2. Measurement of caspase-3 activity in MDA-1986 cells (experiment #1). Treatment groups included untreated control, DMSO control, CDDP, NO1, and a variety of combination treatments (N=5).
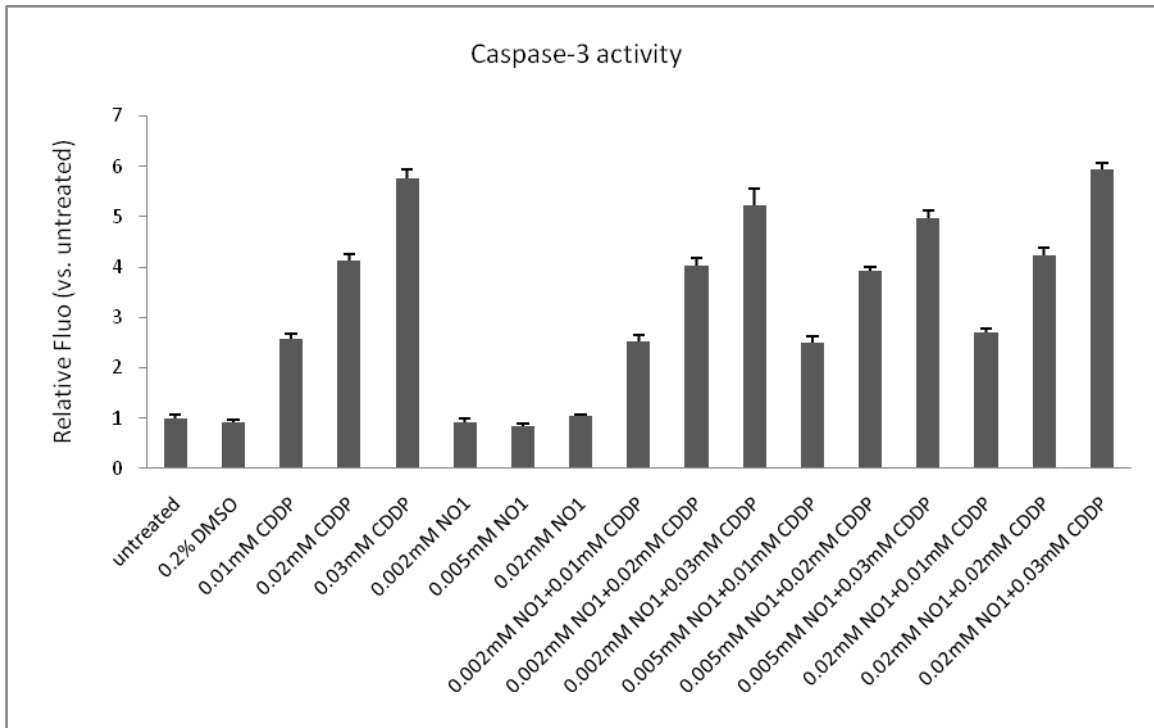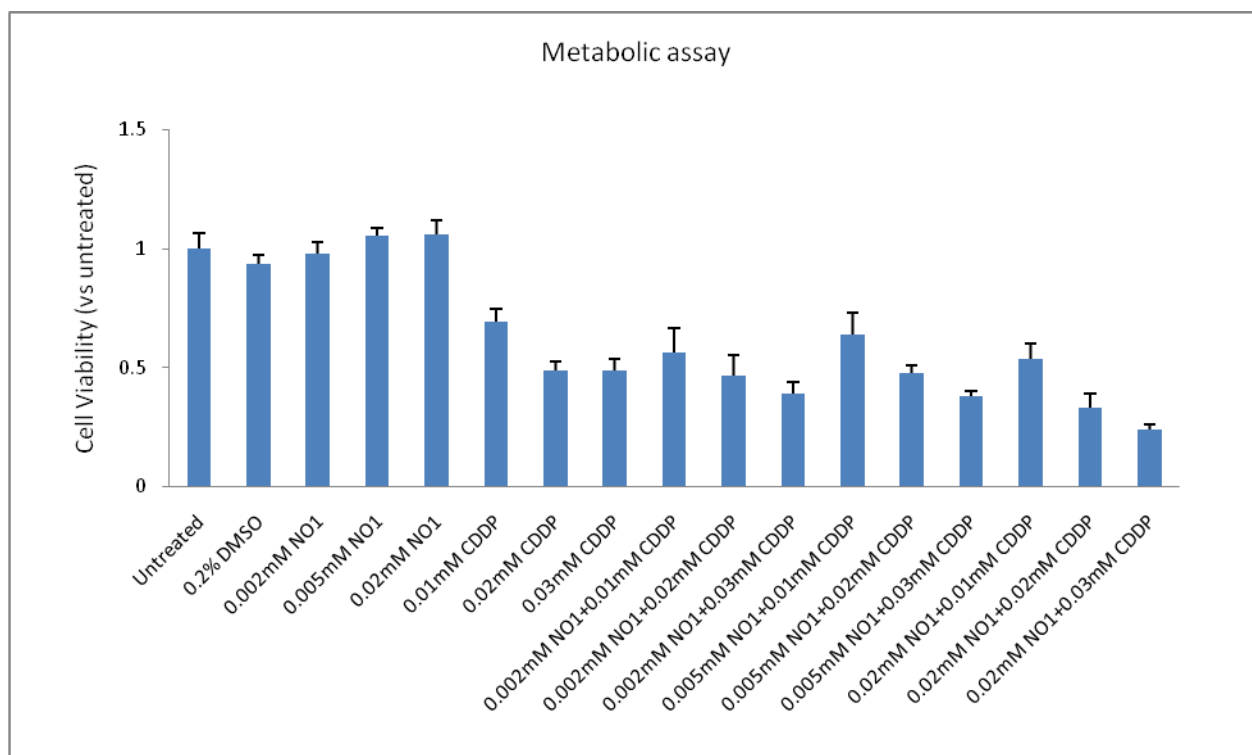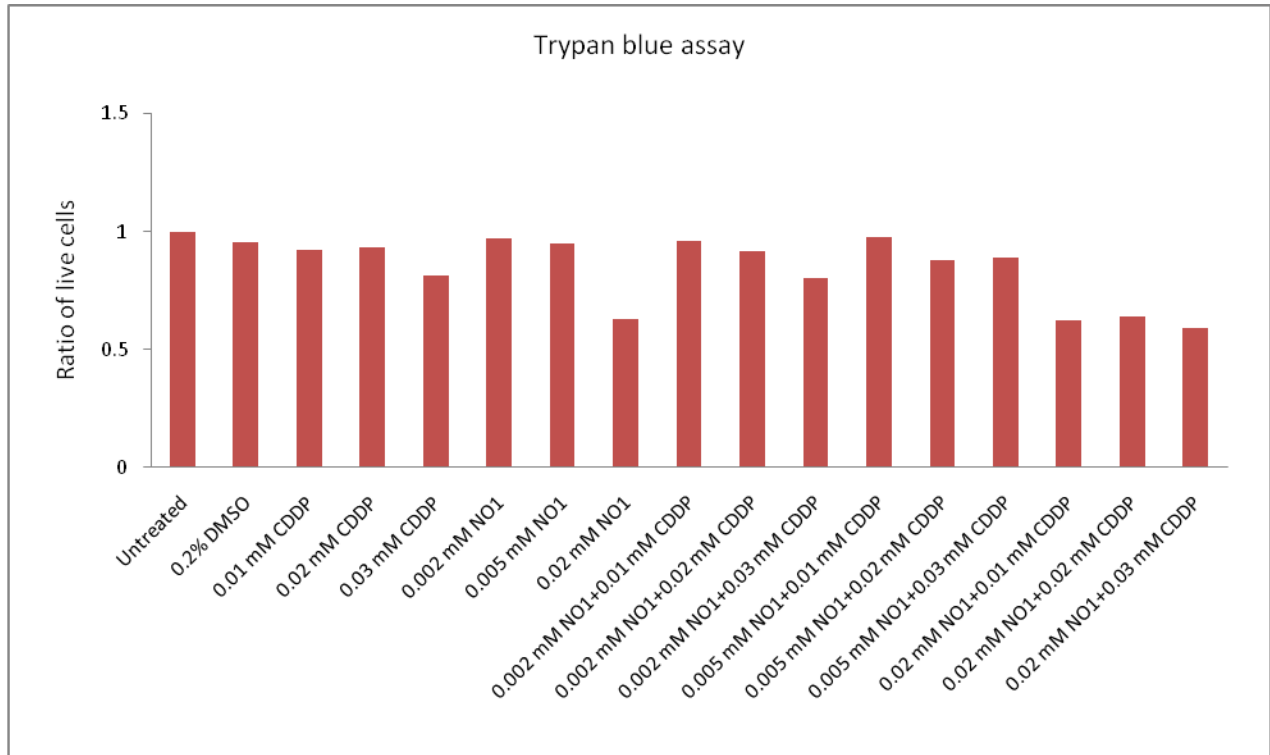
Figure 3. Measurement of caspase-3 activity in MDA-1986 cells (experiment #2). Treatment groups included untreated control, DMSO control, CDDP, NO1, and a variety of combination treatments (N=5).
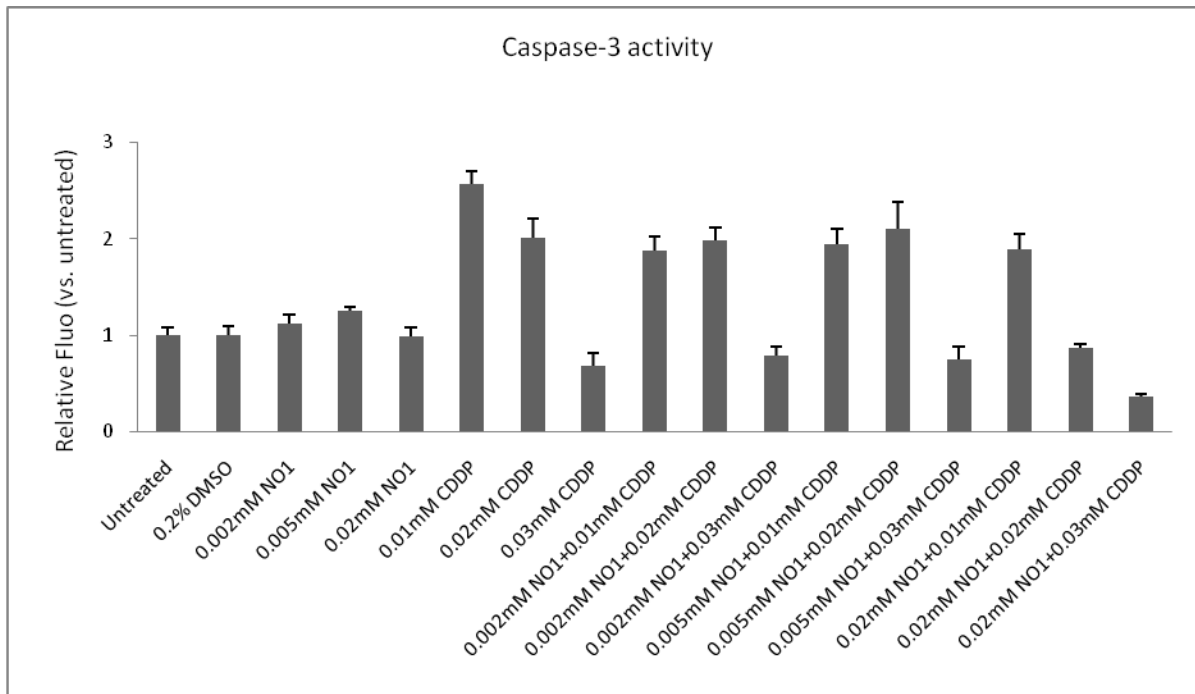
Figure 4. Measurement of caspase-3 activity in MDA-1986 cells (experiment #3). Treatment groups included untreated control, DMSO control, CDDP, NO1, and a variety of combination treatments (N=5).
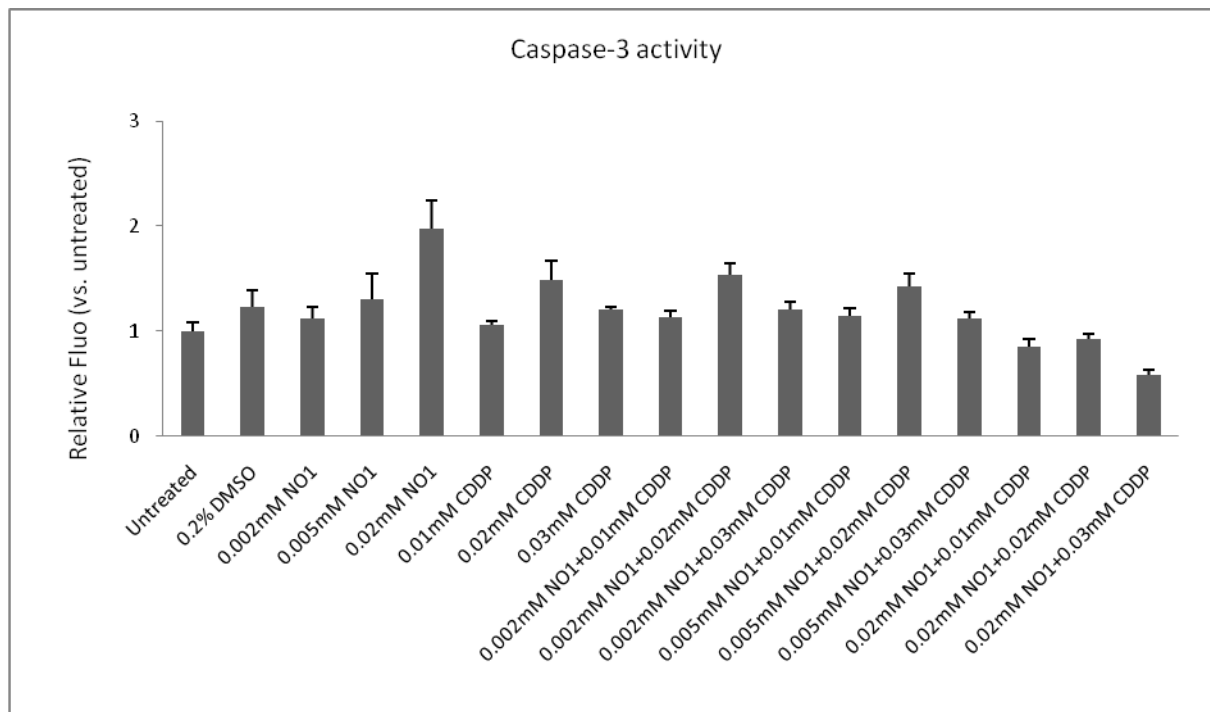
Figure 5. Measurement of caspase-3 activity in MDA-1986 cells (experiment #4). Treatment groups included untreated control, DMSO control, CDDP, NO1, and a variety of combination treatments (N=5).
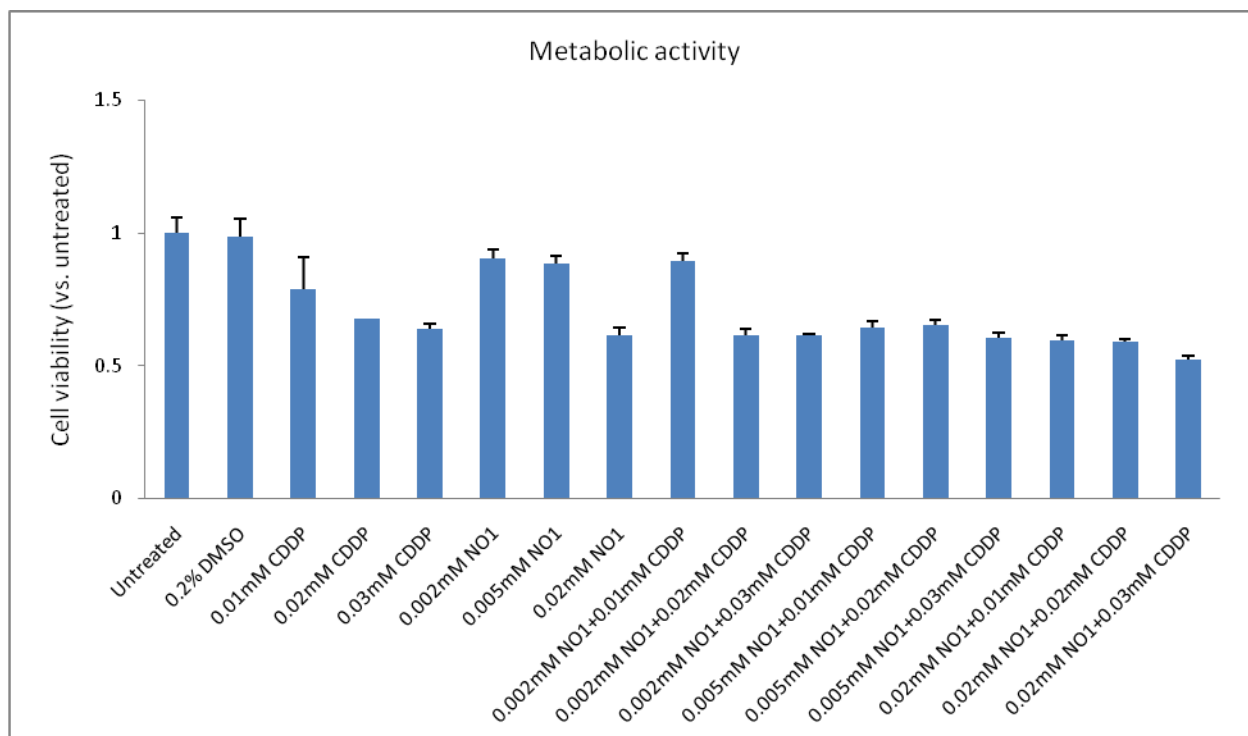
Figure 6. Measurement of metabolic activity in MDA-1986 cells (experiment #1). Treatment groups included untreated control, DMSO control, CDDP, NO1, and a variety of combination treatments. $p < 0.001$ for 0.03 mM CDDP vs. 0.03 mM CDDP+0.02 mM NO1, $p < 0.05$ for 0.02 mM CDDP vs. 0.02 mM CDDP+0.02 mM NO1, $p < 0.05$ for 0.01 mM CDDP vs. 0.01 mM CDDP+0.02 mM NO1 (N=5).
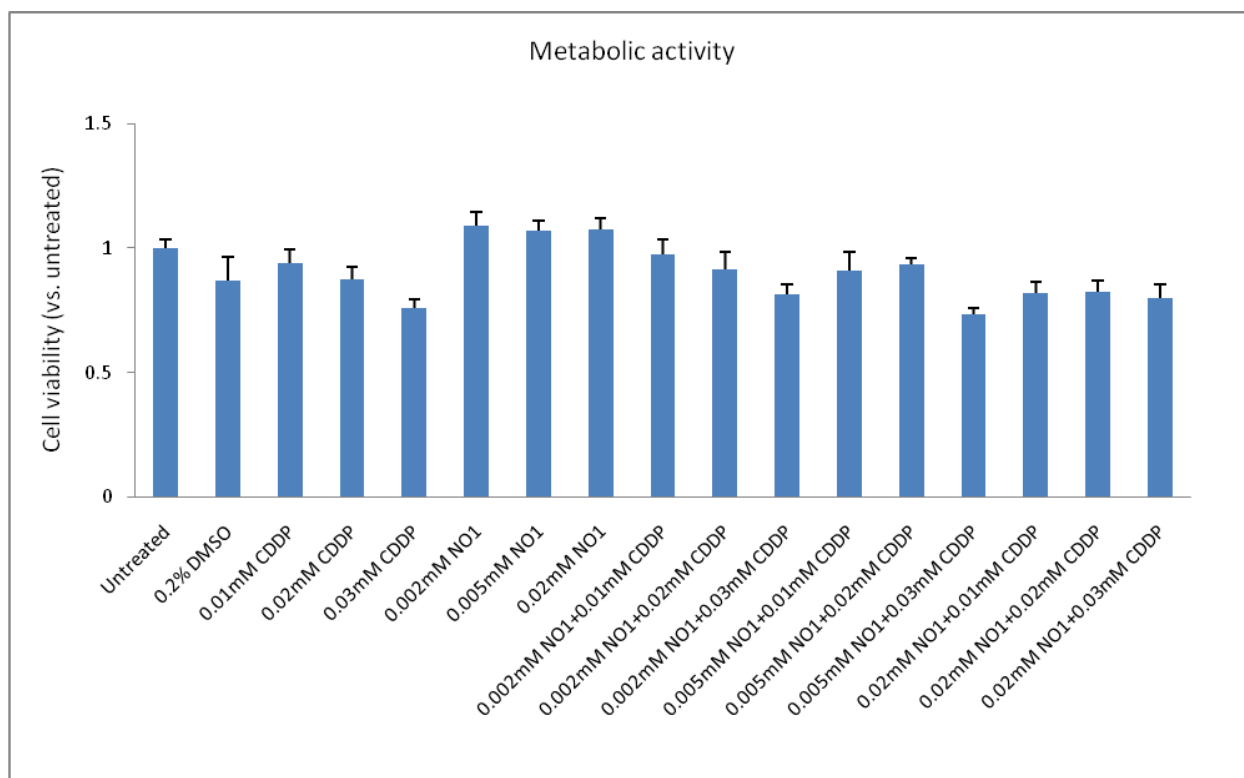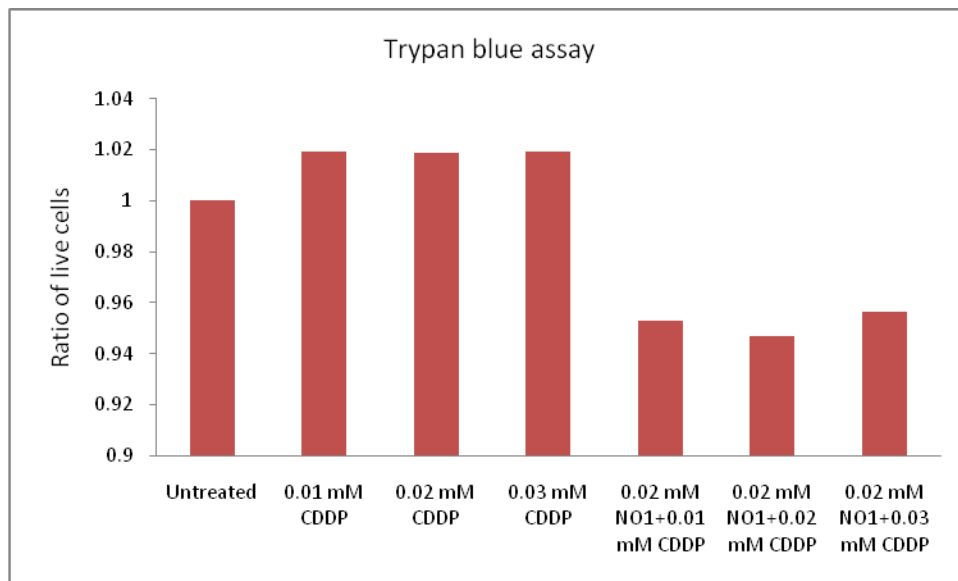
Figure 7. Measurement of metabolic activity in MDA-1986 cells (experiment #2). Treatment groups included untreated control, DMSO control, CDDP, NO1, and a variety of combination treatments. p=0.26 for 0.03 mM CDDP vs. 0.03 mM CDDP+0.02 mM NO1, p=0.19 for 0.02 mM CDDP vs. 0.02 mM CDDP+0.02 mM NO1, p=0.015 for 0.01 mM CDDP vs. 0.01 mM CDDP+0.02 mM NO1 (N=5).
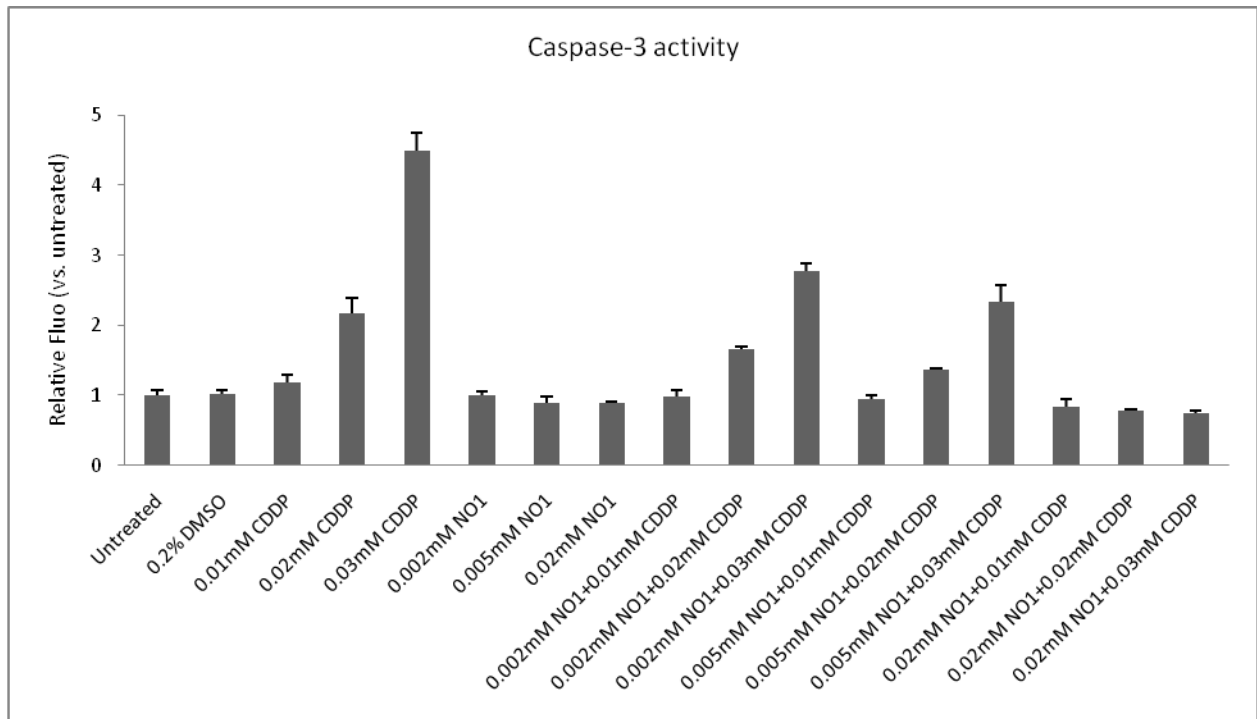
Figure 8. Measurement of metabolic activity in MDA-1986 cells (experiment #3). Treatment groups included untreated control, DMSO control, CDDP, NO1, and a variety of combination treatments. $p=0.0006$ for 0.03 mM CDDP vs. 0.03 mM CDDP+0.02 mM NO1, $p<0.0001$ for 0.02 mM CDDP vs. 0.02 mM CDDP+0.02 mM NO1, $p=0.005$ for 0.01 mM CDDP vs. 0.01 mM CDDP+0.02 mM NO1 (N=5).

Figure 9. Measurement of metabolic activity in MDA-1986 cells (experiment #4). Treatment groups included untreated control, DMSO 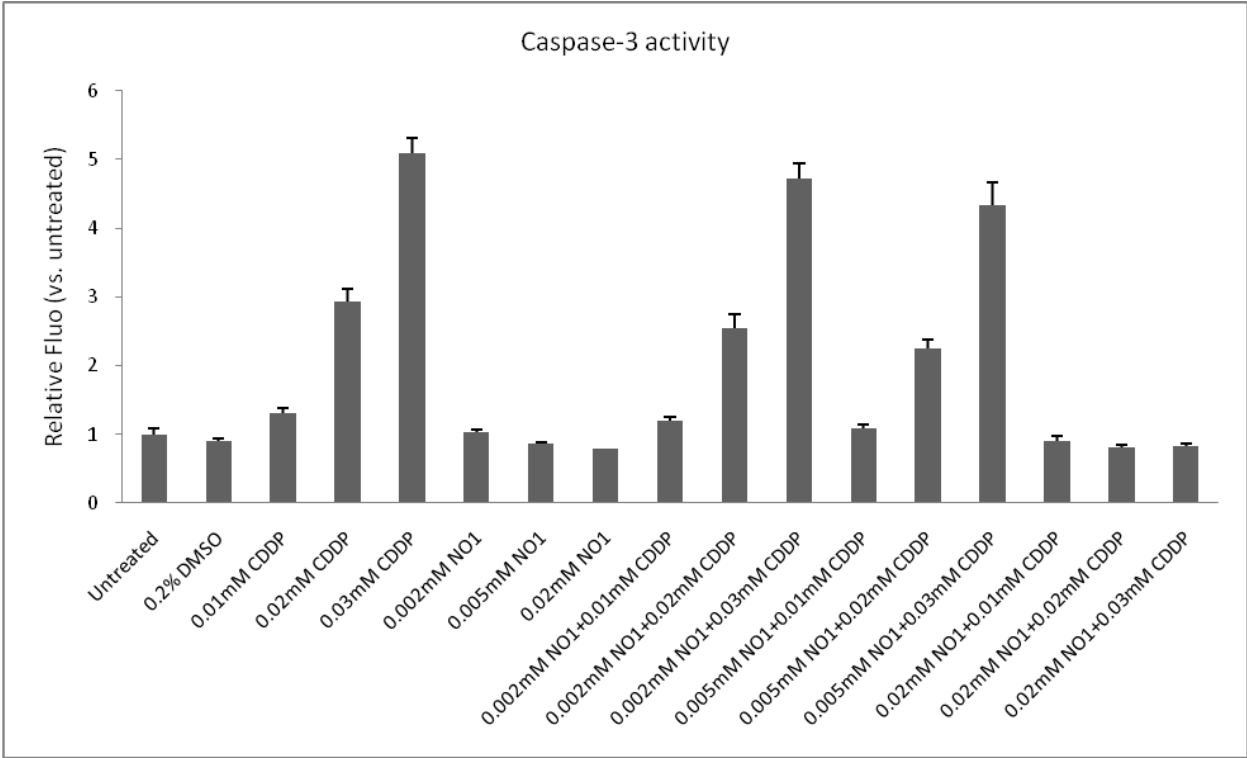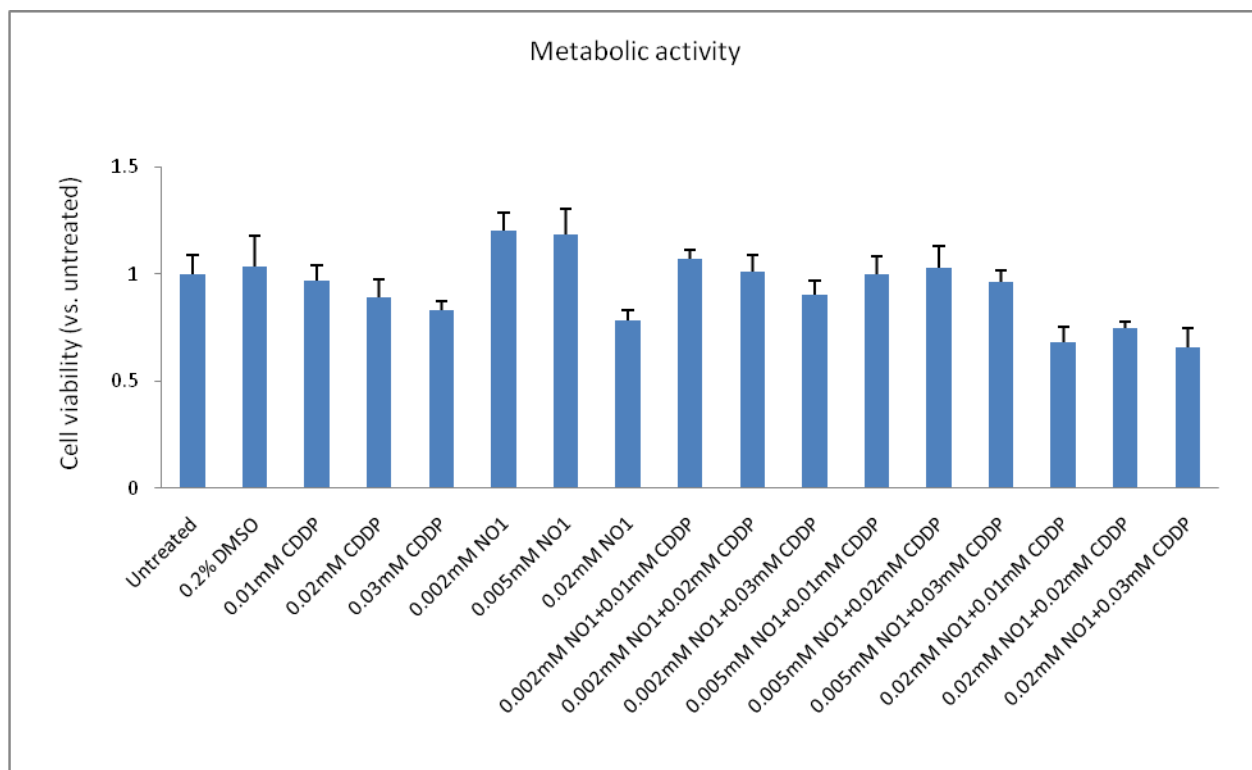control, CDDP, NO1, and a variety of combination treatments. $p<0.0001$ for 0.03 mM CDDP vs. 0.03 mM CDDP+0.02 mM NO1, $p=0.0029$ for 0.02 mM CDDP vs. 0.02 mM CDDP+0.02 mM NO1, $p=0.0026$ for 0.01 mM CDDP vs. 0.01 mM CDDP+0.02 mM NO1 (N=5).

A.

B.

Figure 10. Determination of live cell ratio in MDA-1986 cells (experiment #1, 2 trials (1st trial: (A), 2nd trial: (B)). Treatment groups included untreated control, DMSO control, CDDP, NO1, and a variety of combination treatments. p=0.053 for 0.03 mM CDDP vs. 0.03 mM CDDP+0.02 mM NO1, p=0.0005 for 0.02 mM CDDP vs. 0.02 mM CDDP+0.02 mM NO1, p=0.068 for 0.01 mM CDDP vs. 0.01 mM CDDP+0.02 mM NO1 (N=4).

# 4. Results of caspase-3, resazurin and trypan blue assays in MDA-MB-468LN cells

Figure 11. Measurement of caspase-3 activity in MDA-MB-468LN cells (experiment #5). Treatment groups included untreated control, DMSO control, CDDP, NO1, and a variety of combination treatments (N=5).

Figure 12. Measurement of caspase-3 activity in MDA-MB-468LN cells (experiment #6). Treatment groups included untreated control, DMSO control, CDDP, NO1, and a variety of combination treatments (N=5).

Figure 13. Measurement of metabolic activity in MDA-MB-468LN cells (experiment #5). Treatment groups included untreated control, DMSO control, CDDP, NO1, and a variety of combination treatments. p=0.0026 for 0.03 mM CDDP vs. 0.03 mM CDDP+0.02 mM NO1, p=0.0043 for 0.02 mM CDDP vs. 0.02 mM CDDP+0.02 mM NO1, p=0.0004 for 0.01 mM CDDP vs. 0.01 mM CDDP+0.02 mM NO1 (N=5).
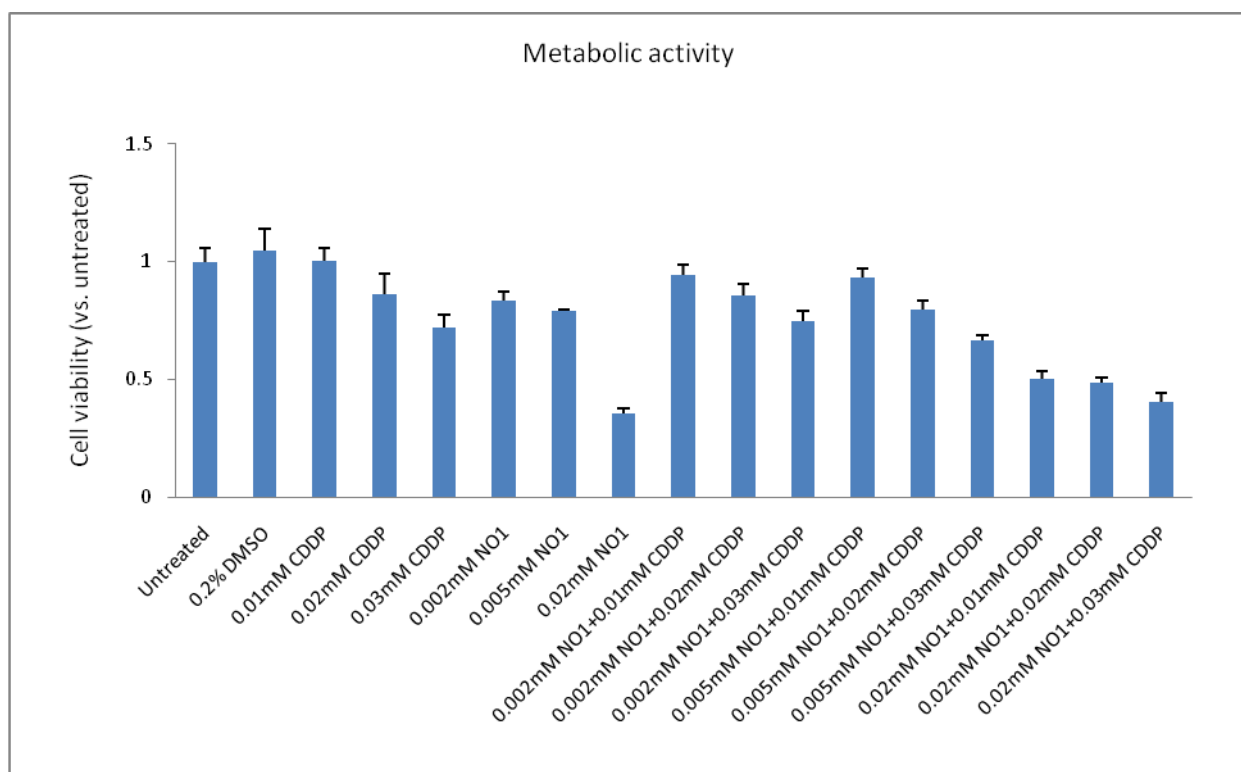
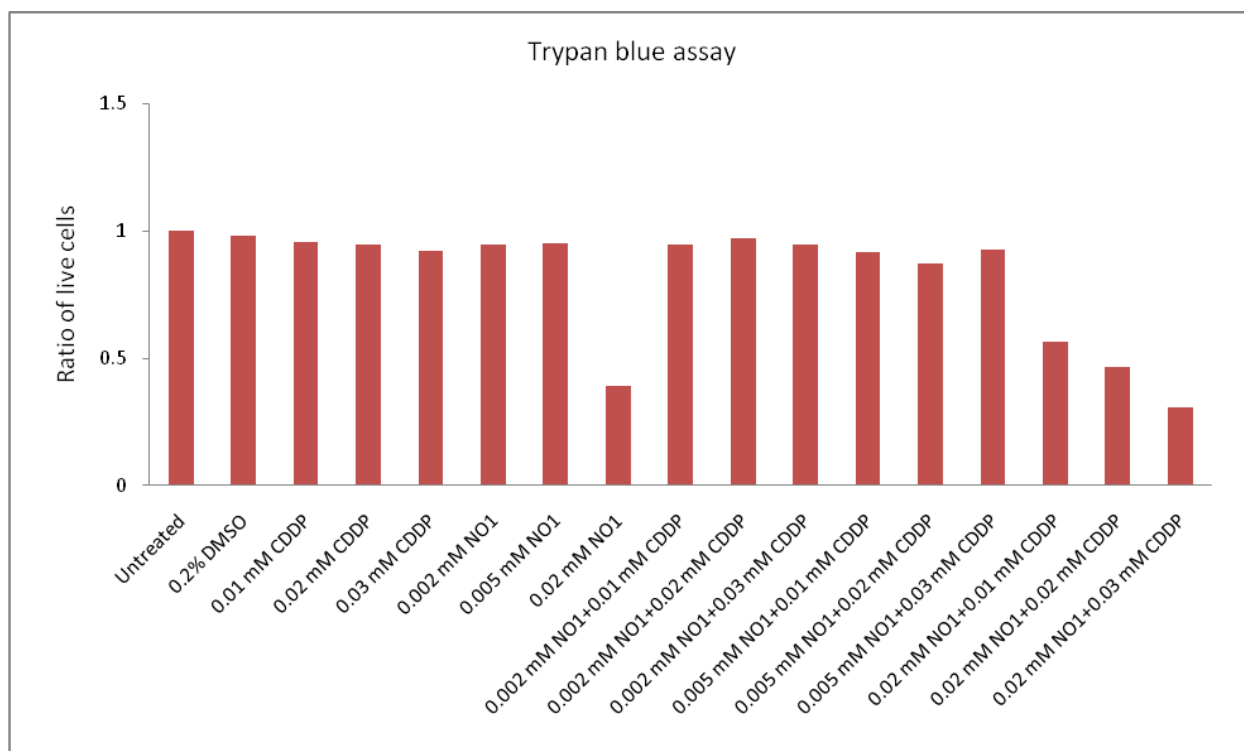**Figure 14.** Measurement of metabolic activity in MDA-MB-468LN cells (experiment #6). Treatment groups included untreated control, DMSO control, CDDP, NO1, and a variety of combination treatments. $p<0.0001$ for 0.03 mM CDDP vs. 0.03 mM CDDP+0.02 mM NO1, $p=0.0002$ for 0.02 mM CDDP vs. 0.02 mM CDDP+0.02 mM NO1, $p=0.0004$ for 0.01 mM CDDP vs. 0.01 mM CDDP+0.02 mM NO1 (N=5).

Figure 15. Determination of live cell ratio in MDA-MB-468LN cells (experiment #5). Treatment groups included untreated control, DMSO control, CDDP, NO1, and a variety of combination treatments. p=0.0003 for 0.03 mM CDDP vs. 0.03 mM CDDP+0.02 mM NO1, p<0.0001 for 0.02 mM CDDP vs. 0.02 mM CDDP+0.02 mM NO1, p=0.0003 for 0.01 mM CDDP vs. 0.01 mM CDDP+0.02 mM NO1 (N=4).

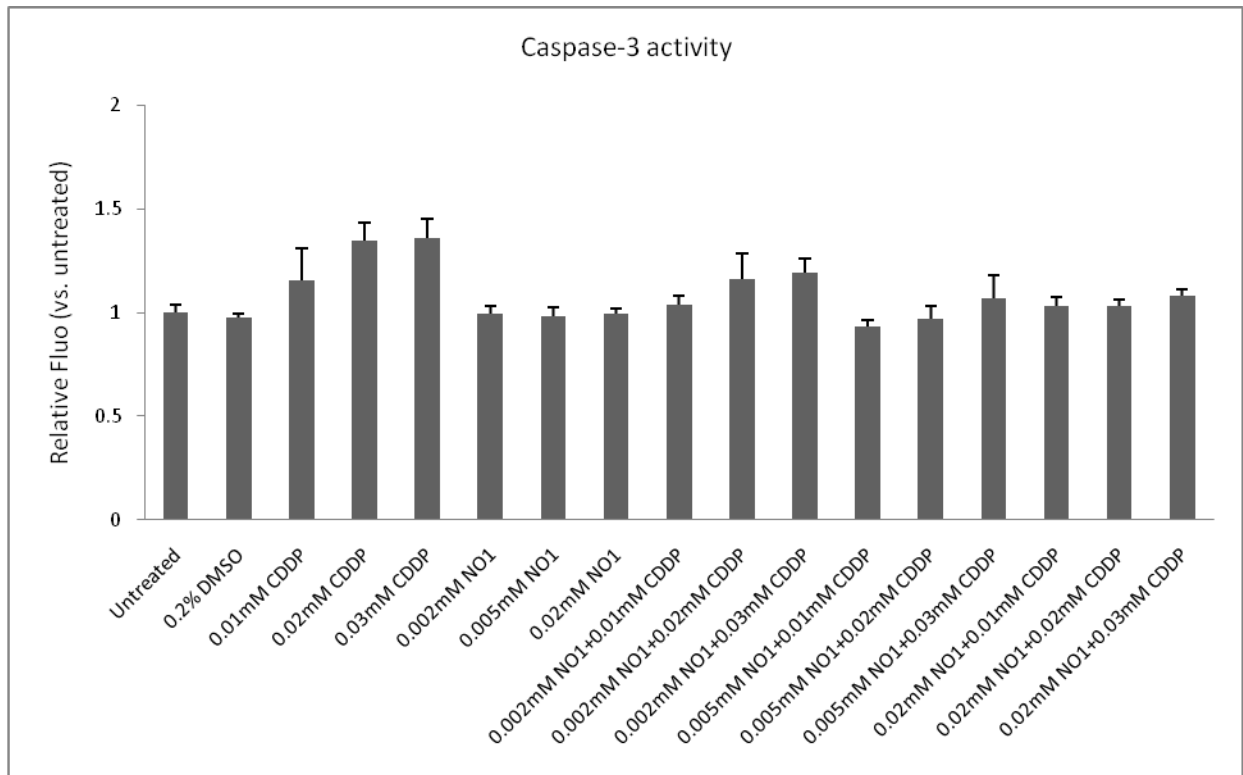**5. Results of caspase-3, resazurin and trypan blue assays in HUVEC cells**

Figure 16. Measurement of caspase-3 activity in HUVEC cells (experiment #7). Treatment groups included untreated control, DMSO control, CDDP, NO1, and a variety of combination treatments (N=5).
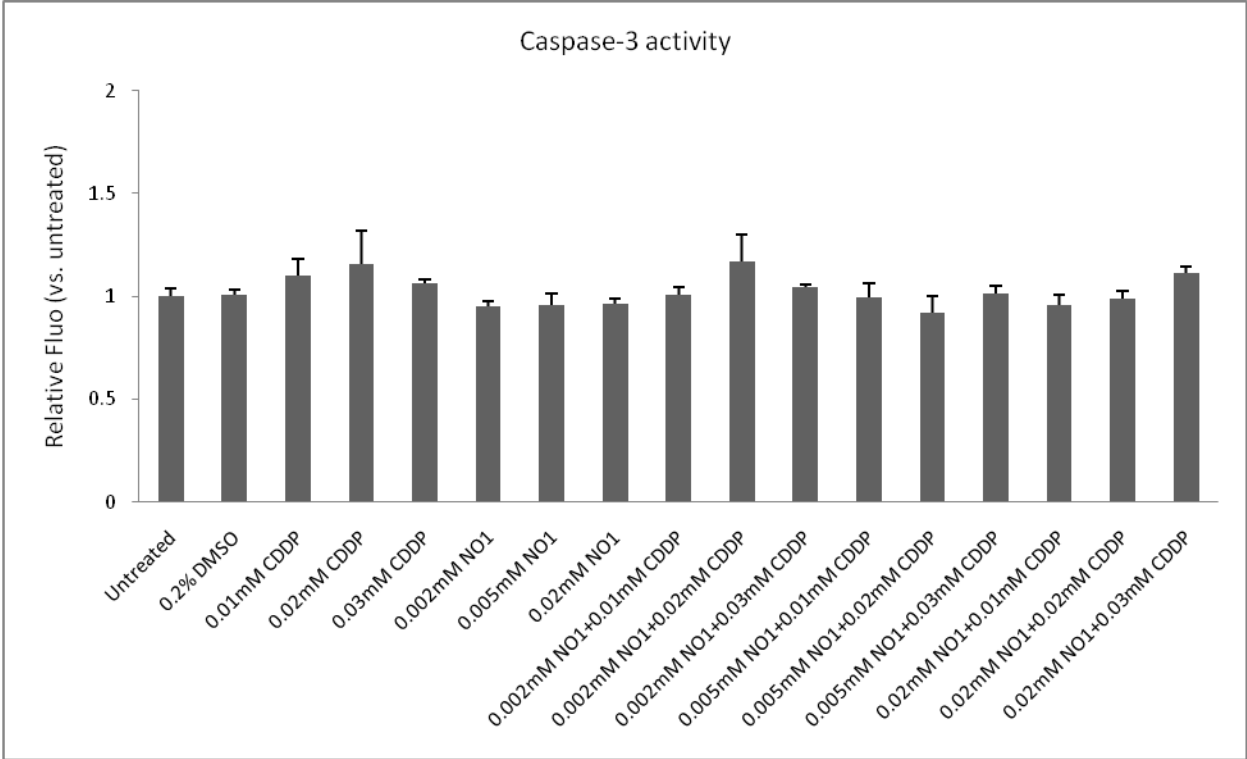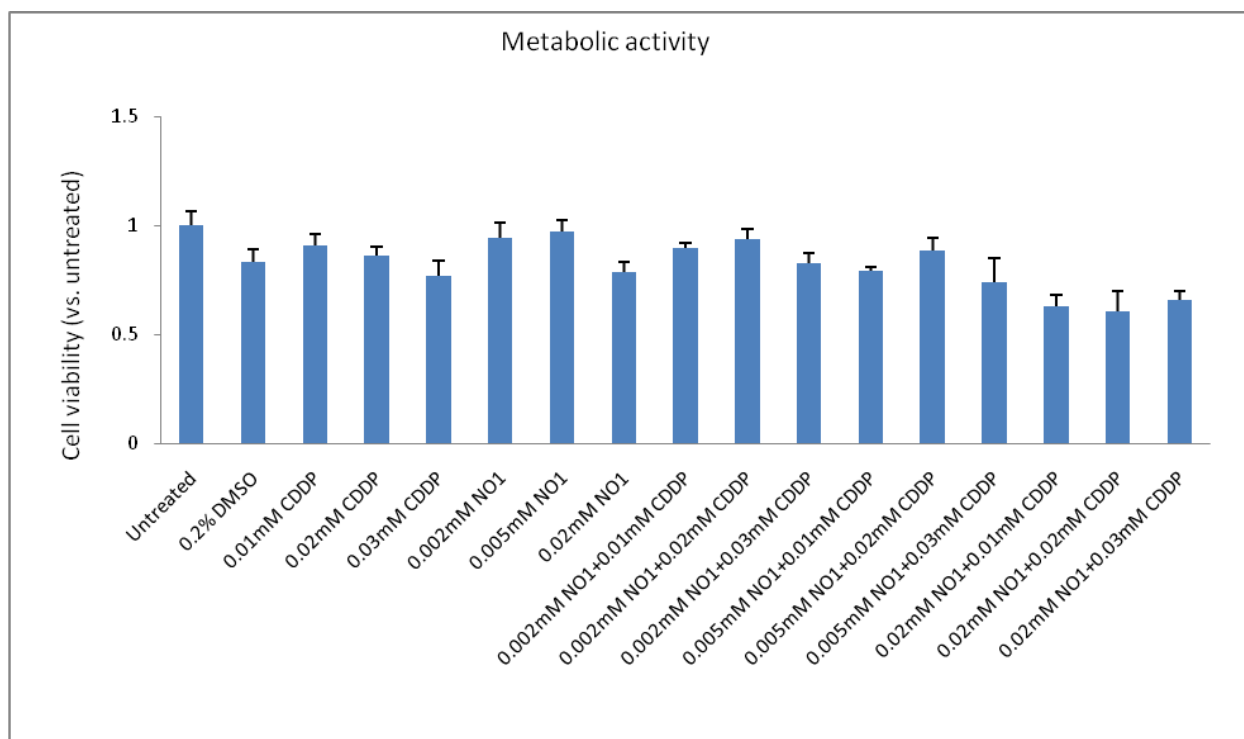
Figure 17. Measurement of caspase-3 activity in HUVEC cells (experiment #8). Treatment groups included untreated control, DMSO control, CDDP, NO1, and a variety of combination treatments (N=5).

Figure 18. Measurement of metabolic activity in HUVEC cells (experiment #7). Treatment groups included untreated control, DMSO control, CDDP, NO1, and a variety of combination treatments. p=0.0028 for 0.03 mM CDDP vs. 0.03 mM CDDP+0.02 mM NO1, p<0.0001 for 0.02 mM CDDP vs. 0.02 mM CDDP+0.02 mM NO1, p<0.0001 for 0.01 mM CDDP vs. 0.01 mM CDDP+0.02 mM NO1 (N=5).
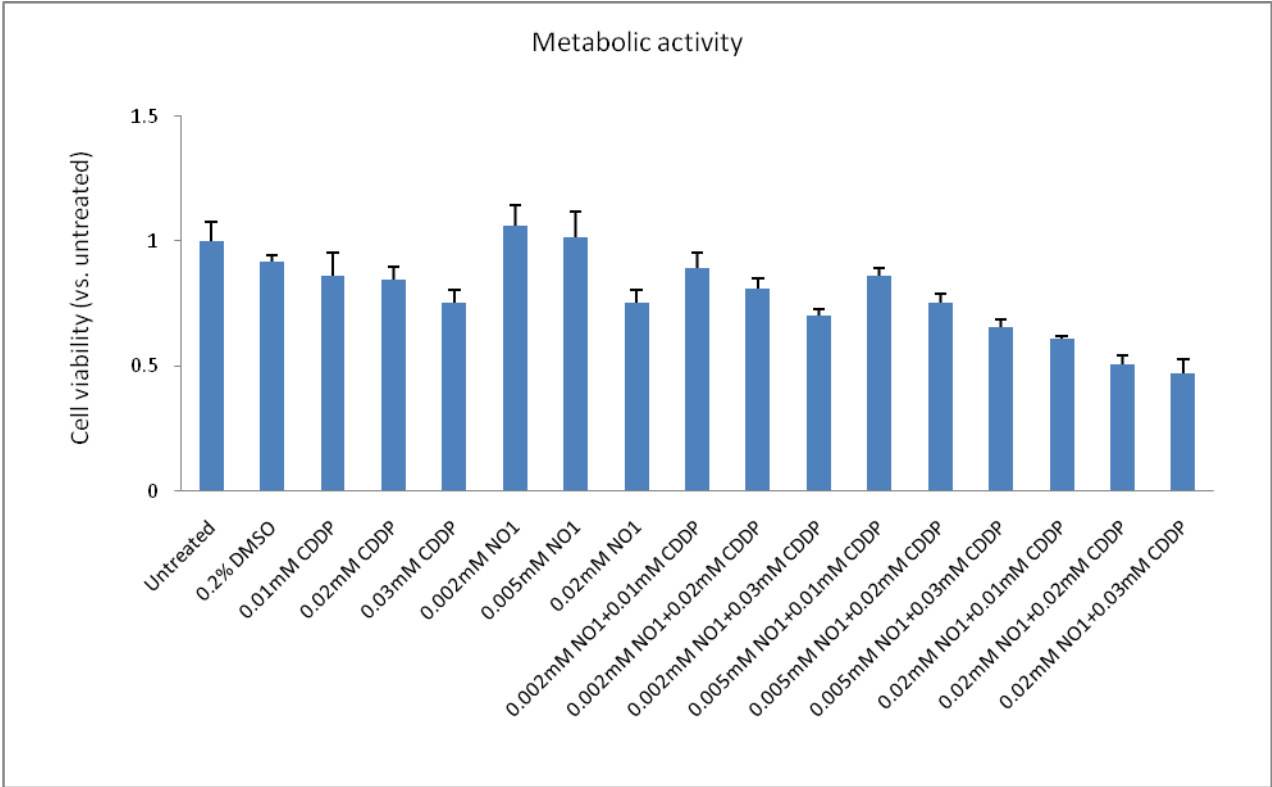
Figure 19. Measurement of metabolic activity in HUVEC cells (experiment #8). Treatment groups included untreated control, DMSO control, CDDP, NO1, and a variety of combination treatments. p<0.0001 for 0.03 mM CDDP vs. 0.03 mM CDDP+0.02 mM NO1, p<0.0001 for 0.02 mM CDDP vs. 0.02 mM CDDP+0.02 mM NO1, p=0.0008 for 0.01 mM CDDP vs. 0.01 mM CDDP+0.02 mM NO1 (N=5).
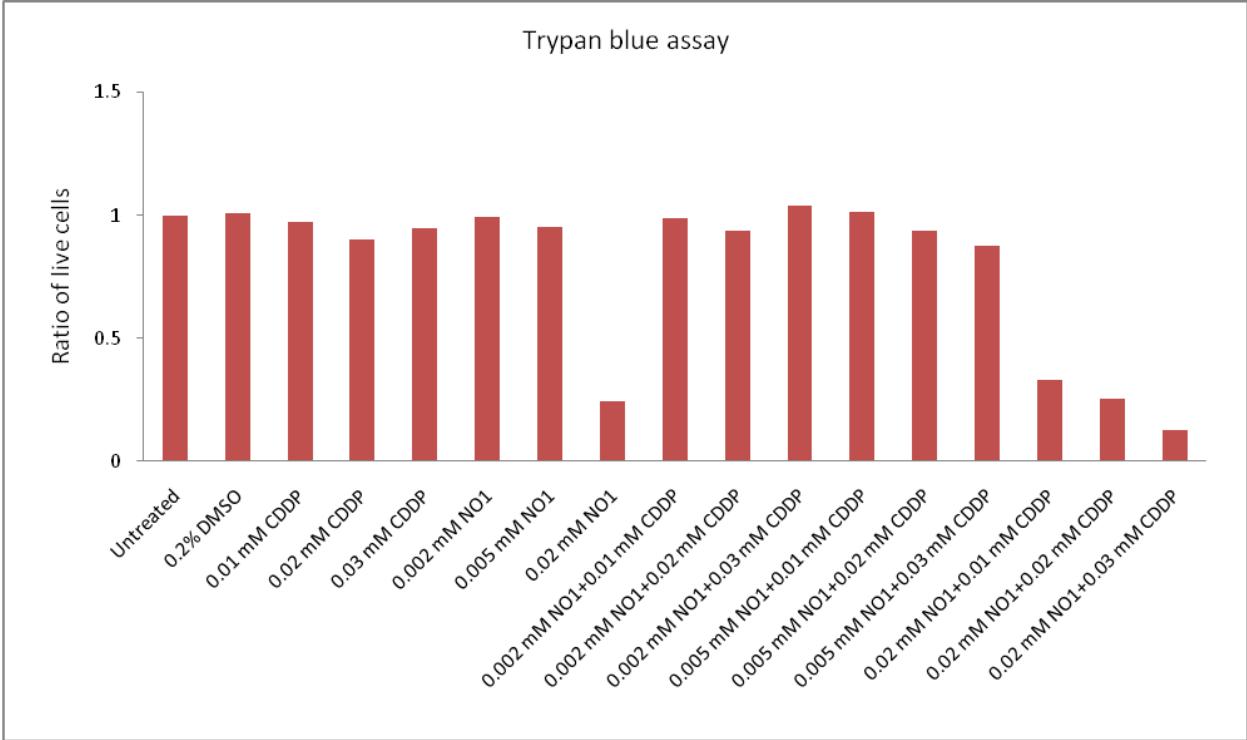
Figure 20. Determination of live cell ratio in HUVEC cells (experiment #7). Treatment groups included untreated control, DMSO control, CDDP, NO1, and a variety of combination treatments. p=0.0003 for 0.03 mM CDDP vs. 0.03 mM CDDP+0.02 mM NO1, p=0.0039 for 0.02 mM CDDP vs. 0.02 mM CDDP+0.02 mM NO1, p=0.003 for 0.01 mM CDDP vs. 0.01 mM CDDP+0.02 mM NO1 (N=4).